## Double Degree Doctorate between


**UNIVERSITA' DEGLI STUDI DI MILANO**
FACOLTA' DI SCIENZE DEL FARMACO
Department of Pharmaceutical Sciences
PhD Course in Pharmaceutical Sciences (XXXI Cycle)

and

**UNIVERSITAT DE BARCELONA**
**Doctoral Program in Biotechnology**
Department of Biochemistry and Molecular Biomedicine
Faculty of Biology


# Bioanalytical and proteomic approaches in the study of pathologic ECs dysfunctionality, oxidative stress and the effects of PFKFB3 modulators

Doctorate Coordinator at Universita' degli Studi di Milano: Prof. Dr. Giancarlo Aldini


Prof. Dr. Marina Carini
Co-Supervisor

Prof. Dr. Marta Cascante Serratosa
Co-Supervisor and Tutor

Nukala Sarath Babu
PhD candidate
R11494


**Academic years 2016-2019**


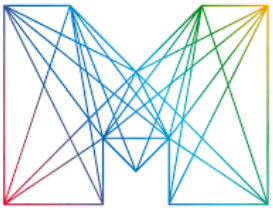

MOGLY NET
LIVING SCIENCE TOGETHER

This PhD programme was founded in the frame of

**HORIZON 2020 - Marie Skłodowska-Curie**

**ITN-European Joint Doctorate**

**MOGLYNET-programme**

"MOGLYNet: *"Mo*dulation of *gly*colytic flux as a *ne*w approach for *t*reatment of atherosclerosis and plaque stabilization: a multidisciplinary study"

*The project leading to this application has received funding from the European Union's Horizon 2020 research and innovation programme under the Marie Skłodowska-Curie grant agreement No 67552.*

# Declaration of Originality

I declare that all the work presented in this thesis is my own, and that all else, figures, images, ideas, quotations, data, results, published or unpublished, have been acknowledged and referenced.

This thesis contains some modified material from my PhD progress reports.

Nukala Sarath Babu

April 2019

# Scientific Contributions

**Publications:**

1. Nukala, S.B., Baron, G., Aldini, G., Carini, M. and D'Amato, A., 2019. Mass spectrometry-based label free quantitative proteomics to study the effect of 3PO drug at cellular level. *ACS Medicinal Chemistry Letters*.
   **DOI:**10.1021/acsmedchemlett.8b00593
2. Quantitative Proteomic Profiling of Pulmonary Endothelial Cells in Chronic Thromboembolic Pulmonary Hypertension
   Sarath Babu Nukala*, Alfonsina D'Amato, Olga Tura-Ceide, Regazzoni Luca, Aldini Gincarlo, Joan Albert Barbera, Marta Cascante, Marina Carini.
   Journal: Journal of Hypertension (Manuscript under preparation)
3. Differentially regulated proteins associated with endothelial dysfunctionality in patients undergoing treatment for acute myocardial infarction.
   Sarath Babu Nukala*, Alfonsina D'Amato, Regazzoni Luca, Aldini Gincarlo, Marta Cascante, Marina Carini.
   Journal: Journal of Hypertension (Manuscript under preparation)

**Oral Presentations:**

- "Bioanalytical and proteomic approaches in the study of pathologic ECs dysfunctionality, oxidative stress and the effects of PFKFB3 modulators", University of Antwerp, Belgium, Feb 2016

- "Proteomics research work in MoGlyNet project", European Molecular Biology Laboratory (EMBL), Germany, July 2016
- "Proteomic approaches in the study of pathologic ECs dysfunctionality", University of Leiden, Netherlands, September 2016.
- "Proteomic profiling of pathological ECs of acute myocardial infarction and chronic thromboembolic pulmonary hypertension", University of Aberdeen, Scotland, May 2017
- "Bioanalytical and proteomic approaches in the study of pathologic ECs dysfunctionality, oxidative stress and the effects of PFKFB3 modulators", Mid-term review meeting, University of Milan, Italy, September 2017.
- "Oxidative stress in the dysfunctional ECs of acute myocardial infarction and chronic thromboembolic pulmonary hypertension", Leiden University Medical Center, Netherlands, April 2018.
- "Mass-spectrometry based label-free quantitative proteomics approach to study the effect of 3PO at cellular level", University of Milan, Italy, September 2018.
- "Bioanalytical and proteomic approaches in the study of pathologic ECs dysfunctionality, oxidative stress and the effects of PFKFB3 modulators, SSPA 2018, Italy, September 2018.
- "Bioanalytical and proteomic approaches in the study of pathologic ECs dysfunctionality, oxidative stress and the effects of PFKFB3 modulators", University of Barcelona, Spain, January 2019.

**Poster Presentations:**

- Nukala Sarath Babu, Alfonsina D'Amato, Luca Regazzoni, Giancarlo Aldini, Mass Spectrometry-Based Label Free Quantitative Proteomics to study the effect of 3-PO in endothelial cells; Italian-Spanish-Portuguese Joint Meeting in Medicinal Chemistry,MedChemSicily2018, abstract page 214 http://www.medchemsicily2018.it/documenti/book_of_abstracts.pdf
- Nukala Sarath Babu, O. Tura , L. Regazzoni , C. Marinello , A. Abdali , G. Aldini, V.F.Smolders, I. Blanco , J.A. Barbera , M. Cascante , M. Carini "Differentially Expressed Proteins in Pulmonary Endothelial Cells in Chronic Thromboembolic Pulmonary Hypertension" American Journal of Respiratory and Critical Care Medicine 2018; 197:A3738ATS International conference, 18-23 May 2018, San Diego, CA. https://www.atsjournals.org/doi/abs/10.1164/ajrccm conference.2018.197.1

- Alfonsina D'Amato, Nukala Sarath Babu, Giancarlo Aldini, Marina Carini. “nLC-MS/MS based Label Free Quantitative Proteomics to study the effects of bioactive compounds” HPLC 2019 Milan.

# Acknowledgements

With honesty and immense pleasure, I express my sincere gratitude to my beloved research guide and mentor ***Prof. Marina Carini***, Department of Pharmaceutical Sciences, University of Milan, Italy for the great supervision, patience, highly valuable and crucial discussions and constant encouragement with respect to the fascinating topic of my research work. I'm very thankful to her for the protection throughout my research period and endless support. Words are not enough to express my feeling towards her for arranging the foundation and ornamentation of my research career.

I express my profound sense of gratitude to my beloved second supervisor ***Prof. Marta Cascante***, Department of Biochemistry and Molecular Biology, University of Barcelona, Spain for the great guidance, support and laboratory facilities provided during the advancement and successful completion of my six months secondment.

I express my heartfelt thanks to ***Prof. Aldini Giancarlo***, Ph.D. coordinator, Department of Pharmaceutical Sciences, University of Milan, Italy for giving a great motivation, good lab environment and support for the successful completion of my research work.

I'm glad to work under the co-supervision of ***Dr. Luca Regazzoni***, Research Scientist, Department of Pharmaceutical Sciences, the University of Milan for the extraordinary support and suggestions not only in the research work but also crucial helps provided during my entire stay in Italy. There are no other words to express my great feelings for his entire assistance.

I'm extremely grateful to ***Dr. Alfonsina D'Amato***, Research Scientist, Department of Pharmaceutical Sciences, University of Milan for the valuable assistance, motivation and suggestions provided in the entire project.

I express my sincere thanks to ***Dr. Olga Tura***, Research Scientist, Department of Pulmonary Medicine, Hospital Clínic-Institutd'Investigacions Biomèdiques August Pi iSunyer (IDIBAPS), University of Barcelona, Spain for the support and crucial discussions for my research work during my stay at University of Barcelona and IDIBAPS.

I would like to extend my sincere thanks to ***Cristina Marinello***, for her technical support and continuous help in the entire period of my research work at the University of Milan. I express my sincere thanks to ***Dr. Ibrahim Halil Polat***, Post-Doctoral Researcher, for his boundless and precious support provided during my secondment at the University of Barcelona.

I express my truthful thanks to my friends, lab mates and colleagues Marco Mol, Ettore, Dr. Giovanna Baron, Anita, Alessandra, Valentina, Francesca, Marco, Giacomo and Dr. Alessandra from the University of Milan; Dr. Silvia Marin, Dr. Miriam Tarrado, Dr. Rolden Cortes, Josep Tarrago, Ines Baptista, Cristina Balcells, Miriam Contreras, and Carles Forguet, from the University of Barcelona, for their moral support and encouragement during my research work.

I would like to extend my honest thanks to all the colleagues in MOGLYNET project Virginia Cristofori, Anahita Abdali, Valerie Smolders, Laura Parma, Fabiana baganha Carreiras, Paola Perrotta, Besa Emini, Carlo De Dominicis, Xiao Hu, Helena Macut, Erika Zodda; and other supervisors Prof. Maria Luisa Gelmi, Prof. Matteo Zanda, Prof. Alessandro Contini. Dr. Stefano Bellosta, Prof. Wim Martinet, Prof. Paul Quax, Prof. Alberto Corsini, Dr. Mirela Delibegovic, Prof. Guido De Mayer, Prof, Joan A. Barbera and Dr. Francesca Clerici for their direct and indirect support in my research work.

I would like to thank ***Sabrina Pavan***, MOGLYNET Project Manager, for providing the support in my entire period of stay. I also express my sincere thanks to ***Marco Dell`Uomo*** and ***Francesca Bizzo*** for the guidance provided during my three months secondment at Ingenus Pharmaceuticals, Switzerland.

Words are not enough for me in conveying my feelings to my parents ***Muneiah Nukala (Late)***; ***Parvathi Nukala*** for their constant adorable affection, love, support, and encouragement throughout my life. I am also grateful to my sisters ***Sarala Ganji, Kavitha Chintaginjala***; brothers-in-laws ***Venkata Subbaiah Ganji, Venkataiah Chintaginjala***. With honesty and enormous pleasure, I express my sincere gratitude to my beloved sister ***Sasikala Bandaru*** and brother-in-law ***Pardha Saradhi Bandaru*** for their continuous love, protection, tremendous support, great motivation and incredible strength provided during the most difficult period of my life.

A final thanks to one and all, I just want you to know that all your help, advice, guidance and friendship was essential to the completion of this thesis.

I'm proud to be a member of MOGLYNET consortium, Department of Pharmaceutical Sciences at the University of Milan, Department of Biochemistry and Molecular Biomedicine at the University of Barcelona that provided a cool and calm climate to complete my research work without any interludes.

***(Nukala Sarath Babu)***

# Abbreviations

| | |
|---|---|
| 3PO | 3-(3-pyridinyl)-1-(4-pyridinyl)-2-propen-1-one |
| ABC | Ammonium bicarbonate |
| ACN | Acetonitrile |
| ACS | Acute coronary syndrome |
| AGEs | Advanced Glycation End-Products |
| AMI | Acute myocardial infarction |
| AOPPs | Advanced Oxidation Protein Products |
| AST | Aspartate aminotransferase, |
| BPA | Balloon pulmonary angioplasty |
| CAD | Coronary artery disease |
| CKD | Chronic kidney disease |
| CK-MB | Creatinine kinase-muscle/brain |
| CTEPH | Chronic thromboembolic pulmonary hypertension |
| CTPA | Computed tomography angiography |
| CVD | cardiovascular disease |
| DCFH-DA | Dichloro-dihydro-fluorescein diacetate |
| DMEM | Dulbecco's Modified Eagle Medium |
| DTT | Dithiothreitol |
| EBM | Endothelial cell basal medium |
| ECG | Electrocardiogram |
| ECs | Endothelial cells |
| EGM | Endothelial cell growth medium |
| ESI | Electrospray ionization |
| FA | Formic acid |
| FBS | Fetal bovine serum |
| GA-1000 | Gentamicin Sulfate-Amphotericin |
| GSH | Glutathione reduced |
| GSSG | Glutathione oxidized |
| HAT | Hypoxanthine-Aminopterin-Thymidine |
| HCAECS | Human coronary artery endothelial cells |
| HCD | Higher-energy collisional dissociation |
| HDL | High-density lipoprotein |
| hEGF | Human endothelial cell growth factor |

| | |
|---|---|
| HEPES | 4-(2-hydroxyethyl)-1-piperazineethanesulfonic acid |
| hFGF | human fibroblast growth factor |
| HPAE | Human pulmonary artery endothelial cells |
| HPLC | High-performance liquid chromatography |
| HSA | Human serum albumin |
| HUVEC | Human umbilical vein endothelial cells |
| IAA | Iodoacetamide |
| ICA | Internal carotid artery |
| LDH | Lactate dehydrogenase |
| LDL | Low-density lipoprotein |
| MS | Mass spectrometry |
| $Na_3VO_4$ | Sodium deoxycholate, sodium orthovanadate |
| NADP | Nicotinamide adenine dinucleotide phosphate |
| NADPH | Nicotinamide Adenine Dinucleotide Phosphate Hydrogen |
| NaF | Sodium fluoride |
| NEM | N-Ethylmaleimide |
| nLC | Nano-Liquid chromatography |
| nLC-HRMS | Nanoscale liquid chromatography high resolution mass spectrometry analysis |
| NP-40 | Tergitol-type NP-40 |
| NYHAFC | New York Heart Association functional class |
| PAH | Pulmonary arterial hypertension |
| PCOs | Protein carbonyls content |
| PE | Pulmonary embolism |
| PEA | Pulmonary endarterectomy |
| PFKFB3 | 6-Phosphofructo-2-Kinase/Fructose-2,6-Biphosphatase 3 |
| PH | Pulmonary hypertension |
| PMA | Phorbol 12-myristate 13-acetate |
| R3-IGF-1 | Long R3 Insulin Like Growth Factor-1 |
| ROS | Reactive oxygen species |
| RT-PCR | Reverse transcription polymerase chain reaction |
| SEM | Standard errors of the mean |
| SMC | Smooth muscle cells |
| SOD | Superoxide dismutase |
| TFA | Trifluoroaceticacid |
| TNFα | Tumor necrosis factor alpha |

| | |
|---|---|
| VEGF | Vascular endothelial growth factor |
| VTE | Venous thromboembolism |
| WHO | World health organization |

# 1 Table of Contents

# List of Figures:

## List of Tables:



## List of Supplementary Figures:



## List of Supplementary Tables:



## List of Appendices:

# PART-I

# 1 Introduction

## A. Endothelial dysfunction and oxidative stress:

The vascular endothelium is crucial for maintaining the vascular homeostasis, platelet activity, leukocyte adhesion, thrombosis and regulation of vascular tone. The vascular endothelium is constituted by a thin layer of an endothelial cell (EC) line that interface between the circulatory system and the rest of the vessel wall.

The vascular endothelium is one of the major targets of oxidative stress, playing an important role in the development of vascular-related disorders, such as atherosclerotic disease[1]. Oxidative stress increases the formation of reactive species (ROS), such as peroxides and hydroxyl radicals. ROS are signalling molecules and are able to induce leukocyte adhesion and promote the vascular endothelial permeability, that leads to the dysfunction of endothelium-related signal transduction pathways as well as redox-regulated transcription factors[2]. ROS cause reorganization of the actin filament, formation of an intracellular gap and changes in the cell shape. The endothelium contains adherents and tight junctions that are responsible for maintaining the restrictive barrier. Figure A1 shows the subcellular endothelial sites regulated by oxidative stress. In the normal structure of vascular endothelium, the lateral cell border contains occluding protein in association with zonula occludens-1 (ZO-1); VE-cadherin in association with a-, b-, and g-catenins; other proteins such as platelet endothelial cell adhesion molecule 1 (PECAM-1). Cortical actin filaments are directly linked with ZO-1, vinculin and α-actinin, that connect catenin to VE-cadherin in actin filament network. Intercellular adhesion molecule-1 (ICAM-1) expressed on the endothelial luminal surface might also involve in cortical actin filaments. ECs continuously express surface adhesion molecules including vascular cell adhesion molecule-1 (VCAM-1), ICAM-1, ICAM-2 and P-selectin (stored in Weible-Palade bodies). However, oxidative stress causes phosphorylation and reorganization of occludin and PECAM-1, reduces levels of vascular endothelium catenins and actin-binding proteins. In the actin filament network, oxidant stress causes the increased formation of stress fibers and decreased cortical actin band, resulting in disruption of the tight and adherens junctions. ROS promote cell contraction and stress fiber formation due to the increased phosphorylation of myosin light chain (MLC). Additionally, oxidative stress functionally upregulates adhesion molecules.

Moreover, the ROS generated at the sites of vascular injury and inflammation might be involved in the destabilization of plaque rupture. At lower concentrations, ROS can act as

signaling molecules involving in the maintenance of cellular activities including cell growth and cell adaptation responses.

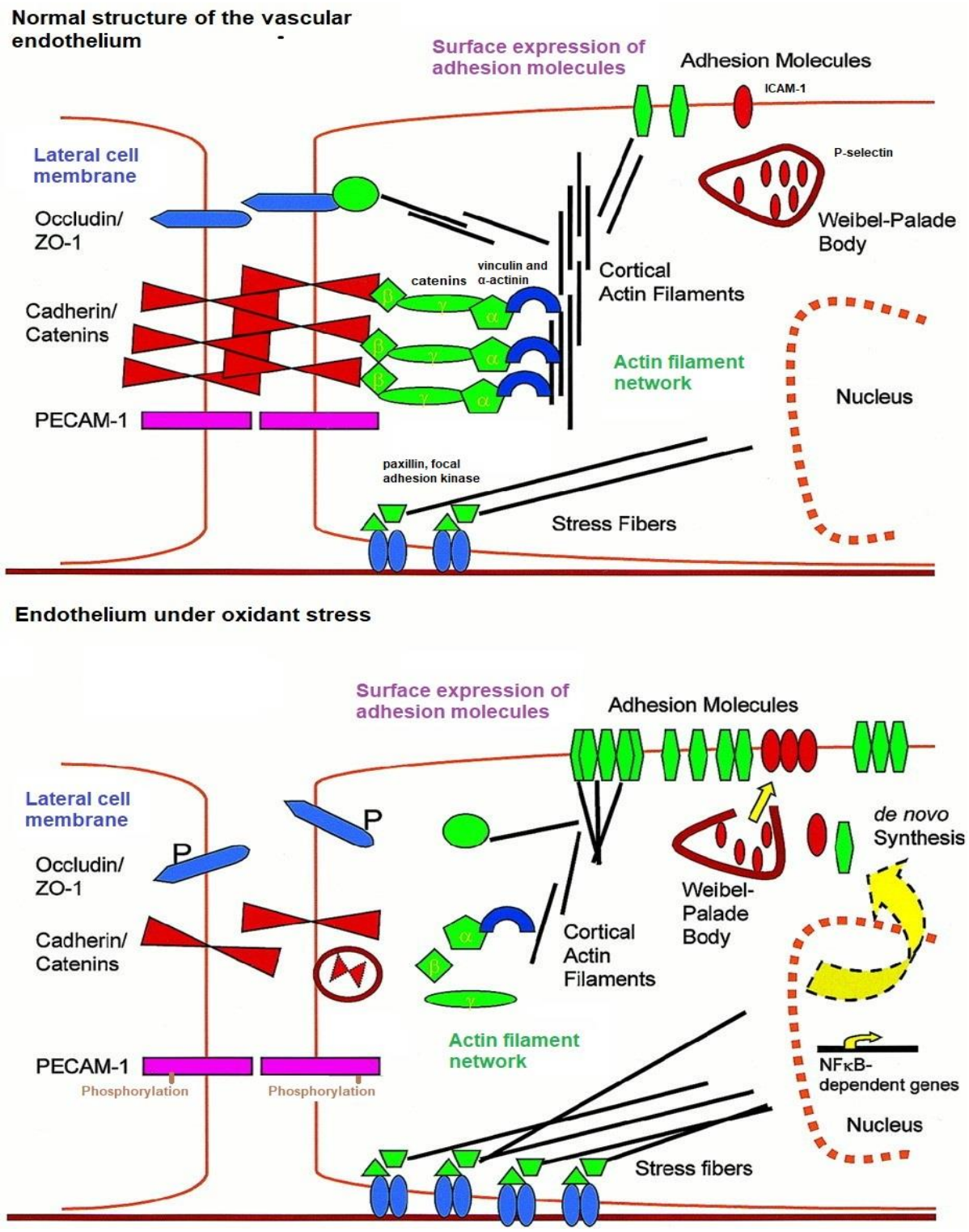


Figure A 1: Subcellular endothelial sites regulated by oxidant stress. (Adapted from Lum et al.[2] and modified)

The stages involved in the endothelial dysfunction of cardiovascular diseases, such as atherosclerosis, are shown in Figure A2. Diabetes, smoking, hypertension, dyslipidemia, obesity, reduced NO availability and aging are the main risk factors of oxidative stress and endothelial dysfunction, which leads to the formation of leukocyte adhesion, inflammation, lipid deposition, vascular smooth muscle cell proliferation, vasoconstriction, platelet aggregation, and thrombosis.

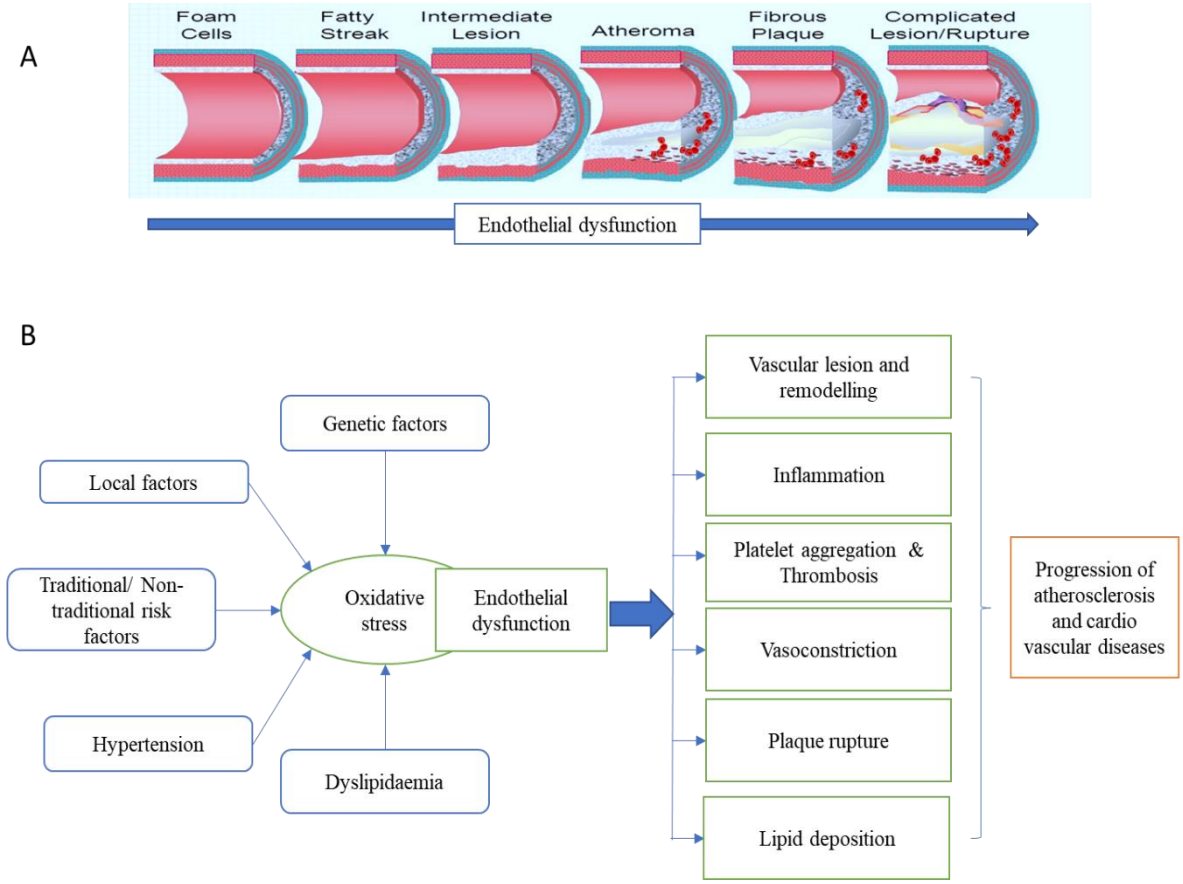


Figure A 2: A) Stages in the development of atherosclerosis. B) Various factors involved in the endothelial dysfunction in atherosclerosis.

The main characteristics of endothelial dysfunction include the reduction of bioavailability of nitric oxide (NO), impairment in the endothelium-derived vasodilators, increase in the production of endothelial-derived contracting factors of proinflammatory, proliferative molecules, and ROS. Endothelial dysfunction is also related to an impaired redox status, and procoagulatory events which are involved in the all stages of atherogenesis [3–5], coronary artery disease, and myocardial ischemia[6–10].

The endothelial dysfunction and oxidative stress play also an important role in the pathogenesis of acute myocardial infarction (AMI) and chronic thromboembolic pulmonary hypertension

(CTEPH)[11,12]. However, the underlying mechanisms involved in the endothelial dysfunctionality of AMI and CTEPH diseases remains unknown.

## A.1 Acute myocardial infarction (AMI):

AMI generally referred as "heart attack" is one of the subgroups of an acute coronary syndrome (ACS), along with unstable angina. The incidence, distribution, and possible control of AMI have changed significantly over the past decades. Despite major improvements achieved from the past decade in the management of patients with AMI, it remains a leading cause of hospitalization, mortality, and morbidity throughout the world. According to the recent studies, more than 2.4 million, 4 million deaths were reported in the USA; Europe and northern Asian countries, respectively[13]. AMI occurs when the supply of oxygen is reduced due to the blockage of coronary arteries of a portion of the heart and the myocardial necrosis increases (Figure A3)[14]. The deficiency of oxygen is intact responsible for the death of myocardial tissue.

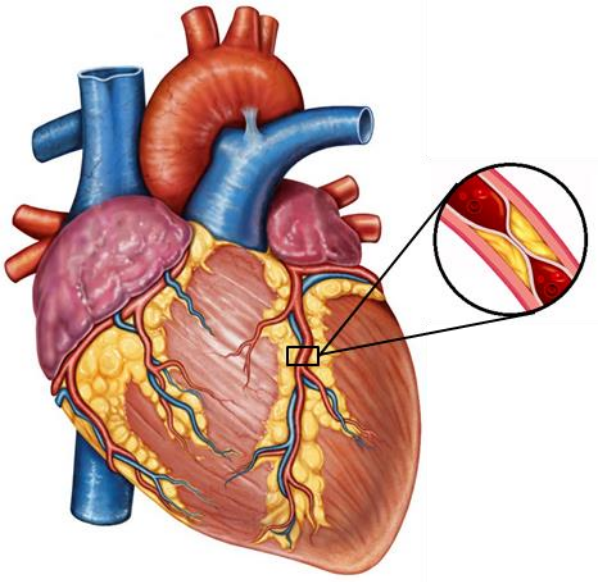

Figure A 3: Plaque formation and myocardial infarction.

Cardiac energy synthesis depends on oxidative metabolism. Occlusion of coronary artery decreases oxygen levels and increases anaerobic-dependent ATP synthesis which results in the energy starvation and cardiac cell necrosis[15]. Subsequent events include the reduced pH, increased concentration of cytosolic calcium ($Ca^{2+}$), loss of cell membrane integrity, and the release of intracellular content to extracellular matrix[16]. An acute and beneficial compensatory phase followed by a chronic maladaptive phase are the two important cardiovascular events associated after MI and before reaching to heart failure. The major mechanisms that initiate the

progression of MI to heart failure are: a) hyperactivity of sympathetic nervous system (SNS) followed by advanced desensitization of β-adrenergic receptors, b) hypersensitivity of renin-angiotensin-aldosterone system (RAAS), c) inflammatory reactions involved in the deposition of fibrotic tissue, d) oxidative stress e) dilated hypertrophy and cardiac remodeling, f) alteration in protein expression profiles and cardiac contractile dynamics, g) energetic substrate remodeling[17–21]. The stimulation of β-adrenergic receptors in the heart, activates signaling pathways related to the excitation-contraction coupling mechanism. Hyperactivation of SNS triggers the cardiac cell growth through the stimulation of MAPK (mitogen-activated protein kinases) and calcineurin-NFAT (calcineurin-nuclear factor of activated T cells) signaling pathways. This leads to the development of cardiac hypertrophy and cardiac remodeling. In addition, angiotensin II increases the production of ROS, collagen, inflammatory cytokines which further facilitates the development of cardiac fibrosis and remodeling.

Furthermore, necrosis of heart tissue leads to the infiltration of leukocytes through the activation of chemotactic gradient in ECs by ischemic-derived ROS[22–24]. The elevated levels of interleukin-1β, tumor necrosis factor-α (TNFα) and interleukin-6 enhance the production of EC adhesions and integrins which induce the extravasation of inflammatory cells into the necrosis site[25–28]. Studies have shown that increased expression of proteolytic activity of matrix metalloproteinases (MMPs) facilitate the immune cell infiltration[24]. Mast cells, ECs, and fibroblasts play a key role in the MI related inflammatory reactions[22]. Studies have shown that ROS and reactive nitric oxide species are involved in the synthesis of collagen through NF-kB activation pathway[24]. Additionally, NADPH oxidases and inducible nitric oxide synthase (iNOS) and xanthine oxidase are involved in collagen synthesis in post-MI events[29].

Emerging studies have shown the qualitative and quantitative changes in the expression of cardiac proteins involved in the MI. The experiments in a rat model showed the reduced expression of SERCA2a (Sarco/endoplasmic reticulum calcium (Ca2+) ATPase cardiac isoform) and PMCA (plasma membrane $Ca^{2+}$ ATPase) proteins with a concomitant increase in left ventricular filling pressure after four weeks of MI[30]. Similar results have been observed in the skinned cardiac fibers of rats at four and eight weeks after MI[31]. The down-regulation of phosphatase enzymes causes the changes in PKA activity inside the dyadic microenvironment which is formed due to the T-tubule of plasma membrane and cistern of sarcoplasmic reticulum[32]. Serum concentration of atrial and brain natriuretic peptides (atrial natriuretic peptide and brain natriuretic peptide) notably ischemic injury and these are markers for MI and progressive heart failure[33,34].

However, the proteomic changes in the AMI endothelial dysfunction and the implication of oxidative stress remain unknown. Therefore, the identification of insights and causes resulting in dysfunctional ECs are crucial to the understanding of the disease and to the development of new therapeutic tools.

## A.2 Chronic thromboembolic pulmonary hypertension (CTEPH):

CTEPH is an orphan, potentially progressive and long-term pulmonary vascular disease caused by chronic obstruction of blood vessels in the pulmonary arteries. It is a distinct form of pulmonary hypertension (PH), characterized by an intraluminal thrombus formation and fibrous stenosis or obstructions in the central pulmonary arteries which causes progressive PH and increased pulmonary vascular resistance and consequent right ventricular failure (Figure A.4, adapted from http://www.phacanada.ca/cteph/)[35–37]. Few investigations have been proposed that the CTEPH is involving in the abnormal vascular remodeling, angiogenesis, fibrinolysis together with endothelial dysfunction [38], autoimmunity[39], inflammation[40], and angiogenesis[41].

In a clinical point of view, the signs and symptoms are non-specific or completely absent in the early stages of the CTEPH. Right heart failure is the sign of an advanced stage of the disease. Exercise intolerance, chest discomfort, haemoptysis (blood in mucus), fatigue, dyspnea (shortness of breath), syncope (fainting), light-headedness and peripheral leg edema (swelling) are the most commonly associated symptoms of CTEPH.

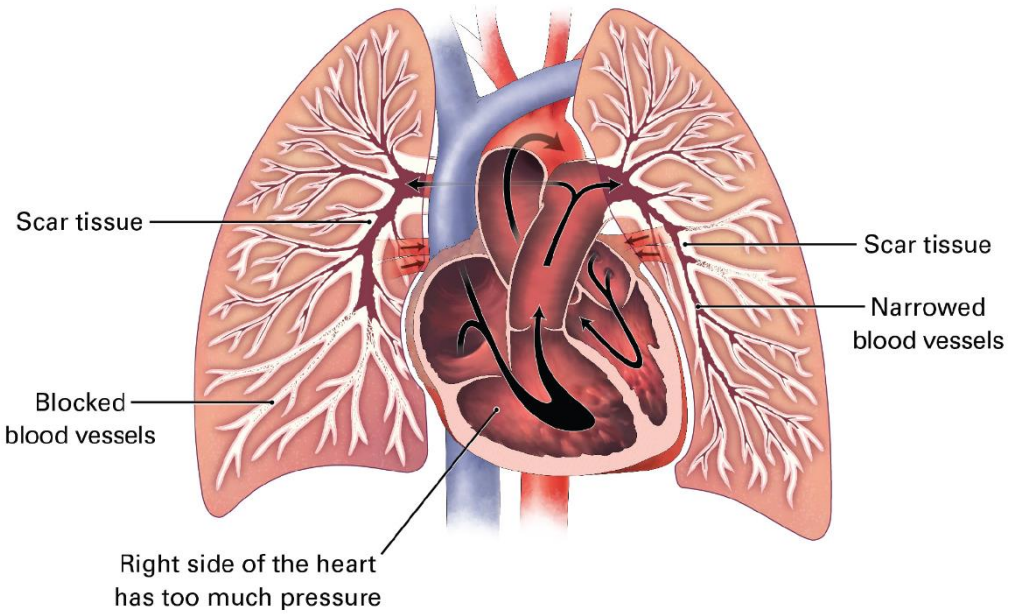


Figure A 4: Chronic thromboembolic pulmonary hypertension

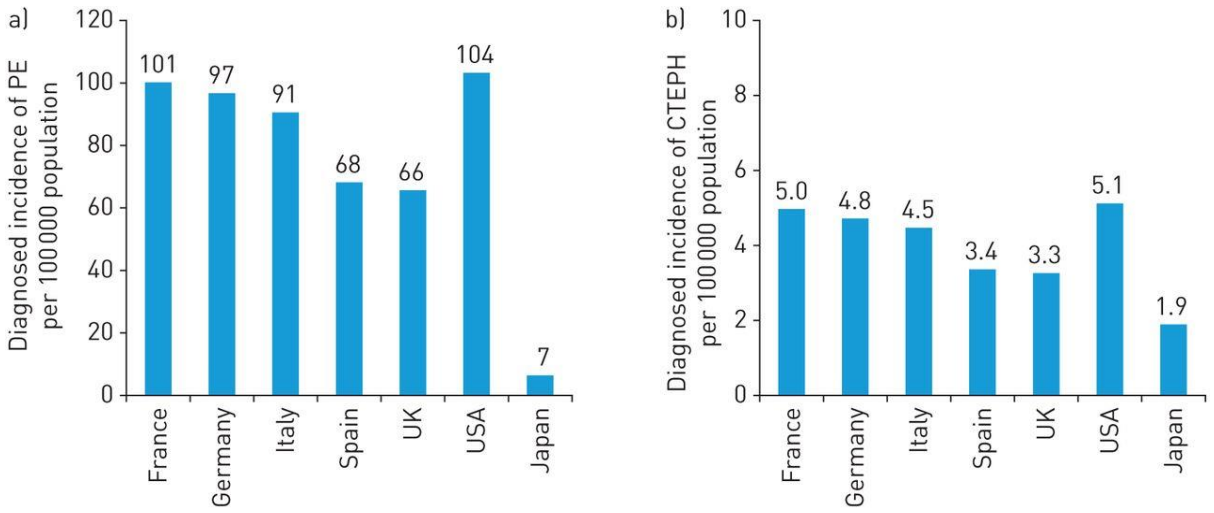


Figure A 5: a) Annual diagnosed incidence of PE, b) annual full incidence of CTEPH per 100000 population in Europe, USA and Japan (crude rates for the year 2015)[37].

Here above mentioned the quantitative epidemiological data of CTEPH, based on the recent investigation of Gall, Henning, et al, with 25 publications and 14 databases. 66-104 cases of crude annual incidence of diagnosed PE per 100000 population were reported, whereas in the case of crude annual full (diagnosed and undiagnosed) 3-5 cases of CTEPH per 100000 population were reported in the USA and Europe. On the other hand, the diagnosed incidence of CTEPH per year was 1.9 per 100000 population in Japan (Figure A.5)[37].

The overview of the pathophysiology of CTEPH is mentioned in Figure A.6. Endothelial dysfunction plays a fundamental role in facilitating the structural changes in the pulmonary vasculature. The pulmonary vascular wall contains fibroblasts in the external layer, smooth muscle cells in the middle layer and a single layer of ECs in an internal intima, which directly connects with blood circulation[42]. Under pathological conditions, the endothelium loses its homeostatic function that causes the disorganization of the vascular wall which is a crucial step in the development of vascular lesions[43]. Uncontrolled or disordered EC proliferation with simultaneous neoangiogenesis results in the formation of glomeruloid structures known as the plexiform lesions, which are common pathological features of the pulmonary vessels of patients with pulmonary arterial hypertension[44]. Moreover, abnormal production of multiple endothelial vasoactive mediators including endothelin-1 (ET-1), NO, thromboxane, prostacyclin, and serotonin have been increasingly recognized in patients with PH. Vascular injury in the combination of altered production of various mediators might expose the underlying vascular tissue to diverse blood-borne factors which further increase pathogenesis.

Endothelial dysfunction might also have an effect in pulmonary vascular homeostasis through the altered production of anticoagulant factors.[44]

When endothelium is activated by disease states, the ECs express specific markers and proteins E-selectin, intercellular adhesion molecule (ICAM)–1, tissue factor, and vascular endothelial growth factor (VEGF) receptors[45,46]. These changes might increase vasoconstriction, proliferation, and coagulability (Figure A.7)[44]. Moreover, several endothelium activation stimuli such as ROS, shear stress and inflammation are known to stimulate the endothelium, causing changes in its proliferation status and production of vasoactive mediators and growth factors[47]. Recent studies have shown the pathogenic role of dysfunctional $K_v$ channels and altered levels of cytosolic $Ca^{2+}$ in the development of pulmonary vascular remodeling in patients with idiopathic pulmonary arterial hypertension (IPAH) [48].

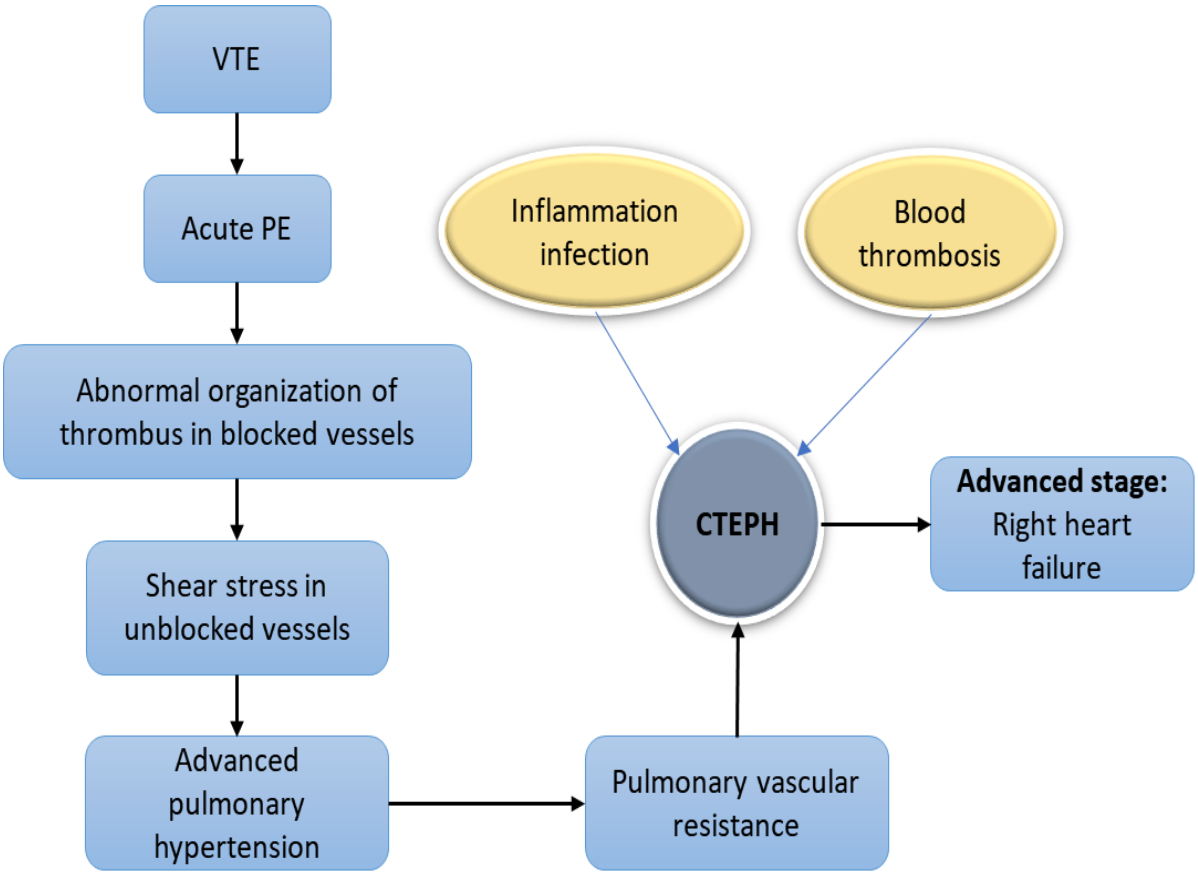


Figure A 6: An overview of the pathophysiology of CTEPH.

Vasocontraction induced under oxidative stress might be one of the important factors in the early stages of PAH and the decrease of NO bioavailability. Inflammation and oxidative stress are essential in PAH with increased lipid peroxidation and reduced antioxidant defenses[49].

Multiple studies have been reported that oxidative stress involved in the pulmonary hypertension[49–52]. However, the comprehensive role of pathological endothelial dysfunctionality during the disease progression mechanism of CTEPH disease remains unclear. Determining the molecular changes and underlying mechanisms that cause the dysfunction of endothelium is currently essential for the identification of early prediction and the development of novel therapeutic strategies.

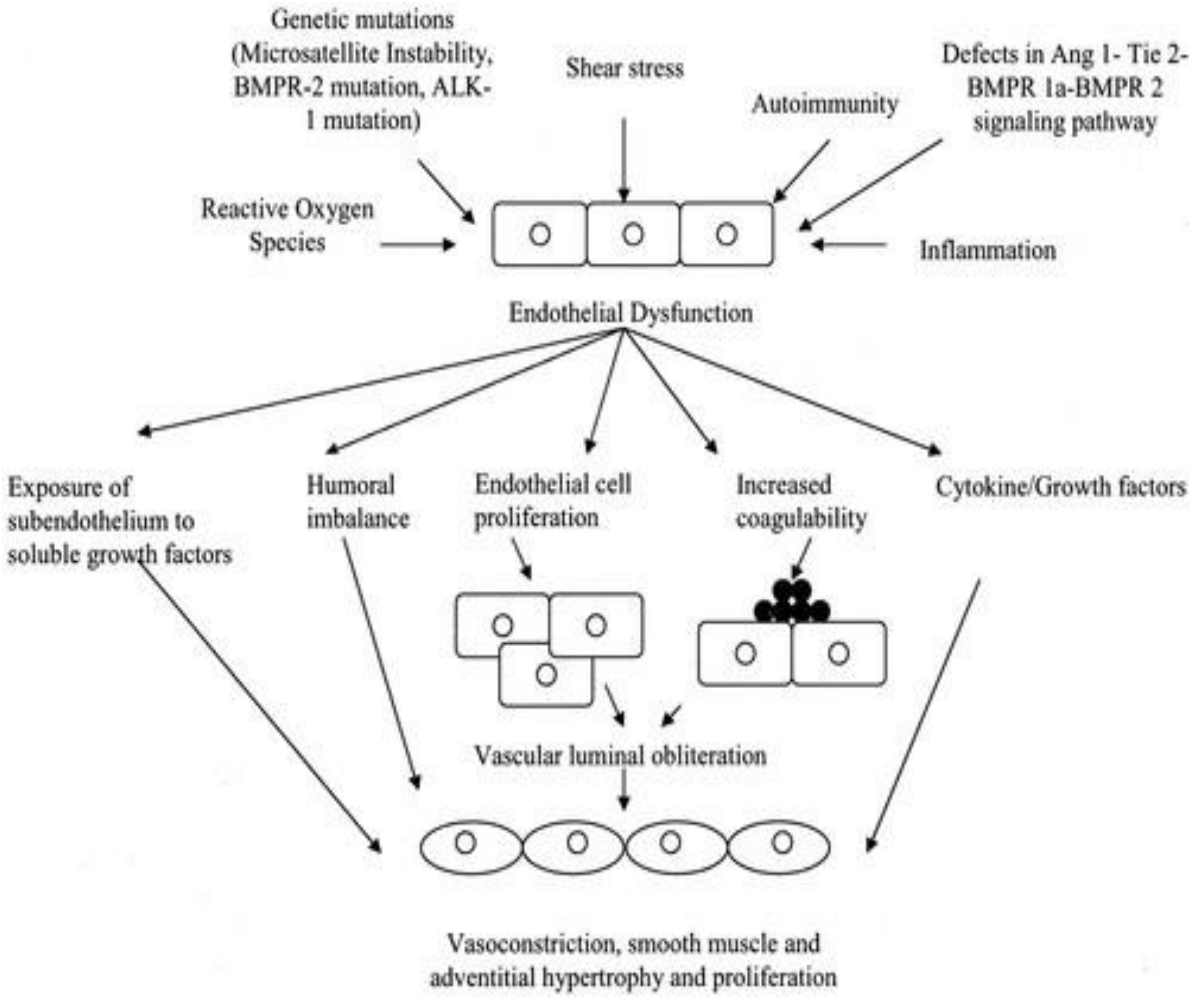


Figure A 7: Mechanistic role of endothelial dysfunction in PH and pulmonary vascular remodeling. Squares indicate endothelial cells; ovals, smooth muscle cells; and closed circles, platelets. Picture adapted from the reference [44]

## B. Bioanalytical approach: deep single-run label free proteomics

Quantitative proteomics is one of the most important approaches in the field of omics, used for the early prediction, disease diagnosis, prognosis and to monitor the molecular proceedings in the different stages of the disease development (Figure B.1). Proteomics includes the characterization of proteome, expression, structure, protein-protein interactions, functions, and modification of proteins at various stages[53,54]. These approaches not only provide a list of identified proteins but also yields a lot of information that allows us to understand physiological changes occurred between two or more states. For instance, disease vs control; treated vs non-treated. From the past decade, many MS-based proteomic approaches have been successfully developed to address the quires related to protein-protein interaction studies, post-translational modifications, and protein expressions or abundances. Labeling quantitative proteomic methods have potential limitations such as long workflow or complex sample preparation, incomplete labeling, very expensive experimental procedures and a limited number of sample analyses.

Therefore, MS-based label-free quantification technique has been developed as a relatively simple, rapid, easy, and inexpensive alternative to other quantitative proteomic approaches. High mass resolution and precision, as well as high peptide identification rates, have been important components in the success of label-free quantification[55]. This approach can be applied to any kind of sample, as well as materials that are not able to be labeled metabolically, for example, several human-based clinical samples. Moreover, this approach requires minimal sample preparation. For instance, primary cells isolated from human specimens, since their growth rate is quite challenging (survive only for the limited number of passages) compared to continuous cancerous cell lines. To understand the high-throughput data and to investigate the underlying mechanisms from omics data network and pathway analysis tools have been developed[56].

The label-free quantitative approach has been applied to pig heart endothelial cells showing the molecular mechanism of several transcription factors and cell surface markers in endocardial endothelium, which might offer new insights into its role in the regulation of cardiac function[57]. In addition, this approach has been used to study the changes in rat cardiac cells treated with protease inhibitors[58]. This approach revealed the district proteomic profiles in the blood serum of a pair of monozygotic (MZ) twins discordant for ischemic stroke (IS) and demonstrated the upregulation of fibulin 1 protein involved in the underlying disease-causing mechanism

in ischemic stroke at molecular level, suggesting that proteomic profiling could be used as a general approach for improved diagnostic, prognostic and therapeutic strategies[59].

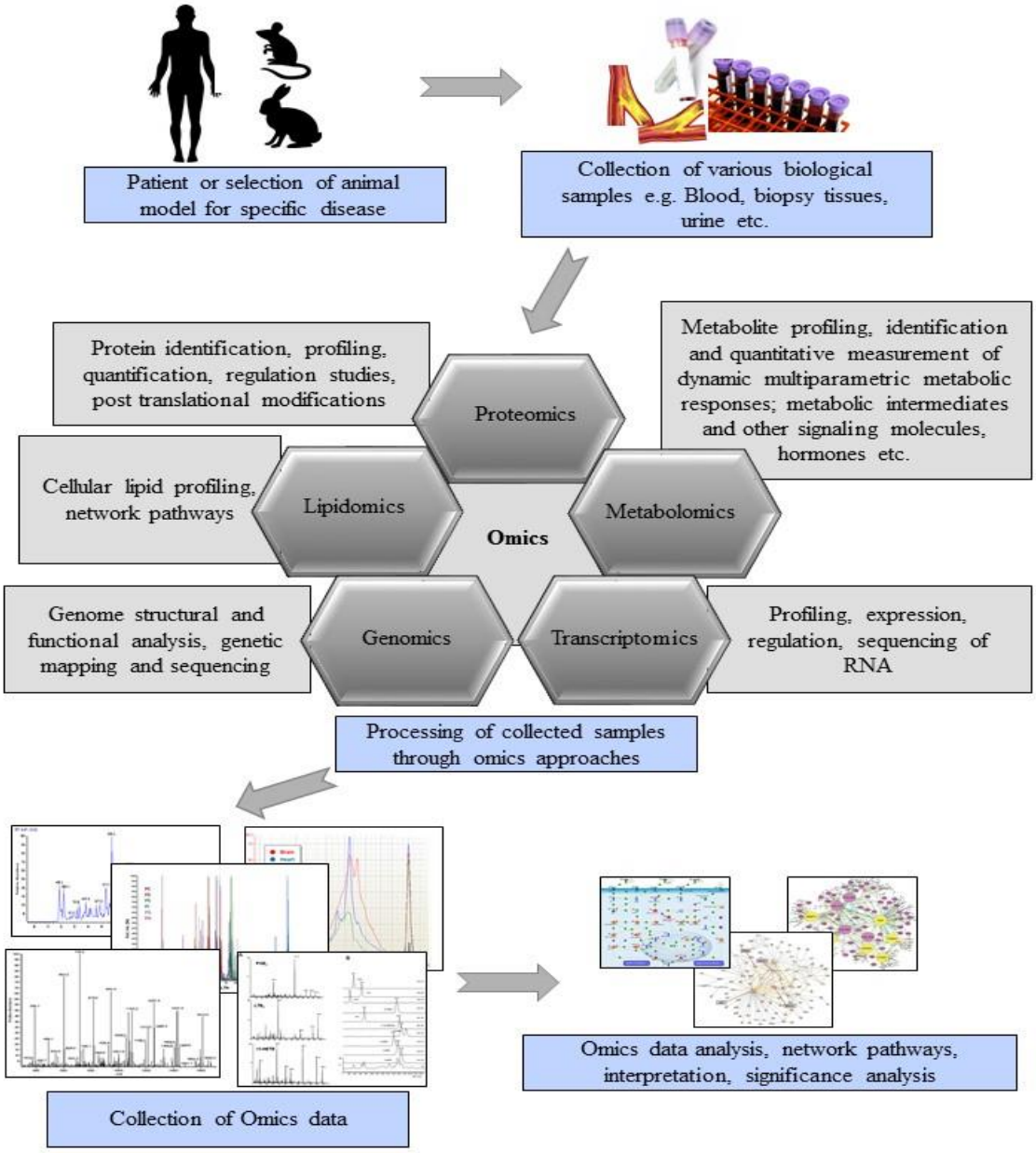


Figure B 1: An overview of omics approach workflow for the cutting-edge research as well as the unbiased discovery of biomarkers.

Quantitative proteomics approach was also applied in the study of endothelial dysfunction induced by advanced glycation end products (AGEs) leading to diabetic cardiovascular complications[60]. Moreover, by using this approach serum protein biomarkers associated with the early phases of formation of carotid atherosclerotic plaques were investigated[61].

Similarly, researchers used this approach to reveal the differences in molecular mechanism of atherosclerosis in the presence or absence of chronic kidney disease (CKD) and demonstrated that proteins involved in inflammation, blood coagulation, oxidative stress, vascular damage, and calcification process exhibited greater alterations in patients with atherosclerosis in the presence of CKD[62]. To determine the effects of chronic ischemia on bladder proteomic profiles and characterization of further downstream signaling pathways, label-free quantitative proteomic analysis was used in bilateral iliac artery atherosclerosis and chronic bladder ischemia diseases in male rats[63]. In addition, the proteome of circulating microparticles in the vascular system was investigated[64].

Therefore, as specified above label-free quantitative approaches have provided powerful tools for analyzing protein changes in large-scale proteomics studies. Consequently, in the present PhD thesis, label-free proteomics quantification and bioinformatic approaches were applied to describe our biological questions.

# 2 Aims of the project

Vascular dysfunction is one of the primary factors in the onset and progression of atherosclerosis and other vascular-related diseases such as AMI and CTEPH. Emerging evidence indicates that pathological blood vessel responses and endothelial dysfunction are associated with metabolic alterations in ECs. The identification of the insights and causes resulting in dysfunctional ECs is crucial for the understanding of the disease and to the development of new therapeutic tools.

Therefore, to study the characteristics of such EC dysfunction in AMI and CTEPH diseases, we aim to determine the quantitative proteomic profile and/or the altered redox status of patient-derived EC lines.

The main aims of the present study were the characterization of AMI and CTEPH patient-derived primary ECs, focusing on:

**PART-I**

1) Network analysis of differentially expressed proteins.
2) Study of oxidative stress/redox status.

**PART-II**

3) Study the effects of PFKFB3 modulators.

# 3 Materials and Methods

## Chemicals and Reagents:

The human vascular endothelial cell line EA. hy926 was a kind gift from Dr. Christina Banfi (Centro cardiologico Monzino, Milan, Italy). AOPP assay kit, protein carbonyl fluorometric assay kit and intracellular ROS assay kit was purchased from Cell Biolabs-OxiSelect™ (San Diego, USA). SOD assay kit, (HAT) media supplement, non-essential amino acids, NaF, NP-40, $Na_3VO_4$, ammonium bicarbonate, phenylmethanesulfonyl fluoride, L-lysine, l-arginine and protease inhibitor cocktail, DTT, ammonium persulfate, ACN, TFA, SDS, IAA, FA, and Bradford reagents were purchased from Sigma Aldrich (St. Louis, USA). GSH/GSSG ratio detection assay kit (Fluorometric - Green), anti-FABP4 polyclonal antibody (15 kDa, Ab66682), was purchased from Abcam (Germany). DMEM high glucose medium, fetal calf serum and fetal bovine serum were purchased from Life technologies (Netherlands). Penicillin-streptomycin, L-glutamine and Trypsin-EDTA were purchased from Lonza (USA). T20 cell counter was purchased from Bio-Rad (USA). EBM™-2, Endothelial Basal Medium-2; EGM™-2 SingleQuots™, Formulates EBM™-2 to EGM™-2; Trypsin/EDTA, HEPES Buffered Saline Solution, Trypsin Neutralizing Solution, HCAECs, HPAEs were purchased from Lonza (Walkersville, USA). Laemmli buffer, 40% acrylamide/Bis solution, TEMED, molecular mass standards and electrophoresis apparatus for one-dimensional electrophoresis, Mini-protein Thx any KD gels and T20 cell counter were supplied by Bio-Rad Laboratories, Inc., Hercules CA. Trypsin Gold, Mass Spectrometry Grade was purchased from Promega (USA). Water and acetonitrile (OPTIMA LC/MS grade) for LC/MS analyses were purchased from Fisher Scientific, UK. Complete protease inhibitor cocktail tablets and sequencing grade trypsin were supplied by Roche Diagnostics (Basel, CH). Anti-VWF monoclonal antibody (250kDa, Sc-21784) was purchased from Santa Cruz, USA. Anti-Actin monoclonal antibody (42kDa, 691001) was purchased from MP Biomedicals.

## 3.1 Control and pathologic endothelial cells of AMI:

Commercially available human coronary artery endothelial cells (HCAEC) were used as controls. Eight individual patient-derived pathological ECs (HCAEC-AMI) were isolated from coronary atherothrombotic specimens in patients undergoing percutaneous coronary intervention with thrombectomy for the treatment of acute ST-segment elevation myocardial infarction (STEMI) at the Royal Infirmary of Edinburgh, Scotland, UK. The study protocol was approved by the Research Ethics Committee and all subjects provided written informed consent. Specimens were washed with phosphate buffered saline (PBS) and manually disaggregated. Tissue explants were seeded into collagen-I coated 6-well plates and maintained under standard cell culture conditions. After 24 hours, tissue explants, non-adherent cells, and debris were aspirated. Medium was changed every other day until the first passage of coronary endothelial outgrowth cells emerged and cells were cultured as previously described[65,66].

These cells were received as a part of MoGlyNet project. All the cell lines in passage 4-5 were obtained from Prof. Marta Cascante from University of Barcelona. Standard guidelines were strictly followed while transporting to maintain the integrity of the cell lines. The isolation and characterization experiments were conducted and validated by other ESR (Early Stage Researcher/Ph.D. student) in the MoGlyNet project consortium.

## 3.2 Control and pathologic endothelial cells of CTEPH:

Commercially available human pulmonary artery endothelial cells (HPAE) were used as controls. Five individual patient-derived pathological ECs corresponding to CTEPH (CTEPH-ECs) were received from Dr. Olga Tura, Research Scientist, Department of Pulmonary Medicine, Hospital Clínic-Institutd'Investigacions Biomèdiques August Pi iSunyer (IDIBAPS), University of Barcelona, Spain.

The specimens containing thromboembolic material with clear thrombus were obtained after pulmonary endarterectomy (PEA) surgery from CTEPH patients at Hospital Clínic-Institutd'Investigacions Biomèdiques August Pi iSunyer (IDIBAPS). Material were washed with PBS and minced into 1-2 mm pieces. Explants were seeded into 0.2% gelatin-coated 6-well plates and maintained under standard cell culture conditions. After 24 hours, tissue explants, non-adherent cells, and debris were aspirated. Medium was changed every other day until the first passage of pulmonary endothelial outgrowth cells emerged and cells were cultured as previously described[65,66].

These cells were received as a part of MoGlyNet project. All the cell lines in passage 4-5 were obtained from Dr. Olga Tura from University of Barcelona. Standard guidelines were strictly followed while transporting to maintain the integrity of the cell lines. The isolation and characterization experiments were conducted and validated by other ESR in the MoGlyNet project consortium.

### 3.3 Growth conditions of control and pathological primary ECs:

All the control ECs and pathological ECs were grown in 0.2% gelatin coated plates with EGM™-2 bulletkit™ medium which contains the EBM™-2 basal medium along with the EGM™-2 singlequots™ kit components (hydrocortisone, hFGF, VEGF, Long R3 Insulin Like Growth Factor-1 (R3-IGF-1), ascorbic acid, hEGF, GA-1000 and heparin), 10% FBS and 1% penicillin-streptomycin antibiotic. Cells were maintained in a 37°C humidified incubator at 5% $CO_2$. All the experiments were performed using the cells in passage number 6-10. Cell stocks were frozen in liquid nitrogen in growth medium supplemented with 40% FBS and 10% v/v DMSO.

### 3.4 Human EA.hy926 endothelial cells:

The permanent human EC line EA.hy926 cells were cultured in high glucose DMEM medium containing HAT (100 mM sodium hypoxanthine, 0.4 mM aminopterin, and 16 mM thymidine), 1% glutamine, 10% FBS and 1% penicillin-streptomycin antibiotic and non-essential amino acids, at 37°C in a humidified atmosphere of 5% CO2. The culture medium was replaced every alternative day. This EC line was particularly selected to study the impact of 3PO and tumor necrosis factor alpha (TNFα) induced inflammation, due to its consistent response and character of constant growth rate when compared to the other primary ECs such as human umbilical vein endothelial cells (HUVEC). Moreover, these cells are very resistant to contamination and do not require more expensive additional growth factors accompanying with the use of primary ECs.

### 3.5 Protein extraction:

Confluent cells were trypsinized and collected by centrifugation at 1200 rpm for 5 min. Harvested cells were washed two times with cold PBS. The cell pellets were resuspended in the solubilization buffer (8 M urea in 50 mM Tris-HCl, 30 mM NaCl, pH: 8.5 and 1% protease inhibitor) and incubated on ice for 5-10 min. Cell lysates were further homogenized by sonication in an ice bath for three times each for 5sec with 30 sec intervals, using an ultra sonicator. Samples were centrifuged at 14000 rpm for 20 min at 4ºC. The protein supernatant

was collected into the new eppendorf tube and pelleted cell debris was discarded. Samples were stored at -80ºC until we use it for further experiments. The protein estimation was carried out by using the Bradford assay.

### 3.6 In-solution trypsin digestion:

10µg of total protein was resuspended in 50 mM ammonium bicarbonate (ABC). Reduction was carried out by incubating 5 mM final concentration of DTT for 30 min at 52°C, followed by an alkylation with 15 mM final concentration of iodoacetamide (IAA) for 20 min in the dark at room temperature. Trypsin digestion was allowed at 37°C overnight, with an enzyme: substrate ratio of 1:10. The resulting peptides were analyzed by nLC-MS/MS.

### 3.7 nLC-HRMS analysis:

Tryptic peptides were analyzed using a Dionex Ultimate 3000 nano-LC system (Sunnyvale CA, USA) connected to an Orbitrap Fusion™ Tribrid™ Mass Spectrometer (Thermo Scientific, Bremen, Germany) equipped with a nano-electrospray ion source. Peptide mixtures were pre-concentrated onto an Acclaim PepMap 100 – 100 µm x 2 cm C18 and separated on EASY-Spray column, 15 cm x 75 µm ID packed with Thermo Scientific Acclaim PepMap RSLC C18, 3 µm, 100 Å. The temperature was setting to 35 °C and the flow rate was 300 nL $min^{-1}$. Mobile phases were the following: 0.1% Formic acid (FA) in water (solvent A); 0.1% FA in water/acetonitrile (solvent B) with 2/8 ratio. Peptides were eluted from the column with the following gradient: 4% to 28% of B for 90 min and then 28% to 40% of B in 10 min, and to 95% within the following 6 min to rinse the column. Column was re-equilibrated for 20 min. Total run time was 130 min. One blank was run between triplicates to prevent sample carryover. MS spectra were collected over an m/z range of 375-1500 Da at 120,000 resolutions, operating in the data dependent mode, cycle time 3 sec between master scans. Higher-energy collisional dissociation (HCD) was performed with collision energy set at 35 eV. Each sample was analyzed in technical triplicates.

### 3.8 Protein identification and quantification:

Data analysis was performed as specified in our publication[67]. Briefly, resulting MS raw files from all the technical and biological replicates were analyzed by using MaxQuant software[68] (version 1.6.2.3). Andromeda search engine was used to identify proteins by target-decoy approach with less than 1% of FDR. In the present study we used *Uniprot_Homo sapiens* database (20,415 entries). Methionine oxidation and acetylation (N terminus) was used as a variable modification. Carbamidomethylation was used as a fixed modification. The label-free

quantification of proteins was obtained by MaxLFQ algorithm in MaxQuant. Match between the runs option was enabled and remaining default parameters were permitted.

### 3.9 Statistical analysis:

An open source Perseus software[69] (version 1.6.1.3; Max Planck Institute of Biochemistry, Germany) was used for the identification of statistically significantly differentially regulated proteins. The resulted data generated from MaxQuant was filtered based on the proteins only identified by site, reverse and potential contaminants. The log 2-fold changes of proteins were estimated by using the comparison of mean LFQ intensities between disease and control groups (HCAEC-AMI vs HCAEC in the case of AMI; whereas in the case of CTEPH, CTEPH-EC vs HPAE). Variabilities of biological replicates were measured with Pearson correlation coefficient values of the LFQ intensities. The differentially regulated proteins with a minimum of two peptides and FDR adjusted p-value < 0.05 were considered as statistically significant.

### 3.10 Gene ontology, network and pathway analysis:

We used Cytoscape software (version 3.6.0; http://cytoscape.org/index.php) to understand the possible network pathways connected with differentially regulated proteins. In particular, we used ClueGo plug-in that generally provides data based on the updated GO terms, BioCarta/Kyoto Encyclopedia of Genes and Genomes (KEGG) pathways[70]. Statistical significance of terms was determined with bid of two-sided enrichment/depletion hypergeometric test and Bonferroni p-value correction. Moreover, we also used the function of GO term fusion for further reduction of redundancy. Remaining default parameters were allowed. IPA (Qiagen) analysis was done based on the manufacturer's instructions.

### 3.11 RNA isolation and cDNA preparation:

Total RNA extraction and conversion to first-strand cDNA were done using iScript RT-qPCR sample preparation reagent (Bio-Rad) and Maxima First Strand cDNA Synthesis Kit (Thermo Scientific), respectively according to the manufacturer's protocol.

a) Briefly, $1x10^5$ control and pathological ECs were seeded in 48 well plates in triplicates. After 24hrs, cells were washed with PBS and added 60µl of iScript RT-qPCR sample preparation reagent. After incubation for 1 minute at room temperature, cell lysate was collected without disturbing the cells and stored at -80º C until we use it for making cDNA.

b) Briefly, $1x10^5$ cells were seeded in 48 well plates in triplicates. Cells were treated in various conditions 1) 3PO (20 µM) for 1hr, 2) TNFα (10 ng/ml) for 24 hrs, 3) 1hr pre-incubation of cells with 3PO, wash with PBS followed by 24 hrs incubation with TNFα, 4) 24 hrs pre-

incubation of cells with TNFα, wash with PBS followed by 1 hr incubation with 3PO, 5) untreated cells, 6) cells treated with vehicle (same amount of DMSO that were used for making the 20 µM concentration of 3PO). After completion of all the treatments, cells were washed with PBS and added 60 µl of iScript RT-qPCR sample preparation reagent. After incubation for 1 minute at room temperature, cell lysate was collected without disturbing the cells and stored at -80º C until we use it for making cDNA.

### 3.12 Quantitative real-time PCR analysis:

Quantitative RT-PCR analysis was performed using an ABI PRISM 7000 Sequence detection system cDNA was amplified in triplicate using Maxima SYBR Green/ROX qPCR Master Mix (Thermo Scientific). The thermal cycling programme started at 95°C for 10 minutes for enzyme activation, followed by 40 cycles of amplification at 95°C for 15 seconds, followed by 60°C for 1 minute. Gene expression was normalized to the housekeeping gene RPLP0. Primer sequences used in this project are listed in Table 3.1, 3.2 and 3.3. Relative expression of targeted genes was determined using the $2^{-\Delta\Delta CT}$ method. P-value below 0.05 were considered as statistically significant.

### 3.13 Western blotting:

Proteins obtained from control and pathological ECs were used to validate the expression pattern by western blot analysis. 30 µg of total proteins were electrophoresed on 8% and 12% SDS-PAGE and transferred by wet-transfer method. Membrane was blocked for 1h at room temperature using blocking buffer (5% milk in PBS with 0.1% tween 20). Primary and secondary antibody dilutions and incubation times were maintained as per the manufacturer instructions. Immunodetection analysis was employed for Von Willebrand factor (VWF), and Actin (ACT) targets using the anti-VWF monoclonal antibody, and anti-Actin (Fisher Scientific) as primary antibodies and respective anti-mouse and anti-rabbit HRP conjugated secondary antibodies (Abcam). Results were obtained by ECL detection method and expression of all target proteins were investigated against the actin housekeeping protein.

### 3.14 Advanced oxidative protein product (AOPP) assay:

Advanced oxidation protein product (AOPP) levels were analyzed by using the OxiSelect AOPP kit (STA318, Cell Biolabs, San Diego, CA, USA). The confluent cells were collected, lysed in buffer (150 mM NaCl, 1% NP-40, 0.5% sodium deoxycholate, 0.1% SDS, 50 mM Tris, pH: 8, 5 mM EDTA and protease inhibitors) and centrifuged for 20 min at 14000 rpm. The pellet containing cell debris was discarded; the protein supernatant was collected. The total

protein concentration was determined by using the Bradford assay. Samples containing 50 µg protein were prepared. Constant volumes of control and pathological cell lysates (200 µL) were added to the wells of a microtiter plate and then exposed to 10 µL of chloramine reaction initiator followed by 20 µL of stop solution. Absorbance was recorded at 340 nm by using the spectrophotometric plate reader (PowerWave biotek). 100, 80, 60, 40, 20, 10, 5 and 0 µM chloramine standards was used. Cell lysates used in this assay was prepared from the ECs in passages between 6-9. Experiments were performed with biological and technical replicates.

### 3.15 Protein carbonyl determination by fluorometric method:

Protein carbonyl content, a general indicator of protein oxidation was measured fluorometrically (480 nm excitation/530 nm emission) using a commercial kit (Cell Biolabs, OxiSelect No. STA-307). Briefly, protein carbonyls were derivatized with the Protein Carbonyl Fluorophore. The Fluorophore binds to the protein carbonyl group in a 1:1 ratio. Proteins are then TCA precipitated and free Fluorophore was removed by washing the protein pellet with acetone. After dissolving the protein pellet in GuHCl, the absorbance of protein-fluorophore product was measured fluorometrically, and the total protein carbonyls were subsequently calculated. Experiments were performed with biological and technical replicates.

### 3.16 Intracellular ROS assay:

ROS were measured by OxiSelect ROS Assay Kit (Cell Biolabs, STA-342). Briefly, the control and pathological ECs were grown in 96 well plate at a density of $9\times10^3$ cells and incubated with the dichloro-dihydro-fluorescein diacetate (DCFH-DA) containing medium at 37°C for 60 minutes in the dark. The confluent cells were lysed, and the fluorescence was recorded by using the fluorometric plate reader at 480 nm/530 nm. Total quantity of ROS was determined based on the comparison with the predetermined DCF standard curve. Experiments were performed with biological and technical replicates.

### 3.17 GSH/GSSG analysis:

GSH/GSSG ratio in control and pathological EC cultures was determined using GSH/GSSG Ratio Detection Assay Kit (Fluorometric-Green) (Abcam Inc. #ab138881) according to the manufacturer's guidelines. The samples were prepared by lysis of total cell protein in 0.5% NP-40 lysis buffer followed by a dilution of 1:50 for GSH analysis. In brief, serial dilution of GSH and GSSG stock standards were prepared along with assay mixtures for detection of GSH and total GSH using 100× Thiol green stock solutions, assay buffer and GSSG probe. A one-step fluorometric reaction of sample with respective assay buffers were incubated for 30 min.

Fluorescence intensity was then monitored at Ex/Em of 490/520 nm. GSSG was determined by subtracting GSH from total GSH. Finally, the ratio of GSH was plotted against GSSG to obtain the GSH activity. Experiments were performed with biological and technical replicates.

### 3.18 NADP/NADPH assay:

NADPH/NADP ratio in control and pathological ECs was determined by using NADP/NADPH quantification kit (Sigma) as per the manufacturer's protocols. Briefly, $1x10^6$ confluent cells were pelleted and washed with cold PBS. Cells were extracted with 800 µl of NADP/NADPH extraction buffer and allowed to incubation for 10 min on ice. Samples were centrifuged at 10000g for 10 min and supernatant used for determining the ratio of NADP and NADPH. To remove the enzymes that may consume NADPH rapidly were removed by filtering through a 10kDA cut-off spin filter (Millipore, UFC501096). An aliquot of the supernatant was heated at 60°C for 30 min to decompose the $NADP^+$, cooled on ice, and spun quickly to remove the precipitate. Another aliquot of the supernatant was not heated. Both aliquots were reacted with $NADP^+$ cycling buffer and enzyme mix (containing glucose-6-phosphate dehydrogenase (G6PDH) for 5 min at room temperature to convert $NADP^+$ to NADPH. The solutions were then incubated with NADPH developer for 2 h and the absorbance measured at 450 nm. The amount of NADPH (heated sample) and the total $NADP^+$ and NADPH (unheated sample) were quantified from an NADPH standard curve. Experiments were performed with biological and technical replicates.

### 3.19 Determination of SOD assay in cells:

Pelleted cells were homogenized in 100 µL of ice cold 0.5% NP-40 lysis buffer. SOD activity was determined by a colorimetric method using a commercially available kit (#19160, Sigma-Aldrich, St. Louis, MO, USA). Briefly, 20 µg of total protein was loaded into 96-well plate in 20 µl volume. Two blanks were maintained with and without addition of enzyme working solution. 200 µl of WST ((2-(4-Iodophenyl)- 3-(4-nitrophenyl)-5-(2,4-disulfophenyl)-2Htetrazolium, monosodium salt) solution was added to samples and blank wells. 20 µl of enzyme working solution was added and allowed for incubation at 37°C for 20 minutes. Absorbance measured at 450 nm using microplate reader. SOD activity was expressed as inhibition rate %. Experiments were performed with biological and technical replicates.

### 3.20 Hoechst assay:

The dosage effect of HM20, HM-21, HM-22 (phosphatase modulators of PFKFB3) and ligand94 (kinase modulator of PFKFB3) compounds synthesized by other ESRs in the

MoglyNet project and commercially available PFKFB3 inhibitor (3PO) were tested *in vitro* on control and pathological ECs of AMI and CTEPH by using Hoechst assay. Cells were incubated with HM20, HM21 and HM22 compounds at 50 µM – 100 µM concentration for 72hrs; and 3PO at 5-30 µM concentration incubation for 72 hrs. After incubation period, cells were washed with 1x PBS and added 100 µl of 0.01% SDS and frozen at -20°C for the overnight. Next day, cells were thawed at 37ºC for 30 min and incubated with 100 µl of HO33342 stain buffer (1 M NaCl, 1 mM EDTA, 10 mM Tris pH 7.4, 7.12 µM of HO33342 stain) for 1hr in the dark. Fluorescence readings were measured at ex:337nm and Em:460 nm by using fluorescence plate reader (FLUORstar* optima). Experiments were performed with biological and technical replicates.

## 3.21 THP1 cells and macrophage differentiation:

To check whether HM-20, HM-21, HM-22 and 3PO inhibiting the activity of PFKFB3, we did a validation experiment using THP1 cells. These cells were grown and maintained in RPMI 1640 medium supplemented with 2 mM L-glutamine, 1.5 g/L sodium bicarbonate, 4.5 g/L glucose, 10 mM HEPES, 1 mM sodium pyruvate with 0.05 mM 2-mercaptoethanol and 10% FBS. Cells were sub cultured when cell concentration reached to $8x10^5$ cells/ml. Media changed for every 2 to 3 days. THP1 cells were differentiated into macrophages by growing in RPMI-1640 medium containing 10 nM PMA (phorbol 12-myristate 13-acetate) for 72hrs. The expression PFKFB3 increased by treating the macrophages with 500 ng/ml of LPS (Lipopolysaccharides) for 30 min. Experiments were performed with biological and technical replicates.

## 3.22 Measurement of cell proliferation with MTT assay:

The cell proliferation inhibitory effect of 3PO was evaluated using MTT reduction assay. Briefly, $5x10^3$ EA.hy926 cells were seeded on a 96-well plate for overnight. Various concentrations of 3PO dissolved in DMSO (10,20,30 and 40 µM) were added to the cells in triplicates and allowed for 24 hrs. 20µl of MTT solution (5 mg/ml) was added and incubated at 37°C for 4 hrs. After the removal of medium containing MTT solution, 100 µl of dimethyl sulfoxide (DMSO) was added to the each well to dissolve purple formazan crystals and the plate was gently shaken for 15 min at room temperature. The optical density was measured at 490 nm using a plate reader (*BioTek's* PowerWave HT, USA). Cells incubated with respective concentration of DMSO (<0.06%) were used as a control for 100% cell proliferation. Statistical analysis was performed in the GraphPad software. Experiments were performed with biological and technical replicates.

### 3.23 3PO and TNFα treatment:

Three types of experimental setups were planned. a) To understand the underlying mechanisms of 3PO in human ECs, EA.hy926 cells were incubated with 20 µM concentration of 3PO dissolved in DMSO. In this study, control cells were incubated with media containing only DMSO in the final concentration of 0.06%. b) to understand the impact of TNFα induced inflammation, cells were incubated with 10 ng/mL concentration of TNFα for 24 hrs. Control cells were incubated in media with PBS c) to understand whether 3PO has a capability to reverse the effect of inflammation, cells were treated with 3PO (20 µM) for 1hr, followed by TNFα (10 ng/mL) incubation for 24hrs. Experiments were performed with biological duplicates and technical triplicates.

### 3.24 Incubation of 3PO and NEM in human serum:

3PO dissolved in DMSO and NEM dissolved in 0.1 M PBS ($Na_2HPO_4$, adjusted to pH 7.4 with $H_3PO_4$) Each compound was tested separately by spiking the final concentration of 1 mM in 300µl of serum. Serum without 3PO/NEM were used as a control. All the samples were allowed for 180 min incubation at temperature 37°C. We tested the reactions at 0h, 1h and 3h.

### 3.25 Extraction of HSA and incubation of NEM and 3PO:

HSA was extracted by using Affi-Gel blue gel (BIO RAD). The column was loaded with 200 µl of 20 mM phosphate buffer ($Na_2HPO_4$, adjusted to pH 7.4 with $H_3PO_4$) and centrifuged at 500 rpm for 1 minute. Serum sample was equilibrated with the same buffer for 15 minutes at room temperature. Equilibrated serum sample was loaded twice in the column and centrifuged for 500 rpm for 1 minute. After washing the column twice with the same buffer, the bounded albumin was eluted by using buffer containing 1.4 M NaCl in 20 mM phosphate buffer pH 7.1.

3PO and NEM was dissolved in methanol and 0.1 M PBS, pH 7.4, respectively. In the first condition, 30 µM concentration of HSA was incubated with 80 µM of NEM. In the second condition, 30 µM concentration of HSA was incubated with 500 µM of 3PO dissolved in 0.1 M PBS, pH 7.4 (Final concentration of methanol was maintained at 1%). HSA dissolved in 0.1 M PBS was used as a control. All the samples were incubated at 37°C and collected at oh, 1hr and 3h for the analysis.

### 3.26 Intact protein analysis:

Intact protein analysis was performed by direct infusion on a triple-quadrupole (TQ) mass spectrometer Finnigan TSQ Quantum Ultra, ThermoQuest, Milan, Italy) equipped with an Electrospray. Finnigan Ion Max source. For MS analyses, samples were desalted by using

Amicon Ultra filter units 0.5 ml, cut-off 10 kDa (Millipore) and washed seven times with water. Samples were then diluted to 1 mg/ml with a final composition of $CH_3CN–H_2O–HCOOH$ (50:50:0.1, v/v/v). Aliquots of 50 µl were injected into the mass spectrometer at a flow rate of 25 µl/min by using a ThermoQuest autosampler. Each sample was analyzed for 5 min under the following instrumental conditions: positive-ion mode; ESI voltage 3.5 kV, capillary temperature 350°C, Q3 scan range 1200–1500 m/z, Q3 power 0.4 amu, scan time 1 s, Q2 gas pressure 1.5 Torr, skimmer offset 10 V, microscan set to 3. Full instrument control and ESI mass spectra acquisitions were carried out by Xcalibur software (version 2.0.7, Thermo Fisher Scientific, Rodano, MI, Italy). Mass spectra deconvolution was performed using MagTran software (version 1.02)[71].

Table 3. 1: List of genes and its forward and reverse primers used for RT-PCR in AMI disease

| S. no | Gene | Symbol | Forward primer | Reverse primer |
|---|---|---|---|---|
| 1 | Multimerin 1 | MMRN1 | GGATTGGAGGTGCTGTCCTG | TCAGCCTGGTTGGTGTGTATC |
| 2 | Gamma-Glutamyltransferase 5 | GGT5 | GGGAGCTCATCATCTCTGCTG | GAGAGAAAGCAGGTTCACAGGG |
| 3 | MACRO Domain Containing 1 | MACROD1 | GTGTTTGGCTACCCCTGTGA | TCAGTCCCGGTCAGGGTG |
| 4 | Malic Enzyme 3 | ME3 | CTTGGTTTCGCTTTGCCTGG | CAGGTGCTCCCAAAGGGTTA |
| 5 | Dipeptidyl Peptidase 7 | DPP7 | CTGGTGTCGGACAGGTTCTG | GACTTCCCGTAGTAGCGGTG |
| 6 | Collagen Type VIII Alpha 1 Chain | COL8A1 | CGAGCTAACCGCACCCTTT | TCACGGGCTCGTTGTTCTTG |
| 7 | Signal transducer and activator of transcription 3 | STAT3 | ATCCTGGTGTCTCCACTGGT | GCTACCTGGGTCAGCTTCAG |
| 8 | integrin beta chain beta 3 | ITGB3 | ACCAGTAACCTGCGGATTGG | CTCATTGAAGCGGGTCACCT |
| 9 | ATPase Plasma Membrane Ca2+ Transporting 4 | ATP2B4 | TGTAGCAGTTGCACCAGTCA | GTGGGTCATGAAGCTGTGGA |
| 10 | CD44 antigen | CD44 | ATCTTGGCATCCCTCTTGGC | CAGTTCTAGCGAGGTGACTGT |
| 11 | Myosin Light Chain 9 | MYL9 | CGAGGATGTGATTCGCAACG | TGTTTGAGGATGCGGGTGAA |
| 12 | Fatty Acid Binding Protein 5 | FABP5 | TCTTGTACCCTGGGAGAGAAGT | GCTGAACCAATGCACCATCTG |
| 13 | Fermitin family homolog 3 | FERMT3 | CCCAGAGCTCAAGGACCATC | AACATCGGGAACCACCTCAC |
| 14 | Ribosomal Protein Lateral Stalk Subunit P0 | RPLP0 | TCGACAATGGCAGCATCTAC | ATCCGTCTCCACAGACAAGG |

Table 3. 2: List of genes and its forward and reverse primers used for RT-PCR in CTEPH disease

| S. no | Gene | Symbol | Forward primer | Reverse primer |
|---|---|---|---|---|
| 1 | Ribosomal Protein Lateral Stalk Subunit P0 | RPLP0 | TCGACAATGGCAGCATCTAC | ATCCGTCTCCACAGACAAGG |
| 2 | Von Willebrand factor | VWF | TGAGGCCTATGGCTTTGTGG | GGTCAAGGTCCCTTCTTGGG |

Table 3. 3: List of genes and its forward and reverse primers used for RT-PCR analysis to check the effect of 3PO in normal and inflamed ECs

| S. no | Gene | Symbol | Forward primer | Reverse primer |
|---|---|---|---|---|
| 1 | β-actin | ACT | AGTGTGACGTGGACATCCGCA | GCCAGGGCAGTGATCTCCTTCT |
| 2 | Interleukin 1 beta | IL1B | ATGCACCTGTACGATCACTG | ACAAGGACATGGAGAACACC |
| 3 | Interleukin 8 | IL8 | ATACTCCAAACCTTTCCACCC | TCTGCACCCAGTTTTCCTTG |
| 4 | Intercellular Adhesion Molecule 1 | ICAM1 | CAGAGGTTGAACCCCACAGT | CCTCTGGCTTCGTCAGAATC |

# 4 Chapters

# Chapter – 1

# 1. Differentially expressed proteins in patient-derived primary endothelial cells of AMI

## 1.1 Abstract:

Endothelial dysfunction is one of the primary factors in the onset and progression of acute myocardial infarction. However, the comprehensive role of pathological endothelial dysfunctionality in the disease progression mechanism remains unclear. An altered protein expression profiling in combination with protein network analysis was employed by using the mass spectrometry-based label-free quantification approach. In the present study, we analysed patient-derived primary endothelial cells which had a less proliferation and migration capacity compared to normal cells. 2246 proteins were identified and quantified. Based on the statistical tests, we identified 335 significantly differentially regulated proteins in HCAEC-AMI ECs compared to the control group. Bioinformatic analysis revealed the alteration of a) metabolism of RNA, b) platelet activation, signaling and aggregation, c) neutrophil degranulation, d) metabolism of amino acids and derivatives, e) cellular responses to stress, and f) response to elevated platelet cytosolic $Ca^{2+}$ pathways. Moreover, the expression pattern of selected genes and proteins was validated at transcriptome and proteome levels, respectively. In conclusion, these results deliver an exclusive representation of the endothelial proteome in AMI, contributing to the understanding of pathophysiology and the starting point for the identification of new drug targets.

## 1.2 Brief introduction:

Vascular endothelium plays a key role in the maintenance of vascular homeostasis and it also acts as a multifunctional organ for vascular tone regulation. Endothelial dysfunction is more frequently observed in the manifestation of cardiovascular risk factors and significantly contributes to the development of atherogenesis, hypertension, peripheral vascular disease, chronic kidney failure, diabetes, viral infections, coronary artery disease, and myocardial ischemia[6–10]. It is characterized by several features including the association of increased production of ROS, growth factors, adhesive molecules; impaired redox status and fibrinolytic ability; a discrepancy in the functions of endothelium-mediated vasodilation, prothrombic and proinflammatory responses[3–5]. However, the occurrence of alterations in endothelial function causes the morphological changes in the atherosclerotic plaques, lesions and also significantly involves in the development of further clinical complications[72].

AMI is one of the leading causes of morbidity and mortality throughout the world and the appearance of this disease predominantly increasing in most of the developing countries. Approximately 15.9 million cases were reported in 2015[73]. It is a subgroup of an acute coronary syndrome, usually occurs with a reduction in myocardial perfusion that leads to the cell necrosis due to the formation of thrombus in coronary arteries. The rupture of an atherosclerotic plaque and unstable angina exposes the blood to thrombogenic lipids, which leads to the activation of clotting factors and platelets. Previous studies have shown that circulating microparticles from patients with AMI causes the endothelial dysfunction and it also occurs severely in young acute myocardial infarction patients correlated with the thrombolysis[74,75].

Emerging data specifies that new pathological blood vessel responses and endothelial dysfunctionality are associated with metabolic alterations in ECs. However, the underlying mechanisms associated with dysfunctional endothelium may be multidimensional and have not been clarified yet. Therefore, identification of insights and causes resulting in dysfunctional ECs are crucial to the understanding of the disease and development of new therapeutic tools.

## 1.3 Results

The aim of this study was to identify the differentially regulated proteins associated with the vascular endothelial dysfunctionality of AMI. For this purpose, pathological primary ECs, isolated from the thrombus material of AMI patients, were used. Patient-derived pathological cells provide

an exclusive opportunity to identify the definite molecular proceedings. The mass spectrometry-based label-free quantitation approach was able to understand the complex network and signaling pathways associated with the endothelial dysfunctionality of AMI.

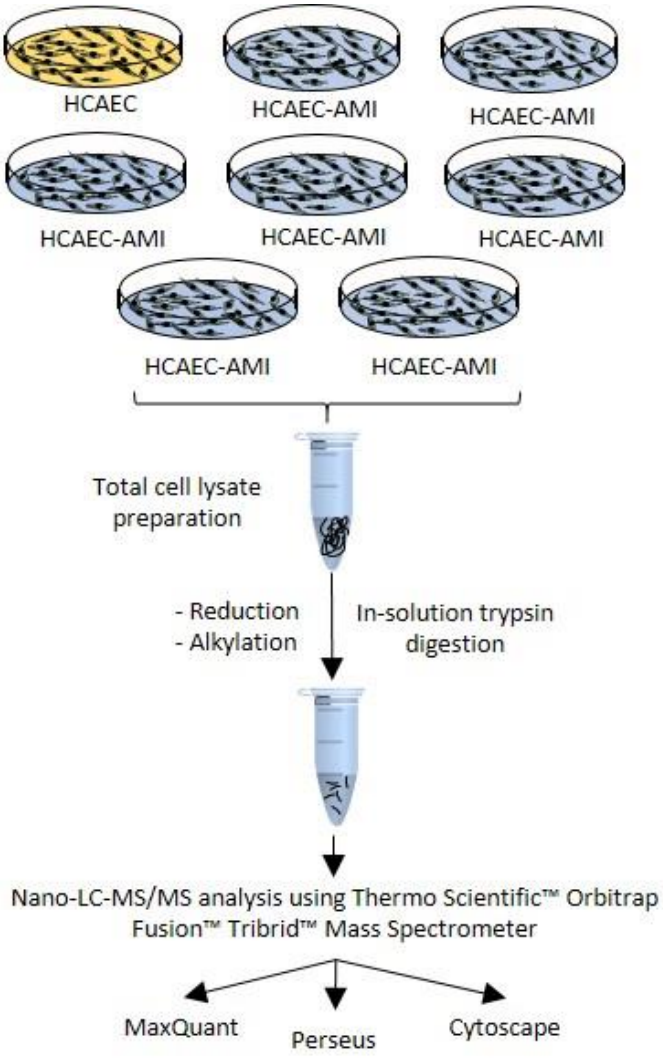


Figure 1.1: Work flow of proteomics approach

The confluent pathological ECs (HCAEC-AMI) and normal human coronary artery endothelial cells (HCAECs) were collected to extract the protein content. Altered protein expression profiling in combination with gene ontology, network and pathway analysis was employed by using the mass spectrometry-based label-free quantification approach to explore the molecular proceedings

(Figure 1.1). Multi scatter plot analysis of peptide intensities resulted in Pearson coefficients higher than 0.98, attesting the high grade of reproducibility of technical and biological replicates.

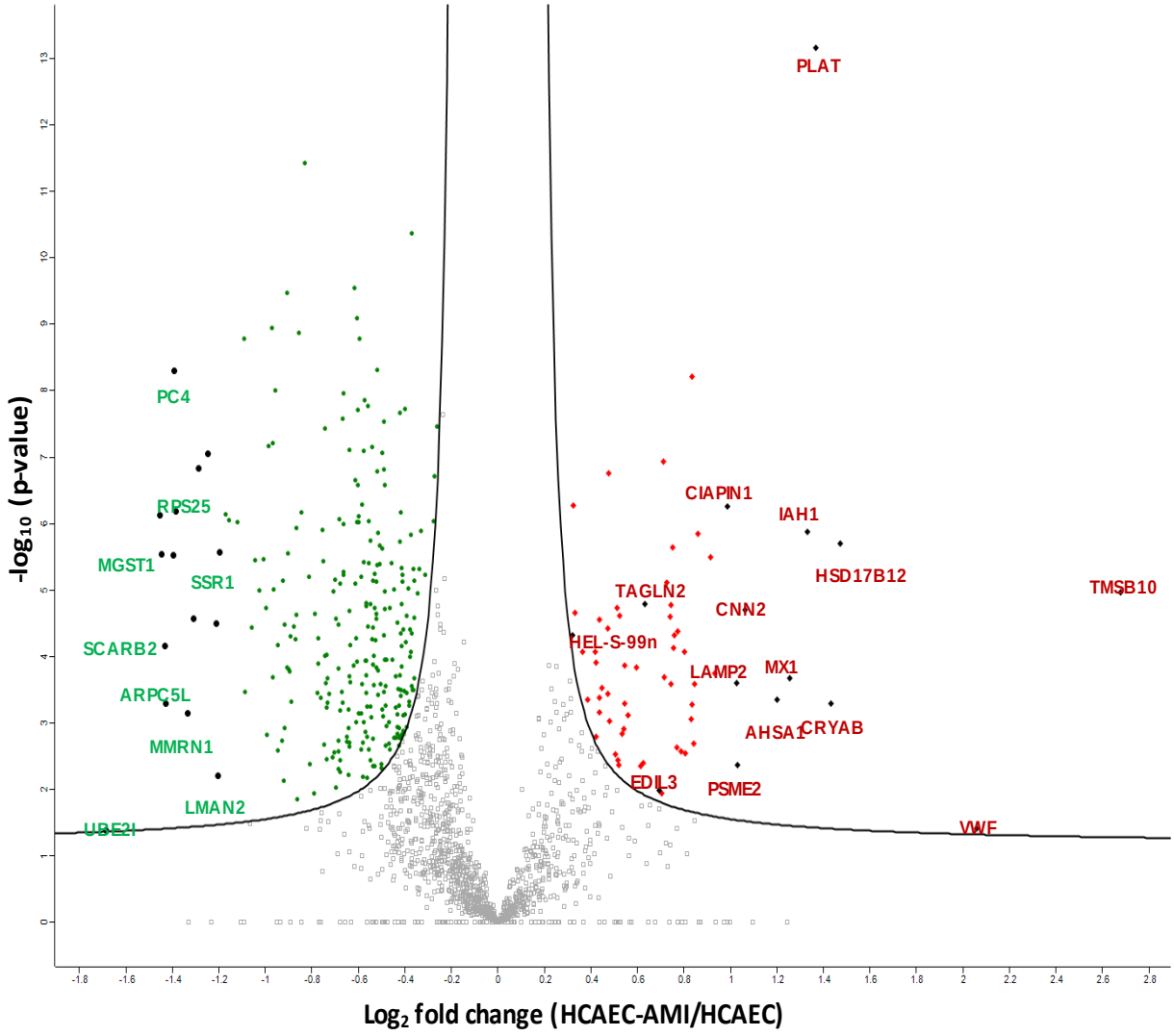


Figure 1.2: Volcano Plot obtained by two-sided t test of the groups: HCAEC-AMI (disease) versus HCAEC (control). The average label-free quantitation (LFQ) intensities of all the technical triplicates and biological replicates of HCAEC-AMI samples compared with the average LFQ intensities of all the technical triplicate and biological replicates of HCAEC samples. Green color indicates the down-regulated proteins, red color represents the upregulated ones.

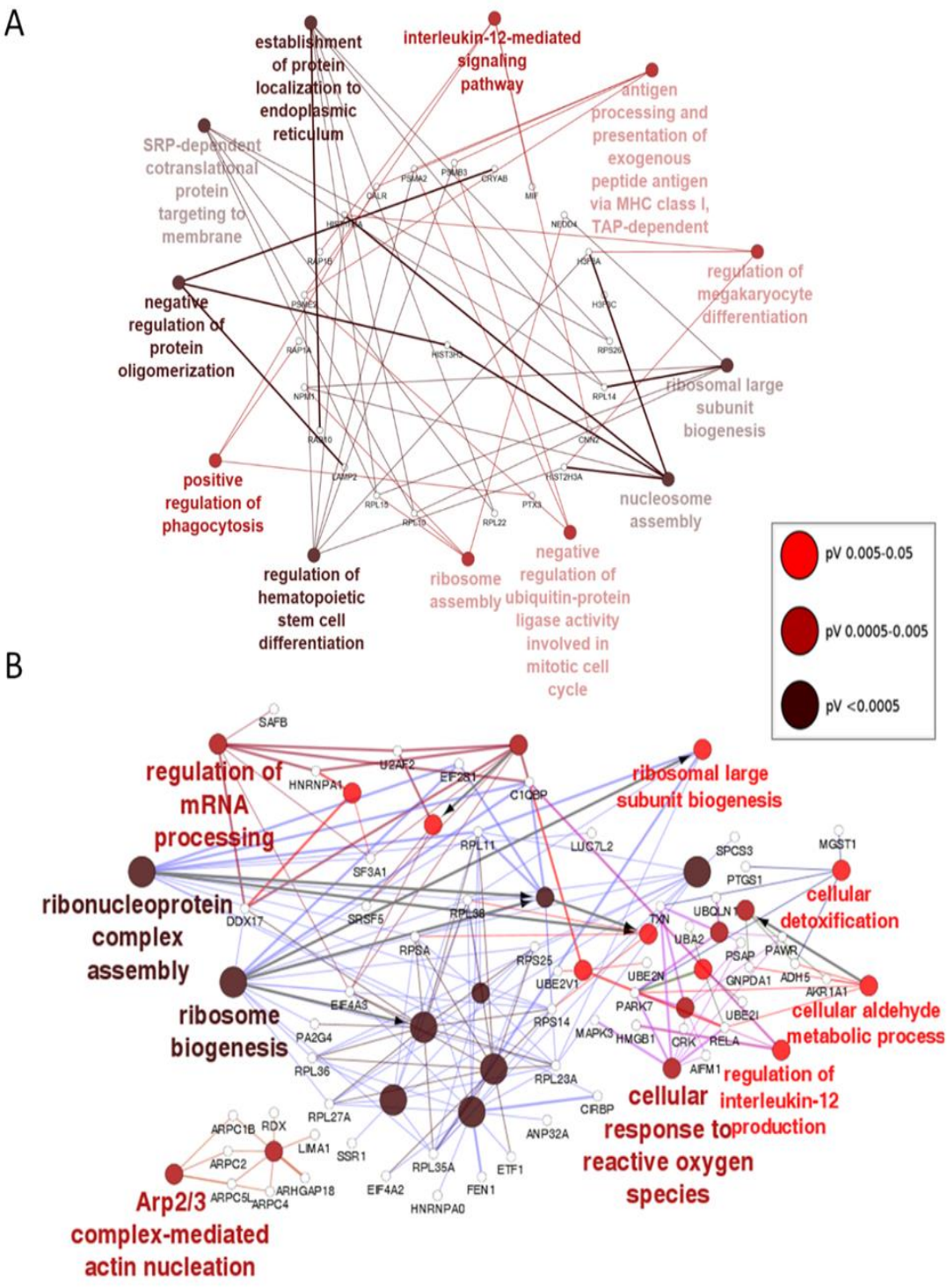


Figure 1.3: Biological process terms associated with up (a) and down (b) regulated proteins found in dysfunctional HCAEC-AMI cells. The significance of the clustering is shown by color code and the size of nodes.

2246 protein and 17653 unique peptides were quantified, consulting the *Uniprot_Homo sapiens* database; the settings of searches were 10 ppm tolerance on peptides, 0.8Da on fragments and less than 1% false discovery rate. The data analysis was performed as specified in our publication[67].

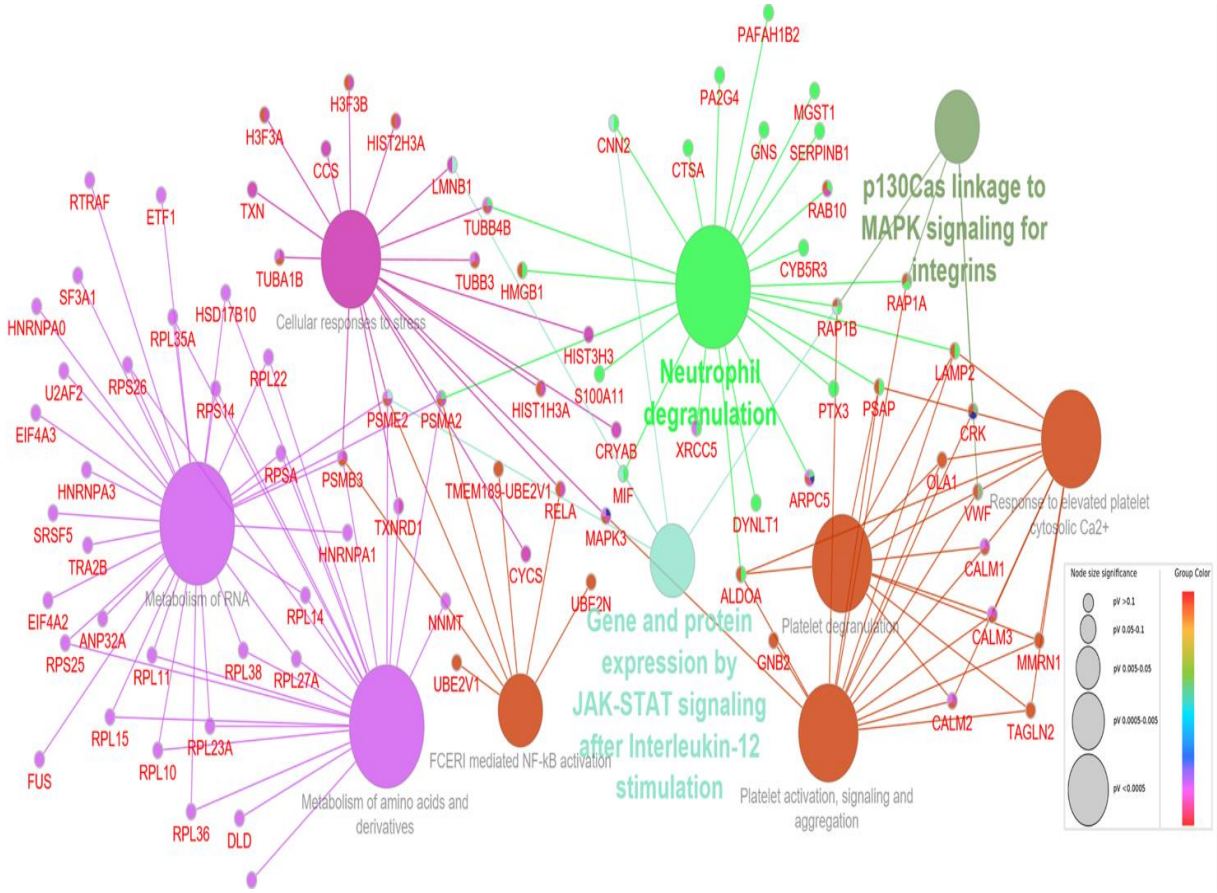


Figure 1.4: Main pathways and involved genes found in dysfunctional HACEC-AMI cells. ClueGo analyses enriched and clustered Reactome pathway terms. The significance of the clustering is shown by color code and the size of nodes.

To discriminate the differentially expressed proteins a two-sided t test was applied to two category groups: HCAEC-AMI (disease) and HCAEC (control). The log2 of ratios of disease versus control (fold change) were plotted against the -log10 of p-value, resulting in the Volcano plot of Figure 1.2. All proteins with a fold change higher than 1.5 and p-value less than 0.05 were considered significant outliers.

335 proteins were differentially regulated, of which 40 up and 123 down-regulated proteins with a fold change higher than 1.5-in the HCAEC-AMI ECs compared to the control group. (Appendix Table-1 and 2).

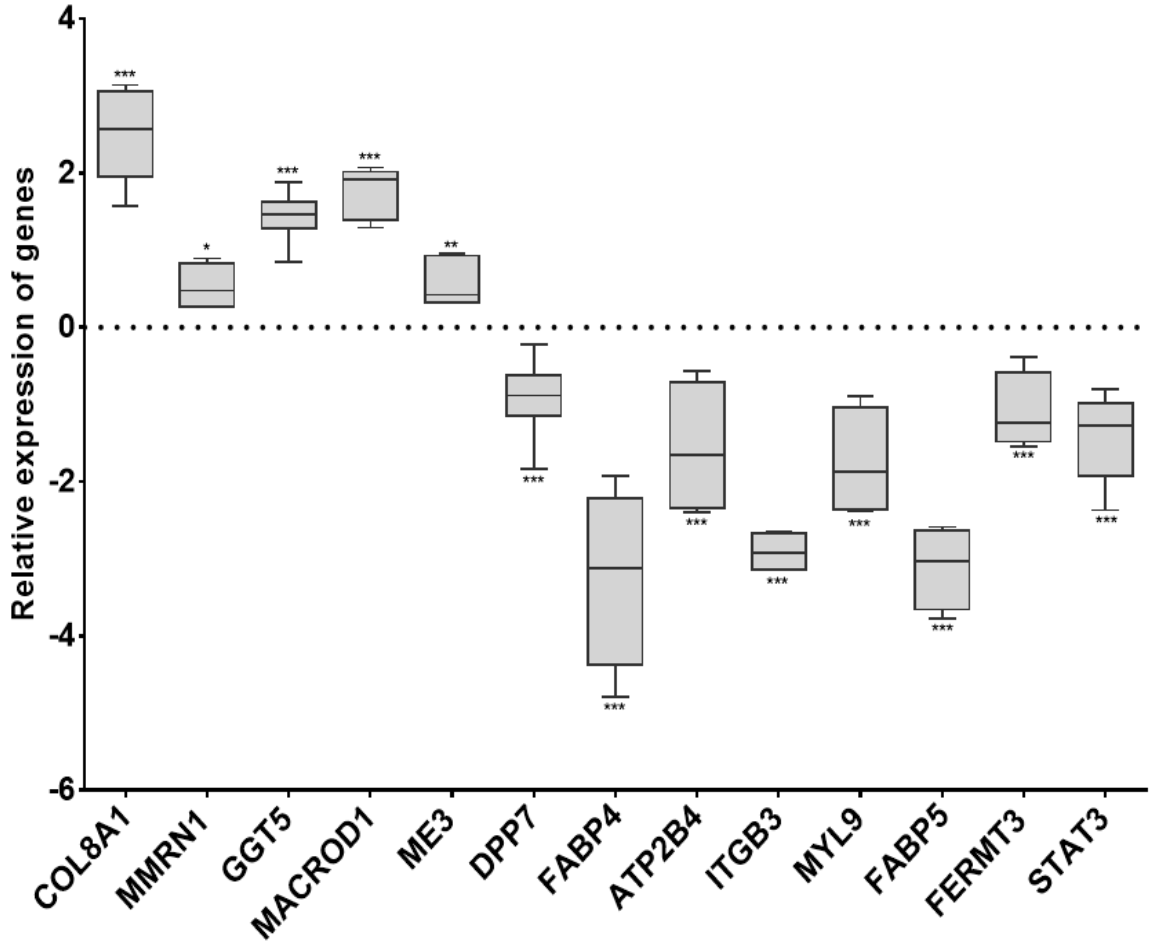


Figure 1.5: Transcript expression levels of selected genes. The expression of selected genes was normalized with RPLP0 housekeeping gene. The boxes display the relative expression of genes in HCAEC-AMI against the HCAEC expression. Data were shown in log2 fold changes of mean ± SD. Differences were considered significant when $p < 0.05$ (*), $0.001 < p < 0.01$ (**), $p < 0.001$ (***).

Majority of upregulated proteins in dysfunctional ECs of AMI are originated from proteasome complex, nucleosome, large ribosomal subunit and cytosolic ribosome (Supplementary Table

1.S.1). The actin-binding protein TMSB10 is showed to be high upregulated protein in dysfunctional ECs with a fold change of 6.4. This protein is involved in the actin filament organization biological process that plays an important role in the organization of the cytoskeleton. Similarly, we identified an important adhesion protein VWF as upregulated protein with a fold change of 4.2. VWF is a key protein that involves in the haemostasis, blood coagulation, platelet degranulation, and activation and extracellular matrix organization. Studies have shown that VWF promotes the formation of a molecular bridge between platelet-surface receptor complex GPIb-IX-V and sub-endothelial collagen matrix, which further increases the binding of plates to the site of vascular injury.

The plasminogen activator (PLAT) protein, involved in tissue remodelling and degradation, was found to be upregulated. Along with these proteins, a platelet-expressed protein HSD17B12 might play a primary role in the dysfunction of ECs. It has a 3-ketoacyl-CoA reductase activity, suggesting a role in lipid metabolism and fatty acid biosynthesis. Moreover, statistically significantly clustered biological processes and the involved genes were reported in Figure 1.3a.

Cytosolic small and large ribosomal subunits and proteasome complex are the main sources for the down-regulated proteins (Supplementary Table 1.S.2). These proteins are involved in ribosome biosynthesis, small and large subunit assembly, regulation of cardiac muscle contraction by calcium ion, regulation of oxidative stress-induced cell death, cellular response to reactive oxygen species and cellular aldehyde metabolic processes (Figure 1.3b). UBE2I (-1.68), SYNE1 (-1.45), and MGST1 (-1.45) showed an extensive down-regulation among all the identified proteins. The MAPEG family (Membrane-Associated Proteins in Eicosanoid and Glutathione metabolism) protein MGST1, involved in the protection of endoplasmic reticulum and outer mitochondrial membrane from oxidative stress. Therefore, the down-regulation of this protein in dysfunctional ECs might indicate the association of increased oxidative stress in endothelial dysfunction of AMI. To better understand the nature of statistically differentially regulated proteins, they were further classified in terms of Reactome pathways. The retrieved data from this analysis showed the association of metabolism of RNA (31 genes, p-value: 4.07E-12); platelet activation, signaling and aggregation (15 genes, p-value: 1.04E-13); neutrophil degranulation (23 genes, p-value: 2.31E-07); metabolism of amino acids and derivatives (22 genes, p-value: 4.04E-12); platelet degranulation (10 genes, p-value: 1.04E-13); cellular responses to stress; and response to elevated

platelet cytosolic Ca2+ pathways (10 genes, p-value: 1.04E-13) in endothelial dysfunction of AMI (Figure 1.4).

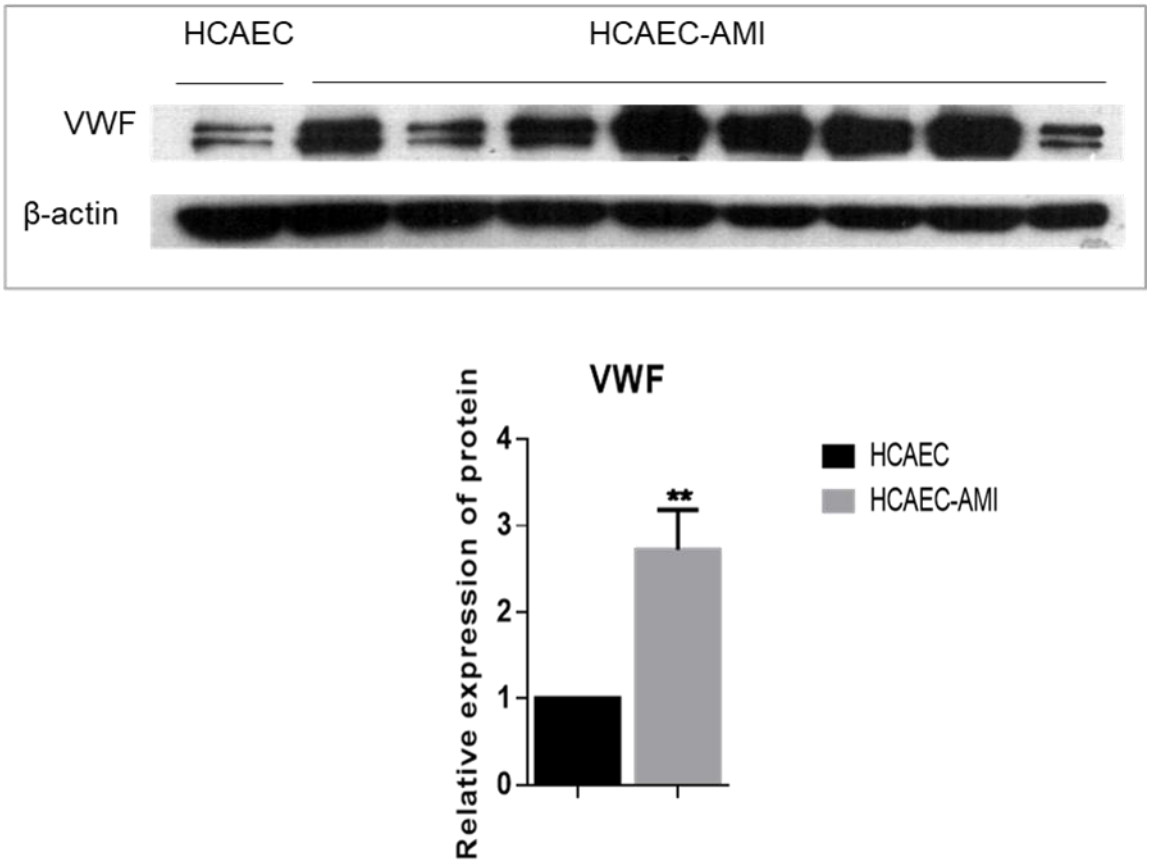


Figure 1.6: Protein expression levels of selected proteins. Bar graph was plotted with mean ± SEM, the x-axis represents the HCAEC-AMI and HCAEC groups and the y-axis represents the relative expression of a respective protein to control. Differences were considered significant when $p < 0.05$ (*), $0.001 < p < 0.01$ (**), $p < 0.001$ (***). β-actin was used as a housekeeping protein.

### 1.3.1 Validation of differentially regulated proteins by RT-PCR analysis:

A total of 13 genes were selected to understand its variation at mRNA level by using quantitative real-time PCR method. The expression of these genes was evaluated using HACEC-AMI cell lines against the HCAECs. The genes such as COL8A1, MMRN1, GGT5, MACROD1, and ME3 were

found to be upregulated and genes including DPP7, FABP4, ATP2B4, ITGB3, MYL9, FABP5, FERMT3 and STAT3 were found to be down-regulated during the endothelial dysfunction of AMI (Figure 1.5).

### 1.3.2. Validation of differentially regulated proteins with western blot analysis:

The differentially expression of VWF was validated by western blot analysis. The peak intensity area of each protein band was calculated using ImageJ software and the data illustrated as histograms after analysing against the ACT as housekeeping protein. As shown in the figure (Figure 1.6), the relative abundance of VWF protein was analogous to the results from label-free quantification study. (2.7-fold change in western blot and 4.2-fold change in proteomics).

## 1.4 Discussion:

A deep understanding of molecular mechanisms of disease is crucial in the discovery of novel therapeutic strategies and in the early prediction to improve the prognosis. Mass spectrometry-based proteomics is one of the advanced tools to identify early biomarkers in the various biological samples. In the present study, for the first time, the changing of proteome profile of patient-derived HCAEC-AMI cells was analysed.

The endothelium which exists between the circulatory system and surrounding tissues plays an important role in the vascular injury. Based on the stress and tissue needs, ECs can induce prothrombotic or antithrombotic events. Usually, healthy ECs express anticoagulant and antiplatelet agents that can be involved in the prevention of fibrin formation and platelet aggregation. Whereas dysfunctional ECs generate aggregation, fibrin formation along with the platelet adhesion. During the final stage, ECs produce pro-fibrinolytic events to enhance the fibrinolysis for the degradation of the clot. On the other hand, ECs under physiological conditions prevent thrombosis by activating the cascade of anticoagulant and antiplatelet mechanisms. In this study TMSB10 and VWF proteins were highly upregulated. TMSB10 has a role in the organization of the cytoskeleton, while the increased expression of VWF clearly explains an enhanced occurrence of thrombosis. VWF also binds to collagen during the damage occurring to the blood vessels. Collagen plays a key role in the maintenance of integrity and elasticity of normal vessel walls as well as atherosclerotic vessel walls and it stimulates the thrombosis formation and scar formation processes particularly in acute myocardial infraction[76] VWF and over expressed

RAP1A, RAP1B proteins are involved in the platelet aggregation, in integrin alpha IIb beta3 signaling and in MAP2K and MAPK activation pathways.

MAPKs is implicated in multiple important cellular processes such as apoptosis, proliferation, motility, differentiation, stress response, and survival. In this study, MAPK3 protein were down-regulated, that correlates with lower proliferation capability.

Recent studies showed that interferon-induced GTP-binding protein MX1 involved in MI and suggested to play a role in the pathology of the disease[77,78]. In this study, MX1 was upregulated with fold change of 2.4, attesting its role in endothelial dysfunction of AMI.

Rap1, which controls the EC function, is one of the critical mediators of FGF-induced ERK activation in human angiogenic process[79]. In this study, upregulation of RAP1a and RAP1b in dysfunctional ECs might explain the strong correlation between endothelial dysfunction, platelet aggregation and angiogenesis in AMI. It might also play a role in the vascular EC protection, based on the results of knockdown studies[80].

The identified differentially regulated proteins in patient cells, such as VWF[81], CRYAB[82], MX1[83], CNN2[84,85], PSME2[86], CIAPIN1[87], TAGLN[88], and EDIL3[89] have been reported to be implicated in AMI, myocardial infarction (MI) vascular injury, morphogenesis, and angiogenesis.

Furthermore, previous studies have shown the increased synthesis of type VIII collagen in the vascular injury of the development process of atherosclerosis in humans and animal models[90,91]. The identified over expressed HSD17B12 protein is a reductase involved in collagen binding activity and long fatty acid chain metabolism. However, in the case of dysfunctional ECs of CTEPH disease, HSD17B12 shown the down regulation, suggesting different role in both different diseases.

MMRN1, belonging to EMILIN family[92], is usually found in platelets, and has an adhesive ligand property in synergy with VWF in platelet adhesion to collagen at the sites of vascular injury[93,94]. The down regulation of MMRN1 protein, was not confirmed by analysis of its gene expression. This lack of correlation is likely due to the differentially regulation of post translated modified form of the protein.

EC apoptosis has a fundamental role in the angiogenesis process and pathological vascular remodelling and regression[95–97]. In this study proteins related to apoptosis pathway resulted

differentially regulated. In particular, CYCS, DNM1L, HMGB1, LMNB1, PSMA4, PSMA7, PSMB5, PSMC5, PSMD13, PSME1, YWHAB, YWHAE showed decreased expression and PSMA2, PSMB3 (1.08-fold change) and PSME2 showed increased expression, attesting their essential role during endothelial reorganization in AMI.

Metabolic alterations and oxidative stress are important influencing factors in the endothelial dysfunctionality of cardiovascular diseases and diabetes [98–100]. Normal ECs constantly produce endothelial nitric oxide synthase (eNOS). The impairment of eNOS–NO system causes the oxidative stress and endothelial dysfunction that further accelerates the atherogenesis. In this investigation, a reduced expression of eNOS activation pathway, described by the down-regulation of CALM1, CALM2, and CALM3 proteins, and the activation of NF-kappaB in B cells, were found. The down-regulation of PARK7, PAWR, PSAP, TXN and UBQLN1 proteins, involved in the regulation of oxidative stress-induced cell death, and the down-regulation of MGST1 protein, involved in the cell protection against oxidative stress, were found. This confirms the involvement of oxidative stress in endothelial dysfunction. The inhibition of vascular oxidative stress and enhancement of eNO production could be a potential therapeutic strategy along with the treatments of established risk factors.

FABP4 is one of the most abundant proteins in fat cells and lipocytes also known as adipocyte cells and it has a major role in proinflammatory activity in macrophages. Previous studies reported overexpression of endothelial FABP4 in response to angiogenic growth actor VEGFA[101]; while other studies demonstrated the correlation between down-regulation of FABP4 and decrease of endothelial cell proliferation [101,102]. According to the gene expression studies, it encourages P38, endothelial nitric-oxide synthase and stem cell factor (SCF)/c-kit pathways[102]. Furthermore, knockdown studies of FABP4 increased the oxidative stress[103]. In the present study, the down-regulation of FABP4 at transcriptome level was found, accordingly with less proliferation and migration capacity of AMI cells (Data not shown; however, these results were validated by other ESR in Prof. Marta Cascante's lab as a part of MoGlyNet project consortium).

Ribosome (including RNA and proteins) is an essential component in the machinery of protein synthesis and ribosomal proteins (RPs) plays a critical role in the cell proliferation, differentiation, apoptosis, DNA repair, and other cellular processes[104]. Studies have shown that the dysfunction of ribosomal biosynthesis may result in abnormal cell proliferation in metabolic disorders and

cancer[105,106]. Moreover, various RPs have been reported to be associated with the progression of cardiovascular diseases[107,108]. However, we observed the down-regulation of several RPs in dysfunctional ECs which are corresponding to the ribosome biogenesis, small and large subunit assembly processes.

In conclusion, the main involved pathways and related proteins have been extensively described by the quantitative and bioinformatic analyses. This can provide new perspectives in drug discovery to treat cardiovascular diseases.

## 1.5 Novelty and significance of the work:

**What is new?**

- This is the first ever study performed to explore the proteomic signatures with patient-derived pathological ECs to unveil underlying pathophysiological mechanisms in endothelial dysfunction associated with AMI.

**What is Relevant?**

- Quantitative proteomic profiling in endothelial dysfunction reveals the differentially regulated proteins that might behave as a biomarker signature of thrombosis, metabolism and oxidative stress.
- The overexpression of VWF strongly associated with thrombus formation, platelet aggregation and angiogenesis that might play a key role endothelial dysfunction of AMI.
- Increased production of oxidants and decreased production of anti-oxidant biomarkers as well as down regulation of protein which had an antioxidant property strongly explained the correlation of the role of oxidative stress in endothelial dysfunction of AMI.

# Chapter -2

# 2 *Differentially Expressed Proteins in Pulmonary Endothelial Cells in Chronic Thromboembolic Pulmonary Hypertension.*

## 2.1 Abstract:

Dysfunction of ECs is one of the major factors involved in the development of CTEPH. Therefore, identification of the molecular mechanisms underlying endothelial dysfunction is crucial to the understanding of the disease and to the expansion of novel therapeutic strategies. The aim of this study was to identify the differentially regulated proteins associated with the vascular dysfunctionality of CTEPH. CTEPH-ECs isolated from specimens obtained in PEA from five patients were analysed. In depth one single run label free quantitative mass spectrometry resulted in a description of an altered protein profiling. 3258 proteins were identified and quantified; 676 were statistically significant differentially regulated proteins. Network analysis revealed the differentially regulation of pathways related to a) neutrophil and platelet degranulation, b) metabolism of lipids, amino acids and selenoamino acids, c) response to elevated cytosolic $Ca^{2+}$, e) detoxification of reactive oxygen species in the dysfunctional CTEPH-ECs.

## 2.2 Brief introduction:

CTEPH is a rare, progressive and discrete pulmonary vascular disease that occurs in the late complication of acute PE followed association with VTE[36,109,110]. The presence of pathological modifications in the pulmonary arteries and their impediments primes to an intensification of pulmonary artery vascular resistance along with the progressive deterioration, which may ultimately lead to the failure of right ventricular. However, according to the recent epidemiological analysis the occurrence of CTEPH will increase in the following decade and it can be considered as life threatening disease with poor prognosis[111,112].

Endothelial dysfunction plays a vital role in the vascular remodelling of pulmonary arteries in PH[113]. The comprehensive role of pathological endothelial dysfunctionality during the disease progression mechanism of CTEPH disease remains unclear. Determining the molecular changes and underlying mechanisms that causes the dysfunction of endothelium is currently essential for the identification of early prediction and the development of novel therapeutic strategies.

## 2.3. Results:

To understand the proteomic changes underlying endothelial dysfunctionality associated with CTEPH, we used patient-derived CTEPH-ECs and healthy HPAEs. 3258 proteins and 27678 unique peptides were identified and quantified. 676 proteins were differentially regulated and considering a threshold of ± 1.5-fold change, 82 proteins were overexpressed, and 227 proteins resulted down-regulated in the CTEPH-ECs compared to the HPAEs group. (Appendix Table 3 and 4). Figure 2.1 shows the distribution of differentially regulated proteins.

Most of the upregulated proteins in dysfunctional ECs of CTEPH were originated from ribosome, large ribosomal subunit and cytosolic ribosome (Supplementary Table 2.S.1). The top three upregulated proteins, PLOD2, TAGLN, TPT1, belong to endoplasmic reticulum, cytoplasm and nucleus, respectively. Network analyses showed the upregulated proteins are involved in various biological processes, such as ribonucleoprotein complex biogenesis, ribosome biogenesis, RNA catabolic process. The enriched biological process terms are described in Figure 2.2.

Vascular endothelium glycoprotein ENG is one of the most important upregulated protein observed in this study. This protein is involved in the positive regulation of angiogenesis, response to hypoxia, positive regulation of collagen biosynthesis and negative regulation of nitric-oxide

(NO) synthase processes. The poly (A) RNA, protein and ATP binding molecular functions were also observed.

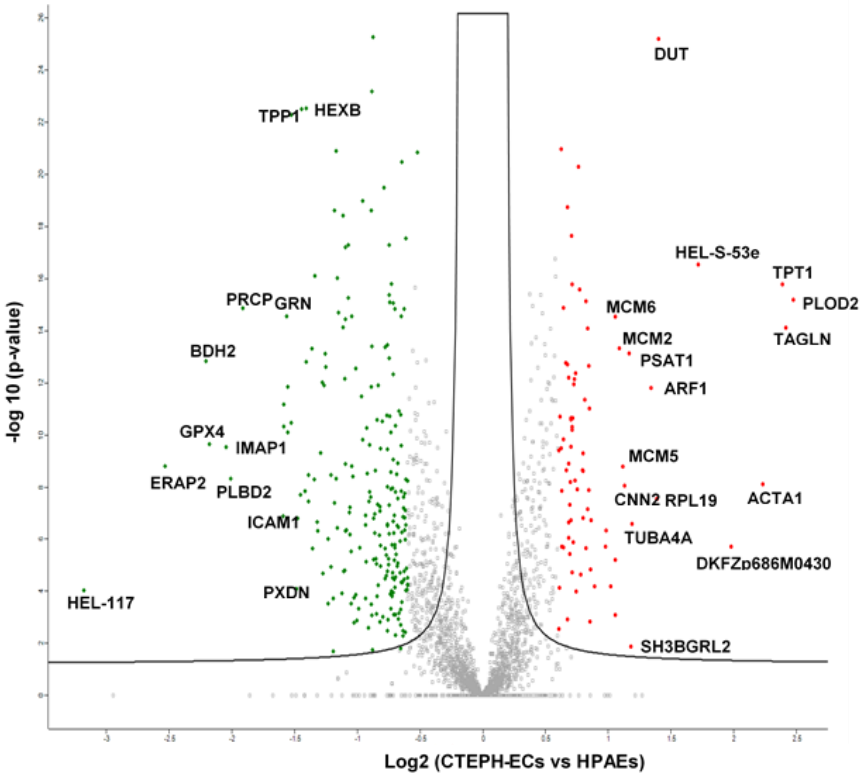


Figure 2.1: Distribution of altered proteins in CTEPH-ECs cells. In the above scatter plot, X-axis represents log2 fold change and y-axis represents -log p-value of significantly differentially regulated proteins. Green colour symbolizes down-regulation, red colour symbolizes upregulation.

The down-regulated proteins belong to the mitochondrion including envelope, matrix, inner membrane, oxidoreductase and respiratory chain; while some are from vacuole and lysosome.

The mitochondrial protein GPX4, cytoplasmimic protein BDH2, endoplasmic reticulum proteins ERAP2 and UCHL1 were the main four down-regulated proteins. GPX4 is an essential antioxidant peroxidase that protect cells from oxidative damage by preventing membrane lipid peroxidation.

However, in our study this protein showed a drastic down-regulation (fold-change of 0.2), suggesting the association of oxidative stress/damage in dysfunctional ECs. Network analyses of down regulated proteins showed the enrichment of biological processes, such as generation of precursor metabolites and energy, mitochondrion organization, ribose phosphate metabolic

process, respiratory electron transport chain, nucleotide metabolic process and cellular lipid metabolic process (Figure 2.3). The enriched molecular function GO terms are instead related to coenzyme binding, oxidoreductase, hydrolase and endopeptidase activities.

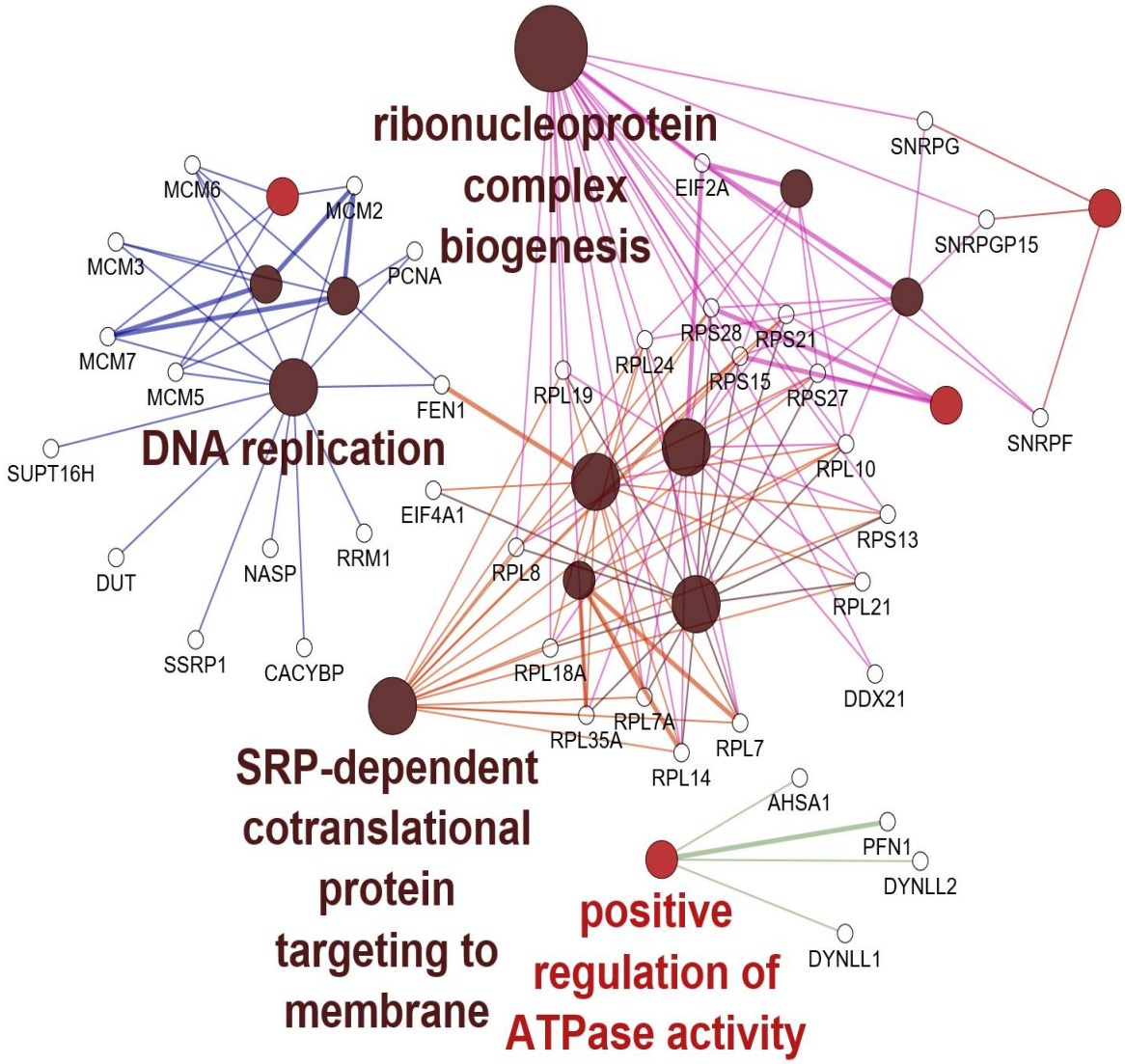


Figure 2.2: Biological process terms associated with up regulated proteins found in dysfunctional CTEPH-ECs. The significance of the clustering is shown by color code and the size of nodes.

Network analyses, based on Reactome terms, resulted in enrichment of pathways, such as metabolism (124 genes, p-value: 6E-08); neutrophil (41 genes, p-value: 1E-08) and platelet degranulation (13 genes, p-value: 1E-05); response to elevated platelet cytosolic Ca2+ (13 genes, p-value: 1E-05); metabolism of lipids (37 genes, p-value: 3E-07), and amino acids (28 genes, p-value: 1E-05); detoxification of reactive oxygen species (6 genes, p-value: 2E-05), pathways

(Figure 2.4). In addition, enriched KEGG terms were arginine and proline metabolism (7 genes, p-value: 6E-04); tryptophan metabolism (8 genes, p-value: 6E-04); beta-alanine metabolism (6 genes, p-value: 6E-04); pyruvate metabolism (8 genes, p-value: 6E-04) and glutathione metabolic (7 genes, p-value: 0.0002) pathways.

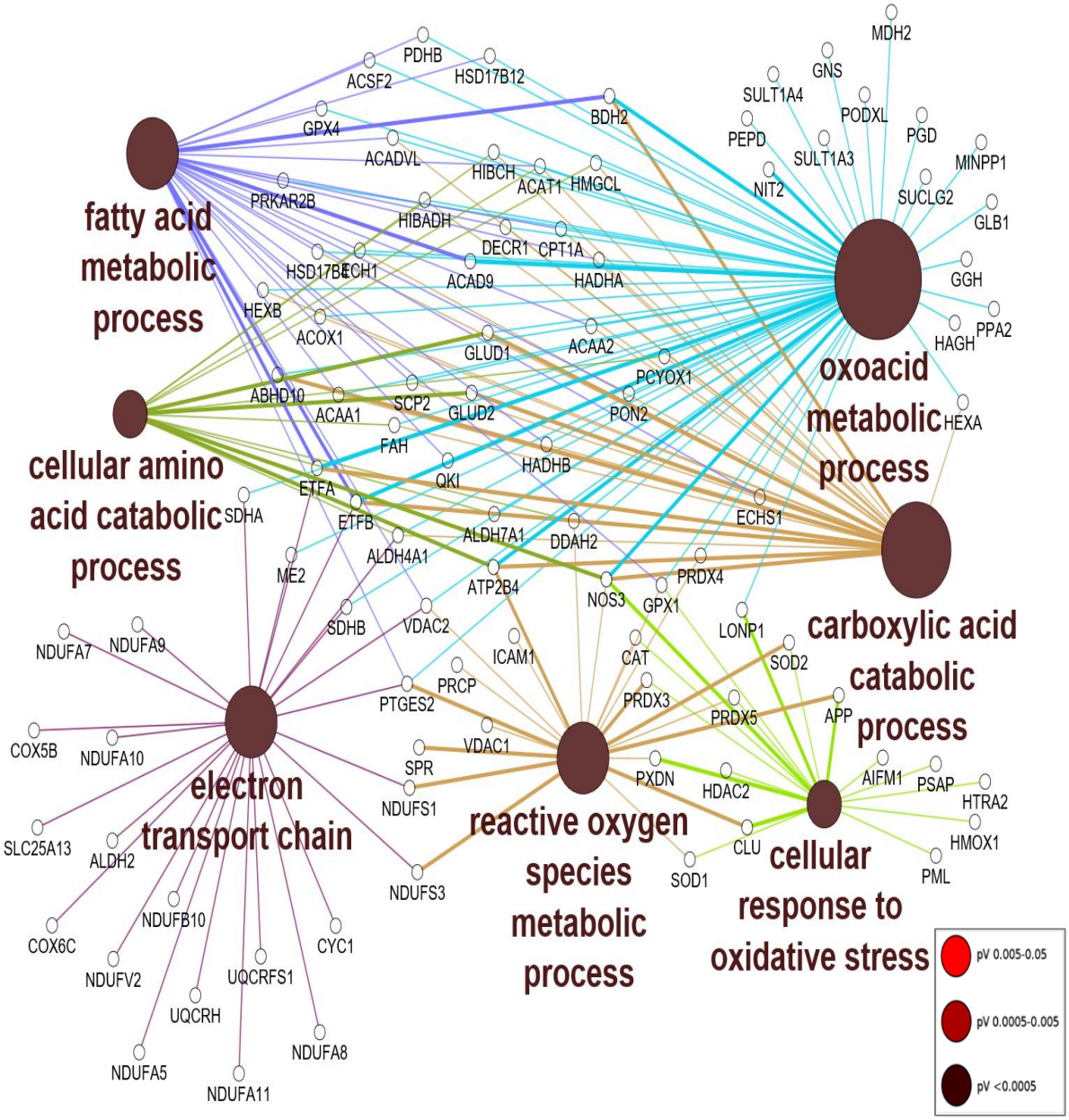


Figure 2.3: Biological process terms associated with down regulated proteins found in dysfunctional CTEPH-ECs. The significance of the clustering is shown by color code and the size of nodes.

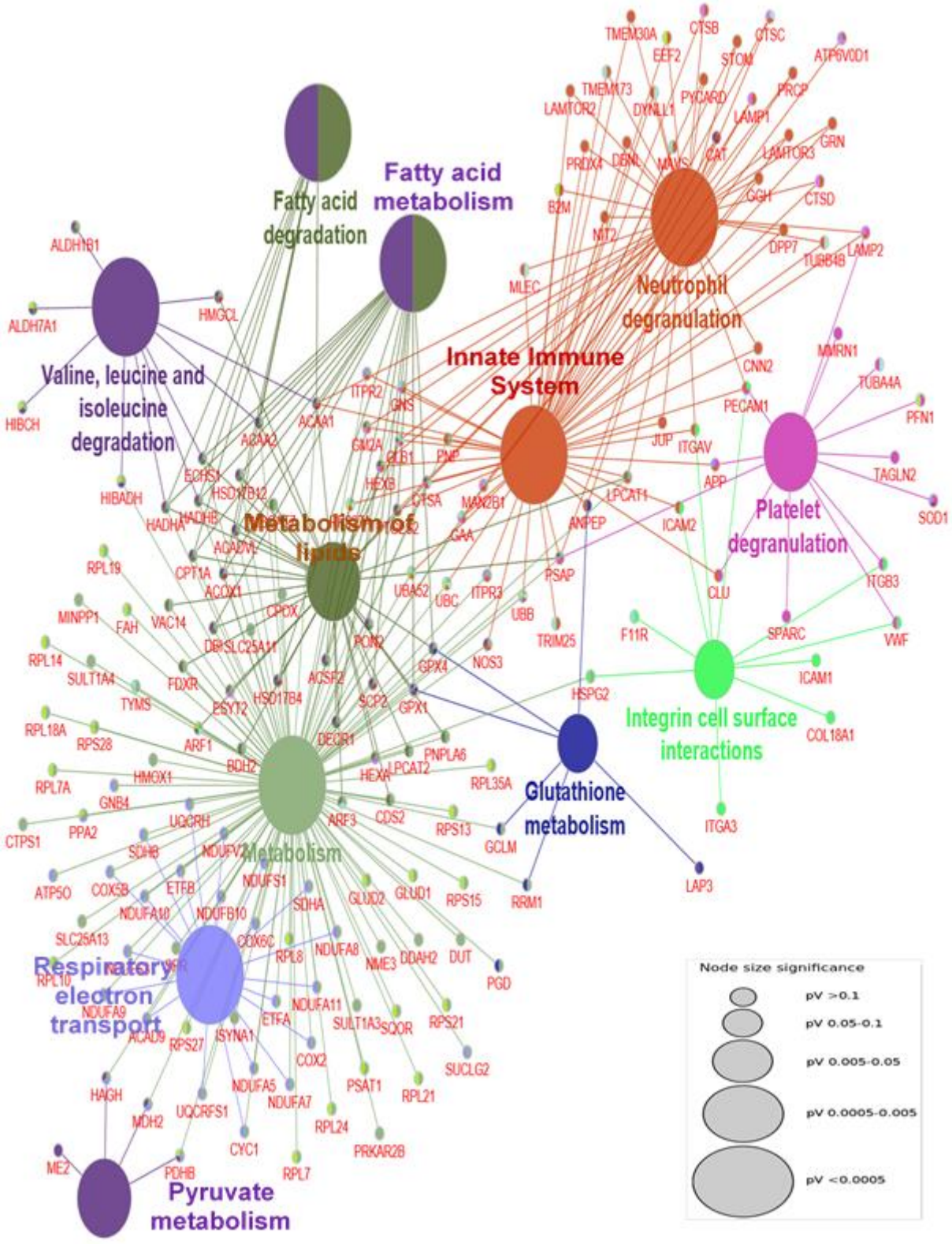


Figure 2.4: Main pathways and respective genes found in dysfunctional CTEPH-ECs.

### 2.2.1 Validation of VWF protein by RT-PCR analysis:

We also validated the gene expression of VWF, protein which we found as down-regulated in the proteomic analysis. As shown in Figure 2.5, the gene expression of VWF was down-regulated at mRNA level.

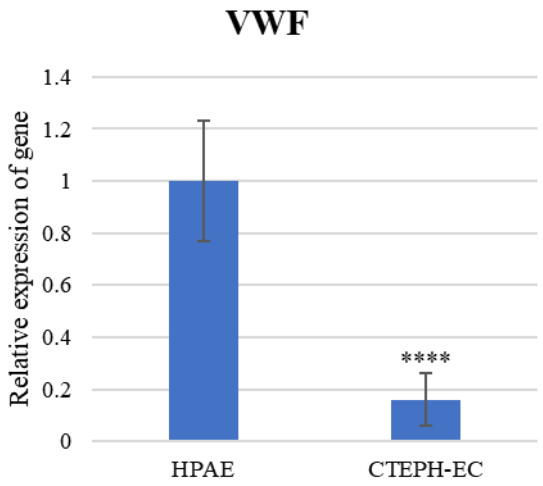


Figure 2.5: Transcript expression levels of VWF gene. The expression of the targeted gene was normalized with RPLP0 housekeeping gene. The boxes display the relative expression of gene in CTEPH-EC against the HPAE expression. Data were shown in mean ± SEM. Differences were considered significant when $p < 0.05$ (*), $0.001 < p < 0.01$ (**), $p < 0.001$ (***), $p < 0.0001$(****).

## 2.3 Discussion:

In our knowledge, this is the first ever study to analyze the proteome profile of patient-derived CTEPH-ECs to understand the underlying mechanisms associated with endothelial dysfunctionality of CTEPH. The quantitative proteomics approach showed PLOD2 as the most upregulated protein attesting its key role in CTEPH, as supported by previous studies in PAH patients [114]. PLOD2 is an attachment site for carbohydrates and it is involved in the stability collagen fibrils. Collagen plays a key role in the maintenance of integrity and elasticity of normal vessel walls as well as atherosclerotic vessel walls and it stimulates the thrombosis formation and scar formation processes particularly in acute myocardial infarction[117]. Under the hypoxic conditions, PLOD2 mediate the remodeling of ECM in synergy with collagen prolyl hydroxylases (P4HA1 and P4HA2)[115]. PLOD2 is involved in collagen deposition[115]. that induces the reduction of vascular elasticity. The increased expression of PLOD2 promotes fibrosis, which usually occurs

because of the injury. COL8A1, involved in the maintenance of vessel wall integrity and structure in atherogenesis[116], was down regulated. On the other hand, TAGLIN showed an extensive upregulation with a fold change of 5.3 in CTEPH-ECs. Recent study has shown that TAGLIN overexpression promoted the proliferation and migration of human pulmonary arterial smooth muscle cells (PASMC), strengthened cytoskeleton; suppression of this protein activated PASMC apoptosis, reducing cell proliferation and migration[117]. The higher expression of TAGLIN might be related to the hyperproliferative phenotype of CTEPH-ECs and it might have an important role in endothelial dysfunction.

Metabolic alterations in ECs are one of the hall marks of endothelial dysfunction in cardiovascular diseases. Among all the identified metabolic pathways, most of the up-regulated proteins are involved in metabolism of pyrimidine, nucleotides, selenoamino acid; and metabolism of amino acids and derivatives pathways, while down-regulated regulated proteins are involved in, tryptophan metabolism, beta-alanine metabolism, pyruvate metabolism glutathione metabolism, arginine and proline metabolism pathways. Haemolysis is one of the common occurrences in pulmonary hypertension and endothelial dysfunction[118,119]. Arginine metabolism changes and reduces NO bioavailability during haemolysis. Proline is an amino acid involved in lung fibrosis, smooth muscle cells proliferation and collagen formation. Low arginine/ornithine ratio has been reported to be associated with high mortality. Under conditions of low arginine and tetrahydrobiopterin, eNOS is uncoupled generating reactive oxygen species[120]. Emerging studies demonstrated that oxidative stress is one of the potential influencing factor in endothelial dysfunction[121,122]. The down regulation of identified GPX4, GPX1, NOS3 proteins attested the increment of oxidative stress. Among these GPX4 found as one of the most down-regulated protein (-4.36-fold change). Under physiological conditions, the antioxidants related to glutathione peroxidase family proteins GPX1 and GPX4 protects the cells from oxidative stress[123]. GPX4 prevents the cells from ferroptosis, a non-apoptotic cell death as consequence of iron-dependent accumulation of lipid reactive oxygen species (ROS)[124]. Elevated levels of GPX1 protected the cultured HPAE from hydrogen peroxide induced cell death[125]. Reduced expression of GPX1 can also lead to inflammatory activation of ECs, that further increase to a proatherogenic endothelial phenotype[126]. Genetic deletion of GPX1 decreased bioavailability of NO and increased the oxidative stress[127]. Moreover, normal ECs always generate endothelial nitric oxide synthase (eNOS), which is essential for maintain various endothelial functions including the vascular

smooth muscle relaxation, vascular endothelial growth factor (VEGF) induced angiogenesis, suppression of inflammatory cell migration and adhesion, angiogenesis, inhibition of thrombosis and coagulation. The impairment of eNOS causes the endothelial dysfunction and oxidative stress which further increases the atherogenesis. The endothelial NOS3 protein, responsible for the production of NO, was found down regulated and vascular endothelium glycoprotein ENG, involved in the negative regulation of NO production, was found up regulated. . Therefore, the reduction in NO bioavailability, resulting from reduced NO production and/or increased NO degradation by superoxide anion, describes the onset of endothelial dysfunction[122]. Furthermore, a drastic alteration in mitochondrial respiratory chain complexes was described by network analyses. COX5B, COX6C, CYC1, ETFA, ETFB, NDUFA10, NDUFA11, NDUFA5, NDUFA7, NDUFA8, NDUFA9, NDUFB10, NDUFS1, NDUFS3, NDUFV2, SDHA, SDHB, SLC25A13, UQCRFS1 and UQCRH proteins are the major down-regulated proteins in mitochondrial respiratory chain complex.

In summary the mechanisms underlying endothelial dysfunction implicates metabolic alterations and oxidative stress related event increment.

## 2.4 Novelty and significance of the study:

**What is new?**

- This is the first ever study performed to explore the proteomic signatures with patient-derived pathological ECs to unveil underlying pathophysiological mechanisms in endothelial dysfunction associated with CTEPH.

**What is Relevant?**

- Quantitative proteomic profiling in endothelial dysfunction reveals the differentially regulated proteins that might behave as a biomarker signature of vascular injury, metabolism and oxidative stress.
- The overexpression of PLOD2 and ENG strongly associated with thrombus formation, platelet aggregation and angiogenesis that might play a key role endothelial dysfunction of CTEPH.
- Increased production of oxidants and decreased production of anti-oxidant biomarkers as well as down regulation of protein which had an antioxidant property strongly explained the correlation of the role of oxidative stress in endothelial dysfunction of CTEPH.

# Chapter - 3

# 3 *Oxidative stress/redox status in HCAEC-AMI and CTEPH-ECs:*

## 3.1 Abstract:

Oxidative stress is one of the major mechanisms involved in the development and progression of several cardiovascular diseases. However, the role of oxidative stress in causing/developing the endothelial dysfunctionality associated with AMI and CTEP diseases remains unknown. Therefore, the aim of this study was focused to investigate the oxidants/redox status in pathological ECs of AMI and CTEPH to elucidate the role of oxidative stress in determining EC dysfunctionality. Quantitative proteomics studies indicated the alteration in the expression of several of proteins, responsible for maintaining the balance between oxidants and antioxidants. To further investigate the status of oxidative stress biomarkers in dysfunctional ECs, the levels of total advanced oxidation protein products (AOPPs), total protein carbonyl content (PCOs), intracellular reactive oxygen species (ROS), ratio of GSH to GSSG, ratio of NADPH to NADP and SOD activity in dysfunctional ECs of AMI and CTEPH were analysed. The differences between pathological ECs and control cells of both AMI and CTEPH diseases resulted significant. The production of AOPPs, PCOs, and intracellular ROS in HCAEC-AMI and CTEPH-ECs were increased. Interestingly, the amount GSH/GSSG and NADPH to NADP ratios in dysfunctional ECs were reduced, a clear indication of oxidative stress involvement in the endothelial dysfunction.

## 3.2 Brief introduction:

Oxidative stress is one of the characteristics of endothelial dysfunction. The oxidative modifications of proteins are an irreversible process, leading to pathological conditions of the vascular system[128]. Hyperglycemia is known to increase oxidative stress[129]. The glycolytic activity is relatively higher in the endothelial cells compared to the other cells. The glycolytic flux in ECs is >200-fold higher than glucose, fatty acid, and glutamine oxidation, resulting in the generation of >85% of the total cellular ATP content[130]. The hyperglycemia promotes the cellular reactive oxygen species (ROS) production through direct glucose auto-oxidation, advanced glycation end product-dependent NADPH activation and mitochondrial superoxide production. Therefore, ROS generated in the atherosclerotic plaque, may be implicated in the disease process and in favouring plaque instability. Oxidative stress occurs due to the imbalance between oxidants and antioxidants that promotes CAD and plaque vulnerability. The cells present in the vascular system such as endothelial cells, adventitial cells, and smooth muscle cells can produce ROS. Due to the increased production of ROS coupled with decreased antioxidant defence, the integrity of the vessel wall is compromised in the patients with vascular diseases. The ROS might activate the signals that further increase endothelial barrier dysfunction, smooth muscle hypercontractility, and vascular remodeling[131]. Studies have been reported the contribution of oxidative stress in the pathogenesis of PAH and atherosclerosis[132–135] and oxidative stress markers increased after MI[136].

AOPPs are a family of compounds generated by protein oxidation and widely recognized as markers for the progression of several diseases like.atherosclerosis[128,137], systemic sclerosis[138], renal complications[139], diabetes mellitus[140], and HIV-positive patients[141].

## 3.3 Results:

AOPPs, PCOs and intracellular ROS were assessed as oxidative biomarkers. The ratio of GSH/GSSG, ratio of NADPH/NADP and SOD activity were evaluated as antioxidative biomarkers.

AOPPs are produced by the cross-link reaction of plasma proteins with chlorinated oxidants, such as hypochlorous acid and chloramines during oxidative stress. The biological role of AOPPs is similar to AGEs proteins. The levels of AOPPs measured in dysfunctional ECs of AMI and CTEPH resulted significantly higher related to control cells (Figure 3.1a and b). These results

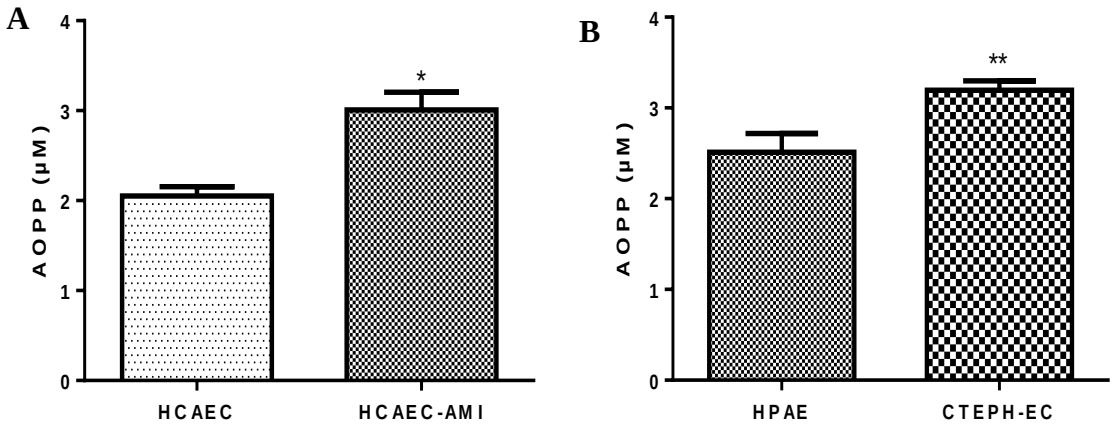


Figure 3.1: Levels of AOPPs in dysfunctional ECs. Patient derived pathological ECs exhibited explicit reactions to oxidative stress. A) Bar graph represents the total quantity AOPPs produced in control and HCAEC-AMI cells (N=12) B) Bar graph represents the total quantity AOPPs produced in control and CTEPH-ECs (N=9). Results were expressed as mean ± SEM. *p-value <0.05, **<0.01, ***<0.001.

indicated that ECs are more susceptible to protein oxidation. Protein carbonylation is one of the protein modifications, usually occurs due to the oxidation of lysine, arginine, threonine and proline amino acids or interaction with ROS and oxidized lipids.

The total protein carbonyls content (PCOs) was also higher related to controls (Figure 3.2a and b). In addition, the levels of intracellular ROS resulted higher in the dysfunctional ECs of AMI and CTEPH(Figure 3.3a and b).

To study the status of antioxidant levels the GSH (reduced) and GSSG (oxidized) ratio was measured. GSH is a major tissue antioxidant that provides reducing equivalents for the glutathione peroxidase (GPx) catalyzed reduction of lipid hydroperoxides to their corresponding alcohols and hydrogen peroxide to water.

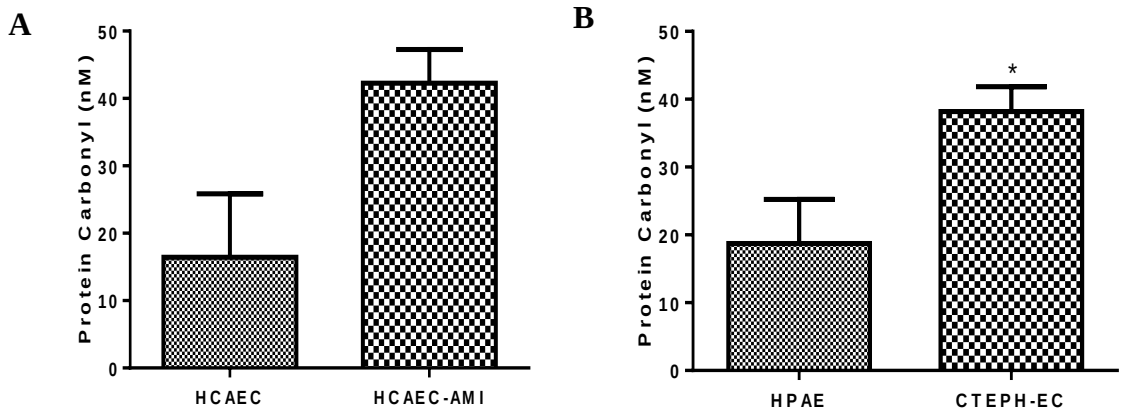


Figure 3.2: Status of PCOs in dysfunctional ECs. A) Bar graph represents the total PCOs produced in control and HCAEC-AMI cells (N=12) B) Bar graph represents the total quantity of PCOs produced in control and CTEPH-ECs (N=6). Results were expressed as means ± SEM. *p-value <0.05, **<0.01, ***<0.001.

In the GPx catalyzed reaction, the formation of a disulfide bond between two GSH molecules gives rise to oxidized glutathione (GSSG). The enzyme glutathione reductase (GR) recycles GSSG to GSH with the simultaneous oxidation of β-nicotinamide adenine dinucleotide phosphate (β-NADPH2). The GSH to GSSG ratios were decreased in the pathological endothelial cells of AMI and CTEPH (Figure 3.4a and b), showing an increase of oxidative stress that induce the accumulation of GSSG.

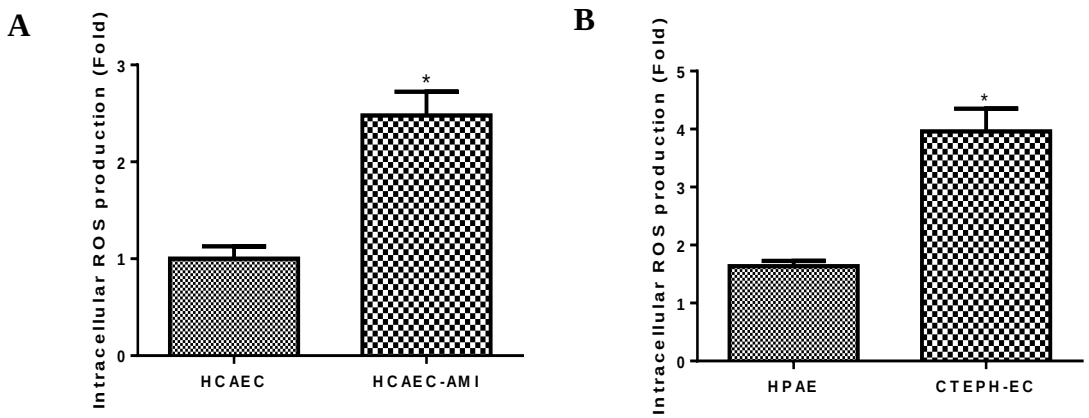


Figure 3.4: Levels of intracellular ROS produced in dysfunctional ECs. A) Bar graph represents the total ROS produced in control and HCAEC-AMI cells (N=21) B) Bar graph represents the total ROS produced in control and CTEPH-ECs (N=15). Results were expressed as means ± SEM. *p-value <0.05, **<0.01, ***<0.001.

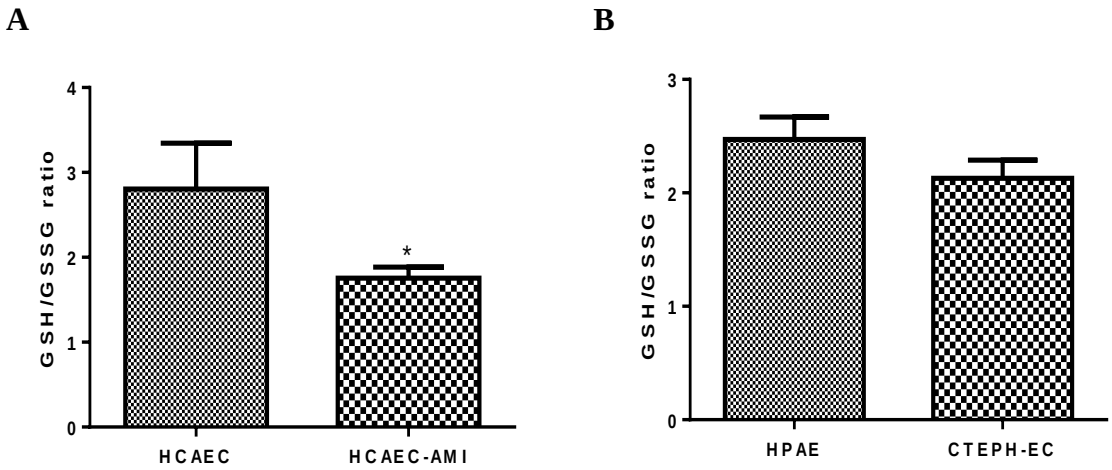


Figure 3.4: Ratio of GSH/GSSG produced in dysfunctional ECs. A) Bar graph represents the ratio of GSH/GSSG in control and HCAEC-AMI cells (N=12) B) Bar graph represents the ratio of GSH/GSSG in control and CTEPH-ECs (N=6). Results were expressed as means ± SEM. *p-value <0.05, **<0.01, ***<0.001.

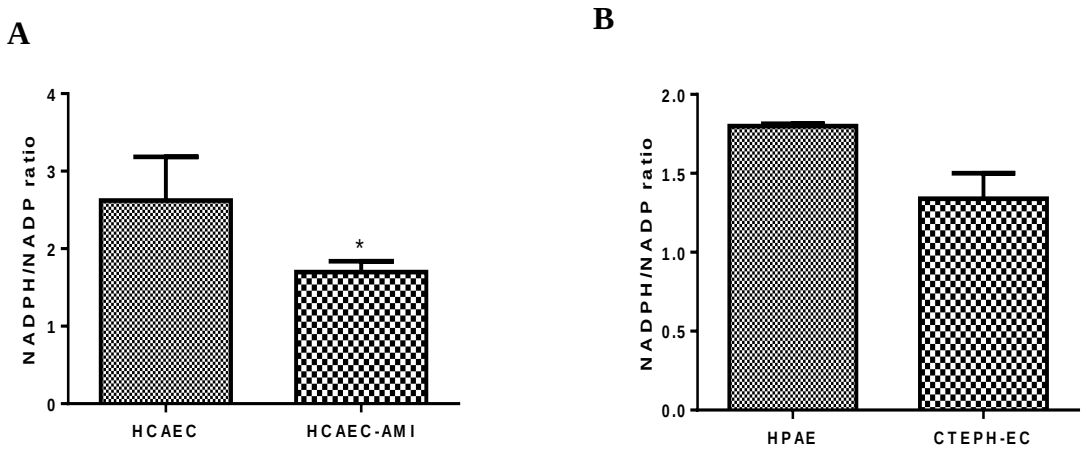


Figure 3.6: Ratio of NADPH/NADP produced in dysfunctional ECs. A) Bar graph represents the ration of NADPH/NADP in control and HCAEC-AMI cells (N=10) B) Bar graph represents the ratio of NADPH/NADP in control, and CTEPH-ECs (N=10). Results were expressed as means ± SEM. *p-value <0.05, **<0.01, ***<0.001.

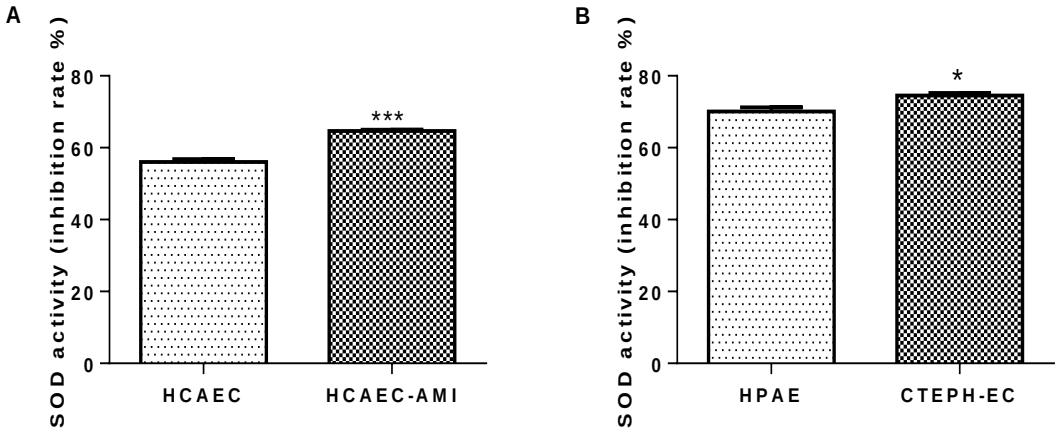


Figure 3.6: SOD activity in dysfunctional Es. A) Bar graph represents the SOD activity in control and HCAEC-AMI cells (N=12) B) Bar graph represents the SOD activity in control and CTEPH-ECs (N=6). SOD activity represented the percentage of the inhibition of water-soluble tetrazolium salt (WST-1). Results were expressed as means ± SEM. *p-value <0.05, **<0.01, ***<0.001.

The ratio of NADPH to NADP were reduced (Figure 3.5a and b) and the SOD activity slightly increased (Figure3.6a and b) in both pathological ECs of AMI and CTEPH. Interestingly these findings indicate the potential role of oxidative stress in both dysfunctionality of endothelial system, coronary artery and pulmonary artery ECs.

## 3.4 Discussion:

In this work, the concentrations of AOPPs and PCOs resulted higher in both AMI and CTEPH diseases. The increased levels of AOPPs might explain the involvement of higher global inflammatory activity in endothelial dysfunction[142]. Increased AOPPs production might be involved in the generation of various types of ROS[143]. The accumulation of ROS has been well established in the pathogenesis of several diseases including diabetes[144], atherosclerosis[145], renal ischemia[146], inflammatory diseases[147]. and cancer[148]. Increased production of ROS in dysfunctional ECs might enhance proinflammatory pathways and affect protein, lipid and enzymatic activity.

When cells are exposed to oxidative stress, the SOD enzyme comes into the action as a cellular defence against oxidative stress caused by free radicals. This enzyme reacts with oxidizing radicals to produce non-radical products. SOD is a copper-containing enzyme, usually occur in cells and tissues such as erythrocytes, liver, and brain. It is a free radical metabolizing enzyme, catalyzing the dismutation of superoxide anion to hydrogen peroxide. It protects the cell membrane from damage caused by highly reactive species. In our analysis, we found a slight increase in the production of SOD in both coronary and pulmonary artery pathological ECs. Low SOD levels have been reported in patients following angina pectoris and myocardial infarction[149]. Based on these findings, it is evident that the level of SOD in the blood of patients suffering from AMI is low when compared to the healthy controls. The down regulation of SOD might be considered as the first line of defence against oxidative stress. Further experiments need to be done to confirm this hypothesis.

Glutathione, a major non-protein thiol in living organisms, plays a central role in coordinating the body's antioxidant defence processes[150–152]. Perturbation of glutathione status of a biological system has been reported to lead to serious consequences. In the present study, low level of GSH in AMI and CTEPH dysfunctional ECs was observed. Interestingly quantitative proteomics analysis showed a down-regulation of GPX4 and GPX1 proteins that catalyse the formation of

glutathione disulphide in presence of hydrogen peroxide (Appendix Table 4). As described before GPX1 decreased the bioavailability of NO and increased the oxidative stress[127]. Therefore, the underlying mechanisms might be attributed to the unavailability of GSH, the substrate for GPX. The capacity of the glutathione system to cope with free radicals mainly depends upon the activity of peroxidase and glutathione reductase. Glutathione reductase (GR) keeps a high ratio of GSH/GSSG in normal cells. In AMI and CTEPH ECs glutathione reductase might be in lower levels, which in turn is linked to the decreased concentration of GPx and reduced glutathione. Moreover, NADPH oxidase-derived ROS play a role in vascular pathology as well as in the maintenance of normal physiological vascular function[153]. NADPH has been suggested to act as an indirectly operating antioxidant, thus maintaining the antioxidative power of glutathione[154]. In the present study, lower level of NADPH was observed in AMI and CTEPH, suggesting the increased oxidative stress in dysfunctional ECs.

# PART-II

# Chapter – 4

# 4 *Effects of PFKFB3 modulators in HCAEC-AMI, CTEPH-EC and Ea. hy926 cells*

## 4.1 Brief introduction:

Endothelium plays an important role in the regulation of vascular tone. Alterations in ECs or endothelial dysfunction are associated with many metabolic abnormalities and vascular diseases such as atherosclerosis, AMI and CTEPH. Recent evidences suggest that ECs in angiogenesis process relied on increased glycolysis activity instead of oxidative phosphorylation to generate energy for maintaining the cellular functions[155,156]. Additionally, the glycolytic flux in ECs are >200-fold than glucose, fatty acid and glutamine oxidation resulting in the generation of >85% of the total cellular ATP content[130]. Moreover, an inflammatory activation of monocytes/macrophages, via Toll-like receptor ligands or pro-inflammatory cytokines, switches their metabolism from oxidative phosphorylation to aerobic glycolysis, further potentiating the inflammatory process[157]. In glycolytic flux, the conversion of fructose-6-phosphate (F-6-P) to fructose-2,6-bisphosphate (F-2,6-P2) is one of the rate-limiting checkpoints modulated by 6-phosphofructo-2-kinase/fructose-2,6-bisphosphatases (PFKFBs), dimeric bifunctional enzymes. Therefore, PFKFBs plays a crucial role in maintain glucose homeostasis and controls the rate of glycolysis in other tissues.

Among four existing PFKFBs isoforms, PFKFB3 is upregulated by inflammatory stimuli. PFKFB3-driven glycolysis is important for angiogenesis and the migration of ECs and PFKFB3-knockdown ECs exhibit defects in the formation of filopodia and lamellipodia[158,159]. Consequently, the significant role of glycolytic enzyme PFKFB3 in angiogenesis delivers opportunities for therapeutic targeting. Strategies targeting pathological angiogenesis have focused primarily on blocking vascular endothelial growth factor (VEGF), but resistance and insufficient efficacy limit its success, mandating alternative antiangiogenic strategies. As a result, there is a strong high need for additional pharmacological interventions that counteract intra-plaque (IP) neovessel formation to prevent plaque rupture and its cardiovascular complications[160].

PFKFB3 has a Kase to Pase activity ratio higher than the other isoforms of the enzyme, and different studies suggest that it is the causative molecule of the so-called “Warburg effect”[161]. PFKFB3’s enzymatic activity is finely controlled by the N-terminal autoregulatory domain (AD)

in the Kase region, possessing a β-hairpin structure (L5-V15). Its interaction with a large portion of the Pase-domain (PD, E344-S363) causes a molecular twist in the protein and increasing the Kase/Pase activity ratio. On the other hand, the deletion of the AD by the alternative mRNA splicing leads to an enzyme with a 7-fold higher Pase activity[162]. Pase activation leads to the reduction of F-2,6-P2, a decrease of PFK-1 activity, and finally to a reduced glycolysis. The cristal structure of PFKFB3 shown in Figure 4.1[163].

Based on the reported implications of PFKFB3 in glycolysis/oxidative stress and, consequently, in related pathological angiogenesis, this enzyme may serve as a very effective therapeutic target in the regulation of the glycolytic pathway to control neovessels formation in the atherogenic process.

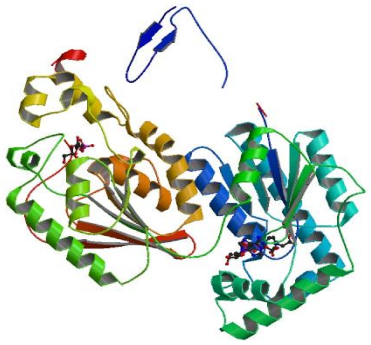

Figure 4.1: Crystal structure of the human inducible form of PFKFB3 from J. Bio. Chem[163]

ECs rely on increased glycolysis activity rather than oxidative phosphorylation to generate energy for maintaining the cellular functions in angiogenesis. The glycolytic activity of ECs is critical for angiogenesis, and it has been demonstrated that reduction of glycolysis by silencing or blocking PFKFB3, results in impairment of EC proliferation, migration, and vascular sprouting *in vitro*[158,164]. Therefore, PFKFBs play a crucial role in maintaining glucose homeostasis and control the rate of glycolysis in other tissues. Among four existing PFKFBs isoforms, PFKFB3 is upregulated by inflammatory stimuli.

As a part of MOGLYNET project, we received three PFKFB3 phosphatase modulators such as HM-20 (YSGFLT), HM-21 (SFLLR-CONH 2) and HM-22 (wGy) from ESR10; Ligand94 from ESR1 as a kinase modulator of PFKFB3. The name, structure and molecular weight of these compounds were specified in Figure 4.2 and Table 4.1.

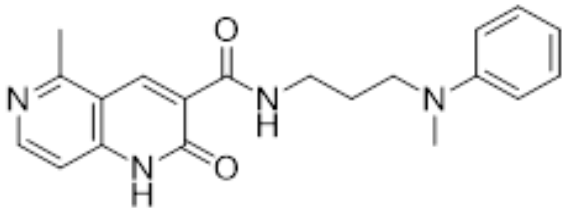

Molecular Weight: 350.42

5-methyl-N-(3-(methyl(phenyl)amino)propyl)-2-oxo-1,6-naphthyridine-3-carboxamide

Figure 4.2: Details of PFKFB3 kinase modulator produced in the MoGlyNet consortium

3PO [(3-(3-Pyridinyl)-1-(4-pyridinyl)-2-propen-1-one), PFKFB3 inhibitor] reduces vessel sprouting also in vivo (IP injection) in EC spheroids, zebrafish embryos, and the mouse retina by inhibiting EC proliferation and migration[160,165,166] Moreover, the compound has been shown to be selectively cytostatic to transformed cells, to suppress the tumorigenic growth of breast adenocarcinoma, leukemia, and lung adenocarcinoma cells *in vivo*[160,167]. More recently, it has been demonstrated that 3PO significantly represses intra-plaque angiogenesis and hemorrhages in mice, demonstrating its potential to prevent plaque rupture[168].

| NAME | SEQUENCE | STRUCTURE | MW |
|---|---|---|---|
| **HM-20** | YSGFLT | 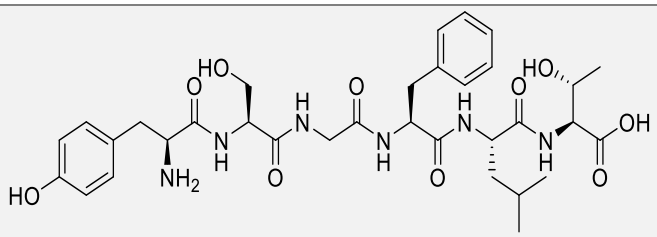 | 686.75 |
| **HM-21** | SFLLR-$CONH_2$ | 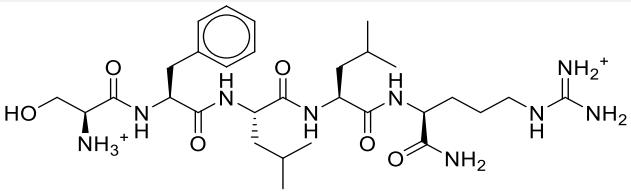 | 633.80 |
| **HM-22** | wGy | 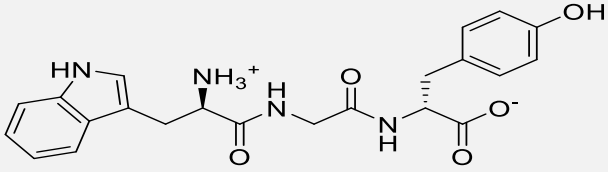 | 424.45 |

Table 4.1: Details of PFKFB3 phosphatase modulators produced in the MoGlyNet consortium

HM-22 has D-amino acids Trp (W) and Tyr (Y). Other amino acids are all L.

HM-21 and HM-22 have a free acid on C-terminal part, while HM-21 has an amide.

## Results:

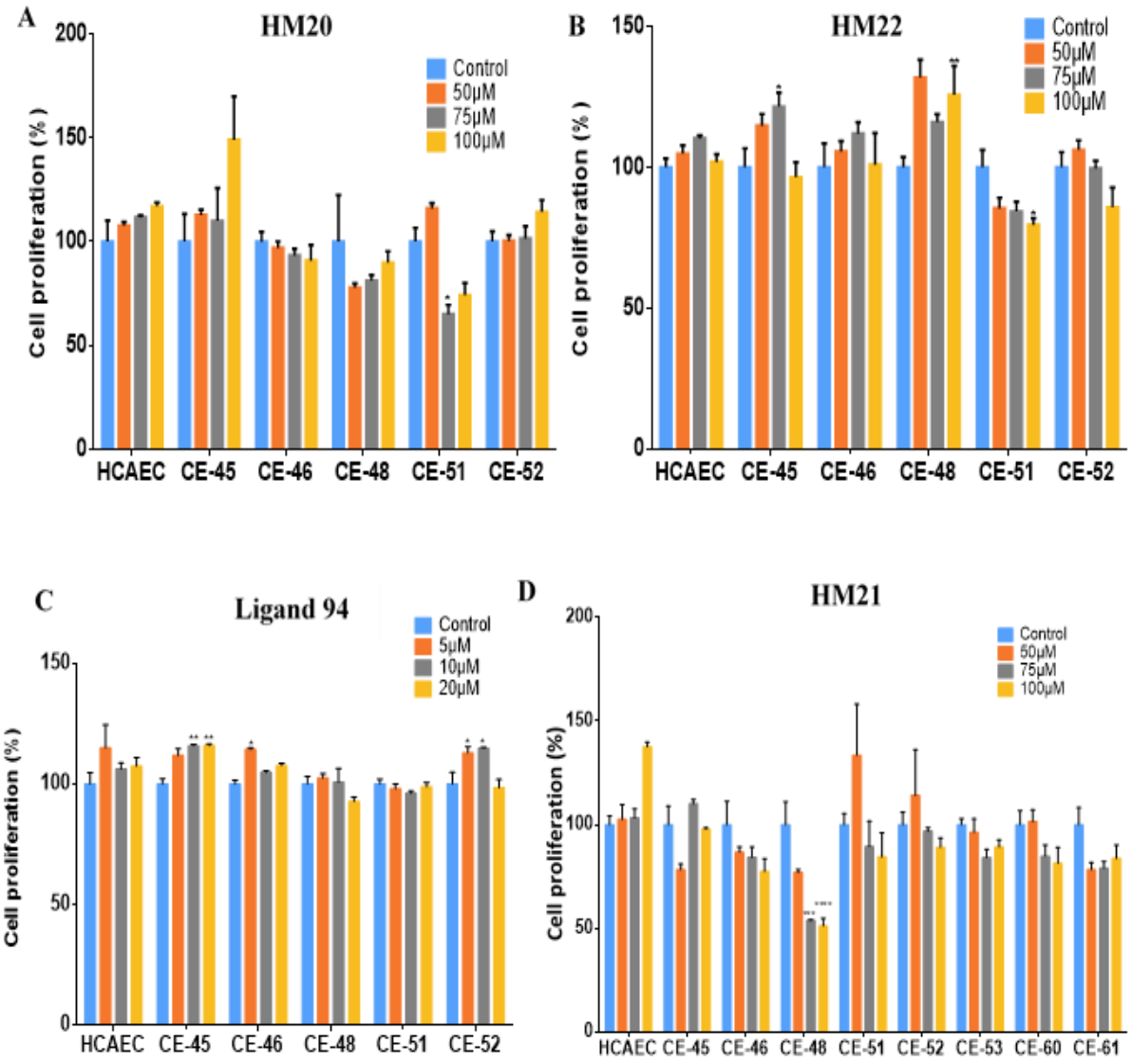


Figure 4.3: Effect of PFKFB3 modulators on HCAEC-AMI cells. CE-45, CE-46, CE-48, CE-51, CE-52, CE-53, CE-60 and CE-61 were corresponding to HACEC-AMI cells. Bar graphs represents the mean ± SEM. *p-value <0.05, **<0.01, ***<0.001.

### 4.1.1 Effect of phosphatase and kinase modulators of PFKFB3 on HCAEC-AMI cells:

Hoechst assay was performed to evaluate the cell proliferation upon incubation with three PFKFB3 phosphatase modulators and one kinase modulator of PFKFB3. HCAEC and HACEC-AMI cells were incubated with 50, 75 and 100µM of HM-20, HM-21 and HM-22; 5,10 and 20µM concentration of ligand 94 for 72hrs.

As shown in Figure - 4.3 A, B and C, HM-20, HM-22 and ligand 94 compounds were not able to reduce the cell proliferation significantly. While, HM-21 (D) showed variable results with pathological ECs.

### 4.1.2 Effect of phosphatase and kinase modulators of PFKFB3 on CTEPH-ECs:

Likewise, Hoechst assay was performed to evaluate the cell proliferation upon incubation with three PFKFB3 phosphatase modulators and one kinase modulator of PFKFB3. HPAE and CTEPH-ECs were incubated with 50, 75 and 100 µM of HM-20, HM-21 and HM-22; 5,10 and 20 µM concentration of ligand 94 for 72 hrs. As shown in Figure 4.4 A, B and C, these compounds were not effective on CTEPH-ECs.

### 4.1.3 *In vitro* screening test for phosphatase modulators of PFKFB3:

To confirm whether these phosphatase modulators targeting PFKFB3, a screening assay by using the macrophages was performed. PFKFB3 expression was activated in macrophages by incubating the cells with lipopolysaccharide (LPS) and cell proliferation was measured by using the Hoechst assay, after 72hrs incubation of PFKFB3 modulators. In this test, the known PFKFB3 inhibitor 3PO used as a positive control. As shown in Figure 4.5, HM-20 and HM22 was not able to show inhibitory effect on PFKFB3, while HM-21 showed inhibitory effect of PFKFB3 at 75 µM. However, HM-21 didn't show significant effect, considering the higher dosage. 3PO instead was able to significantly reduce the cell proliferation at lower concentrations. For this reason, 3PO was used as inhibitor of PFKFB3 for all the other experiments.

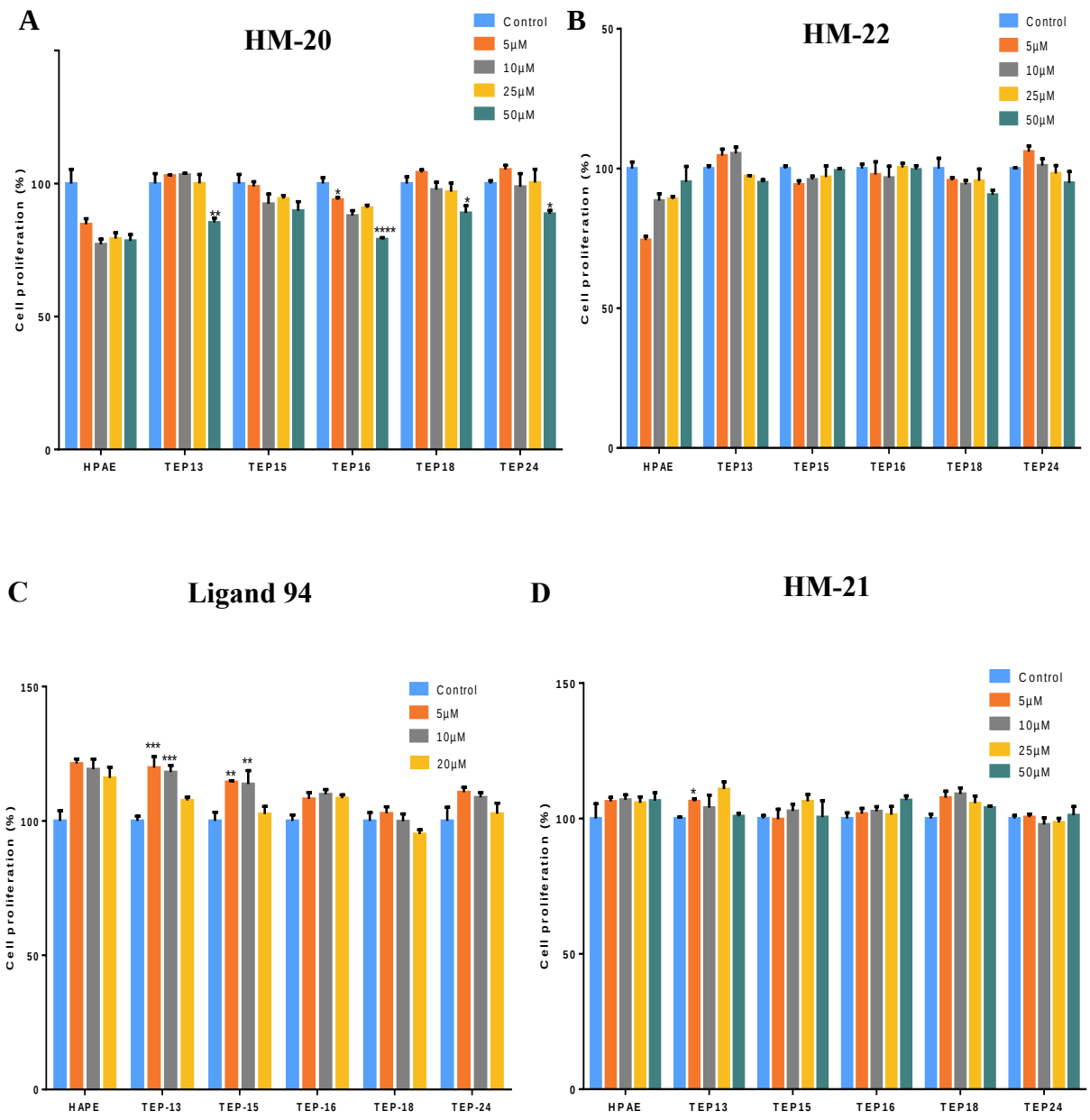


Figure 4.4: Effect of PFKFB3 modulators on CTEPH-ECs. TEP-13, TEP-15, TEP16, TEP-18, TEP-24 were corresponding to CTEPH-ECs. Bar graphs represents the mean ± SEM. *p-value <0.05, **<0.01, ***<0.001.

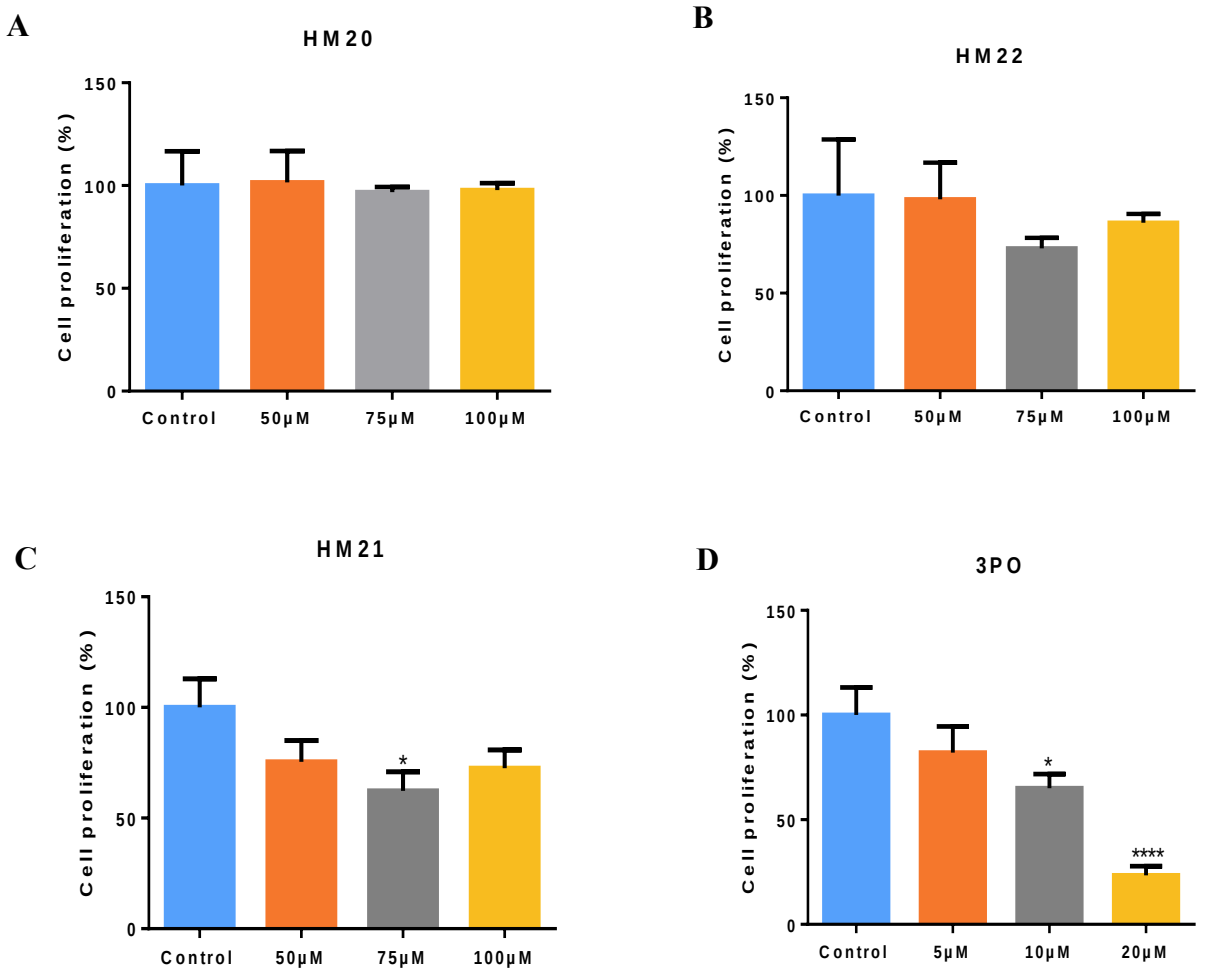


Figure 4.5: *In vitro* screening for phosphatase modulators of PFKFB3 and 3PO. Bar graphs represents the mean ± SEM. *p-value <0.05, **<0.01, ***<0.001.

### 4.1.4 Effect of 3PO on HCAEC-AMI and CTEPH-ECs:

To determine the dosage at which 3PO is able to reduce the proliferation of pathological ECs, Hoechst assay was performed by incubating 3PO at 5 µM-30 µM concentration in HCAEC-AMI and CTEPH-ECs for 72 hrs. As shown in Figure 4.6a, 5 µM concentration of 3PO was able to reduce proliferation in HCAEC-AMI. Similarly, 3PO was able to reduce the CTEPH-ECs proliferation at 20 µM concentration.

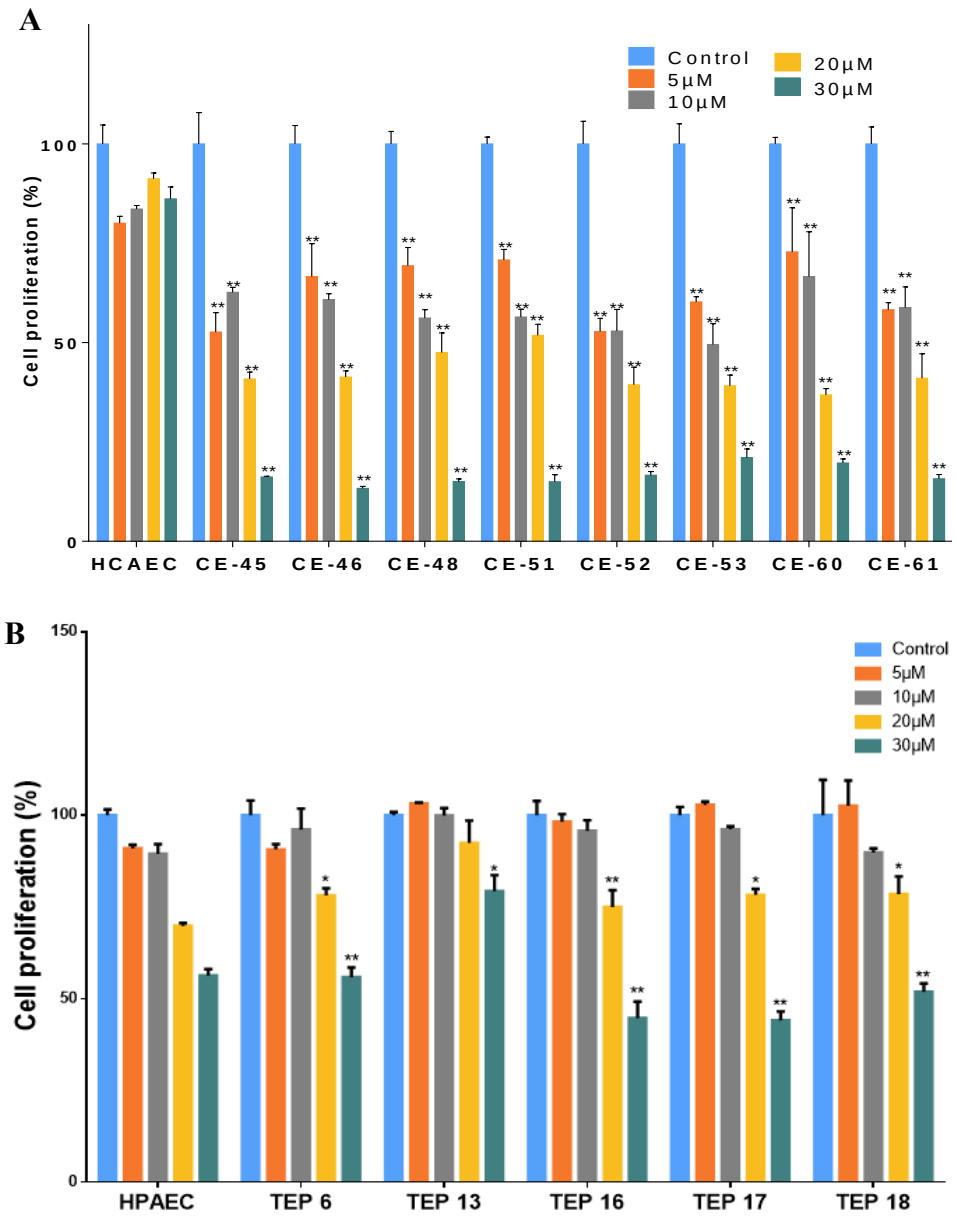


Figure 4.6: Effect of 3PO on A) HCAEC-AMI and B) CTEPH-ECs. Bar graphs represents the mean ± SEM. *p-value <0.05, **<0.01, ***<0.001.

## 4.2 Understanding the mode of action of 3PO in normal and TNFα induced inflamed human ECs by using proteomics approach.

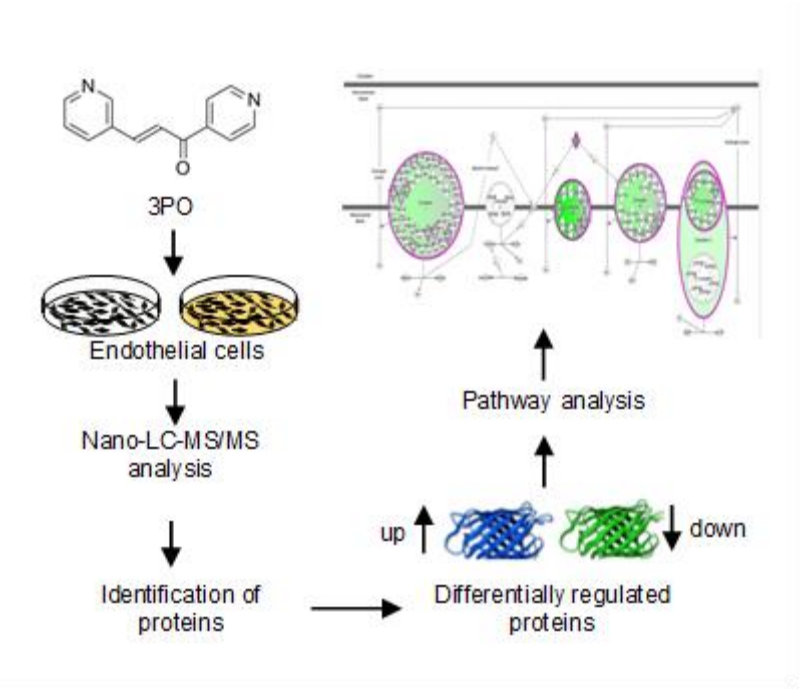


Figure 4.7: Graphical representation of abstract.

### 4.2.1 Abstract:

The molecular mechanism of action of 3PO at EC level under physiological or inflamed conditions remains to be established. Human ECs have been employed to monitor the protein changes induced by 3PO, a compound able to inhibit the glycolytic flux partially and transiently and to reduce pathological angiogenesis in a variety of disease models. Normal and TNFα induced inflamed ECs were incubated with and without 3PO at a concentration (20 μM) able to inhibit cell proliferation without cell death. At the end of the incubation period, samples were submitted to the following steps: a) whole protein extraction, reduction, alkylation, digestion by trypsin; b) peptides separation by nano-LC-MS/MS analysis by using a high-resolution mass spectrometer; c) data analysis including protein identification, quantification and statistical analysis. An altered protein expression profiling in combination with protein network analysis was employed by using a mass spectrometry-based label-free quantification approach to explore the underlying mechanisms of 3PO at cellular level.

### 4.2.2 Brief introduction:

3PO (Figure 4.8a), is a compound able to partially and transiently inhibit glycolysis *in vivo,* to reduce pathological angiogenesis[160], very likely thanks its ability to inhibit the PFKFB3 enzyme[167], an activator of a key glycolytic enzyme, 6-phosphofructo-1-kinase (PFK-1)[160]. However, high dose of 3PO (> 30µM) may cause tumor vessel disintegration and enhance cell dissemination[169]. Hence, identification and characterization of EC proteins whose expression is modulated by the effect of 3PO will expand our understanding of its mode of action. Inflammation, a complex biological response that has a fundamental role in various diseases (autoimmune, neurodegenerative, cardiovascular, cancer and microbial infectious diseases), is now recognized a key factor involved in all the stages of disease progression of atherosclerosis, and novel findings provide an important link among EC dysfunction, angiogenesis, inflammation and EC metabolism in several diseases[170–173]. Moreover, an inflammatory activation of monocytes/macrophages, via Toll-like receptor ligands or pro-inflammatory cytokines, switches their metabolism from oxidative phosphorylation to aerobic glycolysis, further potentiating the inflammatory process[157]. Notwithstanding the plethora of evidence indicating the key role of 3PO in reducing angiogenesis, the molecular mechanism of action of 3PO at EC level under physiological or inflamed conditions remains to be established. Recent findings indicate in fact that 3PO might act through mechanisms that are unrelated to PFKFB3 inhibition[174] and recent studies carried out with recombinant PFKFB3 and

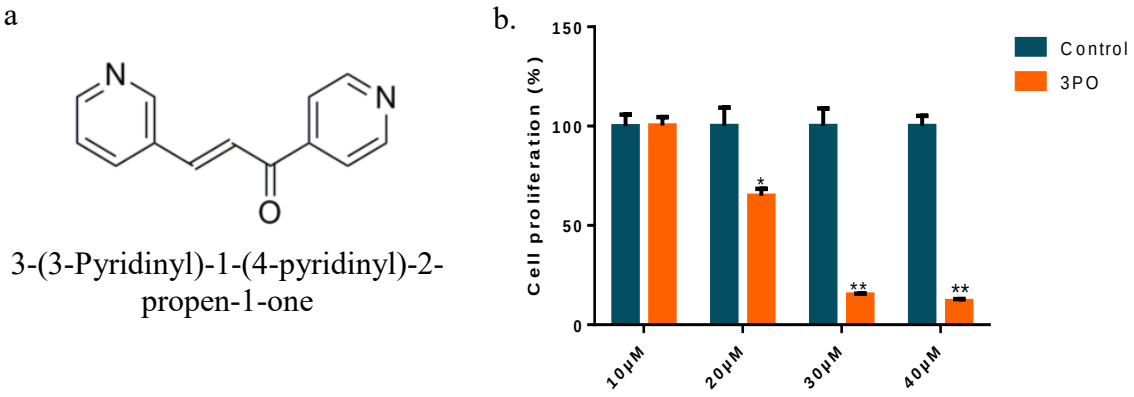


Figure 4.8: a) Structure of 3PO, b) Effect of 3PO on EA.hy926 cells proliferation. ECs were treated with 3PO at various concentrations (10, 20, 30 and 40µM) for 24h and percentage of cell proliferation was assessed by using MTT assay. All data represented as mean ± S.E.M. *P<0.05, **P<0.001 compared with control (N=3).

microscale thermophoresis (to evaluate its interaction with 3PO), did not confirm any binding of the molecule to the enzyme (personal communication).

### 4.2.3 Results and discussion:

To understand the 3PO molecular mechanism of action in the endothelium, in the presence or in absence of an inflammatory agent, EA.hy926 cells, a permanent human endothelial cell line[175] were used as model and tumor necrosis factor alpha (TNF-α), as an inflammatory agent. To check the concentration at which 3PO inhibited EC proliferation, EA. hy926 cells were treated with different 3PO concentrations (10-40μM) for 24 hours, and cell proliferation percentages were determined using MMT assay. As shown in Figure 4.8b, 20μM 3PO was able to have a significant cell proliferation inhibitory effect. (Supplementary Figure S.1 shows the cytotoxic effect of 3PO in Ea.hy926 cells).Therefore, this concentration was selected for further analysis. To induce the inflammation of endothelium, the cells with 10ng/ml concentration of TNFα were treated for 24hrs[176].

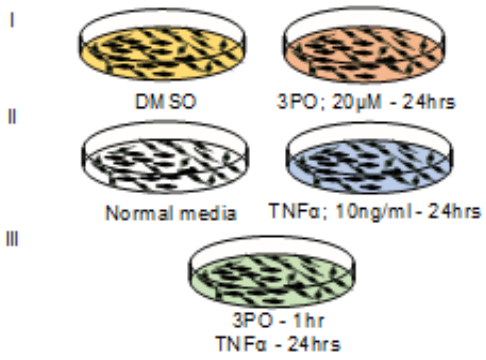


Figure 4.9: Cell treatments for the MS-based label-free quantitative proteomic analysis.

After all the treatments (Figure 4.9), cells were collected and subjected to the following steps: a) protein extraction, reduction, alkylation, in-solution digestion by trypsin; b) peptide separation by nano-LC-MS/MS analysis. The quality and reproducibility of biological replicates were determined by using multi-scatter plot analyses. The average Pearson coefficient was higher than 0.98 among all samples, indicating the high degree of reproducibility (Supplementary Figure S.2).

2214 proteins and 18869 unique peptides were identified and quantified by the Andromeda search engine in MaxQuant using *Uniprot_HomoSapiens* database; search parameters were: 10 ppm tolerance on peptides, 0.8 Da on fragments and less than 1% false discovery rate. A two-sample t-

test was employed using the latest version of Perseus software (v 1.6.1.3), to define the proteins that were differentially regulated in the treated and control groups of samples. 130 and 161 were up and down-regulated proteins in the 3PO treated ECs compared to the control group (Appendix Table 5). The distribution of differentially regulated proteins in ECs upon 3PO treatment is shown in Figure 4.10.

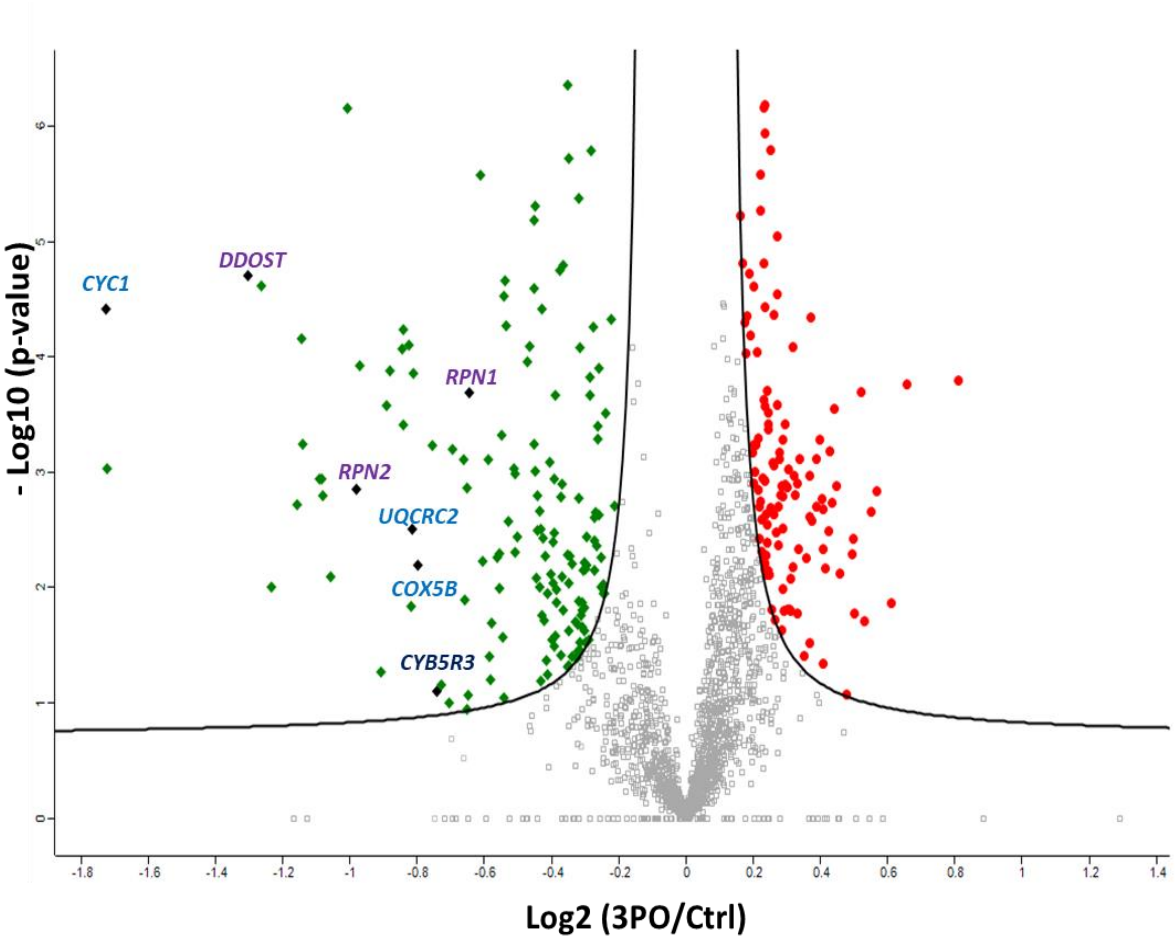


Figure 4.10: Distribution of differentially regulated proteins in ECs after 24h exposure with 3PO. Scatter plots of log2 fold change on x-axis against -log p-value on y-axis of significantly quantified proteins. Data was obtained from technical triplicates and biological duplicates. Green colour indicates down-regulation, red colour represents upregulation.

To describe the protein network, influenced by the drugs (3PO and 3PO/TNFα) Clue-GO plug-in in the latest version of Cytoscape software (v 3.6.0) and Ingenuity Pathway Analyses (IPA, Quiagen) were used. Figure 4.13a shows examples of differentially regulated pathways. Clearly

3PO targets mitochondria and down-regulated substrates such as cytochrome complex, mitochondrial respiratory chain complexes I, III and IV, oxidoreductase complex, mitochondrial membrane. Most of the down-regulated proteins such as CYC1 and ATP5L belong to mitochondrion inner membrane.

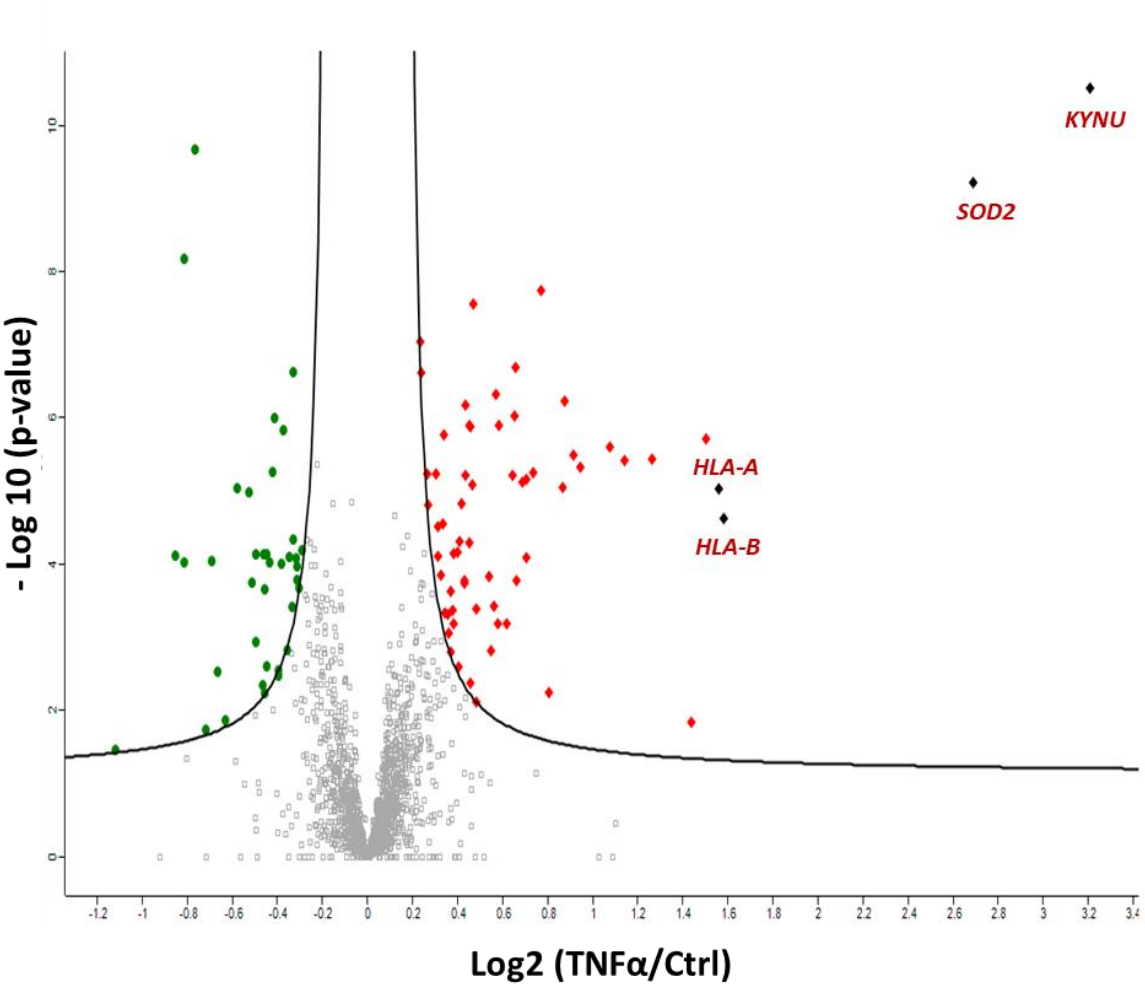


Figure 4.11: Distribution of differentially regulated proteins in ECs after the induction of inflammation with TNFα in the absence of 3PO. Scatter plots of log2 fold change on x-axis against -log p-value on y-axis of significantly quantified proteins. Data was obtained from technical triplicates and biological duplicates. Green colour indicates down-regulation, red colour represents upregulation.

CYC1 is a heme-containing component of the cytochrome b-c1 complex that shuttles electrons between complex III and complex IV in the respiratory chain. In normal conditions, ATP5L or

ATP synthase subunit g, is a part of complex V that produces ATP from ADP in the presence of the proton gradient generated across the membrane by electron transport complexes of the mitochondrial respiratory chain. However, 3PO might be blocking the proton gradient across the membrane via inhibition of the proteins associated with the multiplex complexes of the electron transport chain which may lead to the reduction of ATP synthesis. Therefore, the energy required for cellular metabolic activities and cell proliferation decreases.

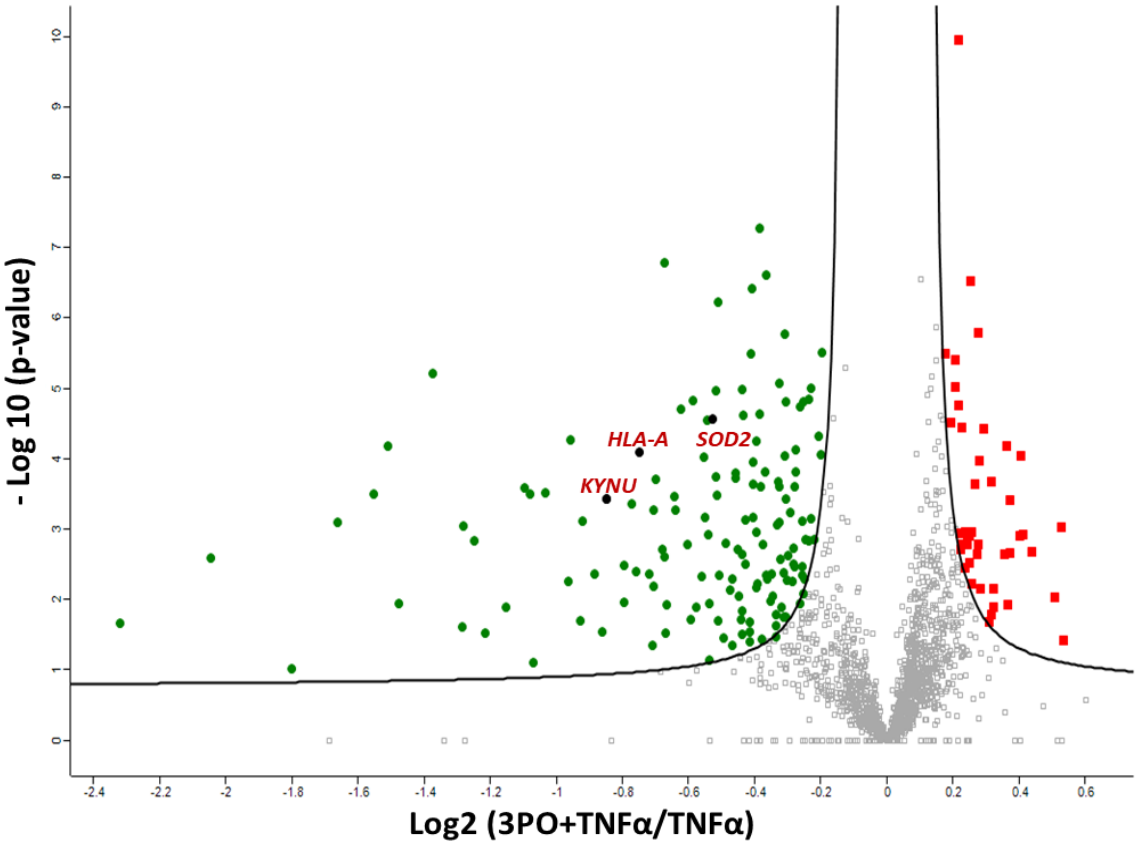


Figure 4.12: Distribution of differentially regulated proteins in ECs after induction of inflammation with TNFα in the presence of 3PO. Scatter plots of log2 fold change on x-axis against -log p-value on y-axis of significantly quantified proteins. Data was obtained from technical triplicates and biological duplicates. Green colour indicates down-regulation, red colour represents upregulation.

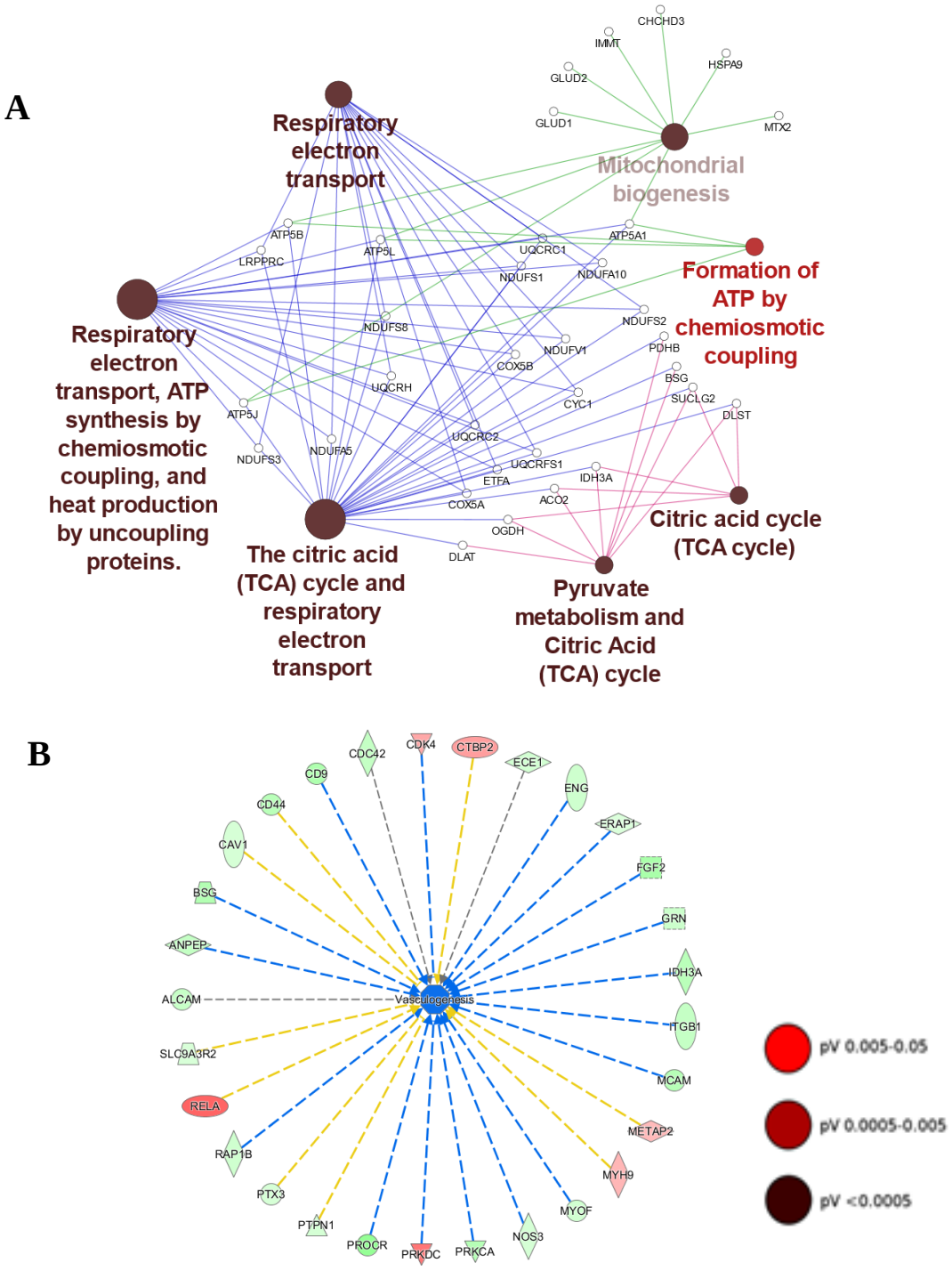


Figure 4.13: Main pathways and respective genes found in different treatments of ECs. ClueGo plugin for Cytoscape software was used for the Reactome network pathway analysis. a) and b) Key pathways of down-regulated proteins in ECs upon 3PO exposure for 24hrs. Significance of the clustering is shown by colour code and the size of nodes. (Figure 4.13b: Green colour indicates down-regulation, red colour represents upregulation of proteins.

Gene ontology enrichment analysis of molecular functions revealed that nucleoside-triphosphatase activity, electron transfer activity, GTPase activity, and coenzyme binding categories were significantly over-represented. In addition, Reactome pathway analysis (Figure 4.13) revealed also the inhibition of the citric acid (TCA) cycle, ATP synthesis by chemiosmotic coupling and pyruvate metabolism pathways. Under physiological conditions, pyruvate generated from glycolysis is converted into acetyl coA that enters into the TCA cycle and the resulting NADH enters into the electron transport chain to produce ATP.

This is essential for cell proliferation and cell metabolic activities. Studies have shown that increased levels of TCA intermediates increase anaerobic pathways and aerobic fatty acid oxidation for ATP production in macrophage-rich atherosclerotic arteries that further potentiate the cell proliferation[177]. Moreover, in the angiogenesis process, pathological cells generate more amount of ATP for their cellular activities. Additionally, as shown in Figure 4.13b, we also observed an inhibition of vasculogenesis pathway by 3PO. The tetraspanin family related cell surface glycoprotein such as CD9, which is a crucial protein in the suppression of cancer cell motility, metastasis, differentiation, signal transduction, and cell adhesion[178] showed down-regulation. It also involves in the platelet activation and aggregation.

The down-regulation of FGF2 by 3PO indicates the reduction of cell division, cell differentiation, cell migration, and angiogenesis[179]. In addition to this, 3PO reduced the expression of PROCR protein, which is implicated in blood coagulation, venous thromboembolism, myocardial infarction, and cancer[180]. Based on these results, we can hypothesize that 3PO might play a vital role in reducing platelet aggregation, blood coagulation, angiogenesis, and tumour formation. On the other hand, we also identified the down-regulation of oxidative phosphorylation, VEGF, cytokine and focal adhesion, and cell movement of endothelial cell signaling pathways by 3PO (Supplementary Figure S.3 to S.7).

In the second step, under the TNFα induced inflamed ECs in the absence of 3PO, 75 up and 48 down-regulated proteins resulted. The distribution of differentially regulated proteins is reported in Figure 4.11, and their log2 fold change are reported in (Appendix Table 6). As, there was an upregulation of inflammatory and oxidative stress-related proteins such as HLA class I histocompatibility antigen A/B, superoxide dismutase (SOD2) and kynureninase (KYNU) proteins.

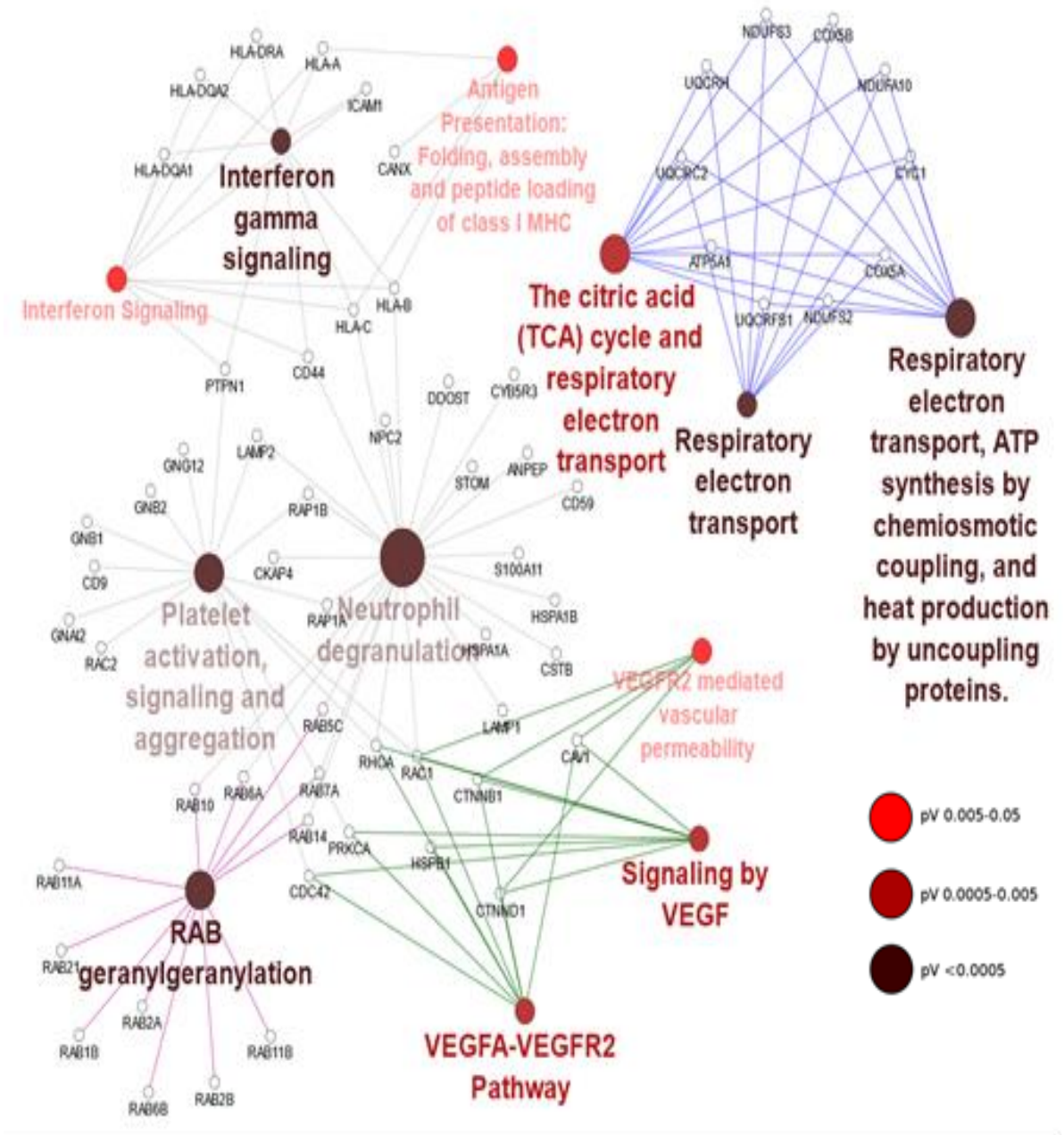


Figure 4.14: Main pathways and respective genes found in different treatments of ECs. ClueGo plugin for Cytoscape software was used for the Reactome network pathway analysis. Major pathways associated with down-regulated genes in inflammatory condition stimulated by using TNFα, in the presence of 3PO. Significance of the clustering is shown by colour code and the size of nodes.

Additionally, in gene ontology enrichment analysis, more than 80% of upregulated proteins are involved in the inflammatory-related biological process including response to interferon-gamma (36.36%), type I interferon signaling pathway (36.36%) and negative regulation of type I interferon production (9.09%). On the other hand, more than 88% of cellular components belong to the MHC class I protein complex. Moreover, network analysis of upregulated proteins revealed the upregulation of pathway represented by enriched KEGG terms: interferon signaling, antigen presentation process, activation of NF-kappa B and regulation of Hypoxia-inducible factor by Oxygen. These results significantly explain the successful induction of inflammation in ECs with the use of TNFα.

In the third step, the anti-inflammatory property of 3PO was evaluated. ECs were treated with 20μM of 3PO for 1hr, followed by 24hrs incubation with 10ng/ml concentration of TNFα . In this analysis, 40 were up and 140 down-regulated proteins, respectively. The distribution of differentially regulated proteins in the presence of 3PO in TNFα induced inflamed ECs were reported in Figure 4.12, and their precise log2 fold change variations is reported in Appendix Table 7. Interestingly, the inflammatory and oxidative stress-related proteins expression completely reversed (Table 4.2), in the presence of 3PO that minimizes the effect of subsequent TNF-alpha treatment. For example, HLA-A showed a fold change of 2.9 in inflamed cells and 0.6 in inflamed cells previously treated with 3PO (Figure 4.11, and 4.12) and SOD 2 showed a fold change of 6.4 in inflamed cells and 0.7 in inflamed cells previous treated with 3PO (Figure 4.11, and 4.12; Table 4.2). In addition, intercellular adhesion molecule 1 (ICAM 1), a specific marker of inflammation, that was down regulated in the presence of 3PO (fold change of 0.7, Appendix Table 7) was also found. Moreover, TCA cycle and respiratory electron transport chain pathways were inhibited as in the 3PO treated cells in the absence of inflammation. The corresponding down-regulated proteins and their interactions in network pathways are reported in Figure 4.14. Several studies have reported that 3PO reduces angiogenesis by inhibiting the activity of vascular endothelial growth factor (VEGF)[160,181]. Similarly, in this study 3PO showed an inhibition of VEGFA-VEGFR2 and VEGF signaling pathways (Figure 4.14). Interestingly, in the presence of 3PO in TNFα induced inflammatory ECs, these pathways were inhibited that resembles the anti-inflammatory property of 3PO. The network analyses highlighted other pathways, such as RAB geranyl-geranylation, neutrophil degranulation, and platelet activation, signaling and aggregation pathways due to the down-regulation of corresponding proteins (Figure 4.14).

| Protein name | Gene Symbol | Log2 (3PO/Ctrl) | Log2 (TNF-α /Ctrl) | Log2 (3PO+TNF-α /TNF-α) |
|---|---|---|---|---|
| Thioredoxin reductase 1, cytoplasmic | TXNRD1 | -0.35 | 0.38 | -0.39 |
| HLA class I histocompatibility antigen | HLA-A; HLA-B | -0.42 | 1.56 | -0.75 |
| Prolyl 4-hydroxylase subunit alpha-2 | P4HA2 | -0.43 | 0.65 | -0.56 |
| Serine palmitoyltransferase 2 | SPTLC2 | -0.43 | -0.30 | -0.28 |
| Kynureninase | KYNU | - | 3.21 | -0.85 |
| Superoxide dismutase;Superoxide dismutase [Mn], mitochondrial | SOD2 | - | 2.69 | -0.53 |
| Guanylate binding protein 1, interferon-inducible, 67kD variant | GBP1 | - | 1.14 | -0.32 |
| Calnexin | CANX | -1.26 | - | -1.38 |
| Dolichyl-diphosphooligosaccharide--protein glycosyltransferase 48 kDa subunit | DDOST | -1.30 | - | -1.66 |
| MICOS complex subunit MIC60 | IMMT | -1.72 | - | -2.05 |
| Cytochrome c1, heme protein, mitochondrial | CYC1 | -1.72 | - | -2.32 |

Table 4.2: Main up and down-regulated proteins in differently treated cells

To further validate the anti-inflammatory effect of 3PO, RT-PCR analysis was performed. As shown in Figure 4.15, the inflammatory marker proteins were upregulated in inflamed ECs.

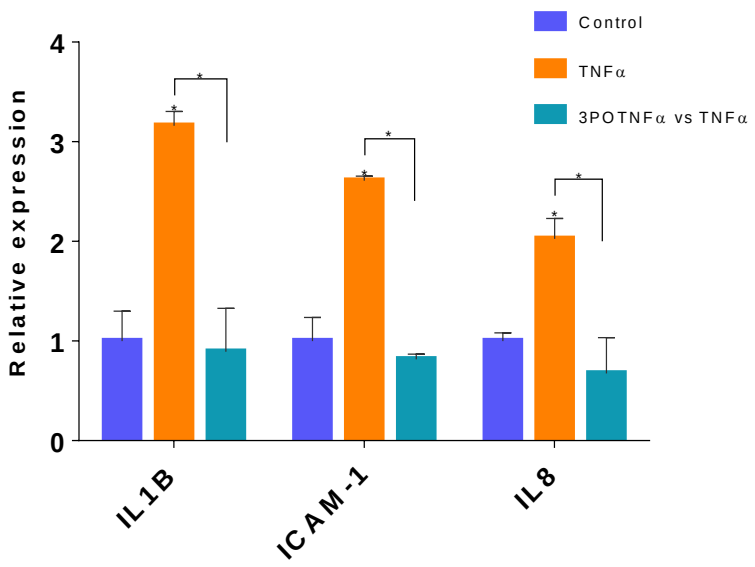


Figure 4.15: Quantitative RT-PCR was performed with inflammatory marker genes such as IL1B, ICAM-1 and IL8 and normalized with β-actin housekeeping gene. TNFα incubated ECs were compared with respective control. Inflamed ECs with 3PO were compared against untreated inflamed ECs (TNFα). The data represented as mean ± SEM (*P<0.05, N=3).

However, after the 3PO treatment, the expressions of ICAM-1, IL1B, and IL8 were reduced. ICAM-1, which was also down regulated in proteomics approach, is one of the plasma marker proteins for endothelial dysfunction or inflammation associated with myocardial infarction and other cardiovascular diseases[182,183] Altogether, the obtained results at proteomic and transcriptome levels clearly indicate the accuracy of network description and the inflammatory preventive character of 3PO by mass spectrometry-based proteomics.

In conclusion 3PO has multiple targets in the ECs, targeting mitochondrial inner membrane and it inhibits the important cellular pathways including the TCA cycle, the mitochondrial respiratory chain, and vasculogenesis that may be useful for understanding an inhibitory effect of 3PO on EC proliferation and migration. Therefore, present data suggests a potential application of this molecule as a starting point in designing novel molecules to prevent diseases where inflammatory reactions are involved, such as in atherosclerosis, cancer or neurodegenerative diseases.

## 4.3 Determination of binding site of 3PO:

After obtaining the significant anti-angiogenic and anti-inflammatory properties of 3PO, we decided to understand the selectivity of 3PO to the specific targets. For this purpose, we challenge the selectivity of 3PO towards human serum and human serum albumin (HSA).

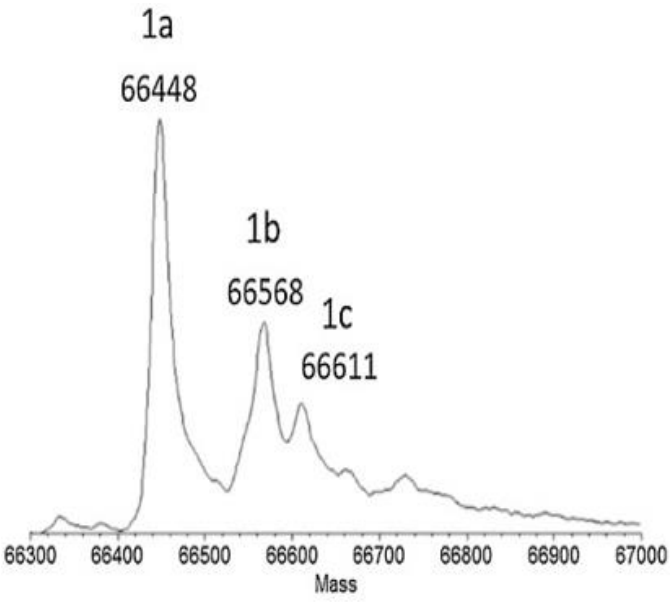


Figure 4.16: Deconvoluted spectrum showing the experimental molecular weight for albumin (1a), cysteinylated albumin (1b) and glycated albumin (1c).

Initially we performed an intact protein analysis of human serum incubating with 3PO by using direct infusion on a triple-quadrupole (TQ) MS. Figure 4.16, showed the deconvoluted mass spectrum of albumin contained in a blank sample, which consisted of serum incubated for 3h at 37°C. In detail, the spectrum showing a triplet of signals attributed to albumin, cysteinylated albumin and glycated albumin (Figure 4.16, peaks a–c, respectively)[184]. Similarly, the shape of the serum spectrum remained same at the beginning of spiking with 1mM 3PO (data not shown).

The HSA spectrum acquired after 15min, 1h and 3h incubation with 3PO. The deconvolution of the mass spectrum acquired allowed the identification of an adduct. This adduct was detected at 66661 Da (Figure 4.17, 1d) that increased in intensity from 15 min to 1h and remained same at 3h. It has a nominal shift of 210 Da, which corresponds to the nominal mass of 3PO. Interestingly, the albumin and its cysteinylated and glycated forms were still detectable (Figure 4.17, 1b and 1c, respectively).

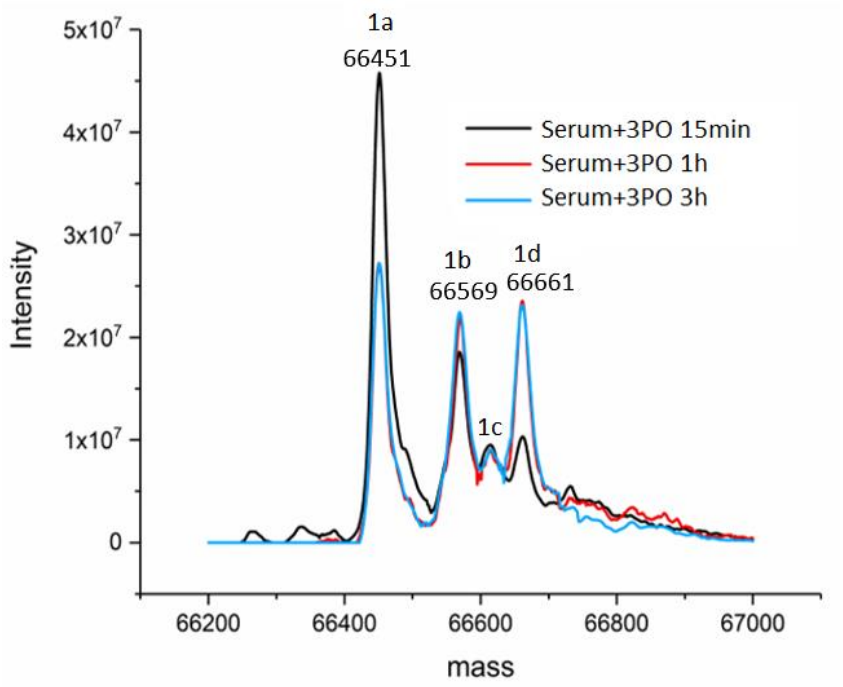


Figure 4.17: Deconvoluted spectrum of albumin in serum spiked with 3PO. Native albumin (1a), cysteinylated albumin (1b), glycated albumin (1c) and adduct formed by 3PO (1d).

However, the intensity of native albumin peak was reduced as the intensity of adduct increased with incubation time. Therefore, the spectrum of serum incubated with 3PO showed one new signal at 15 min after the start of incubation. The shape and relative abundances of the peaks corresponding to adduct increased up to 1h and did not change thereafter. We performed these experiments in the complex environment of serum which contains approximately 62% of albumin, 38% of globulin and less than 1% of regulatory proteins. To validate these findings, we extracted albumin from serum and repeated the incubation with 3PO for 1h at 37°C (Experimental protocol specified in F.26 under materials and methods section).

The HSA spectrum acquired after 1h incubation with 3PO by using ion trap MS instrument. The deconvolution of the mass spectrum acquired allowed the identification of an adduct. This adduct was detected at 66649±4 Da (Figure 4.17, 1d). It has a nominal shift of 210±4 Da, which corresponds to the nominal mass of 3PO. As we identified in the case of complex serum, the cysteinylated and glycated forms were detectable in the isolated albumin from serum (Figure 4.18, 1b and 1c, respectively). However, the intensity of native albumin peak was reduced as the new peak corresponding to 3PO adduct appeared after 1h incubation time.

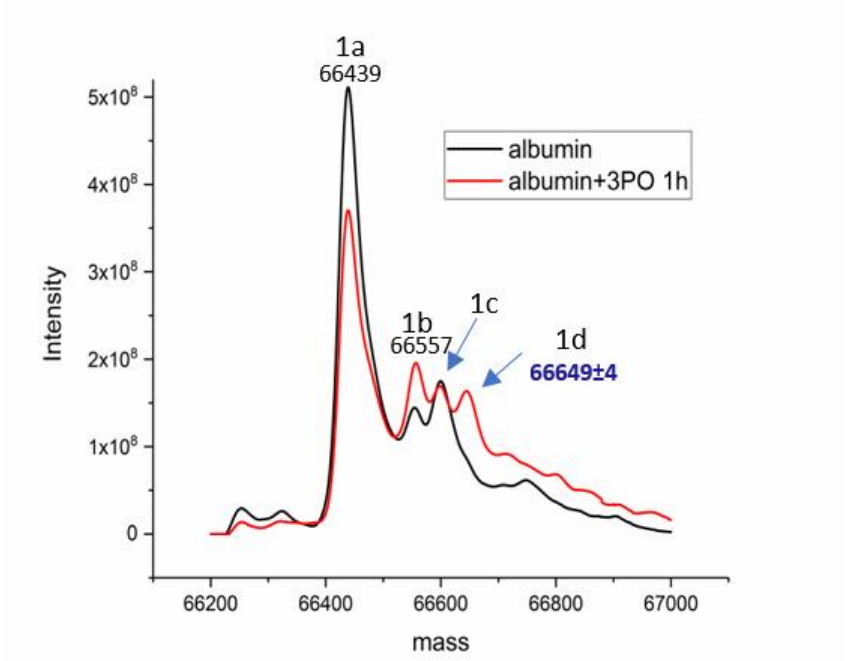


Figure 4.18: Deconvoluted spectrum of albumin isolated from human serum spiked with 3PO. Native albumin (1a), cysteinylated albumin (1b), glycated albumin (1c) and adduct formed by 3PO (1d).

After obtaining these results, we hypothesized that 3PO might be having a binding site on the Cys34 reside of the albumin. In order to confirm our hypothesis, we did indirect validation experiment with N-ethylmaleimide (NEM). NEM is known reagent for the covalent binding of Cys34 residue in proteins[185–187]. HSA contains 35 cysteine residues of which 34 are involved in intramolecular disulphide bonds thus contributing to overall tertiary structure. One free cysteine residue, Cys34, is the major extracellular source of redox active thiol group (-SH) which accounts for ≈ 80% of thiols in plasma[188].

The HSA spectrum acquired after 1h incubation with NEM. The deconvolution of the mass spectrum acquired allowed the identification of mass shift for the NEM modified albumin peak (Figure 4.19, 1a). This peak was detected at 66562 Da, which is compatible with the expected value for NEM adduct (66564) with an accuracy of -30 ppm. Similarly, we have seen the mass shift in the cysteinylated and glycated forms, and they were still detectable (Figure 4.19, 1b and 1c, respectively). These results demonstrate the blocking of Cys34 residue of albumin after 1h incubation with NEM at 37°C.

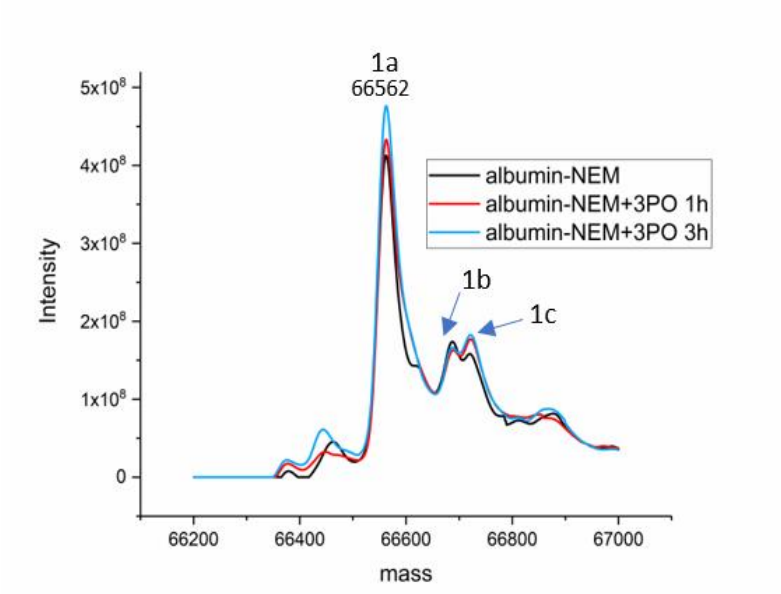


Figure 4.19: Deconvoluted spectrum of albumin extracted serum and spiked with NEM and 3PO. NEM modified albumin (1a), cysteinylated albumin (1b), glycated albumin (1c). No 3PO adduct formation in the sample spiked with NEM.

In the next step, we incubated the Cys34 blocked albumin with 3PO to check whether 3PO is able form the adduct. The hypothesis behind this experiment is that if 3PO has a different target site, other than free Cys34 , we would identify an extra peak even after blocking Cys34 residue with NEM. Notably in this analysis, as shown in Figure 4.19, we did not identify any extra peaks at 1hr and 3hr incubation with 3PO in NEM modified albumin. Therefore, based on the identified results we obtained a partial confirmation that 3PO has a specific target site at Cys34 residue of albumin. Cys blockage might explain the interfering action of 3PO with cell respiration as we identified in the proteomic analysis.

## 4.4 Future experiments:

In order to get direct evidence of our hypothesis, we designed a new experiment. To clarify which are the modified albumin hotspots for 3PO, we will perform a shotgun digestion of albumin after 1-3h incubation with 3PO, followed by a standard LC-MS/MS analysis. The peptide identifications will be performed by using proteome discover software. 3PO was described as a glycolytic pathway blocker, but this can be exerted to thiol alkylation as for IAA, which is toxic.

# 5 Industrial secondment

During the industrial secondment at Ingenus Pharmaceuticals, the following competences were acquired related to quality assurance (QA) and quality control (QC):

- Training in multiple SOPs and GMPs
- Data integrity.
- Two stages of filtration, filling, vial washing, capping, lyophilization stages.
- Bacterial infection tests: LAL-Test-Gel clot technique.
- Examination of microbial contamination of the water network and treated water.
- Media fill operations -Visual inspection of the media fill vials.
- Performance qualification protocol summary reports.
- Visible particles in injection
- Statistical control of the visual inspection of the product.
- Visible inspection of product according to cGMPs.
- Analytical method for Paclitaxel injection.
- Analytical method for irinotecan hydrochloride injection.
- Analytical method for docetaxel injection.
- Analytical method for Topotecan injection.
- Analytical method for Hydrochloride injection.
- Stability study control for 1-12 months at 25-40ºC.
- Management of reagents and consumables in chemical laboratory.

# 6 Conclusions and general discussion of the study

The comprehensive role of pathological endothelial dysfunctionality in the onset and progression of atherosclerosis and other vascular related diseases such as acute myocardial infarction (AMI) and chronic thromboembolic pulmonary disease (CTEPH) remains far from being fully understood. Therefore, notwithstanding dysfunction of ECs is one of the major factors involved in the development of vascular diseases, identification of the molecular mechanisms underlying endothelial dysfunction is crucial not only to the understanding of the diseases, but also to development of new targeting drugs aimed to correct endothelial functional imbalance through innovative therapeutic strategies.

For these reasons, in the first part of the project, we have explored, by using different experimental approaches, the redox status and proteomic profiles of pathological EC cells, in an attempt to unveil underlying pathophysiological mechanisms in endothelial dysfunction associated with both AMI and CTEPH diseases.

Oxidative stress parameters and the redox status have been determined in different EC lines and under different experimental conditions with the main aim to elucidate the role of oxidative stress in determining EC dysfunctionality. Such screenings carried out by conventional methodologies (UV and fluorometric assay, immunodetection of oxidatively-modified proteins), indicated an increased production of oxidants (intracellular ROS) and of oxidative stress markers (AOPPs, PCOs) and decreased levels of cellular antioxidants (GSH/GSSH, NADPH/NADP), in both pathological ECs from AMI and CTEPH patients. We observed almost similar results in both pathological cell types, supporting the involvement of oxidative stress in the endothelial dysfunction mechanism of both the diseases.

The network analyses of differentially expressed proteins, quantified by mass spectrometry-based label-free approach, allowed the description of the two endothelial dysfunction diseases. However, in the original Moglynet project other mass spectrometric methods were reported, such as the isobaric tag (iTRAQ) and the stable isotope labeling by amino acids in cell culture (SILAC) methods. These methods, even if they also allow the relative quantitation of proteins, require long workflow or complex sample preparation, very expensive experimental procedures and the labeling reactions can be incomplete. The label free approach instead allows the quantitative correlation of several unlabeled samples, using normalized peak intensities. The major drawback of this strategy is the necessity of a high reproducible liquid chromatographic runs and mass

detection and fragmentation processes between analyses, attested by the statistical correlation between peak intensity of peptides in the biological and technical replicates. In addition, the required normalization between samples implicates the analyses of several replicates.

The network analyses, using the differentially expressed proteins (335 and 676 proteins) in AMI and CTEPH ECs versus controls, reveal the biomarker signature of vascular injury, thrombosis, metabolism and oxidative stress. The expression pattern of selected genes and proteins was also validated at transcriptome and proteome levels, respectively. In particular, the overexpression of VWF in AMI-ECs and of PLOD2 and ENG in CTEPH cells is strongly associated with thrombus formation, platelet aggregation and angiogenesis that might play a key role endothelial dysfunction of both the diseases. Hence, if we compare the molecular mechanisms associated with endothelial dysfunction in both AMI and CTEPH, we clearly identify the association to thrombus formation, collagen deposition, vascular remodeling, platelet aggregation, metabolic alterations and oxidative stress related events. However, the involved proteins and the relative differentially expressed pathways, that might act as markers in these molecular proceedings are different in the two cell types. Therefore, the pathophysiology of endothelial dysfunction in AMI and CTEPH diseases is different.

Furthermore, the down regulation of proteins with antioxidant property in both AMI and CTEPH cell types well correlates to the increased production of oxidants and decreased production of anti-oxidant biomarkers, and strongly confirm the role of oxidative stress in endothelial dysfunction of both AMI and CPTH diseases.

From all these considerations we can conclude that our present results deliver an exclusive representation of the endothelial proteome in both AMI and CTEPH diseases, contributing to the understanding of pathophysiology and building the foundation for the identification of new drug targets.

In the original project, the proteomic approach would also have been applied to the study of new inhibitors of the glycolytic pathway, involved in the processes of angiogenesis responsible for the progressive and unstable vascular disease leading to plaque rupture and subsequent occlusion of the arteries (myocardial infarction or stroke as final events). The project focused on the enzyme PFKFB3 (PFKFB3-driven glycolysis has been shown to be involved in angiogenesis), with the final aim to counteract neovessel formation in order to prevent plaque rupture and its

cardiovascular complications. Unfortunately, the phosphatase and kinase modulators of PFKFB3 synthesized in the MoGlyNet consortium, were shown to be less potent than 3PO, the prototype of PFKFB3 inhibitors involved in the reduction of EC migration and proliferation and able to partially and transiently inhibit glycolysis *in vivo*. Therefore, in this project, we applied the same mass spectrometry-based label free quantitative proteomic approach above described to analyze the effects of 3PO in human ECs. Notwithstanding the plethora of evidence indicating the key role of 3PO in reducing angiogenesis, the molecular mechanism of action and the toxicity of 3PO at EC level under physiological or inflamed conditions remains to be established. In this part of the study, the network analyses, using the differentially expressed proteins, 130 and 161 up and down-regulated proteins in the 3PO- treated ECs compared to the control group, allowed the description of 3PO effect in the cells. In particular 3PO targets mitochondria and down-regulated substrates such as cytochrome complex, mitochondrial respiratory chain complexes I, III and IV, oxidoreductase complex, and protein complex present in the mitochondrial inner membrane. 3PO inhibits the important cellular pathways including the TCA cycle and vasculogenesis that may be useful not only for understanding the inhibitory effect of 3PO on EC proliferation and migration, but also for explaining the toxicity of the compound and why it was important to optimize the toxicological profile of the molecule. Furthermore, emerging studies revealed the strong association among endothelial dysfunction, angiogenesis and inflammation. Therefore, to check whether 3PO has an anti-inflammatory property, we induced inflammation in ECs by using TNFα. As expected, in this analysis, we identified the association of inflammatory related pathways. Interestingly, after treating the inflamed ECs, the expression of inflammatory related proteins completely reversed, suggesting the potential anti-inflammatory property of 3PO. Therefore, our present data confirm a potential application of this molecule as a starting point in designing novel molecules to prevent diseases where inflammatory reactions are involved, such as in atherosclerosis, cancer or neurodegenerative diseases.

In conclusion the network analyses in combination with quantitative proteomics is able to describe the pathological changes occurring in a disease state, and also the impact of a biologically-active molecule at cell level, attesting its powerful application in medicinal chemistry.

# 7 Bibliography

1. Gimbrone, M. A. & García-Cardeña, G. Vascular endothelium, hemodynamics, and the pathobiology of atherosclerosis. *Cardiovasc. Pathol.* **22,** 9–15 (2013).

2. Lum, H. & Roebuck, K. A. Oxidant stress and endothelial cell dysfunction. *Am. J. Physiol. Physiol.* **280,** C719–C741 (2001).

3. Sena, C. M., Pereira, A. M. & Seiça, R. Endothelial dysfunction — A major mediator of diabetic vascular disease. *Biochim. Biophys. Acta - Mol. Basis Dis.* **1832,** 2216–2231 (2013).

4. Addabbo, F., Montagnani, M. & Goligorsky, M. S. Mitochondria and reactive oxygen species. *Hypertens. (Dallas, Tex. 1979)* **53,** 885–92 (2009).

5. Taddei, S., Ghiadoni, L., Virdis, A., Versari, D. & Salvetti, A. Mechanisms of Endothelial Dysfunction: Clinical Significance and Preventive Non-Pharmacological Therapeutic Strategies. *Curr. Pharm. Des.* **9,** 2385–2402 (2003).

6. Celermajer, D. S. Endothelial Dysfunction: Does It Matter? Is It Reversible? *J. Am. Coll. Cardiol.* **30,** 325–333 (1997).

7. Vilahur, G. *et al.* Polyphenol-enriched Diet Prevents Coronary Endothelial Dysfunction by Activating the Akt/eNOS Pathway. *Rev. Española Cardiol. (English Ed.* **68,** 216–225 (2015).

8. Hasdai, D., Gibbons, R. J., Holmes, D. R., Higano, S. T. & Lerman, A. Coronary endothelial dysfunction in humans is associated with myocardial perfusion defects. *Circulation* **96,** 3390–3395 (1997).

9. Zeiher, A. M., Krause, T., Schächinger, V., Minners, J. & Moser, E. Impaired endothelium-dependent vasodilation of coronary resistance vessels is associated with exercise-induced myocardial ischemia. *Circulation* **91,** 2345–52 (1995).

10. Zeiher, A. M., Drexler, H., Wollschläger, H. & Just, H. Modulation of coronary vasomotor tone in humans. Progressive endothelial dysfunction with different early stages of coronary atherosclerosis. *Circulation* **83,** 391–401 (1991).

11. Do.e, Z. *et al.* Evidence for Rho-Kinase Activation in Patients With Pulmonary Arterial Hypertension. *Circ. J.* **73,** 1731–1739 (2009).

12. Chibana, H. *et al.* Pulmonary artery dysfunction in chronic thromboembolic pulmonary hypertension. *Int. J. Cardiol. Hear. Vasc.* **17,** 30–32 (2017).

13. Reed, G. W., Rossi, J. E. & Cannon, C. P. Acute myocardial infarction. *Lancet (London, England)* **389,** 197–210 (2017).

14. Steg, P. G. *et al.* ESC Guidelines for the management of acute myocardial infarction in patients presenting with ST-segment elevation. *Eur. Heart J.* **33,** 2569–2619 (2012).

15. Ventura-Clapier, R., Garnier, A., Veksler, V. & Joubert, F. Bioenergetics of the failing heart. *Biochim. Biophys. Acta - Mol. Cell Res.* **1813,** 1360–1372 (2011).

16. Orogo, A. M. & Gustafsson, Å. B. Cell death in the myocardium: My heart won't go on. *IUBMB Life* **65,** 651–656 (2013).

17. Fukushima, A., Milner, K., Gupta, A. & Lopaschuk, G. Myocardial Energy Substrate Metabolism in Heart Failure : from Pathways to Therapeutic Targets. *Curr. Pharm. Des.* **21,** 3654–3664 (2015).

18. Münzel, T., Gori, T., Keaney, J. F., Maack, C. & Daiber, A. Pathophysiological role of oxidative stress in systolic and diastolic heart failure and its therapeutic implications. *Eur. Heart J.* **36,** 2555–2564 (2015).

19. Dhalla, N. S., Rangi, S., Babick, A. P., Zieroth, S. & Elimban, V. Cardiac remodeling and subcellular defects in heart failure due to myocardial infarction and aging. *Heart Fail. Rev.* **17,** 671–681 (2012).

20. Bers, D. M. Altered Cardiac Myocyte Ca Regulation In Heart Failure. *Physiology* **21,** 380–387 (2006).

21. Braunwald, E. Biomarkers in Heart Failure. *N. Engl. J. Med.* **358,** 2148–2159 (2008).

22. Gabriel-Costa, D. The pathophysiology of myocardial infarction-induced heart failure. *Pathophysiology* **25,** 277–284 (2018).

23. Fan, H. *et al.* Oxygen radicals trigger activation of NF-κB and AP-1 and upregulation of ICAM-1 in reperfused canine heart. *Am. J. Physiol. Circ. Physiol.* **282,** H1778–H1786 (2002).

24. Sun, Y. Myocardial repair/remodelling following infarction: roles of local factors. *Cardiovasc. Res.* **81,** 482–490 (2008).

25. Ono, K., Matsumori, A., Shioi, T., Furukawa, Y. & Sasayama, S. Cytokine Gene Expression After Myocardial Infarction in Rat Hearts. *Circulation* **98,** 149–156 (1998).

26. Gwechenberger, M. *et al.* Cardiac Myocytes Produce Interleukin-6 in Culture and in Viable Border Zone of Reperfused Infarctions. *Circulation* **99,** 546–551 (1999).

27. Irwin, M. W. *et al.* Tissue Expression and Immunolocalization of Tumor Necrosis Factor-α in Postinfarction Dysfunctional Myocardium. *Circulation* **99,** 1492–1498 (1999).

28. Frangogiannis, N. G. The inflammatory response in myocardial injury, repair and remodelling. *Nat. Rev. Cardiol.* **11,** 255–265 (2014).

29. Grieve, D. J., Byrne, J. A., Cave, A. C. & Shah, A. M. Role of Oxidative Stress in Cardiac Remodelling after Myocardial Infarction. *Hear. Lung Circ.* **13,** 132–138 (2004).

30. Mackiewicz, U. *et al.* Sarcolemmal Ca2+-ATPase ability to transport Ca2+ gradually diminishes after myocardial infarction in the rat. *Cardiovasc. Res.* **81,** 546–554 (2008).

31. Costa, D. G. *et al.* LASSBio-294, A Compound With Inotropic and Lusitropic Activity, Decreases Cardiac Remodeling and Improves Ca2+ Influx Into Sarcoplasmic Reticulum After Myocardial Infarction. *Am. J. Hypertens.* **23,** 1220–1227 (2010).

32. Curran, J., Hinton, M. J., Ríos, E., Bers, D. M. & Shannon, T. R. β-Adrenergic Enhancement of Sarcoplasmic Reticulum Calcium Leak in Cardiac Myocytes Is Mediated by Calcium/Calmodulin-Dependent Protein Kinase. *Circ. Res.* **100,** 391–398 (2007).

33. Asakura, M. *et al.* Rationale and Design of a Large-Scale Trial Using Atrial Natriuretic Peptide (ANP) as an Adjunct to Percutaneous Coronary Intervention for ST-Segment Elevation Acute Myocardial Infarction. *Circ. J.* **68,** 95–100 (2004).

34. Tsai, S.-H., Lin, Y.-Y., Chu, S.-J., Hsu, C.-W. & Cheng, S.-M. Interpretation and Use of Natriuretic Peptides in Non-Congestive Heart Failure Settings. *Yonsei Med. J.* **51,** 151 (2010).

35. Hoeper, M. M. *et al.* Chronic thromboembolic pulmonary hypertension. *lancet Respir. Med.* **2,** 573–582 (2014).

36. Fedullo, P., Kerr, K. M., Kim, N. H. & Auger, W. R. Chronic Thromboembolic Pulmonary Hypertension. *Am. J. Respir. Crit. Care Med.* **183,** 1605–1613 (2011).

37. Gall, H. *et al.* An epidemiological analysis of the burden of chronic thromboembolic pulmonary hypertension in the USA, Europe and Japan. *Eur. Respir. Rev.* **26,** 160121 (2017).

38. Sakao, S. *et al.* Endothelial-like cells in chronic thromboembolic pulmonary hypertension: crosstalk with myofibroblast-like cells. *Respir. Res.* **12,** 109 (2011).

39. Changal, K., Sofi, F., Altaf, S., … A. R.-C. reports in & 2016, undefined. ANA negative systemic lupus erythematosus leading to CTEPH, TTP-like thrombocytopenia, and skin ulcers. *hindawi.com* at <https://www.hindawi.com/journals/crirh/2016/4507247/abs/>

40. Wynants, M., Quarck, R., … A. R.-E. & 2012, undefined. Effects of C-reactive protein on human pulmonary vascular cells in chronic thromboembolic pulmonary hypertension. *Eur Respir. Soc* at <http://erj.ersjournals.com/content/40/4/886.short>

41. Bonderman, D., Jakowitsch, J., … B. R.-, biology, and vascular & 2008, undefined. Role for staphylococci in misguided thrombus resolution of chronic thromboembolic pulmonary hypertension. *Am Hear. Assoc* at <http://atvb.ahajournals.org/content/28/4/678.short>

42. Jeffery, T. K. & Morrell, N. W. Molecular and cellular basis of pulmonary vascular remodeling in pulmonary hypertension. *Prog. Cardiovasc. Dis.* **45,** 173–202 (2002).

43. Xu, W. & Erzurum, S. C. in *Comprehensive Physiology* **1,** 357–372 (John Wiley & Sons, Inc., 2010).

44. Budhiraja, R., Tuder, R. M. & Hassoun, P. M. Endothelial dysfunction in pulmonary hypertension. *Circulation* **109,** 159–65 (2004).

45. Aird, W. C. Endothelial cell dynamics and complexity theory. *Crit. Care Med.* **30,** S180–S185 (2002).

46. Ranchoux, B. *et al.* Endothelial dysfunction in pulmonary arterial hypertension: an evolving landscape (2017 Grover Conference Series). *Pulm. Circ.* **8,** 2045893217752912 (2018).

47. Smolders, V. F. *et al.* Metabolic Alterations in Cardiopulmonary Vascular Dysfunction. *Front. Mol. Biosci.* **5,** 120 (2019).

48. Makino, A., Firth, A. L. & Yuan, J. X.-J. in *Comprehensive Physiology* **1,** 1555–1602 (John Wiley & Sons, Inc., 2011).

49. Reis, G. S. *et al.* Oxidative-stress biomarkers in patients with pulmonary hypertension. *Pulm. Circ.* **3,** 856–61 (2013).

50. Bowers, R. *et al.* Oxidative Stress in Severe Pulmonary Hypertension. *Am. J. Respir. Crit. Care Med.* **169,** 764–769 (2004).

51. Jernigan, N. L. *et al.* Contribution of reactive oxygen species to the pathogenesis of pulmonary arterial hypertension. *PLoS One* **12,** e0180455 (2017).

52. Zuo, L., Rose, B. A., Roberts, W. J., He, F. & Banes-Berceli, A. K. Molecular Characterization of Reactive Oxygen Species in Systemic and Pulmonary Hypertension. *Am. J. Hypertens.* **27,** 643–650 (2014).

53. Fields, S. Proteomics: Proteomics in genomeland. *Science* (2001). doi:10.1126/science.291.5507.1221

54. Anderson, N. L. & Anderson, N. G. Proteome and proteomics: New technologies, new concepts, and new words. in *Electrophoresis* (1998). doi:10.1002/elps.1150191103

55. Cox, J. *et al.* Accurate proteome-wide label-free quantification by delayed normalization and maximal peptide ratio extraction, termed MaxLFQ. *Mol. Cell. Proteomics* **13,** 2513–26 (2014).

56. Lai, E.-Y., Chen, Y.-H. & Wu, K.-P. A knowledge-based T2-statistic to perform pathway analysis for quantitative proteomic data. *PLOS Comput. Biol.* **13,** e1005601 (2017).

57. Jaleel, A., Aneesh Kumar, A., Ajith Kumar, G. S., Surendran, A. & Kartha, C. C. Label-free quantitative proteomics analysis reveals distinct molecular characteristics in endocardial endothelium. *Mol. Cell. Biochem.* **451,** 1–10 (2019).

58. Coliva, G., Duarte, S., Pérez-Sala, D. & Fedorova, M. Impact of inhibition of the autophagy-lysosomal pathway on biomolecules carbonylation and proteome regulation in rat cardiac cells. *Redox Biol.* 101123 (2019). doi:10.1016/J.REDOX.2019.101123

59. Vadgama, N., Lamont, D., Hardy, J., Nasir, J. & Lovering, R. C. Distinct proteomic profiles in monozygotic twins discordant for ischaemic stroke. *Mol. Cell. Biochem.* 1–9 (2019). doi:10.1007/s11010-019-03501-2

60. Banarjee, R., Sharma, A., Bai, S., Deshmukh, A. & Kulkarni, M. Proteomic study of endothelial dysfunction induced by AGEs and its possible role in diabetic cardiovascular complications. *J. Proteomics* **187,** 69–79 (2018).

61. Bhosale, S. D. *et al.* Serum Proteomic Profiling to Identify Biomarkers of Premature Carotid Atherosclerosis. *Sci. Rep.* **8,** 9209 (2018).

62. Luczak, M. *et al.* Label-Free Quantitative Proteomics Reveals Differences in Molecular Mechanism of Atherosclerosis Related and Non-Related to Chronic Kidney Disease. *Int. J. Mol. Sci.* **17,** (2016).

63. Su, N. *et al.* Quantitative Proteomic Analysis of Differentially Expressed Proteins and Downstream Signaling Pathways in Chronic Bladder Ischemia. *J. Urol.* **195,** 515–523 (2016).

64. Braga-Lagache, S. *et al.* Robust Label-free, Quantitative Profiling of Circulating Plasma Microparticle (MP) Associated Proteins. *Mol. Cell. Proteomics* **15,** 3640–3652 (2016).

65. Tura, O. *et al.* Late Outgrowth Endothelial Cells Resemble Mature Endothelial Cells and Are Not Derived from Bone Marrow. *Stem Cells* **31,** 338–348 (2013).

66. Brittan, M. *et al.* Impaired vascular function and repair in patients with premature coronary artery disease. *Eur. J. Prev. Cardiol.* **22,** 1557–1566 (2015).

67. Nukala, S. B., Baron, G., Aldini, G., Carini, M. & D'Amato, A. Mass Spectrometry-based Label-free Quantitative Proteomics To Study the Effect of 3PO Drug at Cellular Level. *ACS Med. Chem. Lett.* acsmedchemlett.8b00593 (2019). doi:10.1021/acsmedchemlett.8b00593

68. Cox, J. & Mann, M. MaxQuant enables high peptide identification rates, individualized p.p.b.-range mass accuracies and proteome-wide protein quantification. *Nat. Biotechnol.* **26,** 1367–1372 (2008).

69. Tyanova, S. *et al.* The Perseus computational platform for comprehensive analysis of (prote)omics data. *Nat. Methods* **13,** 731–740 (2016).

70. Bindea, G. *et al.* ClueGO: a Cytoscape plug-in to decipher functionally grouped gene ontology and pathway annotation networks. *Bioinformatics* **25,** 1091–3 (2009).

71. Zhang, Z. & Marshall, A. G. A universal algorithm for fast and automated charge state

deconvolution of electrospray mass-to-charge ratio spectra. *J. Am. Soc. Mass Spectrom.* **9,** 225–233 (1998).

72. Ross, R. The pathogenesis of atherosclerosis: a perspective for the 1990s. *Nature* **362,** 801–809 (1993).

73. GBD 2015 Disease and Injury Incidence and Prevalence Collaborators, T. *et al.* Global, regional, and national incidence, prevalence, and years lived with disability for 310 diseases and injuries, 1990-2015: a systematic analysis for the Global Burden of Disease Study 2015. *Lancet (London, England)* **388,** 1545–1602 (2016).

74. Boulanger, C. M. *et al.* Circulating microparticles from patients with myocardial infarction cause endothelial dysfunction. *Circulation* **104,** 2649–52 (2001).

75. Chen, S.-M. *et al.* Endothelial dysfunction in young patients with acute ST-elevation myocardial infarction. *Heart Vessels* **26,** 2–9 (2011).

76. Peuhkurinen, K., Risteli, L., Jounela, A. & Risteli, J. Changes in interstitial collagen metabolism during acute myocardial infarction treated with streptokinase or tissue plasminogen activator. *Am. Heart J.* **131,** 7–13 (1996).

77. Chen, Y.-F. *et al.* Regulation of Gene Expression with Thyroid Hormone in Rats with Myocardial Infarction. *PLoS One* **7,** e40161 (2012).

78. Zhao, Q., Wu, K., Li, N., Li, Z. & Jin, F. Identification of potentially relevant genes for myocardial infarction using RNA sequencing data analysis. *Exp. Ther. Med.* **15,** 1456–1464 (2018).

79. Yan, J., Li, F., Ingram, D. A. & Quilliam, L. A. Rap1a is a key regulator of fibroblast growth factor 2-induced angiogenesis and together with Rap1b controls human endothelial cell functions. *Mol. Cell. Biol.* **28,** 5803–10 (2008).

80. Birukova, A. A. *et al.* Prostacyclin post-treatment improves LPS-induced acute lung injury and endothelial barrier recovery via Rap1. *Biochim. Biophys. Acta* **1852,** 778–91 (2015).

81. Wang, X. *et al.* Kinetics of plasma von Willebrand factor in acute myocardial infarction patients: a meta-analysis. *Oncotarget* **8,** 90371–90379 (2017).

82. Mitra, A. *et al.* Role of α-crystallin B as a regulatory switch in modulating cardiomyocyte apoptosis by mitochondria or endoplasmic reticulum during cardiac hypertrophy and myocardial infarction. *Cell Death Dis.* **4,** e582–e582 (2013).

83. Zhao, Q., Wu, K., Li, N., Li, Z. & Jin, F. Identification of potentially relevant genes for myocardial infarction using RNA sequencing data analysis. *Exp. Ther. Med.* **15,** 1456–1464 (2018).

84. Chen, J., Yu, L., Zhang, S. & Chen, X. Network Analysis-Based Approach for Exploring the Potential Diagnostic Biomarkers of Acute Myocardial Infarction. *Front. Physiol.* **7,** 615 (2016).

85. Ahammad, I. Identification of Key Proteins Associated with Myocardial Infarction using Bioinformatics and Systems Biology. doi:10.1101/308544

86. Wang, Y. *et al.* Bioinformatic Analysis of the Possible Regulative Network of miR-30a/e in Cardiomyocytes 2 Days Post Myocardial Infarction. *Acta Cardiol. Sin.* **34,** 175–188 (2018).

87. Zhang, Y., Fang, J. & Ma, H. Inhibition of miR-182-5p protects cardiomyocytes from hypoxia-induced apoptosis by targeting CIAPIN1. *Biochem. Cell Biol.* **96,** 646–654 (2018).

88. Derda, A. A. *et al.* Gene expression profile analysis of aortic vascular smooth muscle cells reveals

upregulation of cadherin genes in myocardial infarction patients. *Physiol Genomics* **50,** 648–657 (2018).

89. Jiang, S.-H. *et al.* Overexpressed EDIL3 predicts poor prognosis and promotes anchorage-independent tumor growth in human pancreatic cancer. *Oncotarget* **7,** 4226–40 (2016).

90. Sibinga, N. E. *et al.* Collagen VIII is expressed by vascular smooth muscle cells in response to vascular injury. *Circ. Res.* **80,** 532–41 (1997).

91. Sinha, S., Kielty, C. M., Heagerty, A. M., Canfield, A. E. & Shuttleworth, C. A. Upregulation of collagen VIII following porcine coronary artery angioplasty is related to smooth muscle cell migration not angiogenesis. *Int. J. Exp. Pathol.* **82,** 295–302 (2001).

92. Jeimy, S. B., Tasneem, S., Cramer, E. M. & Hayward, C. P. M. Multimerin 1. *Platelets* **19,** 83–95 (2008).

93. Reheman, A., Tasneem, S., Ni, H. & Hayward, C. P. M. Mice with deleted multimerin 1 and alpha-synuclein genes have impaired platelet adhesion and impaired thrombus formation that is corrected by multimerin 1. *Thromb. Res.* **125,** e177-83 (2010).

94. TASNEEM, S. *et al.* Platelet adhesion to multimerin 1 *in vitro* : influences of platelet membrane receptors, von Willebrand factor and shear. *J. Thromb. Haemost.* **7,** 685–692 (2009).

95. Chavakis, E. & Dimmeler, S. Regulation of endothelial cell survival and apoptosis during angiogenesis. *Arterioscler. Thromb. Vasc. Biol.* **22,** 887–93 (2002).

96. Folkman, J. Angiogenesis and apoptosis. *Semin. Cancer Biol.* **13,** 159–167 (2003).

97. Carmeliet, P. Angiogenesis in health and disease. *Nat. Med.* **9,** 653–660 (2003).

98. Goveia, J., Stapor, P. & Carmeliet, P. Principles of targeting endothelial cell metabolism to treat angiogenesis and endothelial cell dysfunction in disease. *EMBO Mol. Med.* **6,** 1105–20 (2014).

99. Cai, H. & Harrison, D. G. Endothelial dysfunction in cardiovascular diseases: the role of oxidant stress. *Circ. Res.* **87,** 840–4 (2000).

100. Ceriello, A. *et al.* Effect of atorvastatin and irbesartan, alone and in combination, on postprandial endothelial dysfunction, oxidative stress, and inflammation in type 2 diabetic patients. *Circulation* **111,** 2518–24 (2005).

101. Elmasri, H. *et al.* Fatty acid binding protein 4 is a target of VEGF and a regulator of cell proliferation in endothelial cells. *FASEB J.* **23,** 3865–3873 (2009).

102. Elmasri, H. *et al.* Endothelial cell-fatty acid binding protein 4 promotes angiogenesis: role of stem cell factor/c-kit pathway. *Angiogenesis* **15,** 457–468 (2012).

103. Kajimoto, K., Minami, Y. & Harashima, H. Cytoprotective role of the fatty acid binding protein 4 against oxidative and endoplasmic reticulum stress in 3T3-L1 adipocytes. *FEBS Open Bio* **4,** 602–610 (2014).

104. Wang, W. *et al.* Ribosomal proteins and human diseases: pathogenesis, molecular mechanisms, and therapeutic implications. *Med. Res. Rev.* **35,** 225–85 (2015).

105. Ruggero, D. & Pandolfi, P. P. Does the ribosome translate cancer? *Nat. Rev. Cancer* **3,** 179–192 (2003).

106. Wang, W. *et al.* Ribosomal proteins and human diseases: pathogenesis, molecular mechanisms, and

therapeutic implications. *Med. Res. Rev.* **35,** 225–85 (2015).

107. Di, R. *et al.* S6K inhibition renders cardiac protection against myocardial infarction through PDK1 phosphorylation of Akt. *Biochem. J.* **441,** 199–207 (2012).

108. Casad, M. E. *et al.* Cardiomyopathy is associated with ribosomal protein gene haplo-insufficiency in Drosophila melanogaster. *Genetics* **189,** 861–70 (2011).

109. Humbert, M. Pulmonary arterial hypertension and chronic thromboembolic pulmonary hypertension: Pathophysiology. *European Respiratory Review* **19,** 59–63 (2010).

110. Lang, I. Advances in understanding the pathogenesis of chronic thromboembolic pulmonary hypertension. *Br. J. Haematol.* **149,** 478–483 (2010).

111. Gall, H. *et al.* An epidemiological analysis of the burden of chronic thromboembolic pulmonary hypertension in the USA, Europe and Japan. *Eur. Respir. Rev.* **26,** 160121 (2017).

112. Jenkins, D., Mayer, E., Screaton, N. & Madani, M. State-of-the-art chronic thromboembolic pulmonary hypertension diagnosis and management. *Eur. Respir. Rev.* **21,** 32–9 (2012).

113. Budhiraja, R., Tuder, R., Circulation, P. H.- & 2004, undefined. Endothelial dysfunction in pulmonary hypertension. *Am Hear. Assoc* at <http://circ.ahajournals.org/content/109/2/159.short>

114. Zhao, Y. D. *et al.* A Biochemical Approach to Understand the Pathogenesis of Advanced Pulmonary Arterial Hypertension: Metabolomic Profiles of Arginine, Sphingosine-1-Phosphate, and Heme of Human Lung. *PLoS One* **10,** e0134958 (2015).

115. Gilkes, D. M., Bajpai, S., Chaturvedi, P., Wirtz, D. & Semenza, G. L. Hypoxia-inducible factor 1 (HIF-1) promotes extracellular matrix remodeling under hypoxic conditions by inducing P4HA1, P4HA2, and PLOD2 expression in fibroblasts. *J. Biol. Chem.* **288,** 10819–29 (2013).

116. Xu, R. *et al.* NC1 domain of human type VIII collagen (alpha 1) inhibits bovine aortic endothelial cell proliferation and causes cell apoptosis. *Biochem. Biophys. Res. Commun.* **289,** 264–268 (2001).

117. Huang, L. *et al.* Transgelin as a potential target in the reversibility of pulmonary arterial hypertension secondary to congenital heart disease. *J. Cell. Mol. Med.* **22,** 6249–6261 (2018).

118. Machado, R. F. & Gladwin, M. T. Pulmonary hypertension in hemolytic disorders: pulmonary vascular disease: the global perspective. *Chest* **137,** 30S–38S (2010).

119. Minneci, P. C. *et al.* Hemolysis-associated endothelial dysfunction mediated by accelerated NO inactivation by decompartmentalized oxyhemoglobin. *J. Clin. Invest.* **115,** 3409–17 (2005).

120. Mathew, R., Huang, J., Wu, J. M., Fallon, J. T. & Gewitz, M. H. Hematological disorders and pulmonary hypertension. *World J. Cardiol.* **8,** 703 (2016).

121. Cai, H. & Harrison, D. G. Endothelial dysfunction in cardiovascular diseases: the role of oxidant stress. *Circ. Res.* **87,** 840–4 (2000).

122. Incalza, M. A. *et al.* Oxidative stress and reactive oxygen species in endothelial dysfunction associated with cardiovascular and metabolic diseases. *Vascul. Pharmacol.* **100,** 1–19 (2018).

123. Higashi, Y., Pandey, A., Goodwin, B. & Delafontaine, P. Insulin-like growth factor-1 regulates glutathione peroxidase expression and activity in vascular endothelial cells: Implications for atheroprotective actions of insulin-like growth factor-1. *Biochim. Biophys. Acta* **1832,** 391–9 (2013).

124. Yang, W. S. *et al.* Regulation of Ferroptotic Cancer Cell Death by GPX4. *Cell* **156,** 317–331 (2014).

125. Zhang, Y., Handy, D. E. & Loscalzo, J. Adenosine-Dependent Induction of Glutathione Peroxidase 1 in Human Primary Endothelial Cells and Protection Against Oxidative Stress. *Circ. Res.* **96,** 831–837 (2005).

126. Barroso, M. *et al.* Inhibition of cellular methyltransferases promotes endothelial cell activation by suppressing glutathione peroxidase 1 protein expression. *J. Biol. Chem.* **289,** 15350–62 (2014).

127. Forgione, M. A. *et al.* Cellular glutathione peroxidase deficiency and endothelial dysfunction. *Am. J. Physiol. Circ. Physiol.* **282,** H1255–H1261 (2002).

128. Gryszczyńska, B. *et al.* Advanced Oxidation Protein Products and Carbonylated Proteins as Biomarkers of Oxidative Stress in Selected Atherosclerosis-Mediated Diseases. *Biomed Res. Int.* **2017,** 4975264 (2017).

129. Kitano, D. *et al.* A comparative study of time-specific oxidative stress after acute myocardial infarction in patients with and without diabetes mellitus. *BMC Cardiovasc. Disord.* **16,** 102 (2016).

130. De Bock, K., Georgiadou, M. & Carmeliet, P. Role of endothelial cell metabolism in vessel sprouting. *Cell Metabolism* (2013). doi:10.1016/j.cmet.2013.08.001

131. Birukov, K. G. Cyclic Stretch, Reactive Oxygen Species, and Vascular Remodeling. *Antioxid. Redox Signal.* **11,** 1651–1667 (2009).

132. DeMarco, V. G. *et al.* Oxidative stress contributes to pulmonary hypertension in the transgenic (mRen2)27 rat. *Am. J. Physiol. Circ. Physiol.* **294,** H2659–H2668 (2008).

133. Rawat, D. K. *et al.* Increased Reactive Oxygen Species, Metabolic Maladaptation, and Autophagy Contribute to Pulmonary Arterial Hypertension–Induced Ventricular Hypertrophy and Diastolic Heart Failure. *Hypertension* **64,** 1266–1274 (2014).

134. Iwata, K. *et al.* Deficiency of NOX1/Nicotinamide Adenine Dinucleotide Phosphate, Reduced Form Oxidase Leads to Pulmonary Vascular Remodeling. *Arterioscler. Thromb. Vasc. Biol.* **34,** 110–119 (2014).

135. Aggarwal, S., Gross, C. M., Sharma, S., Fineman, J. R. & Black, S. M. in *Comprehensive Physiology* **3,** 1011–1034 (John Wiley & Sons, Inc., 2013).

136. Kasap, S., Gönenç, A., Şener, D. E. & Hisar, İ. Serum Cardiac Markers in Patients with Acute Myocardial Infarction: Oxidative Stress, C-Reactive Protein and N-Terminal Probrain Natriuretic Peptide. *J. Clin. Biochem. Nutr.* **41,** 50–57 (2007).

137. Yang, X. *et al.* [Increased levels of advanced oxidation protein products are associated with atherosclerosis in chronic kidney disease]. *Zhonghua nei ke za zhi* **44,** 342–6 (2005).

138. Fonteneau, G. *et al.* Serum-Mediated Oxidative Stress from Systemic Sclerosis Patients Affects Mesenchymal Stem Cell Function. *Front. Immunol.* **8,** 988 (2017).

139. Mohammedi, K. *et al.* Manganese Superoxide Dismutase (SOD2) Polymorphisms, Plasma Advanced Oxidation Protein Products (AOPP) Concentration and Risk of Kidney Complications in Subjects with Type 1 Diabetes. *PLoS One* **9,** e96916 (2014).

140. Taylor, E. L., Armstrong, K. R., Perrett, D., Hattersley, A. T. & Winyard, P. G. Optimisation of an Advanced Oxidation Protein Products Assay: Its Application to Studies of Oxidative Stress in Diabetes Mellitus. *Oxid. Med. Cell. Longev.* **2015,** 496271 (2015).

141. Morimoto, H. K. *et al.* Role of metabolic syndrome and antiretroviral therapy in adiponectin levels and oxidative stress in HIV-1 infected patients. *Nutrition* **30,** 1324–1330 (2014).

142. Skvarilová, M., Bulava, A., Stejskal, D., Adamovská, S. & Bartek, J. Increased level of advanced oxidation products (AOPP) as a marker of oxidative stress in patients with acute coronary syndrome. *Biomed. Pap. Med. Fac. Univ. Palacky. Olomouc. Czech. Repub.* **149,** 83–7 (2005).

143. Vona, R. *et al.* Oxidative stress in the pathogenesis of systemic scleroderma: An overview. *J. Cell. Mol. Med.* **22,** 3308–3314 (2018).

144. Fakhruddin, S., Alanazi, W. & Jackson, K. E. Diabetes-Induced Reactive Oxygen Species: Mechanism of Their Generation and Role in Renal Injury. *J. Diabetes Res.* **2017,** 1–30 (2017).

145. Kattoor, A. J., Pothineni, N. V. K., Palagiri, D. & Mehta, J. L. Oxidative Stress in Atherosclerosis. *Curr. Atheroscler. Rep.* **19,** 42 (2017).

146. Granger, D. N. & Kvietys, P. R. Reperfusion injury and reactive oxygen species: The evolution of a concept. *Redox Biol.* **6,** 524–551 (2015).

147. Forrester, S. J., Kikuchi, D. S., Hernandes, M. S., Xu, Q. & Griendling, K. K. Reactive Oxygen Species in Metabolic and Inflammatory Signaling. *Circ. Res.* **122,** 877–902 (2018).

148. Kumari, S., Badana, A. K., G, M. M., G, S. & Malla, R. Reactive Oxygen Species: A Key Constituent in Cancer Survival. *Biomark. Insights* **13,** 1177271918755391 (2018).

149. van Deel, E. D. *et al.* Extracellular superoxide dismutase protects the heart against oxidative stress and hypertrophy after myocardial infarction. *Free Radic. Biol. Med.* **44,** 1305–1313 (2008).

150. Kidd, P. M. *Glutathione: Systemic Protectant Against Oxidative and Free Radical Damage Dedicated to the memory of Professor Daniel Mazia, my PhD mentor and a pioneer in cell biology*. *Alternative Medicine Review x* **2,** (1997).

151. McLeay, Y., Stannard, S., Houltham, S. & Starck, C. Dietary thiols in exercise: oxidative stress defence, exercise performance, and adaptation. *J. Int. Soc. Sports Nutr.* **14,** 12 (2017).

152. Tardiolo, G. *et al.* Overview on the Effects of N-Acetylcysteine in Neurodegenerative Diseases. *Molecules* **23,** 3305 (2018).

153. Konior, A., Schramm, A., Czesnikiewicz-Guzik, M. & Guzik, T. J. NADPH Oxidases in Vascular Pathology. *Antioxid. Redox Signal.* **20,** 2794–2814 (2014).

154. Kirsch, M. & De Groot, H. NAD(P)H, a directly operating antioxidant? *FASEB J.* **15,** 1569–74 (2001).

155. Stapor, P., Wang, X., Goveia, J., Moens, S. & Carmeliet, P. Angiogenesis revisited-role and therapeutic potential of targeting endothelial metabolism. *J. Cell Sci. Comment. Artic. Ser. CELL Biol. Dis.* doi:10.1242/jcs.153908

156. Goveia, J., Stapor, P. & Carmeliet, P. Principles of targeting endothelial cell metabolism to treat angiogenesis and endothelial cell dysfunction in disease. *EMBO Mol. Med.* **6,** 1105–20 (2014).

157. Nishizawa, T. *et al.* An in vivo test of the hypothesis that glucose in myeloid cells stimulates inflammation and atherosclerosis. *Cell Rep* **7,** 356–365 (2014).

158. De Bock, K. *et al.* Role of PFKFB3-driven glycolysis in vessel sprouting. *Cell* **154,** 651–63 (2013).

159. Xu, Y. *et al.* Endothelial PFKFB3 plays a critical role in angiogenesis. *Arterioscler. Thromb. Vasc. Biol.* **34,** 1231–9 (2014).

160. Schoors, S. *et al.* Partial and transient reduction of glycolysis by PFKFB3 blockade reduces

pathological angiogenesis. *Cell Metab.* **19,** 37–48 (2014).

161. Marsin, A.-S. *et al.* Phosphorylation and activation of heart PFK-2 by AMPK has a role in the stimulation of glycolysis during ischaemia. *Curr. Biol.* **10,** 1247–1255 (2000).

162. Manes, N. P. & El-Maghrabi, M. R. The kinase activity of human brain 6-phosphofructo-2-kinase/fructose-2,6-bisphosphatase is regulated via inhibition by phosphoenolpyruvate. *Arch. Biochem. Biophys.* **438,** 125–136 (2005).

163. Kim, S.-G., Manes, N. P., El-Maghrabi, M. R. & Lee, Y.-H. Crystal structure of the hypoxia-inducible form of 6-phosphofructo-2-kinase/fructose-2,6-bisphosphatase (PFKFB3): a possible new target for cancer therapy. *J. Biol. Chem.* **281,** 2939–44 (2006).

164. Xu, Y. *et al.* Endothelial PFKFB3 plays a critical role in angiogenesis. *Arterioscler. Thromb. Vasc. Biol.* **34,** 1231–9 (2014).

165. Perrotta, P. *et al.* Pharmacological strategies to inhibit intra-plaque angiogenesis in atherosclerosis. *Vascul. Pharmacol.* (2018). doi:10.1016/J.VPH.2018.06.014

166. Cantelmo, A. R. *et al.* Inhibition of the Glycolytic Activator PFKFB3 in Endothelium Induces Tumor Vessel Normalization, Impairs Metastasis, and Improves Chemotherapy. *Cancer Cell* **30,** 968–985 (2016).

167. Clem, B. *et al.* Small-molecule inhibition of 6-phosphofructo-2-kinase activity suppresses glycolytic flux and tumor growth. *Mol. Cancer Ther.* **7,** 110–20 (2008).

168. Veken, B. Van Der, Meyer, G. De & Martinet, W. Inhibition of glycolysis reduces intraplaque angiogenesis in a mouse model of advanced atherosclerosis. *Atherosclerosis* **263,** e23 (2017).

169. Conradi, L.-C. *et al.* Tumor vessel disintegration by maximum tolerable PFKFB3 blockade. *Angiogenesis* **20,** 599–613 (2017).

170. Vila, V. *et al.* Inflammation, endothelial dysfunction and angiogenesis markers in chronic heart failure patients. *Int. J. Cardiol.* **130,** 276–277 (2008).

171. Steyers, C., Miller, F., Steyers, C. M. & Miller, F. J. Endothelial Dysfunction in Chronic Inflammatory Diseases. *Int. J. Mol. Sci. 2014, Vol. 15, Pages 11324-11349* **15,** 11324–11349 (2014).

172. Yang, X., Chang, Y. & Wei, W. Endothelial Dysfunction and Inflammation: Immunity in Rheumatoid Arthritis. *Mediators Inflamm.* **2016,** 1–9 (2016).

173. Zhu, M.-T. *et al.* Endothelial dysfunction and inflammation induced by iron oxide nanoparticle exposure: Risk factors for early atherosclerosis. *Toxicol. Lett.* **203,** 162–171 (2011).

174. Boyd, S. *et al.* Structure-Based Design of Potent and Selective Inhibitors of the Metabolic Kinase PFKFB3. *J. Med. Chem.* **58,** 3611–3625 (2015).

175. Ahn, K., Pan, S., Beningo, K. & Hupe, D. A permanent human cell line (EA.hy926) preserves the characteristics of endothelin converting enzyme from primary human umbilical vein endothelial cells. *Life Sci.* **56,** 2331–2341 (1995).

176. D'Alessio, A., Al-Lamki, R. S., Bradley, J. R. & Pober, J. S. Caveolae participate in tumor necrosis factor receptor 1 signaling and internalization in a human endothelial cell line. *Am. J. Pathol.* **166,** 1273–82 (2005).

177. Yamashita, A. *et al.* Increased Metabolite Levels of Glycolysis and Pentose Phosphate Pathway in

Rabbit Atherosclerotic Arteries and Hypoxic Macrophage. *PLoS One* **9,** e86426 (2014).

178. Jiang, X., Zhang, J. & Huang, Y. Tetraspanins in cell migration. *Cell Adh. Migr.* **9,** 406–15 (2015).

179. Mori, S. *et al.* The integrin-binding defective FGF2 mutants potently suppress FGF2 signalling and angiogenesis. *Biosci. Rep.* **37,** (2017).

180. Dennis, J. *et al.* The endothelial protein C receptor (PROCR) Ser219Gly variant and risk of common thrombotic disorders: a HuGE review and meta-analysis of evidence from observational studies. *Blood* **119,** 2392–400 (2012).

181. Cully, M. A new way to starve vascular endothelial cells. *Nat. Rev. Drug Discov.* **13,** 176–177 (2014).

182. Ridker, P. M., Hennekens, C. H., Roitman-Johnson, B., Stampfer, M. J. & Allen, J. Plasma concentration of soluble intercellular adhesion molecule 1 and risks of future myocardial infarction in apparently healthy men. *Lancet (London, England)* **351,** 88–92 (1998).

183. Hwang, S. J. *et al.* Circulating adhesion molecules VCAM-1, ICAM-1, and E-selectin in carotid atherosclerosis and incident coronary heart disease cases: the Atherosclerosis Risk In Communities (ARIC) study. *Circulation* **96,** 4219–25 (1997).

184. Regazzoni, L., Colombo, S., Mazzolari, A., Vistoli, G. & Carini, M. Serum albumin as a probe for testing the selectivity of irreversible cysteine protease inhibitors: The case of vinyl sulfones. *J. Pharm. Biomed. Anal.* **124,** 294–302 (2016).

185. Anraku, M. *et al.* Quantitative Analysis of Cysteine-34 on the Anitioxidative Properties of Human Serum Albumin in Hemodialysis Patients. *J. Pharm. Sci.* **100,** 3968–3976 (2011).

186. Kim, H.-J., Ha, S., Lee, H. Y. & Lee, K.-J. ROSics: Chemistry and proteomics of cysteine modifications in redox biology. *Mass Spectrom. Rev.* **34,** 184–208 (2015).

187. Gryzunov, Y. A. *et al.* Binding of fatty acids facilitates oxidation of cysteine-34 and converts copper-albumin complexes from antioxidants to prooxidants. *Arch. Biochem. Biophys.* **413,** 53–66 (2003).

188. Plantier, J.-L., Duretz, V., Devos, V., Urbain, R. & Jorieux, S. Comparison of antioxidant properties of different therapeutic albumin preparations. *Biologicals* **44,** 226–233 (2016).

# 8 Appendices

Appendix Table 1: List of upregulated proteins associated with endothelial dysfunction in AMI.

| Protein ID | Protein names | Gene names | Log2 (HCAEC-AMI vs HCAEC) | -LOG(P-value) |
|---|---|---|---|---|
| P63313 | Thymosin beta-10 | TMSB10 | 2.68 | 4.97 |
| P04275 | von Willebrand factor;von Willebrand antigen 2 | VWF | 2.06 | 1.41 |
| B4DWS6 | Very-long-chain 3-oxoacyl-CoA reductase | HSD17B12 | 1.47 | 5.70 |
| E9PR44 | Alpha-crystallin B chain | CRYAB | 1.43 | 3.29 |
| B4DRD3 | Tissue-type plasminogen activator;Tissue-type plasminogen activator chain A;Tissue-type plasminogen activator chain B | PLAT | 1.37 | 13.16 |
| A0A140VJL6 | Isoamyl acetate-hydrolyzing esterase 1 homolog | IAH1 | 1.33 | 5.87 |
| P20591 | Interferon-induced GTP-binding protein Mx1;Interferon-induced GTP-binding protein Mx1, N-terminally processed | MX1 | 1.25 | 3.67 |
| O95433 | Activator of 90 kDa heat shock protein ATPase homolog 1 | AHSA1 | 1.20 | 3.35 |
| B4DDF4 | Calponin;Calponin-2 | CNN2 | 1.06 | 4.70 |
| Q86SZ7 | Proteasome activator complex subunit 2 | PSME2 | 1.03 | 2.36 |
| B4E2S7 | Lysosome-associated membrane glycoprotein 2 | LAMP2 | 1.03 | 3.60 |
| Q6FI81 | Anamorsin | CIAPIN1 | 0.99 | 6.26 |
| A0A0S2Z4G7 | Nucleophosmin | NPM1 | 0.93 | 3.75 |
| A0A024R6I3 | Transmembrane emp24 domain-containing protein 10 | TMED10 | 0.91 | 5.50 |
| Q6IBN4 | Enoyl-CoA delta isomerase 2, mitochondrial | PECI | 0.86 | 5.85 |
| O94874 | E3 UFM1-protein ligase 1 | UFL1 | 0.85 | 3.59 |
| O15511 | Actin-related protein 2/3 complex subunit 5 | ARPC5 | 0.84 | 2.69 |
| A0A024R3C4 | KDEL motif-containing protein 2 | KDELC2 | 0.84 | 3.28 |
| Q5RLJ0 | UPF0568 protein C14orf166 | C14orf166 | 0.83 | 8.21 |
| Q9UPN1 | Serine/threonine-protein phosphatase;Serine/threonine-protein phosphatase PP1-gamma catalytic subunit | PPP1CC | 0.83 | 3.05 |
| A0A024RA52 | Proteasome subunit alpha type;Proteasome subunit alpha type-2 | PSMA2 | 0.81 | 2.55 |
| X5D2T3 | 60S ribosomal protein L10 | RPL10 | 0.80 | 4.07 |
| P61026 | Ras-related protein Rab-10 | RAB10 | 0.79 | 2.57 |
| B7ZAY2 | Ras-related protein Rap-1b;Ras-related protein Rap-1b-like protein;Ras-related protein Rap-1A | RAP1B | 0.77 | 4.39 |
| Q5U0D2 | Transgelin | TAGLN | 0.77 | 2.63 |
| Q6IPH7 | | RPL14 | 0.76 | 4.33 |
| O15231 | Zinc finger protein 185 | ZNF185 | 0.76 | 4.13 |
| P51571 | Translocon-associated protein subunit delta | SSR4 | 0.75 | 5.64 |
| J3KQ32 | Obg-like ATPase 1 | OLA1 | 0.74 | 4.78 |
| A0A024RB14 | 40S ribosomal protein S26;Putative 40S ribosomal protein S26-like 1 | RPS26 | 0.74 | 3.59 |
| Q13509 | Tubulin beta-3 chain | TUBB3 | 0.74 | 4.60 |

| | | | | |
|---|---|---|---|---|
| A0A024R7B7 | Hsp90 co-chaperone Cdc37;Hsp90 co-chaperone Cdc37, N-terminally processed | CDC37 | 0.72 | 5.11 |
| B7Z3K3 | Inositol-3-phosphate synthase 1 | ISYNA1 | 0.71 | 3.68 |
| B3KT06 | Tubulin alpha-1B chain | TUBA1B | 0.71 | 6.93 |
| A0A024R1M8 | Apolipoprotein L2 | APOL2 | 0.71 | 1.95 |
| O43854 | EGF-like repeat and discoidin I-like domain-containing protein 3 | EDIL3 | 0.69 | 1.98 |
| P37802 | Transgelin-2 | TAGLN2 | 0.63 | 4.79 |
| P63172 | Dynein light chain Tctex-type 1 | DYNLT1 | 0.63 | 2.39 |
| B4DFL1 | Dihydrolipoyl dehydrogenase;Dihydrolipoyl dehydrogenase, mitochondrial | DLD | 0.61 | 2.36 |
| V9HW44 | Platelet-activating factor acetylhydrolase IB subunit beta | HEL-S-303 | 0.60 | 3.84 |

Appendix Table 2: List of down-regulated proteins associated with endothelial dysfunctionality in AMI.

| Protein ID | Protein names | Gene names | Log2 (HCAEC-AMI vs HCAEC) | -LOG(P-value) |
|---|---|---|---|---|
| H3BPC4 | SUMO-conjugating enzyme UBC9 | UBE2I | -1.68 | 1.38 |
| E7ENN3 | Nesprin-1 | SYNE1 | -1.45 | 6.12 |
| F5H7F6 | Microsomal glutathione S-transferase 1 | MGST1 | -1.45 | 5.54 |
| A0A1W2PRF6 | Lysosome membrane protein 2 | SCARB2 | -1.43 | 4.16 |
| B3KPC7 | Actin-related protein 2/3 complex subunit 5;Actin-related protein 2/3 complex subunit 5-like protein | ARPC5L | -1.43 | 3.29 |
| A8K651 | Complement component 1 Q subcomponent-binding protein, mitochondrial | C1QBP | -1.39 | 5.53 |
| Q9BQQ5 | 60S ribosomal protein L27a | L27a | -1.39 | 8.30 |
| P62851 | 40S ribosomal protein S25 | RPS25 | -1.38 | 6.19 |
| Q13201 | Multimerin-1;Platelet glycoprotein Ia*;155 kDa platelet multimerin | MMRN1 | -1.33 | 3.14 |
| Q9Y5B9 | FACT complex subunit SPT16 | SUPT16H | -1.31 | 4.57 |
| Q96FQ6 | Protein S100-A16 | S100A16 | -1.29 | 6.83 |
| Q6IBA2 | Activated RNA polymerase II transcriptional coactivator p15 | PC4 | -1.25 | 7.05 |
| Q13151 | Heterogeneous nuclear ribonucleoprotein A0 | HNRNPA0 | -1.21 | 4.49 |
| B4DWN1 | Vesicular integral-membrane protein VIP36 | LMAN2 | -1.20 | 2.20 |
| C9J3L8 | Translocon-associated protein subunit alpha | SSR1 | -1.20 | 5.57 |
| Q2TAM5 | Transcription factor p65 | RELA | -1.17 | 6.14 |
| P29966 | Myristoylated alanine-rich C-kinase substrate | MARCKS | -1.15 | 6.06 |
| H0YN26 | Acidic leucine-rich nuclear phosphoprotein 32 family member A | ANP32A | -1.12 | 6.03 |
| Q53FJ5 | Prosaposin;Saposin-A;Saposin-B-Val;Saposin-B;Saposin-C;Saposin-D | PSAP | -1.09 | 8.79 |
| Q13404 | Ubiquitin-conjugating enzyme E2 variant 1 | UBE2V1 | -1.09 | 3.47 |

| | | | | |
|---|---|---|---|---|
| A0A140VJK1 | Glutaredoxin-3 | GLRX3 | -1.06 | 4.43 |
| F8W6I7 | Heterogeneous nuclear ribonucleoprotein A1;Heterogeneous nuclear ribonucleoprotein A1, N-terminally processed;Heterogeneous nuclear ribonucleoprotein A1-like 2 | HNRNPA1 | -1.05 | 5.46 |
| A0A024R3J7 | Dolichyl-diphosphooligosaccharide--protein glycosyltransferase subunit STT3A | hCG_2032701 | -1.03 | 5.00 |
| Q9Y3U8 | 60S ribosomal protein L36 | RPL36 | -1.01 | 5.47 |
| P51858 | Hepatoma-derived growth factor | HDGF | -1.00 | 4.74 |
| F5GXX5 | Dolichyl-diphosphooligosaccharide--protein glycosyltransferase subunit DAD1 | DAD1 | -0.99 | 2.82 |
| Q5T7C4 | High mobility group protein B1;Putative high mobility group protein B1-like 1 | HMGB1 | -0.99 | 7.17 |
| B4DTT0 | N-acetylglucosamine-6-sulfatase | DKFZp686E12166 | -0.97 | 8.94 |
| O14907 | Tax1-binding protein 3 | TAX1BP3 | -0.97 | 3.69 |
| A0A024R4X0 | NADH-cytochrome b5 reductase;NADH-cytochrome b5 reductase 3;NADH-cytochrome b5 reductase 3 membrane-bound form;NADH-cytochrome b5 reductase 3 soluble form | CYB5R3 | -0.97 | 7.22 |
| H9ZYJ2 | Thioredoxin | TXN | -0.96 | 5.01 |
| B5BU25 | Splicing factor U2AF 65 kDa subunit | U2AF2 | -0.96 | 8.00 |
| Q86U79 | Adenosine kinase | ADK | -0.95 | 2.58 |
| L7RT18 | Adapter molecule crk | CRK | -0.94 | 4.18 |
| V9HW48 | SH3 domain-binding glutamic acid-rich-like protein | HEL-S-115 | -0.93 | 2.73 |
| A0A140VJF4 | Biliverdin reductase A | BLVRA | -0.93 | 5.15 |
| E9PI87 | Oxidoreductase HTATIP2 | HTATIP2 | -0.92 | 2.13 |
| J3KNF4 | Copper chaperone for superoxide dismutase | CCS | -0.92 | 4.48 |
| Q6FGV9 | Phosphomevalonate kinase | PMVK | -0.92 | 2.92 |
| P20700 | Lamin-B1 | LMNB1 | -0.91 | 9.48 |
| Q6FGY1 | Hippocalcin-like protein 1 | HPCAL1 | -0.91 | 3.83 |
| A0A024R258 | Ubiquilin-1;Ubiquilin-4 | UBQLN1 | -0.90 | 5.55 |
| Q53XX5 | Cold-inducible RNA-binding protein | CIRBP | -0.90 | 3.80 |
| Q59H57 | RNA-binding protein FUS | FUS | -0.90 | 3.77 |
| B4E324 | Carboxypeptidase;Lysosomal protective protein;Lysosomal protective protein 32 kDa chain;Lysosomal protective protein 20 kDa chain | CTSA | -0.89 | 4.30 |
| K7ESE8 | Bleomycin hydrolase | BLMH | -0.89 | 3.32 |
| P46926 | Glucosamine-6-phosphate isomerase 1;Glucosamine-6-phosphate isomerase | GNPDA1 | -0.88 | 4.45 |
| B7Z4K8 | Basic leucine zipper and W2 domain-containing protein 2 | BZW2 | -0.87 | 4.26 |
| B7Z2Z1 | Scaffold attachment factor B1 | SAFB | -0.87 | 5.93 |
| Q6IRT1 | S-(hydroxymethyl)glutathione dehydrogenase;Alcohol dehydrogenase class-3 | ADH5 | -0.87 | 4.62 |
| P15531 | Nucleoside diphosphate kinase A | NME1 | -0.86 | 1.85 |
| A2A2D0 | Stathmin | STMN1 | -0.86 | 8.87 |
| C9JFR7 | Cytochrome c | CYCS | -0.84 | 6.18 |
| A8K2W3 | Serum deprivation-response protein | SDPR | -0.83 | 11.43 |

| | | | | |
|---|---|---|---|---|
| F5GYN4 | Ubiquitin thioesterase OTUB1 | OTUB1 | -0.81 | 5.20 |
| O75436 | Vacuolar protein sorting-associated protein 26A | VPS26A | -0.81 | 2.38 |
| V9HW74 | Ubiquitin carboxyl-terminal hydrolase;Ubiquitin carboxyl-terminal hydrolase isozyme L1 | HEL-117 | -0.79 | 1.94 |
| A0A0S2Z410 | 3-hydroxyacyl-CoA dehydrogenase type-2 | HSD17B10 | -0.79 | 4.64 |
| H3BPQ3 | Protein NDRG4 | NDRG4 | -0.78 | 3.46 |
| Q5T9B9 | Endoglin | ENG | -0.77 | 3.90 |
| A0A087X296 | Prostaglandin G/H synthase 1 | PTGS1 | -0.77 | 4.28 |
| J3K000 | Xaa-Pro dipeptidase | PEPD | -0.76 | 3.38 |
| A0A024RAV2 | ATP-dependent DNA helicase Q1 | RECQL | -0.76 | 5.90 |
| A0A024R3Z6 | Basic leucine zipper and W2 domain-containing protein 1 | BZW1 | -0.75 | 5.44 |
| P18077 | 60S ribosomal protein L35a | RPL35A | -0.75 | 2.68 |
| Q6FH49 | Nicotinamide N-methyltransferase | NNMT | -0.74 | 4.02 |
| V9HWI0 | Alcohol dehydrogenase [NADP(+)] | HEL-S-165mP | -0.74 | 7.43 |
| B3KMZ6 | SUMO-activating enzyme subunit 2 | UBA2 | -0.74 | 3.60 |
| E9PJ81 | UBX domain-containing protein 1 | UBXN1 | -0.74 | 2.45 |
| B4DIZ2 | Ubiquitin-conjugating enzyme E2 K | UBE2K | -0.74 | 3.24 |
| A5PLK7 | Protein RCC2 | RCC2 | -0.73 | 4.02 |
| B0YJ88 | Radixin | RDX | -0.73 | 3.67 |
| A0A024R883 | V-type proton ATPase subunit G 1 | ATP6V1G1 | -0.73 | 3.30 |
| A0A024R3W7 | Elongation factor 1-beta | EEF1B2 | -0.73 | 3.44 |
| Q5IST1 | Serine/arginine-rich splicing factor 5 | SFRS5 | -0.71 | 2.49 |
| A0A024R8W0 | Eukaryotic initiation factor 4A-III;Eukaryotic initiation factor 4A-III, N-terminally processed | DDX48 | -0.71 | 4.98 |
| Q6FHX6 | Flap endonuclease 1 | FEN1 | -0.70 | 2.56 |
| Q53HS0 | Glutamine--tRNA ligase | QARS | -0.70 | 5.15 |
| O95831 | Apoptosis-inducing factor 1, mitochondrial | AIFM1 | -0.70 | 2.02 |
| O15400 | Syntaxin-7 | STX7 | -0.70 | 4.56 |
| Q5T123 | SH3 domain-binding glutamic acid-rich-like protein 3 | SH3BGRL3 | -0.69 | 4.48 |
| Q9HDC9 | Adipocyte plasma membrane-associated protein | APMAP | -0.69 | 2.58 |
| Q05BM8 | Polypeptide N-acetylgalactosaminyltransferase;Polypeptide N-acetylgalactosaminyltransferase 1;Polypeptide N-acetylgalactosaminyltransferase 1 soluble form | GALNT1 | -0.69 | 3.82 |
| Q9BRL5 | | CALM3 | -0.69 | 2.73 |
| J3QRT5 | Intercellular adhesion molecule 2 | ICAM2 | -0.69 | 2.31 |
| F8WCF6 | Actin-related protein 2/3 complex subunit 4 | ARPC4-TTLL3 | -0.68 | 6.06 |
| I3L2L5 | Protein FAM195B | FAM195B | -0.68 | 3.19 |
| B3KN57 | Sorting nexin-2 | SNX2 | -0.68 | 5.10 |
| F8VQE1 | LIM domain and actin-binding protein 1 | LIMA1 | -0.68 | 2.45 |
| D3DP46 | Signal peptidase complex subunit 3 | SPCS3 | -0.68 | 2.27 |
| A0A024R9D2 | Protein LYRIC | MTDH | -0.67 | 3.46 |

| | | | | |
|---|---|---|---|---|
| P35580 | Myosin-10 | MYH10 | -0.67 | 7.58 |
| K7ES31 | Eukaryotic translation initiation factor 3 subunit K | EIF3K | -0.67 | 3.30 |
| J3KT73 | 60S ribosomal protein L38 | RPL38 | -0.66 | 6.00 |
| P62263 | 40S ribosomal protein S14 | RPS14 | -0.66 | 7.96 |
| P62495 | Eukaryotic peptide chain release factor subunit 1 | ETF1 | -0.66 | 5.27 |
| Q53XC0 | Eukaryotic translation initiation factor 2 subunit 1 | EIF2S1 | -0.66 | 5.24 |
| Q96C90 | Protein phosphatase 1 regulatory subunit 14B | PPP1R14B | -0.65 | 2.71 |
| F5H2R5 | Rho GDP-dissociation inhibitor 2 | ARHGDIB | -0.65 | 2.80 |
| A4D275 | Actin-related protein 2/3 complex subunit 1B | ARPC1B | -0.64 | 2.92 |
| Q14240 | Eukaryotic initiation factor 4A-II;Eukaryotic initiation factor 4A-II, N-terminally processed | EIF4A2 | -0.64 | 3.21 |
| B4E3A8 | Leukocyte elastase inhibitor | HEL57 | -0.64 | 2.22 |
| A0A024R1K8 | Splicing factor 3A subunit 1 | SF3A1 | -0.64 | *2.65* |
| H7BY10 | 60S ribosomal protein L23a | RPL23A | -0.64 | 3.71 |
| Q96IZ0 | PRKC apoptosis WT1 regulator protein | PAWR | -0.64 | 4.69 |
| A8K719 | Core-binding factor subunit beta | CBFB | -0.64 | 2.71 |
| A0A024RDB0 | Ubiquitin-like modifier-activating enzyme 6 | UBE1L2 | -0.64 | 7.12 |
| A0A0A6YYJ8 | Putative RNA-binding protein Luc7-like 2 | LUC7L2 | -0.64 | 3.62 |
| A0A140VJP5 | S-adenosylmethionine synthase isoform type-2;S-adenosylmethionine synthase | MAT2A | -0.64 | 4.18 |
| Q53R19 | Actin-related protein 2/3 complex subunit 2 | ARPC2 | -0.62 | 3.86 |
| A0A1X7SBZ2 | Probable ATP-dependent RNA helicase DDX17 | DDX17 | -0.62 | 9.54 |
| A9UK01 | Rho GTPase-activating protein 18 | ARHGAP18 | -0.61 | 5.11 |
| A0A024RB85 | Proliferation-associated protein 2G4 | PA2G4 | -0.61 | 6.66 |
| V9HW41 | Ubiquitin-conjugating enzyme E2 N | HEL-S-71 | -0.61 | 3.01 |
| Q5VVD0 | 60S ribosomal protein L11 | RPL11 | -0.61 | 4.27 |
| P51991 | Heterogeneous nuclear ribonucleoprotein A3 | HNRNPA3 | -0.61 | 9.09 |
| A0A024R5Q7 | Adenylosuccinate synthetase isozyme 2 | ADSS | -0.61 | 6.02 |
| Q59GU6 | Sorting nexin-1 | SNX1 | -0.61 | 3.93 |
| P13010 | X-ray repair cross-complementing protein 5 | XRCC5 | -0.60 | 6.59 |
| C9J9K3 | 40S ribosomal protein SA | RPSA | -0.60 | 7.71 |
| A0A0A0MRM8 | Unconventional myosin-VI | MYO6 | -0.60 | 3.14 |
| L7RXH5 | Mitogen-activated protein kinase;Mitogen-activated protein kinase 3 | MAPK3 | -0.60 | 6.02 |
| V9HWC2 | Protein deglycase DJ-1 | HEL-S-67p | -0.60 | 6.11 |

Appendix Table 3: List of upregulated proteins associated with endothelial dysfunctionality in CTEPH.

| Protein ID | Protein names | Gene names | Log 2 (CTEPH-EC/HPAE) | -LOG(P-value) |
|---|---|---|---|---|
| O00469 | Procollagen-lysine,2-oxoglutarate 5-dioxygenase 2 | PLOD2 | 2.47 | 15.22 |
| Q5U0D2 | Transgelin | TAGLN | 2.41 | 14.14 |
| A0A0P1J1R0 | Translationally-controlled tumor protein | TPT1 | 2.38 | 15.80 |
| P68133 | Actin, alpha skeletal muscle;Actin, alpha cardiac muscle 1;Actin, gamma-enteric smooth muscle;Actin, aortic smooth muscle | ACTA1 | 2.23 | 8.13 |
| Q5CZB5 | Uncharacterized protein DKFZp686M0430 | DKFZp686M0430 | 1.98 | 5.73 |
| V9HW83 | Retinal dehydrogenase 1 | HEL-S-53e | 1.71 | 16.57 |
| H0YNW5 | Deoxyuridine 5-triphosphate nucleotidohydrolase, mitochondrial | DUT | 1.40 | 25.23 |
| J3QR09 | Ribosomal protein L19;60S ribosomal protein L19 | RPL19 | 1.38 | 7.55 |
| Q5ISS1 | ADP-ribosylation factor 1;ADP-ribosylation factor 3 | ARF1 | 1.34 | 11.81 |
| P68366 | Tubulin alpha-4A chain | TUBA4A | 1.18 | 6.60 |
| Q9UJC5 | SH3 domain-binding glutamic acid-rich-like protein 2 | SH3BGRL2 | 1.17 | 1.90 |
| A0A024R222 | Phosphoserine aminotransferase | PSAT1 | 1.16 | 13.15 |
| B4DDF4 | Calponin;Calponin-2 | CNN2 | 1.13 | 8.08 |
| B1AHB1 | DNA helicase;DNA replication licensing factor MCM5 | MCM5 | 1.11 | 8.80 |
| B3KXZ4 | DNA helicase;DNA replication licensing factor MCM2 | MCM2 | 1.08 | 13.33 |
| Q14566 | DNA replication licensing factor MCM6 | MCM6 | 1.05 | 14.57 |
| Q8WX93 | Palladin | PALLD | 1.05 | 5.21 |
| O95433 | Activator of 90 kDa heat shock protein ATPase homolog 1 | AHSA1 | 1.05 | 3.11 |
| K7ELC2 | 40S ribosomal protein S15 | RPS15 | 1.02 | 4.20 |
| Q53Y97 | Thymidylate synthase | TYMS | 0.98 | 6.36 |
| Q02952 | A-kinase anchor protein 12 | AKAP12 | 0.97 | 5.74 |
| P63279 | SUMO-conjugating enzyme UBC9 | UBE2I | 0.89 | 4.20 |
| P07108 | Acyl-CoA-binding protein | DBI | 0.86 | 6.75 |
| Q49AN9 | Small nuclear ribonucleoprotein G;Putative small nuclear ribonucleoprotein G-like protein 15 | SNRPG | 0.86 | 4.87 |
| B7Z6Y2 | Myc box-dependent-interacting protein 1 | BIN1 | 0.85 | 2.86 |
| Q6FHX6 | Flap endonuclease 1 | FEN1 | 0.84 | 11.02 |
| Q7Z726 | Importin subunit alpha;Importin subunit alpha-1 | KPNA2 | 0.84 | 7.92 |
| Q9UBB4 | Ataxin-10 | ATXN10 | 0.84 | 12.66 |
| V9HWH6 | Purine nucleoside phosphorylase | HEL-S-156an | 0.83 | 14.10 |

| | | | | |
|---|---|---|---|---|
| Q6IPH7 | | RPL14 | 0.83 | 7.18 |
| D3DT44 | Glutamate--cysteine ligase regulatory subunit | GCLM | 0.82 | 5.69 |
| P07737 | Profilin-1 | PFN1 | 0.82 | 15.14 |
| P62424 | 60S ribosomal protein L7a | RPL7A | 0.81 | 11.37 |
| Q6IBA2 | Activated RNA polymerase II transcriptional coactivator p15 | PC4 | 0.80 | 6.84 |
| P17812 | CTP synthase 1;CTP synthase | CTPS1 | 0.80 | 8.65 |
| A4D177 | Chromobox protein homolog 3 | CBX3 | 0.79 | 9.30 |
| P40222 | Alpha-taxilin | TXLNA | 0.79 | 8.67 |
| F6WIT2 | Serine/threonine-protein phosphatase 2A activator | PPP2R4 | 0.78 | 4.67 |
| Q9Y5B9 | FACT complex subunit SPT16 | SUPT16H | 0.77 | 15.60 |
| A0A024R4Z6 | FACT complex subunit SSRP1 | SSRP1 | 0.76 | 20.30 |
| B4DNN4 | Ribonucleoside-diphosphate reductase;Ribonucleoside-diphosphate reductase large subunit | RRM1 | 0.75 | 7.94 |
| P61960 | Ubiquitin-fold modifier 1 | UFM1 | 0.74 | 4.00 |
| Q9UNN8 | Endothelial protein C receptor | PROCR | 0.74 | 12.38 |
| Q53HJ4 | DNA helicase;DNA replication licensing factor MCM3 | MCM3 | 0.73 | 8.26 |
| A0A0S2Z4A5 | DNA replication licensing factor MCM7;DNA helicase | MCM7 | 0.73 | 12.17 |
| P37802 | Transgelin-2 | TAGLN2 | 0.72 | 11.98 |
| P18077 | 60S ribosomal protein L35a | RPL35A | 0.72 | 5.90 |
| M0R117 | 60S ribosomal protein L18a | RPL18A | 0.71 | 10.66 |
| Q16222 | UDP-N-acetylhexosamine pyrophosphorylase;UDP-N-acetylgalactosamine pyrophosphorylase;UDP-N-acetylglucosamine pyrophosphorylase | UAP1 | 0.71 | 10.20 |
| P20290 | Transcription factor BTF3 | BTF3 | 0.71 | 4.73 |
| A0A024RDE8 | PDZ and LIM domain protein 5 | PDLIM5 | 0.71 | 10.34 |
| A0A024RDY0 | Importin-5 | RANBP5 | 0.71 | 15.80 |
| P18124 | 60S ribosomal protein L7 | RPL7 | 0.70 | 17.65 |
| Q71UA6 | Amino acid transporter;Neutral amino acid transporter B(0) | SLC1A5 | 0.70 | 10.66 |
| Q9BY44 | Eukaryotic translation initiation factor 2A;Eukaryotic translation initiation factor 2A, N-terminally processed | EIF2A | 0.70 | 10.62 |
| Q5ISS7 | 60S ribosomal protein L10 | RPL10 | 0.70 | 6.74 |
| Q8IZ29 | Tubulin beta-4B chain | TUBB2C | 0.70 | 9.57 |
| P62917 | 60S ribosomal protein L8 | RPL8 | 0.69 | 8.20 |
| Q658N3 | Protein Dr1 | DKFZp666G145 | 0.69 | 5.45 |
| C9JXB8 | 60S ribosomal protein L24 | RPL24 | 0.69 | 7.33 |
| A0A024R6Y2 | Nuclear transport factor 2 | NUTF2 | 0.68 | 6.07 |
| Q9NR30 | Nucleolar RNA helicase 2 | DDX21 | 0.68 | 12.20 |
| Q8WVC2 | 40S ribosomal protein S21 | RPS21 | 0.68 | 8.93 |

| | | | | |
|---|---|---|---|---|
| Q9UJU6 | Drebrin-like protein | DBNL | 0.68 | 6.66 |
| A8K7F6 | Eukaryotic initiation factor 4A-I | EIF4A1 | 0.67 | 18.76 |
| A0A024QZ77 | EF-hand domain-containing protein D2 | EFHD2 | 0.67 | 2.95 |
| A8K2X4 | Endoglin | ENG | 0.67 | 12.73 |
| Q53H03 | Nuclear autoantigenic sperm protein | NASP | 0.66 | 8.66 |
| P62277 | 40S ribosomal protein S13 | RPS13 | 0.66 | 12.79 |
| Q6FI35 | Proliferating cell nuclear antigen | PCNA | 0.64 | 14.91 |
| A0A024R904 | Calcyclin-binding protein | CACYBP | 0.64 | 9.86 |
| A8K6Q8 | Transferrin receptor protein 1;Transferrin receptor protein 1, serum form | TFRC | 0.64 | 5.69 |
| B2R4R9 | 40S ribosomal protein S28 | RPS28 | 0.63 | 5.72 |
| P42677 | 40S ribosomal protein S27 | RPS27 | 0.63 | 7.87 |
| P13639 | Elongation factor 2 | EEF2 | 0.62 | 21.00 |
| O14929 | Histone acetyltransferase type B catalytic subunit | HAT1 | 0.62 | 9.51 |
| A0A140VK94 | Ran-specific GTPase-activating protein | RANBP1 | 0.61 | 10.73 |
| A0A024QYX3 | RNA-binding protein 3 | RBM3 | 0.61 | 4.16 |
| P62306 | Small nuclear ribonucleoprotein F | SNRPF | 0.60 | 2.57 |
| A0A0S2Z4R1 | Tyrosine--tRNA ligase, cytoplasmic;Tyrosine--tRNA ligase, cytoplasmic, N-terminally processed;Tyrosine--tRNA ligase | YARS | 0.60 | 9.43 |

Appendix Table 4: List of down-regulated proteins associated with endothelial dysfunctionality in CTEPH.

| Protein ID | Protein names | Gene names | Log2 (CTEPH-EC/HPAE) | -LOG(P-value) |
|---|---|---|---|---|
| V9HW74 | Ubiquitin carboxyl-terminal hydrolase;Ubiquitin carboxyl-terminal hydrolase isozyme L1 | HEL-117 | -3.17 | 4.04 |
| B2R769 | Endoplasmic reticulum aminopeptidase 2 | ERAP2 | -2.53 | 8.81 |
| A0A024RDG9 | 3-hydroxybutyrate dehydrogenase type 2 | BDH2 | -2.21 | 12.83 |
| K7ERP4 | Glutathione peroxidase;Phospholipid hydroperoxide glutathione peroxidase, mitochondrial | GPX4 | -2.18 | 9.66 |
| A0A090N8Z4 | GTPase IMAP family member 1 | IMAP1 | -2.04 | 9.55 |
| Q8NHP8 | Putative phospholipase B-like 2;Putative phospholipase B-like 2 32 kDa form;Putative phospholipase B-like 2 45 kDa form | PLBD2 | -2.01 | 8.33 |
| A0A024R5L0 | Lysosomal Pro-X carboxypeptidase | PRCP | -1.91 | 14.87 |
| Q5NKV8 | Intercellular adhesion molecule 1 | ICAM1 | -1.59 | 6.89 |
| P30837 | Aldehyde dehydrogenase X, mitochondrial | ALDH1B1 | -1.58 | 10.33 |
| Q5TBU5 | Adipogenesis regulatory factor | hCG_1773630 | -1.58 | 11.17 |
| B4DJI2 | Granulins;Acrogranin;Paragranulin;Granulin-1;Granulin-2;Granulin-3;Granulin-4;Granulin-5;Granulin-6;Granulin-7 | GRN | -1.56 | 14.56 |

| | | | | |
|---|---|---|---|---|
| Q96DI8 | Heme oxygenase 1 | HMOX1 | -1.55 | 10.09 |
| P04040 | Catalase | CAT | -1.55 | 11.85 |
| B4DSE2 | Tripeptidyl-peptidase 1 | TPP1 | -1.53 | 22.28 |
| Q14165 | Malectin | MLEC | -1.52 | 10.46 |
| Q92626 | Peroxidasin homolog | PXDN | -1.48 | 4.09 |
| Q7Z7M4 | Superoxide dismutase;Superoxide dismutase [Mn], mitochondrial | SOD2 | -1.47 | 6.81 |
| A0A090N8H2 | GTPase IMAP family member 8 | hIAN6 | -1.45 | 7.71 |
| B4DTT0 | N-acetylglucosamine-6-sulfatase | DKFZp686E12166 | -1.44 | 22.53 |
| A0A024RA75 | 3-hydroxyisobutyrate dehydrogenase;3-hydroxyisobutyrate dehydrogenase, mitochondrial | HIBADH | -1.42 | 7.84 |
| P36551 | Oxygen-dependent coproporphyrinogen-III oxidase, mitochondrial | CPOX | -1.41 | 12.80 |
| Q5URX0 | Beta-hexosaminidase;Beta-hexosaminidase subunit beta;Beta-hexosaminidase subunit beta chain B;Beta-hexosaminidase subunit beta chain A | HEXB | -1.41 | 22.55 |
| A0A090N7X0 | GTPase IMAP family member 4 | HIMAP4 | -1.39 | 8.48 |
| B3KQQ0 | Peptidyl-prolyl cis-trans isomerase FKBP9 | FKBP9 | -1.39 | 7.45 |
| A0A024R8Q1 | Lysosomal alpha-glucosidase;76 kDa lysosomal alpha-glucosidase;70 kDa lysosomal alpha-glucosidase | GAA | -1.36 | 13.32 |
| A0A140VJL0 | 3-hydroxyisobutyryl-CoA hydrolase, mitochondrial | HIBCH | -1.35 | 5.65 |
| A8K335 | Gamma-glutamyl hydrolase | GGH | -1.34 | 8.29 |
| A0A0C4DFN8 | NADPH:adrenodoxin oxidoreductase, mitochondrial | FDXR | -1.34 | 16.12 |
| Q53H18 | Beta-galactosidase | GLB1 | -1.32 | 6.66 |
| Q9NSC5 | Homer protein homolog 3 | HOMER3 | -1.31 | 6.31 |
| Q6IB89 | NADH dehydrogenase [ubiquinone] 1 alpha subcomplex subunit 7 | NDUFA7 | -1.29 | 9.31 |
| Q9Y2Q5 | Ragulator complex protein LAMTOR2 | LAMTOR2 | -1.28 | 12.02 |
| P49407 | Beta-arrestin-1 | ARRB1 | -1.27 | 4.68 |
| P04275 | von Willebrand factor;von Willebrand antigen 2 | VWF | -1.26 | 11.90 |
| O75923 | Dysferlin | DYSF | -1.25 | 13.11 |
| Q53FB6 | Aldehyde dehydrogenase, mitochondrial | ALDH2 | -1.25 | 12.60 |
| A8K9J6 | CD276 antigen | CD276 | -1.23 | 3.52 |
| B4DJQ8 | Dipeptidyl peptidase 1;Dipeptidyl peptidase 1 exclusion domain chain;Dipeptidyl peptidase 1 heavy chain;Dipeptidyl peptidase 1 light chain | CTSC | -1.23 | 6.01 |
| Q9BVJ8 | Beta-hexosaminidase;Beta-hexosaminidase subunit alpha | HEXA | -1.21 | 4.95 |
| P51970 | NADH dehydrogenase [ubiquinone] 1 alpha subcomplex subunit 8 | NDUFA8 | -1.21 | 8.46 |
| Q8TDB4 | Protein MGARP | MGARP | -1.19 | 3.74 |
| Q8IWP6 | | | -1.19 | 1.70 |
| Q9UHL4 | Dipeptidyl peptidase 2 | DPP7 | -1.18 | 7.40 |

| | | | | | |
|---|---|---|---|---|---|
| P16284 | Platelet endothelial cell adhesion molecule | PECAM1 | | -1.18 | 18.62 |
| A0A024RAD8 | Delta-1-pyrroline-5-carboxylate dehydrogenase, mitochondrial | ALDH4A1 | | -1.17 | 8.33 |
| A0A1B0GW44 | Cathepsin D;Cathepsin D light chain;Cathepsin D heavy chain | HEL-S-130P | | -1.17 | 20.91 |
| B2R7D2 | Multiple inositol polyphosphate phosphatase 1 | MINPP1 | | -1.16 | 6.44 |
| A0A024RAB6 | Basement membrane-specific heparan sulfate proteoglycan core protein;Endorepellin;LG3 peptide | HSPG2 | | -1.16 | 16.03 |
| Q9Y4D7 | Plexin-D1 | PLXND1 | | -1.15 | 14.69 |
| Q96CM8 | Acyl-CoA synthetase family member 2, mitochondrial | ACSF2 | | -1.12 | 3.92 |
| B7Z8A2 | Prenylcysteine oxidase 1 | PCYOX1 | | -1.11 | 14.14 |
| P35580 | Myosin-10 | MYH10 | | -1.11 | 18.41 |
| Q14XT3 | Cytochrome c oxidase subunit 2 | COX2 | | -1.11 | 4.76 |
| Q9NV96 | Cell cycle control protein 50A | TMEM30A | | -1.10 | 4.80 |
| B4E324 | Carboxypeptidase;Lysosomal protective protein;Lysosomal protective protein 32 kDa chain;Lysosomal protective protein 20 kDa chain | CTSA | | -1.10 | 12.17 |
| Q53FJ5 | Prosaposin;Saposin-A;Saposin-B-Val;Saposin-B;Saposin-C;Saposin-D | PSAP | | -1.10 | 14.44 |
| P49006 | MARCKS-related protein | MARCKSL1 | | -1.10 | 8.90 |
| A0A024R9D7 | 2,4-dienoyl-CoA reductase, mitochondrial | DECR1 | | -1.09 | 17.20 |
| Q6DHZ2 | cAMP-dependent protein kinase type II-beta regulatory subunit | PRKAR2B | | -1.09 | 6.33 |
| A0A096LPI6 | ES1 protein homolog, mitochondrial | C21orf33 | | -1.09 | 6.35 |
| P38117 | Electron transfer flavoprotein subunit beta | ETFB | | -1.07 | 15.26 |
| A0A024RC61 | Aminopeptidase N | ANPEP | | -1.07 | 17.29 |
| Q96DP0 | | | | -1.06 | 7.04 |
| B4DKM6 | Serum paraoxonase/arylesterase 2 | PON2 | | -1.06 | 6.17 |
| Q96N83 | Podocalyxin | PODXL | | -1.06 | 7.24 |
| A0A0S2Z5A5 | Septin-9 | | 9-Sep | -1.05 | 3.53 |
| B4DEH0 | 39S ribosomal protein L10, mitochondrial | MRPL10 | | -1.05 | 5.53 |
| A0A024R8T3 | Acyl-coenzyme A oxidase;Peroxisomal acyl-coenzyme A oxidase 1 | ACOX1 | | -1.04 | 8.80 |
| B4E2S7 | Lysosome-associated membrane glycoprotein 2 | LAMP2 | | -1.04 | 14.55 |
| Q8WYJ5 | Histidine triad nucleotide-binding protein 2, mitochondrial | HINT2 | | -1.03 | 8.40 |
| B3KNK4 | Phosphatidate cytidylyltransferase;Phosphatidate cytidylyltransferase 2 | CDS2 | | -1.03 | 2.80 |
| Q53YE7 | Amine oxidase [flavin-containing] A | MAOA | | -1.02 | 3.77 |
| A0A0S2Z3L0 | Electron transfer flavoprotein subunit alpha, mitochondrial | ETFA | | -1.01 | 12.57 |
| L7UUZ7 | Integrin beta;Integrin beta-3 | ITGB3 | | -1.01 | 3.87 |
| Q8NG19 | Collagen alpha-1(XVIII) chain;Endostatin | COL18A1 | | -1.00 | 2.89 |
| B5MDU6 | UPF0554 protein C2orf43 | LDAH | | -0.99 | 3.34 |
| B7Z3K3 | Inositol-3-phosphate synthase 1 | ISYNA1 | | -0.98 | 5.69 |

| | | | | |
|---|---|---|---|---|
| B3KRY3 | Lysosome-associated membrane glycoprotein 1 | LAMP1 | -0.97 | 11.48 |
| Q14258 | E3 ubiquitin/ISG15 ligase TRIM25 | TRIM25 | -0.96 | 9.81 |
| P30084 | Enoyl-CoA hydratase, mitochondrial | ECHS1 | -0.96 | 19.00 |
| H7C0V9 | Amyloid beta A4 protein;N-APP;Soluble APP-alpha;Soluble APP-beta;C99;Beta-amyloid protein 42;Beta-amyloid protein 40;C83;P3(42);P3(40);C80;Gamma-secretase C-terminal fragment 59;Gamma-secretase C-terminal fragment 57;Gamma-secretase C-terminal fragment 50;C31 | APP | -0.94 | 6.91 |
| P17900 | Ganglioside GM2 activator;Ganglioside GM2 activator isoform short | GM2A | -0.94 | 3.73 |
| A0A0B4J2A4 | 3-ketoacyl-CoA thiolase, mitochondrial | ACAA2 | -0.93 | 6.54 |
| B7Z7Z3 | Nitric oxide synthase;Nitric oxide synthase, endothelial | NOS3 | -0.93 | 5.13 |
| P11233 | Ras-related protein Ral-A | RALA | -0.93 | 10.27 |
| A0A1B0GTY9 | Alpha-aminoadipic semialdehyde dehydrogenase | ALDH7A1 | -0.92 | 8.53 |
| J3K000 | Xaa-Pro dipeptidase | PEPD | -0.91 | 2.61 |
| B2RAZ4 | Apoptosis-associated speck-like protein containing a CARD | PYCARD | -0.91 | 7.44 |
| A8K6H1 | Endoplasmic reticulum aminopeptidase 1 | ERAP1 | -0.90 | 9.62 |
| A0A024R5C4 | Reticulon;Reticulon-3 | RTN3 | -0.90 | 7.81 |
| P21912 | Succinate dehydrogenase [ubiquinone] iron-sulfur subunit, mitochondrial | SDHB | -0.89 | 7.61 |
| Q6FHM4 | Cytochrome c oxidase subunit 5B, mitochondrial | COX5B | -0.89 | 11.86 |
| B2R659 | Peroxisomal multifunctional enzyme type 2;(3R)-hydroxyacyl-CoA dehydrogenase;Enoyl-CoA hydratase 2 | HSD17B4 | -0.89 | 18.62 |
| P16930 | Fumarylacetoacetase | FAH | -0.89 | 3.50 |
| P55084 | Trifunctional enzyme subunit beta, mitochondrial;3-ketoacyl-CoA thiolase | HADHB | -0.88 | 23.18 |
| P30048 | Thioredoxin-dependent peroxide reductase, mitochondrial | PRDX3 | -0.88 | 13.39 |
| Q9H1E3 | Nuclear ubiquitous casein and cyclin-dependent kinase substrate 1 | NUCKS1 | -0.88 | 3.09 |
| B3KWW5 | Galectin;Galectin-9 | LGALS9 | -0.88 | 1.76 |
| A0A0A0MR02 | Voltage-dependent anion-selective channel protein 2 | VDAC2 | -0.87 | 25.28 |
| Q7Z531 | GTP:AMP phosphotransferase AK3, mitochondrial | AK3 | -0.87 | 6.81 |
| Q9UF24 | NADH dehydrogenase [ubiquinone] iron-sulfur protein 3, mitochondrial | DKFZp586K0821 | -0.87 | 5.21 |
| A0A024R670 | Synaptojanin-2-binding protein | SYNJ2BP | -0.86 | 6.97 |
| Q7Z434 | Mitochondrial antiviral-signaling protein | MAVS | -0.86 | 6.23 |
| L7RXH0 | Integrin alpha-V;Integrin alpha-V heavy chain;Integrin alpha-V light chain | ITGAV | -0.86 | 8.63 |
| Q14571 | Inositol 1,4,5-trisphosphate receptor type 2 | ITPR2 | -0.85 | 5.26 |
| E9PIN3 | Nuclear RNA export factor 1 | NXF1 | -0.85 | 5.05 |
| Q59E90 | Alpha-mannosidase;Lysosomal alpha-mannosidase;Lysosomal alpha-mannosidase A | MAN2B1 | -0.85 | 3.12 |

| | | | | |
|---|---|---|---|---|
| | peptide;Lysosomal alpha-mannosidase B peptide;Lysosomal alpha-mannosidase C peptide;Lysosomal alpha-mannosidase D peptide;Lysosomal alpha-mannosidase E peptide | | | |
| Q9Y277 | Voltage-dependent anion-selective channel protein 3 | VDAC3 | -0.84 | 10.59 |
| Q2TAB3 | Sulfotransferase;Sulfotransferase 1A4;Sulfotransferase 1A3 | SULT1A4 | -0.84 | 3.81 |
| Q13011 | Delta(3,5)-Delta(2,4)-dienoyl-CoA isomerase, mitochondrial | ECH1 | -0.84 | 7.34 |
| B2RAQ8 | Carnitine O-palmitoyltransferase 1, liver isoform | CPT1A | -0.83 | 11.90 |
| Q9UHA4 | Ragulator complex protein LAMTOR3 | LAMTOR3 | -0.83 | 4.23 |
| A1L0T0 | Acetolactate synthase-like protein | ILVBL | -0.82 | 6.15 |
| K7EQ77 | NADH dehydrogenase [ubiquinone] 1 alpha subcomplex subunit 11 | NDUFA11 | -0.82 | 7.26 |
| B4DMP4 | Protein VAC14 homolog | VAC14 | -0.82 | 2.82 |
| Q8IY17 | Neuropathy target esterase | PNPLA6 | -0.82 | 7.08 |
| A0A087WUQ6 | Glutathione peroxidase;Glutathione peroxidase 1 | GPX1 | -0.82 | 5.76 |
| A0A024R9B7 | Cytochrome c oxidase subunit 6C | COX6C | -0.82 | 4.96 |
| V9HW53 | N(G),N(G)-dimethylarginine dimethylaminohydrolase 2 | HEL-S-277 | -0.81 | 9.48 |
| Q9BTT5 | NADH dehydrogenase [ubiquinone] 1 alpha subcomplex subunit 9, mitochondrial | NDUFA9 | -0.80 | 10.54 |
| B1AK13 | Hydroxymethylglutaryl-CoA lyase, mitochondrial | HMGCL | -0.80 | 3.02 |
| A0A1L1UHR1 | Voltage-dependent anion-selective channel protein 1 | VDAC1 | -0.79 | 19.49 |
| Q9UEH5 | NADH dehydrogenase [ubiquinone] flavoprotein 2, mitochondrial | NDUFV2 | -0.78 | 13.38 |
| X5CKB3 | Antigen peptide transporter 1 | TAP1 | -0.78 | 4.50 |
| Q5RKT7 | Ubiquitin-40S ribosomal protein S27a;Ubiquitin;40S ribosomal protein S27a;Ubiquitin-60S ribosomal protein L40;Ubiquitin;60S ribosomal protein L40;Polyubiquitin-B;Ubiquitin;Polyubiquitin-C;Ubiquitin | RPS27A | -0.78 | 5.64 |
| H7BXI1 | Extended synaptotagmin-2 | ESYT2 | -0.77 | 5.40 |
| H7BYY1 | | TPM1 | -0.77 | 4.61 |
| A0A024R325 | Succinyl-CoA ligase subunit beta;Succinyl-CoA ligase [GDP-forming] subunit beta, mitochondrial | SUCLG2 | -0.76 | 10.74 |
| Q68DH9 | Calcium-transporting ATPase;Plasma membrane calcium-transporting ATPase 4 | DKFZp686M088 | -0.76 | 6.53 |
| A8K2W3 | Serum deprivation-response protein | SDPR | -0.76 | 6.57 |
| K7EJE8 | Lon protease homolog, mitochondrial;Lon protease homolog | LONP1 | -0.76 | 8.01 |
| A0A0A0MS41 | Sideroflexin;Sideroflexin-3 | SFXN3 | -0.76 | 4.78 |
| P52209 | 6-phosphogluconate dehydrogenase, decarboxylating | PGD | -0.76 | 9.45 |

| | | | | |
|---|---|---|---|---|
| P10909 | Clusterin;Clusterin beta chain;Clusterin alpha chain;Clusterin | CLU | -0.76 | 2.50 |
| D3DQH8 | SPARC | SPARC | -0.76 | 13.46 |
| B4DP06 | | | -0.75 | 2.91 |
| Q96PU8 | Protein quaking | QKI | -0.75 | 5.25 |
| Q9UHS8 | Sulfide:quinone oxidoreductase, mitochondrial | hCG_2001986 | -0.75 | 5.02 |
| Q53SW4 | NADH dehydrogenase [ubiquinone] 1 alpha subcomplex subunit 10, mitochondrial | NDUFA10 | -0.75 | 6.21 |
| B3KPA6 | Very long-chain specific acyl-CoA dehydrogenase, mitochondrial | ACADVL | -0.75 | 17.29 |
| A0A1W2PQT3 | NAD-dependent malic enzyme, mitochondrial | ME2 | -0.75 | 7.30 |
| Q9NZM1 | Myoferlin | MYOF | -0.74 | 12.95 |
| A0A024QZ30 | Succinate dehydrogenase [ubiquinone] flavoprotein subunit, mitochondrial | SDHA | -0.74 | 15.39 |
| A0A140VJX1 | Acetyl-CoA acetyltransferase, mitochondrial | ACAT1 | -0.74 | 15.09 |
| A0A024RAS8 | Heme-binding protein 1 | HEBP1 | -0.74 | 10.73 |
| Q9BS40 | Latexin | LXN | -0.74 | 3.90 |
| Q9NUJ1 | Mycophenolic acid acyl-glucuronide esterase, mitochondrial | ABHD10 | -0.73 | 8.58 |
| P29590 | Protein PML | PML | -0.73 | 7.94 |
| V9HWC9 | Superoxide dismutase [Cu-Zn] | HEL-S-44 | -0.73 | 10.11 |
| Q6DKJ4 | Nucleoredoxin | NXN | -0.73 | 3.32 |
| D3DVF0 | Junctional adhesion molecule A | F11R | -0.73 | 4.02 |
| E9KL44 | Trifunctional enzyme subunit alpha, mitochondrial;Long-chain enoyl-CoA hydratase;Long chain 3-hydroxyacyl-CoA dehydrogenase | HADHA | -0.73 | 15.80 |
| Q9UNW9 | RNA-binding protein Nova-2 | NOVA2 | -0.72 | 5.79 |
| A0A0S2Z487 | Junction plakoglobin | JUP | -0.72 | 3.81 |
| Q13201 | Multimerin-1;Platelet glycoprotein Ia*;155 kDa platelet multimerin | MMRN1 | -0.72 | 4.71 |
| A0A024R3J7 | Dolichyl-diphosphooligosaccharide--protein glycosyltransferase subunit STT3A | hCG_2032701 | -0.72 | 7.94 |
| Q99584 | Protein S100-A13 | S100A13 | -0.72 | 4.51 |
| E5KRK5 | NADH-ubiquinone oxidoreductase 75 kDa subunit, mitochondrial | NDUFS1 | -0.71 | 15.06 |
| B4DMF5 | Glutamate dehydrogenase;Glutamate dehydrogenase 1, mitochondrial;Glutamate dehydrogenase 2, mitochondrial | GLUD1 | -0.71 | 12.33 |
| B2RA03 | Keratin, type I cytoskeletal 18 | KRT18 | -0.71 | 9.05 |
| Q9H845 | Acyl-CoA dehydrogenase family member 9, mitochondrial | ACAD9 | -0.71 | 3.95 |
| Q9Y6C9 | Mitochondrial carrier homolog 2 | MTCH2 | -0.71 | 6.69 |
| A8K761 | NADH dehydrogenase [ubiquinone] 1 beta subcomplex subunit 10 | NDUFB10 | -0.71 | 6.24 |
| Q9HAV0 | Guanine nucleotide-binding protein subunit beta-4 | GNB4 | -0.71 | 3.12 |
| A0A024R745 | NADH dehydrogenase [ubiquinone] 1 alpha subcomplex subunit 5 | NDUFA5 | -0.71 | 4.45 |
| D3DTC2 | Lysophosphatidylcholine acyltransferase 1 | AYTL2 | -0.71 | 6.93 |

| | | | | |
|---|---|---|---|---|
| H3BPK3 | Hydroxyacylglutathione hydrolase, mitochondrial | HAGH | -0.70 | 5.20 |
| V9HW38 | Cytosol aminopeptidase | HEL-S-106 | -0.70 | 14.85 |
| Q56VL3 | OCIA domain-containing protein 2 | OCIAD2 | -0.70 | 5.69 |
| P47985 | Cytochrome b-c1 complex subunit Rieske, mitochondrial;Cytochrome b-c1 complex subunit 11 | UQCRFS1 | -0.70 | 4.14 |
| A8K734 | Hedgehog-interacting protein | HHIP | -0.70 | 5.80 |
| Q53GX6 | Nucleobindin-1 | NUCB1 | -0.70 | 10.35 |
| Q567R0 | Cytochrome b-c1 complex subunit 6, mitochondrial | UQCRH | -0.70 | 4.56 |
| O15173 | Membrane-associated progesterone receptor component 2 | PGRMC2 | -0.70 | 7.83 |
| A0A0S2Z4V6 | Wolframin | WFS1 | -0.69 | 2.31 |
| Q7L5N7 | Lysophosphatidylcholine acyltransferase 2 | LPCAT2 | -0.69 | 3.09 |
| A0A090N7T9 | Secernin-1 | SCRN1 | -0.69 | 5.43 |
| A0A024R2M6 | 3-ketoacyl-CoA thiolase, peroxisomal | ACAA1 | -0.68 | 8.49 |
| Q14573 | Inositol 1,4,5-trisphosphate receptor type 3 | ITPR3 | -0.68 | 6.51 |
| B3KUJ5 | Histone deacetylase;Histone deacetylase 2 | HDAC2 | -0.68 | 4.98 |
| A0A024R882 | Erythrocyte band 7 integral membrane protein | STOM | -0.68 | 5.08 |
| B4DL49 | Cathepsin B;Cathepsin B light chain;Cathepsin B heavy chain | CTSB | -0.68 | 7.58 |
| B2R761 | Non-specific lipid-transfer protein | SCP2 | -0.68 | 8.91 |
| Q9NUF9 | Nucleoside diphosphate kinase;Nucleoside diphosphate kinase 3 | c371H6.2 | -0.67 | 2.95 |
| O95831 | Apoptosis-inducing factor 1, mitochondrial | AIFM1 | -0.67 | 6.45 |
| A0A0C4DG44 | Serine protease HTRA2, mitochondrial | HTRA2 | -0.67 | 3.17 |
| I3L1P8 | Mitochondrial 2-oxoglutarate/malate carrier protein | SLC25A11 | -0.67 | 10.93 |
| E9PKG6 | Nucleobindin-2;Nesfatin-1 | NUCB2 | -0.66 | 5.93 |
| Q53FG6 | Splicing factor 3B subunit 4 | SF3B4 | -0.66 | 4.72 |
| Q9H7Z7 | Prostaglandin E synthase 2;Prostaglandin E synthase 2 truncated form | PTGES2 | -0.66 | 3.30 |
| Q0QF37 | Malate dehydrogenase;Malate dehydrogenase, mitochondrial | MDH2 | -0.65 | 10.78 |
| Q9H857 | 5-nucleotidase domain-containing protein 2 | NT5DC2 | -0.65 | 2.71 |
| Q86WV6 | Stimulator of interferon genes protein | TMEM173 | -0.65 | 4.36 |
| P48047 | ATP synthase subunit O, mitochondrial | ATP5O | -0.65 | 14.55 |
| Q8TBT6 | Cytochrome c1, heme protein, mitochondrial | CYC1 | -0.65 | 9.60 |
| V9HW35 | Peroxiredoxin-5, mitochondrial | HEL-S-55 | -0.65 | 7.84 |
| F5GXX5 | Dolichyl-diphosphooligosaccharide--protein glycosyltransferase subunit DAD1 | DAD1 | -0.65 | 6.26 |
| I6L9C8 | Zinc finger protein 428 | ZNF428 | -0.64 | 3.59 |
| A8K401 | Prohibitin | PHB | -0.64 | 20.47 |
| C9JG87 | 39S ribosomal protein L39, mitochondrial | MRPL39 | -0.64 | 4.36 |
| B4E0X1 | Beta-2-microglobulin;Beta-2-microglobulin;Beta-2-microglobulin form pI 5.3 | B2M | -0.64 | 2.50 |

| | | | | |
|---|---|---|---|---|
| Q53GR7 | Calcium-binding mitochondrial carrier protein Aralar2 | SLC25A13 | -0.63 | 6.87 |
| D3DSR9 | Tumor necrosis factor receptor superfamily member 10B | TNFRSF10B | -0.63 | 2.29 |
| Q8NCF7 | Phosphate carrier protein, mitochondrial | SLC25A3 | -0.63 | 7.61 |
| B4E0H8 | Integrin alpha-3;Integrin alpha-3 heavy chain;Integrin alpha-3 light chain | ITGA3 | -0.63 | 7.20 |
| J3QRT5 | Intercellular adhesion molecule 2 | ICAM2 | -0.63 | 4.46 |
| Q9UNM1 | 10 kDa heat shock protein, mitochondrial | EPFP1 | -0.63 | 14.84 |
| B4DWN1 | Vesicular integral-membrane protein VIP36 | LMAN2 | -0.63 | 4.77 |
| O15400 | Syntaxin-7 | STX7 | -0.62 | 6.82 |
| Q53GQ0 | Very-long-chain 3-oxoacyl-CoA reductase | HSD17B12 | -0.62 | 6.35 |
| Q9HDC9 | Adipocyte plasma membrane-associated protein | APMAP | -0.62 | 7.78 |
| E5KS95 | Elongation factor Ts, mitochondrial | TSFM | -0.62 | 2.42 |
| Q0PNF2 | Stabilin-1 | STAB1 | -0.62 | 7.12 |
| B4DDH8 | Lysophospholipid acyltransferase 7 | MBOAT7 | -0.62 | 5.98 |
| Q9H2U2 | Inorganic pyrophosphatase 2, mitochondrial | PPA2 | -0.61 | 6.56 |
| A0A024R3X4 | 60 kDa heat shock protein, mitochondrial | HSPD1 | -0.61 | 17.54 |
| P35270 | Sepiapterin reductase | SPR | -0.61 | 4.04 |
| P11177 | Pyruvate dehydrogenase E1 component subunit beta, mitochondrial | PDHB | -0.61 | 8.30 |
| Q9Y512 | Sorting and assembly machinery component 50 homolog | SAMM50 | -0.61 | 4.88 |
| A0A024R1M8 | Apolipoprotein L2 | APOL2 | -0.60 | 4.05 |
| F8W031 | | CNPY2 | -0.60 | 8.25 |
| B2RAW0 | Disabled homolog 2 | DAB2 | -0.60 | 4.25 |
| Q9Y5J9 | Mitochondrial import inner membrane translocase subunit Tim8 B | TIMM8B | -0.60 | 4.23 |

Appendix Table 5: List of statistically significantly differentially regulated proteins in normal ECs upon exposure to 3PO for 24hrs.

| Protein ID | Protein names | Gene names | log2 (3PO/Control) | -LOG(P-value) |
|---|---|---|---|---|
| Q5TDE9 | Cancer-related nucleoside-triphosphatase | C1orf57;NTPCR | 0.81 | 3.81 |
| Q59E89 | DnaJ homolog subfamily B member 4 | DNAJB4 | 0.65 | 3.76 |
| A0A158RFU3 | Parathymosin | PTMS | 0.61 | 1.87 |
| Q59GN2 | Putative 60S ribosomal protein L39-like 5;60S ribosomal protein L39 | RPL39P5;RPL39 | 0.57 | 2.85 |
| A0A140VK41 | Ribose-phosphate pyrophosphokinase 2 | PRPS2 | 0.55 | 2.66 |
| Q2TSD2 | Nucleolysin TIAR | TIAL1 | 0.53 | 1.71 |
| Q92522 | Histone H1x | H1FX | 0.52 | 3.70 |
| Q8WUW1 | Protein BRICK1 | BRK1 | 0.50 | 1.78 |
| Q2TAM5 | Transcription factor p65 | RELA | 0.50 | 2.43 |

| | | | | |
|---|---|---|---|---|
| A8MZF9 | Developmentally-regulated GTP-binding protein 2 | DRG2 | 0.49 | 2.29 |
| H3BUG4 | Anamorsin | CIAPIN1 | 0.48 | 1.08 |
| Q5QPM7 | Proteasome inhibitor PI31 subunit | PSMF1 | 0.46 | 2.13 |
| Q92621 | Nuclear pore complex protein Nup205 | NUP205 | 0.45 | 2.88 |
| P78527 | DNA-dependent protein kinase catalytic subunit | PRKDC | 0.44 | 3.56 |
| Q05D78 | Double-strand break repair protein MRE11A | MRE11A | 0.43 | 2.74 |
| A0A024R964 | Serine/threonine-protein kinase Nek7 | NEK7 | 0.43 | 3.18 |
| F5H5V4 | 26S proteasome non-ATPase regulatory subunit 9 | PSMD9 | 0.42 | 2.50 |
| B4E043 | KH domain-containing, RNA-binding, signal transduction-associated protein 1;KH domain-containing, RNA-binding, signal transduction-associated protein 3;KH domain-containing, RNA-binding, signal transduction-associated protein 2 | KHDRBS1;KHDRBS3;KHDRBS2 | 0.41 | 2.17 |
| Q6FGB3 | Pterin-4-alpha-carbinolamine dehydratase | PCBD;PCBD1 | 0.41 | 2.68 |
| P08579 | U2 small nuclear ribonucleoprotein B | SNRPB2 | 0.41 | 2.34 |
| Q6FGM6 | Peptidyl-prolyl cis-trans isomerase D | PPID | 0.41 | 1.34 |
| Q15645 | Pachytene checkpoint protein 2 homolog | TRIP13 | 0.40 | 2.77 |
| B2RAH5 | Protein phosphatase 1 regulatory subunit;Protein phosphatase 1 regulatory subunit 12A | PPP1R12A | 0.40 | 3.29 |
| B4DXG8 | Exosome complex component RRP45 | EXOSC9 | 0.39 | 3.12 |
| B7ZLC9 | Gem-associated protein 5 | GEMIN5 | 0.39 | 2.71 |
| I3L3P7 | 40S ribosomal protein S15a | RPS15A;hCG_1994130 | 0.37 | 2.58 |
| P62277 | 40S ribosomal protein S13 | RPS13 | 0.37 | 4.35 |
| O94906 | Pre-mRNA-processing factor 6 | PRPF6 | 0.37 | 2.62 |
| B4DLP1 | IST1 homolog | IST1 | 0.37 | 1.53 |
| E9PD53 | Structural maintenance of chromosomes protein;Structural maintenance of chromosomes protein 4 | SMC4 | 0.37 | 2.98 |
| Q9BZK7 | F-box-like/WD repeat-containing protein TBL1XR1;F-box-like/WD repeat-containing protein TBL1X | TBL1XR1;TBL1X | 0.36 | 2.26 |
| B3KMP2 | Anaphase-promoting complex subunit 7 | ANAPC7 | 0.35 | 1.42 |
| B3KY03 | Condensin complex subunit 1 | NCAPD2 | 0.35 | 1.26 |
| V9HWI1 | Flavin reductase (NADPH) | HEL-S-10;BLVRB | 0.34 | 3.12 |
| Q53G42 | m7GpppX diphosphatase | DCPS | 0.33 | 2.34 |
| P62851 | 40S ribosomal protein S25 | RPS25 | 0.33 | 1.78 |
| P62906 | 60S ribosomal protein L10a;Ribosomal protein | RPL10A | 0.33 | 2.91 |
| B7ZLZ7 | Structural maintenance of chromosomes protein;Structural maintenance of chromosomes protein 2 | SMC2;SMC2L1 | 0.32 | 2.81 |
| E5RHG8 | Transcription elongation factor B polypeptide 1 | TCEB1 | 0.32 | 2.98 |
| Q63HR1 | Plasminogen activator inhibitor 1 RNA-binding protein | DKFZp686P17171;SERBP1 | 0.32 | 2.18 |
| A0A024R0H7 | Methylosome protein 50 | WDR77 | 0.32 | 4.09 |
| Q5SQP8 | C-terminal-binding protein 2 | CTBP2 | 0.31 | 1.80 |

| | | | | |
|---|---|---|---|---|
| B2R928 | Mitogen-activated protein kinase kinase kinase kinase;Mitogen-activated protein kinase kinase kinase kinase 5 | MAP4K5 | 0.31 | 2.09 |
| A0A024QZ77 | EF-hand domain-containing protein D2 | EFHD2 | 0.31 | 1.81 |
| B4DPV7 | Cysteine--tRNA ligase, cytoplasmic | CARS | 0.30 | 3.03 |
| J3QLE5 | Small nuclear ribonucleoprotein-associated protein;Small nuclear ribonucleoprotein-associated protein N;Small nuclear ribonucleoprotein-associated proteins B and B | SNRPN;SNRPB | 0.30 | 2.87 |
| A0A024R5S5 | Eukaryotic translation initiation factor 3 subunit J | EIF3S1;EIF3J | 0.30 | 1.81 |
| Q5IFJ8 | 26S proteasome non-ATPase regulatory subunit 5 | PSMD5 | 0.29 | 3.42 |
| Q9Y3Z3 | Deoxynucleoside triphosphate triphosphohydrolase SAMHD1 | SAMHD1 | 0.29 | 2.89 |
| A0A023T787 | RNA-binding protein 8A | RBM8;RBM8A | 0.29 | 1.81 |
| B7Z3M6 | Phosphomannomutase;Phosphomannomutase 2 | PMM2 | 0.29 | 1.99 |
| Q1W6G4 | Putative RNA-binding protein Luc7-like 1 | LUC7L | 0.29 | 3.29 |
| O14776 | Transcription elongation regulator 1 | TCERG1 | 0.29 | 2.52 |
| P63279 | SUMO-conjugating enzyme UBC9 | UBE2I | 0.29 | 2.79 |
| P17096 | High mobility group protein HMG-I/HMG-Y | HMGA1 | 0.28 | 1.64 |
| B4DNR3 | Alpha/beta hydrolase domain-containing protein 14B | ABHD14B;HEL-S-299 | 0.28 | 2.89 |
| Q59GU6 | Sorting nexin-1 | SNX1 | 0.28 | 2.81 |
| Q53H22 | Amidophosphoribosyltransferase | PPAT | 0.28 | 1.59 |
| F8VYH9 | Cyclin-dependent kinase 4 | CDK4 | 0.28 | 3.12 |
| A0A024R4M0 | 40S ribosomal protein S9 | RPS9 | 0.28 | 3.18 |
| Q96EM0 | Trans-3-hydroxy-L-proline dehydratase | L3HYPDH | 0.27 | 2.71 |
| A0A1U9X9D5 | Valine--tRNA ligase | VARS | 0.27 | 2.37 |
| Q13242 | Serine/arginine-rich splicing factor 9 | SRSF9 | 0.27 | 4.55 |
| F8VPD4 | CAD protein;Glutamine-dependent carbamoyl-phosphate synthase;Aspartate carbamoyltransferase;Dihydroorotase | CAD | 0.27 | 5.05 |
| Q9NYG1 | Caldesmon | CALD1 | 0.27 | 3.59 |
| Q32Q12 | Nucleoside diphosphate kinase;Nucleoside diphosphate kinase B | NME1-NME2;NME2;NME1 | 0.27 | 2.49 |
| E9PJ81 | UBX domain-containing protein 1 | UBXN1;LOC51035 | 0.27 | 1.56 |
| B5LY71 | Uridine 5-monophosphate synthase;Orotate phosphoribosyltransferase;Orotidine 5-phosphate decarboxylase;Orotidine 5-phosphate decarboxylase | UMPS | 0.26 | 1.73 |
| P49006 | MARCKS-related protein | MARCKSL1 | 0.26 | 2.64 |
| Q53F35 | Acidic leucine-rich nuclear phosphoprotein 32 family member B | ANP32B | 0.26 | 3.07 |
| A0A024R3V0 | SPATS2-like protein | DNAPTP6;SPATS2L | 0.26 | 4.37 |
| P19623 | Spermidine synthase | SRM | 0.26 | 3.09 |
| B4DHG4 | Exocyst complex component 5 | EXOC5 | 0.25 | 1.81 |

| | | | | |
|---|---|---|---|---|
| A8K9K6 | Nucleolar protein 56 | NOP56 | 0.25 | 2.70 |
| A0A024R652 | C-1-tetrahydrofolate synthase, cytoplasmic;Methylenetetrahydrofolate dehydrogenase;Methenyltetrahydrofolate cyclohydrolase;Formyltetrahydrofolate synthetase;C-1-tetrahydrofolate synthase, cytoplasmic, N-terminally processed | MTHFD1 | 0.25 | 5.80 |
| E9PID8 | Cleavage stimulation factor subunit 2 | CSTF2 | 0.25 | 2.12 |
| V9HW92 | PDZ and LIM domain protein 1 | HEL-S-112;PDLIM1 | 0.25 | 3.52 |
| A0A0A6YYJ8 | Putative RNA-binding protein Luc7-like 2 | LUC7L2 | 0.24 | 3.38 |
| O15042 | U2 snRNP-associated SURP motif-containing protein | U2SURP | 0.24 | 2.15 |
| A0A024R222 | Phosphoserine aminotransferase | PSAT1 | 0.24 | 3.42 |
| A0A140VK39 | Protein phosphatase methylesterase 1 | PPME1 | 0.24 | 2.39 |
| Q9Y266 | Nuclear migration protein nudC | NUDC;NPD011 | 0.24 | 2.55 |
| B7Z1N6 | Fructose-bisphosphate aldolase;Fructose-bisphosphate aldolase C | ALDOC | 0.24 | 2.12 |
| J3KP15 | Serine/arginine-rich splicing factor 2 | SRSF2;SFRS2 | 0.24 | 3.72 |
| Q4ZG72 | ATP-dependent RNA helicase DDX18 | DDX18 | 0.24 | 2.64 |
| P60866 | 40S ribosomal protein S20 | RPS20 | 0.24 | 2.28 |
| Q10567 | AP-1 complex subunit beta-1 | AP1B1 | 0.24 | 2.93 |
| A0A0S2Z4G7 | Nucleophosmin | NPM1 | 0.23 | 3.58 |
| Q53FW2 | Ribose-phosphate pyrophosphokinase 1 | PRPS1 | 0.23 | 6.19 |
| Q9NRN7 | L-aminoadipate-semialdehyde dehydrogenase-phosphopantetheinyl transferase | AASDHPPT | 0.23 | 2.16 |
| A0A024R1N1 | Myosin-9 | MYH9 | 0.23 | 5.94 |
| Q9H1E3 | Nuclear ubiquitous casein and cyclin-dependent kinase substrate 1 | NUCKS1;NUCKS | 0.23 | 2.21 |
| Q12792 | Twinfilin-1 | TWF1 | 0.23 | 4.44 |
| A0A024RDL8 | Argininosuccinate lyase | ASL | 0.23 | 2.27 |
| P12268 | Inosine-5-monophosphate dehydrogenase 2 | IMPDH2 | 0.23 | 4.82 |
| J3QRS9 | BUB3-interacting and GLEBS motif-containing protein ZNF207 | ZNF207;DKFZp761N202 | 0.23 | 3.63 |
| P50991 | T-complex protein 1 subunit delta | CCT4 | 0.23 | 6.17 |
| B4DDM5 | Peroxisomal multifunctional enzyme type 2;(3R)-hydroxyacyl-CoA dehydrogenase;Enoyl-CoA hydratase 2 | HSD17B4 | 0.23 | 2.96 |
| B3KUJ5 | Histone deacetylase;Histone deacetylase 2 | HDAC2 | 0.22 | 2.31 |
| H7BYY1 | Tropomyosin 1 (Alpha), isoform CRA_m | TPM1 | 0.22 | 2.60 |
| A0A140VJE3 | Methionine aminopeptidase 2;Methionine aminopeptidase | METAP2 | 0.22 | 2.75 |
| Q15056 | Eukaryotic translation initiation factor 4H | EIF4H;WBSCR1 | 0.22 | 2.07 |
| P38159 | RNA-binding motif protein, X chromosome;RNA-binding motif protein, X chromosome, N-terminally processed;RNA binding motif protein, X-linked-like-1 | RBMX;RBMXL1 | 0.22 | 5.28 |
| Q8TBK5 | 60S ribosomal protein L6 | RPL6 | 0.22 | 5.59 |

| | | | | |
|---|---|---|---|---|
| Q6FHM6 | NHP2-like protein 1;NHP2-like protein 1, N-terminally processed | NHP2L1 | 0.22 | 2.43 |
| F1T0I1 | Protein transport protein Sec16A | SEC16A | 0.22 | 2.71 |
| Q5JSH3 | WD repeat-containing protein 44 | WDR44;DKFZp761M142 | 0.22 | 2.24 |
| A0A024R8W0 | Eukaryotic initiation factor 4A-III;Eukaryotic initiation factor 4A-III, N-terminally processed | DDX48;EIF4A3 | 0.21 | 3.30 |
| A8KAQ5 | U1 small nuclear ribonucleoprotein 70 kDa | SNRP70;SNRNP70 | 0.21 | 2.85 |
| A0A024QZC0 | Ataxin-2-like protein | ATXN2L | 0.21 | 4.05 |
| Q8IX12 | Cell division cycle and apoptosis regulator protein 1 | CCAR1 | 0.21 | 2.38 |
| Q59ET3 | T-complex protein 1 subunit zeta | CCT6A | 0.21 | 3.25 |
| D3DWL9 | Cleavage and polyadenylation specificity factor subunit 1 | CPSF1 | 0.20 | 3.01 |
| B2R6U8 | Cleavage and polyadenylation specificity factor subunit 5 | NUDT21 | 0.20 | 4.61 |
| P37108 | Signal recognition particle 14 kDa protein | SRP14 | 0.20 | 2.59 |
| Q9NR30 | Nucleolar RNA helicase 2 | DDX21 | 0.20 | 3.25 |
| A0A0S2Z4I9 | Vasodilator-stimulated phosphoprotein | VASP | 0.20 | 2.91 |
| P23526 | Adenosylhomocysteinase | AHCY | 0.20 | 3.18 |
| B4E266 | Leucine--tRNA ligase, cytoplasmic | LARS | 0.19 | 4.19 |
| B2RBA6 | DNA helicase;DNA replication licensing factor MCM7 | MCM7 | 0.19 | 2.91 |
| Q96BS4 | rRNA 2-O-methyltransferase fibrillarin | FBL | 0.19 | 2.90 |
| P28074 | Proteasome subunit beta type-5 | PSMB5 | 0.19 | 2.97 |
| Q13151 | Heterogeneous nuclear ribonucleoprotein A0 | HNRNPA0 | 0.19 | 4.73 |
| A0A087WY71 | AP-2 complex subunit mu | AP2M1 | 0.19 | 3.16 |
| B5MDF5 | GTP-binding nuclear protein Ran | RAN | 0.18 | 4.36 |
| Q6NXR8 | 40S ribosomal protein S3a | RPS3A | 0.18 | 3.38 |
| P62424 | 60S ribosomal protein L7a | RPL7A;RP-L7a | 0.18 | 4.04 |
| J3KTA4 | Probable ATP-dependent RNA helicase DDX5 | DDX5;DKFZp686J01190 | 0.17 | 4.31 |
| A0A140VK49 | Staphylococcal nuclease domain-containing protein 1 | SND1 | 0.17 | 4.82 |
| Q14566 | DNA replication licensing factor MCM6 | MCM6 | 0.16 | 5.23 |
| Q5JR08 | Rho-related GTP-binding protein RhoC;Transforming protein RhoA | RHOC;hCG_2043376;RHOA | -0.21 | 2.71 |
| V9HW43 | Heat shock protein beta-1 | HEL-S-102;HSPB1 | -0.22 | 4.32 |
| B7Z766 | Hypoxia up-regulated protein 1 | HYOU1 | -0.24 | 3.51 |
| O75937 | DnaJ homolog subfamily C member 8 | DNAJC8 | -0.24 | 1.95 |
| Q6I9U3 | Cation-dependent mannose-6-phosphate receptor | M6PR | -0.24 | 1.95 |
| Q14376 | UDP-glucose 4-epimerase | GALE | -0.24 | 2.02 |
| B4DS43 | Acetyltransferase component of pyruvate dehydrogenase complex;Dihydrolipoyllysine-residue acetyltransferase component of pyruvate dehydrogenase complex, mitochondrial | DLAT | -0.25 | 2.26 |
| V9HW35 | Peroxiredoxin-5, mitochondrial | HEL-S-55;PRDX5 | -0.25 | 2.01 |

| | | | | |
|---|---|---|---|---|
| Q5VSQ6 | Prolyl 4-hydroxylase subunit alpha-1 | P4HA1 | -0.26 | 2.62 |
| V9HWH9 | Protein S100;Protein S100-A11;Protein S100-A11, N-terminally processed | HEL-S-43;S100A11 | -0.26 | 3.90 |
| G3XAI2 | Laminin subunit beta-1 | LAMB1 | -0.26 | 3.40 |
| Q6FHM2 | Guanine nucleotide-binding protein G(I)/G(S)/G(T) subunit beta-2 | GNB2 | -0.26 | 3.29 |
| Q5T6L4 | Argininosuccinate synthase | ASS;ASS1 | -0.26 | 1.72 |
| Q9H3N1 | Thioredoxin-related transmembrane protein 1 | TMX1 | -0.26 | 1.63 |
| Q9BY42 | Protein RTF2 homolog | RTFDC1 | -0.27 | 2.36 |
| C9JTN7 | Nucleolysin TIA-1 isoform p40 | TIA1 | -0.27 | 2.65 |
| Q5T8U5 | Surfeit locus protein 4 | SURF4 | -0.27 | 2.15 |
| A0A0A7E7X3 | Endoplasmic reticulum aminopeptidase 1 | ERAP1;ARTS-1 | -0.27 | 2.40 |
| H3BS70 | Enoyl-CoA delta isomerase 1, mitochondrial | ECI1;DCI | -0.27 | 2.61 |
| A8K6Q8 | Transferrin receptor protein 1;Transferrin receptor protein 1, serum form | TFRC | -0.28 | 4.26 |
| A8K5I0 | Heat shock 70 kDa protein 1B;Heat shock 70 kDa protein 1A | HEL-S-103;HSPA1B;HSPA1A | -0.28 | 5.79 |
| A0A158RFU6 | Ras-related protein Rab-7a | RAB7A | -0.28 | 3.83 |
| Q6FHJ5 | Secretory carrier-associated membrane protein 3 | SCAMP3 | -0.29 | 3.67 |
| Q15843 | NEDD8 | NEDD8;NEDD8-MDP1 | -0.29 | 1.55 |
| Q6NTG0 | Na(+)/H(+) exchange regulatory cofactor NHE-RF2 | SLC9A3R2 | -0.30 | 1.47 |
| J3KMY5 | Epididymal secretory protein E1 | NPC2 | -0.30 | 2.44 |
| Q8IXB1 | DnaJ homolog subfamily C member 10 | DNAJC10 | -0.30 | 2.20 |
| Q6PKB3 | 28S ribosomal protein S27, mitochondrial | MRPS27 | -0.30 | 1.53 |
| A0A0R4J2G3 | Neutral cholesterol ester hydrolase 1 | NCEH1 | -0.30 | 1.42 |
| B2RCZ7 | Persulfide dioxygenase ETHE1, mitochondrial | ETHE1 | -0.30 | 2.16 |
| A0A140VJX1 | Acetyl-CoA acetyltransferase, mitochondrial | ACAT1 | -0.30 | 1.82 |
| A0A024RBX6 | Pirin | PIR | -0.30 | 2.22 |
| E9PDF2 | 2-oxoglutarate dehydrogenase, mitochondrial | OGDH | -0.30 | 1.63 |
| P31947 | 14-3-3 protein sigma | SFN | -0.31 | 2.15 |
| J3QQR8 | Intercellular adhesion molecule 2 | ICAM2 | -0.31 | 1.80 |
| D6RDG7 | Sideroflexin-1 | SFXN1 | -0.31 | 1.87 |
| A0A024R325 | Succinyl-CoA ligase subunit beta;Succinyl-CoA ligase [GDP-forming] subunit beta, mitochondrial | SUCLG2 | -0.31 | 1.66 |
| A0A087WTB8 | Ubiquitin carboxyl-terminal hydrolase;Ubiquitin carboxyl-terminal hydrolase isozyme L3 | UCHL3 | -0.31 | 1.76 |
| A0A087WUN7 | SRA stem-loop-interacting RNA-binding protein, mitochondrial | SLIRP | -0.31 | 1.35 |
| D6RAN4 | 60S ribosomal protein L9 | RPL9 | -0.31 | 1.46 |
| P26022 | Pentraxin-related protein PTX3 | PTX3 | -0.31 | 1.52 |
| Q2TNI1 | Caveolin;Caveolin-1 | CAV1 | -0.32 | 4.08 |
| B7Z4V2 | Stress-70 protein, mitochondrial | HEL-S-124m;HSPA9 | -0.32 | 1.39 |

| | | | | |
|---|---|---|---|---|
| B2R6K4 | Guanine nucleotide-binding protein G(I)/G(S)/G(T) subunit beta-1 | GNB1 | -0.32 | 5.38 |
| B7Z7Z3 | Nitric oxide synthase;Nitric oxide synthase, endothelial | NOS3 | -0.32 | 2.77 |
| A8K3M3 | Tyrosine-protein phosphatase non-receptor type;Tyrosine-protein phosphatase non-receptor type 1 | PTPN1 | -0.32 | 1.89 |
| P49411 | Elongation factor Tu, mitochondrial | TUFM | -0.32 | 1.44 |
| B2RDJ6 | Probable cytosolic iron-sulfur protein assembly protein CIAO1 | CIAO1 | -0.32 | 1.68 |
| A0A087WVM4 | Monofunctional C1-tetrahydrofolate synthase, mitochondrial | MTHFD1L | -0.33 | 1.39 |
| Q69YG1 | Myotrophin | DKFZp761E1322; MTPN | -0.33 | 1.70 |
| A0A024QYX3 | RNA-binding protein 3 | RBM3 | -0.34 | 1.31 |
| A0A024R745 | NADH dehydrogenase [ubiquinone] 1 alpha subcomplex subunit 5 | NDUFA5 | -0.34 | 2.21 |
| Q567R0 | Cytochrome b-c1 complex subunit 6, mitochondrial | UQCRH | -0.34 | 1.25 |
| V9HW26 | ATP synthase subunit alpha;ATP synthase subunit alpha, mitochondrial | HEL-S-123m;ATP5A1 | -0.34 | 1.40 |
| B4DKB2 | Endothelin-converting enzyme 1 | ECE1 | -0.35 | 2.27 |
| Q6FGE5 | Protein S100-A10 | S100A10 | -0.35 | 1.62 |
| Q6NZ59 | ATP synthase-coupling factor 6, mitochondrial | ATP5J | -0.35 | 1.32 |
| B2R5P6 | Thioredoxin reductase 1, cytoplasmic | TXNRD1 | -0.35 | 5.72 |
| A0A140VJQ4 | Ornithine aminotransferase, mitochondrial;Ornithine aminotransferase, hepatic form;Ornithine aminotransferase, renal form | OAT | -0.35 | 2.04 |
| B7Z2Z1 | Scaffold attachment factor B1 | SAFB | -0.35 | 2.28 |
| P11177 | Pyruvate dehydrogenase E1 component subunit beta, mitochondrial | PDHB | -0.35 | 1.31 |
| Q9NZM1 | Myoferlin | MYOF | -0.35 | 6.35 |
| P04899 | Guanine nucleotide-binding protein G(i) subunit alpha-2 | GNAI2;WUGSC:H_LUCA16.1 | -0.36 | 4.80 |
| E5KNY5 | Leucine-rich PPR motif-containing protein, mitochondrial | LRPPRC | -0.37 | 1.80 |
| Q53FM7 | NADH dehydrogenase [ubiquinone] iron-sulfur protein 3, mitochondrial | NDUFS3;DKFZp586K0821 | -0.37 | 2.90 |
| Q9BRX8 | Redox-regulatory protein FAM213A | FAM213A | -0.37 | 2.09 |
| A0A024RB87 | Ras-related protein Rap-1b;Ras-related protein Rap-1A;Ras-related protein Rap-1b-like protein | RAP1B;RAP1A | -0.37 | 1.41 |
| B4DZ08 | Aconitate hydratase, mitochondrial | ACO2;ACON | -0.37 | 2.78 |
| P80217 | Interferon-induced 35 kDa protein | IFI35 | -0.37 | 1.18 |
| Q5T9B9 | Endoglin | ENG | -0.37 | 4.75 |
| Q96AG4 | Leucine-rich repeat-containing protein 59 | LRRC59 | -0.38 | 1.15 |
| B4DMF5 | Glutamate dehydrogenase;Glutamate dehydrogenase 1, mitochondrial;Glutamate dehydrogenase 2, mitochondrial | GLUD1;GLUD2 | -0.38 | 1.99 |
| Q6IB91 | Phosphoenolpyruvate carboxykinase [GTP], mitochondrial | PCK2 | -0.39 | 1.88 |
| Q460N5 | Poly [ADP-ribose] polymerase 14 | PARP14 | -0.39 | 1.58 |

| | | | | |
|---|---|---|---|---|
| B4DJI2 | Granulins;Acrogranin;Paragranulin;Granulin-1;Granulin-2;Granulin-3;Granulin-4;Granulin-5;Granulin-6;Granulin-7 | GRN | -0.39 | 3.67 |
| G3V0I5 | NADH dehydrogenase [ubiquinone] flavoprotein 1, mitochondrial | NDUFV1 | -0.39 | 2.47 |
| B3KPA6 | Very long-chain specific acyl-CoA dehydrogenase, mitochondrial | ACADVL | -0.39 | 2.94 |
| B3KM58 | cDNA FLJ10358 fis, clone NT2RM2001238, highly similar to Glutaminase kidney isoform, mitochondrial | DKFZp686O15119 | -0.39 | 1.49 |
| B4E2V5 | Erythrocyte band 7 integral membrane protein | STOM | -0.40 | 2.39 |
| A0A024R3X4 | 60 kDa heat shock protein, mitochondrial | HSPD1 | -0.40 | 2.03 |
| B7Z792 | NADH dehydrogenase [ubiquinone] iron-sulfur protein 2, mitochondrial | NDUFS2 | -0.40 | 1.55 |
| A0A0G2JP90 | Nodal modulator 1;Nodal modulator 3;Nodal modulator 2 | NOMO1;NOMO3; NOMO2 | -0.40 | 2.11 |
| A0A024R9D7 | 2,4-dienoyl-CoA reductase, mitochondrial | DECR1;DECR | -0.40 | 3.09 |
| Q30118 | HLA class II histocompatibility antigen, DR alpha chain;HLA class II histocompatibility antigen, DQ alpha 2 chain | HLA-DRA;HLA-DRA1;HLA-DQA1;HLA-DQA1/DRA;HLA-DQA2 | -0.41 | 1.25 |
| E9KL44 | Trifunctional enzyme subunit alpha, mitochondrial;Long-chain enoyl-CoA hydratase;Long chain 3-hydroxyacyl-CoA dehydrogenase | HADHA | -0.41 | 1.95 |
| P55084 | Trifunctional enzyme subunit beta, mitochondrial;3-ketoacyl-CoA thiolase | HADHB | -0.41 | 1.37 |
| Q9H7V3 | Non-specific protein-tyrosine kinase;Proto-oncogene tyrosine-protein kinase Src;Tyrosine-protein kinase Fyn;Tyrosine-protein kinase Yes;Tyrosine-protein kinase Lck | YES1;SRC;FYN;LCK | -0.42 | 2.27 |
| M4RCG9 | HLA class I histocompatibility antigen, A-30 alpha chain;HLA class I histocompatibility antigen, A-24 alpha chain;HLA class I histocompatibility antigen, A-69 alpha chain;HLA class I histocompatibility antigen, A-2 alpha chain;HLA class I histocompatibility antigen, A-68 alpha chain;HLA class I histocompatibility antigen, A-23 alpha chain;HLA class I histocompatibility antigen, A-11 alpha chain;HLA class I histocompatibility antigen, A-3 alpha chain;HLA class I histocompatibility antigen, A-36 alpha chain;HLA class I histocompatibility antigen, A-1 alpha chain;HLA class I histocompatibility antigen, Cw-5 alpha chain;HLA class I histocompatibility antigen, Cw-8 alpha chain | HLA-A;HLA;HLA-B;HLA-A24AK;MHC class I HLA-A;HLA-A*0226;HLA-A*02;HLA-C;HLA-Cw;HLA A | -0.42 | 1.72 |
| Q05DA4 | Prolyl 4-hydroxylase subunit alpha-2 | P4HA2;DKFZp686M0919 | -0.43 | 2.43 |
| Q13011 | Delta(3,5)-Delta(2,4)-dienoyl-CoA isomerase, mitochondrial | ECH1 | -0.43 | 1.76 |
| F5GXJ9 | CD166 antigen | ALCAM | -0.43 | 4.42 |

| | | | | |
|---|---|---|---|---|
| Q6IBS5 | Dihydrolipoyllysine-residue succinyltransferase component of 2-oxoglutarate dehydrogenase complex, mitochondrial | DLST | -0.43 | 1.19 |
| E9KL42 | Acyl-coenzyme A thioesterase 1;Acyl-coenzyme A thioesterase 2, mitochondrial | ACOT1;ACOT2 | -0.43 | 2.50 |
| A4D1N4 | MICOS complex subunit MIC19 | CHCHD3 | -0.43 | 2.67 |
| A0A024R6H1 | Serine palmitoyltransferase 2 | SPTLC2 | -0.43 | 2.01 |
| Q9UJZ1 | Stomatin-like protein 2, mitochondrial | STOML2 | -0.44 | 2.80 |
| C9JNK6 | Metaxin-2 | MTX2 | -0.44 | 2.49 |
| V9HW31 | ATP synthase subunit beta;ATP synthase subunit beta, mitochondrial | HEL-S-271;ATP5B | -0.44 | 2.08 |
| P05556 | Integrin beta-1 | ITGB1 | -0.45 | 5.31 |
| B4E0H8 | Integrin alpha-3;Integrin alpha-3 heavy chain;Integrin alpha-3 light chain | ITGA3 | -0.45 | 3.01 |
| A0A024RAE4 | Cell division control protein 42 homolog | CDC42;hCG_39634 | -0.45 | 5.19 |
| A0A1W2PPX5 | Lysosome membrane protein 2 | SCARB2 | -0.45 | 3.25 |
| A0A024RC61 | Aminopeptidase N | ANPEP | -0.45 | 4.59 |
| E9PNW4 | CD59 glycoprotein | CD59 | -0.46 | 4.09 |
| Q9Y305 | Acyl-coenzyme A thioesterase 9, mitochondrial | ACOT9 | -0.47 | 3.95 |
| P54709 | Sodium/potassium-transporting ATPase subunit beta-3 | ATP1B3 | -0.50 | 2.44 |
| Q9BYN0 | Sulfiredoxin-1 | SRXN1 | -0.51 | 2.31 |
| A0A0A0MS41 | Sideroflexin;Sideroflexin-3 | SFXN3 | -0.51 | 2.99 |
| B4DJB4 | Isocitrate dehydrogenase [NAD] subunit, mitochondrial;Isocitrate dehydrogenase [NAD] subunit alpha, mitochondrial | IDH3A | -0.53 | 2.58 |
| H0YD13 | CD44 antigen | CD44 | -0.53 | 4.27 |
| Q96N83 | Podocalyxin | PODXL | -0.54 | 4.66 |
| P05023 | Sodium/potassium-transporting ATPase subunit alpha-1 | ATP1A1 | -0.54 | 4.53 |
| Q58FF8 | Putative heat shock protein HSP 90-beta 2 | HSP90AB2P | -0.54 | 1.05 |
| B3KRJ9 | Splicing regulatory glutamine/lysine-rich protein 1 | SREK1;DKFZp667P103 | -0.54 | 1.57 |
| B3KRY3 | Lysosome-associated membrane glycoprotein 1 | LAMP1 | -0.55 | 3.32 |
| A0A024R6S1 | DnaJ homolog subfamily A member 2 | DNAJA2 | -0.55 | 2.29 |
| B3KXZ9 | Cell surface glycoprotein MUC18 | MCAM | -0.56 | 2.00 |
| Q2TSD3 | Protein kinase C;Protein kinase C alpha type | PRKCA | -0.56 | 2.26 |
| H0YLU7 | Electron transfer flavoprotein subunit alpha, mitochondrial | ETFA | -0.58 | 1.69 |
| E9PKH6 | NADH dehydrogenase [ubiquinone] iron-sulfur protein 8, mitochondrial | NDUFS8 | -0.58 | 1.20 |
| A0A087WUV8 | Basigin | BSG;hEMMPRIN | -0.58 | 1.40 |
| K7EJE8 | Lon protease homolog, mitochondrial;Lon protease homolog | LONP1 | -0.59 | 3.12 |
| Q9UM02 | Prolyl endopeptidase | PREP | -0.60 | 2.23 |
| B4DPP0 | Tetraspanin;CD9 antigen | CD9;BTCC-1 | -0.61 | 5.58 |
| Q96HX3 | Dolichyl-diphosphooligosaccharide--protein glycosyltransferase subunit 1 | RPN1 | -0.64 | 3.70 |

| | | | | |
|---|---|---|---|---|
| Q9HDC9 | Adipocyte plasma membrane-associated protein | APMAP | -0.65 | 1.07 |
| D9ZGF5 | Fibroblast growth factor;Fibroblast growth factor 2 | FGF2 | -0.65 | 0.95 |
| B4DJ81 | NADH-ubiquinone oxidoreductase 75 kDa subunit, mitochondrial | NDUFS1 | -0.65 | 2.86 |
| Q8TCS8 | Polyribonucleotide nucleotidyltransferase 1, mitochondrial | PNPT1 | -0.66 | 1.89 |
| Q53SW4 | NADH dehydrogenase [ubiquinone] 1 alpha subcomplex subunit 10, mitochondrial | NDUFA10 | -0.66 | 3.11 |
| A8K132 | Glutaminase kidney isoform, mitochondrial | GLS | -0.70 | 3.20 |
| A0A024R7H5 | Bone marrow stromal antigen 2 | BST2 | -0.70 | 1.00 |
| Q9H8H0 | Nucleolar protein 11 | NOL11 | -0.73 | 1.15 |
| A0A024R4X0 | NADH-cytochrome b5 reductase;NADH-cytochrome b5 reductase 3;NADH-cytochrome b5 reductase 3 membrane-bound form;NADH-cytochrome b5 reductase 3 soluble form | CYB5R3 | -0.74 | 1.10 |
| Q9Y277 | Voltage-dependent anion-selective channel protein 3 | VDAC3 | -0.76 | 3.24 |
| P10606 | Cytochrome c oxidase subunit 5B, mitochondrial | COX5B | -0.80 | 2.20 |
| Q9UNN8 | Endothelial protein C receptor | PROCR | -0.81 | 3.86 |
| H3BRG4 | Cytochrome b-c1 complex subunit 2, mitochondrial | UQCRC2 | -0.81 | 2.50 |
| H3BNX8 | Cytochrome c oxidase subunit 5A, mitochondrial | COX5A | -0.82 | 1.84 |
| Q6NZX3 | 5-nucleotidase | NT5E | -0.82 | 4.10 |
| Q53FB6 | Aldehyde dehydrogenase, mitochondrial | ALDH2 | -0.84 | 3.41 |
| B4E2Z3 | 4F2 cell-surface antigen heavy chain | SLC3A2 | -0.84 | 4.24 |
| A0A024RBH2 | Cytoskeleton-associated protein 4 | CKAP4 | -0.84 | 4.07 |
| P47985 | Cytochrome b-c1 complex subunit Rieske, mitochondrial;Cytochrome b-c1 complex subunit 11 | UQCRFS1 | -0.88 | 3.88 |
| P31930 | Cytochrome b-c1 complex subunit 1, mitochondrial | UQCRC1 | -0.89 | 3.58 |
| E9PN17 | ATP synthase subunit g, mitochondrial | ATP5L | -0.91 | 1.27 |
| A0A024QZT0 | Voltage-dependent anion-selective channel protein 2 | VDAC2 | -0.97 | 3.92 |
| B2RE46 | Dolichyl-diphosphooligosaccharide--protein glycosyltransferase subunit 2 | RPN2 | -0.98 | 2.85 |
| P05141 | ADP/ATP translocase 2;ADP/ATP translocase 2, N-terminally processed | SLC25A5 | -1.01 | 6.16 |
| B2R4R0 | Histone H4 | HIST1H4H;HIST1H4A | -1.06 | 2.09 |
| B4DND4 | Gamma-glutamyltransferase 5;Gamma-glutamyltransferase 5 heavy chain;Gamma-glutamyltransferase 5 light chain | GGT5 | -1.08 | 2.80 |
| P68431 | Histone H3.1 | HIST1H3A | -1.08 | 2.95 |
| F8VVM2 | Phosphate carrier protein, mitochondrial | SLC25A3 | -1.09 | 2.94 |
| A0A1L1UHR1 | Voltage-dependent anion-selective channel protein 1 | VDAC1 | -1.14 | 3.25 |

| | | | | |
|---|---|---|---|---|
| Q6I9V5 | ADP/ATP translocase 3;ADP/ATP translocase 3, N-terminally processed;ADP/ATP translocase 1 | SLC25A6;SLC25A4 | -1.14 | 4.16 |
| Q5TEC6 | Histone H3 | HIST2H3PS2 | -1.16 | 2.72 |
| Q9UHS8 | Sulfide:quinone oxidoreductase, mitochondrial | hCG_2001986;SQRDL | -1.23 | 2.00 |
| P27824 | Calnexin | CANX | -1.26 | 4.62 |
| A0A0C4DGS1 | Dolichyl-diphosphooligosaccharide--protein glycosyltransferase 48 kDa subunit | DDOST | -1.30 | 4.71 |
| Q16891 | MICOS complex subunit MIC60 | IMMT | -1.72 | 3.03 |
| Q8TBT6 | Cytochrome c1, heme protein, mitochondrial | CYC1 | -1.72 | 4.42 |

Appendix Table 6: List of statistically significantly differentially regulated proteins in TNFα induced inflamed ECs in the absence of 3PO.

| Protein ID | Protein names | Gene symbol | log2 (TNFα/Control | -LOG(P-value) |
|---|---|---|---|---|
| Q16719 | Kynureninase | KYNU | 3.21 | 10.50 |
| Q7Z7M4 | Superoxide dismutase;Superoxide dismutase [Mn], mitochondrial | SOD2 | 2.69 | 9.22 |
| M4RCG9 | HLA class I histocompatibility antigen, A-30 alpha chain;HLA class I histocompatibility antigen, A-24 alpha chain;HLA class I histocompatibility antigen, A-69 alpha chain;HLA class I histocompatibility antigen, A-2 alpha chain;HLA class I histocompatibility antigen, A-68 alpha chain;HLA class I histocompatibility antigen, A-23 alpha chain;HLA class I histocompatibility antigen, A-11 alpha chain;HLA class I histocompatibility antigen, A-3 alpha chain;HLA class I histocompatibility antigen, A-36 alpha chain;HLA class I histocompatibility antigen, A-1 alpha chain;HLA class I histocompatibility antigen, Cw-5 alpha chain;HLA class I histocompatibility antigen, Cw-8 alpha chain | HLA-A;HLA;HLA-B;HLA-A24AK;MHC class I HLA-A;HLA-A*0226;HLA-A*02;HLA-C;HLA-Cw;HLA A | 1.56 | 5.02 |
| P09914 | Interferon-induced protein with tetratricopeptide repeats 1 | IFIT1 | 1.50 | 5.71 |
| K7EM56 | 40S ribosomal protein S15 | RPS15 | 1.44 | 1.84 |
| Q460N5 | Poly [ADP-ribose] polymerase 14 | PARP14 | 1.26 | 5.43 |
| Q5D1D5 | Guanylate binding protein 1 | N/A | 1.14 | 5.43 |
| Q96AZ6 | Interferon-stimulated gene 20 kDa protein | ISG20 | 1.08 | 5.60 |
| Q8TDB6 | E3 ubiquitin-protein ligase DTX3L | DTX3L | 0.94 | 5.33 |
| A0A024QYT5 | Plasminogen activator inhibitor 1 | SERPINE1 | 0.91 | 5.49 |
| P26022 | Pentraxin-related protein PTX3 | PTX3 | 0.88 | 6.24 |
| Q5ISL3 | Catenin beta-1 | CTNNB1 | 0.87 | 5.06 |

| | | | | |
|---|---|---|---|---|
| B4E0X1 | Beta-2-microglobulin;Beta-2-microglobulin;Beta-2-microglobulin form pI 5.3 | B2M | 0.80 | 2.23 |
| Q86SZ7 | Proteasome activator complex subunit 2 | PSME2 | 0.77 | 7.74 |
| P19474 | E3 ubiquitin-protein ligase TRIM21 | TRIM21 | 0.73 | 5.25 |
| B2R6L0 | Tubulin beta-2A chain | TUBB2A;TUBB2B;DKFZp566F223 | 0.71 | 5.16 |
| P80723 | Brain acid soluble protein 1 | BASP1 | 0.71 | 4.09 |
| A2ACR1 | Proteasome subunit beta type;Proteasome subunit beta type-9 | PSMB9 | 0.69 | 5.11 |
| A0A096LNZ9 | Ubiquitin-like protein ISG15 | ISG15 | 0.66 | 3.78 |
| Q9H444 | Charged multivesicular body protein 4b | CHMP4B | 0.66 | 6.69 |
| Q05DA4 | Prolyl 4-hydroxylase subunit alpha-2 | P4HA2;DKFZp686M0919 | 0.65 | 6.02 |
| P80217 | Interferon-induced 35 kDa protein | IFI35 | 0.64 | 5.22 |
| O14933 | Ubiquitin/ISG15-conjugating enzyme E2 L6 | UBE2L6 | 0.62 | 3.18 |
| A0A024R7A8 | Aldose reductase | AKR1B1 | 0.58 | 5.90 |
| Q59F45 | Mothers against decapentaplegic homolog;Mothers against decapentaplegic homolog 3;Mothers against decapentaplegic homolog 2;Mothers against decapentaplegic homolog 9 | SMAD3;SMAD2;SMAD9 | 0.58 | 3.19 |
| P20591 | Interferon-induced GTP-binding protein Mx1;Interferon-induced GTP-binding protein Mx1, N-terminally processed | MX1 | 0.57 | 6.33 |
| Q13287 | N-myc-interactor | NMI | 0.56 | 3.43 |
| A0A024R7H5 | Bone marrow stromal antigen 2 | BST2 | 0.55 | 2.81 |
| A8ASI8 | BH3-interacting domain death agonist;BH3-interacting domain death agonist p15;BH3-interacting domain death agonist p13;BH3-interacting domain death agonist p11 | BID | 0.54 | 3.83 |
| P07305 | Histone H1.0;Histone H1.0, N-terminally processed | H1F0 | 0.48 | 3.39 |
| A8KA84 | 2-5-oligoadenylate synthase 3 | OAS3 | 0.48 | 2.11 |
| V9HWB7 | Aconitate hydratase;Cytoplasmic aconitate hydratase | HEL60;ACO1;IRP1 | 0.47 | 7.56 |
| A0A0K0K1L8 | Proteasome activator complex subunit 1 | PSME1 | 0.46 | 5.09 |
| E9PK52 | Band 4.1-like protein 2 | EPB41L2 | 0.46 | 2.38 |
| A0A024R972 | Laminin subunit gamma-1 | LAMC1 | 0.46 | 5.87 |
| Q9UKY7 | Protein CDV3 homolog | CDV3 | 0.45 | 5.89 |
| C9JBL0 | Nuclear autoantigen Sp-100 | SP100 | 0.45 | 5.89 |
| P49407 | Beta-arrestin-1 | ARRB1 | 0.45 | 4.29 |
| C9J0H3 | Phospholipid scramblase 1 | PLSCR1 | 0.44 | 1.92 |
| P17900 | Ganglioside GM2 activator;Ganglioside GM2 activator isoform short | GM2A | 0.43 | 2.17 |
| P29966 | Myristoylated alanine-rich C-kinase substrate | MARCKS | 0.43 | 6.18 |
| A0A024R542 | 182 kDa tankyrase-1-binding protein | TNKS1BP1 | 0.43 | 5.22 |
| B3KMR5 | RRP12-like protein | RRP12 | 0.43 | 3.77 |
| Q92522 | Histone H1x | H1FX | 0.43 | 3.75 |

| | | | | |
|---|---|---|---|---|
| P42224 | Signal transducer and activator of transcription 1-alpha/beta;Signal transducer and activator of transcription | STAT1 | 0.42 | 4.83 |
| B2R6X6 | Peptidyl-prolyl cis-trans isomerase;Peptidyl-prolyl cis-trans isomerase F, mitochondrial | PPIF | 0.41 | 2.04 |
| A8K5I0 | Heat shock 70 kDa protein 1B;Heat shock 70 kDa protein 1A | HEL-S-103;HSPA1B;HSPA1A | 0.41 | 4.31 |
| P16401 | Histone H1.5 | HIST1H1B | 0.40 | 2.60 |
| A0A024R442 | Aspartyl aminopeptidase | DNPEP | 0.40 | 4.16 |
| A0A087X0V5 | 2-5-oligoadenylate synthase 2 | OAS2 | 0.38 | 2.31 |
| B2R5P6 | Thioredoxin reductase 1, cytoplasmic | TXNRD1 | 0.38 | 4.14 |
| D3DUZ3 | Gamma-interferon-inducible protein 16 | IFI16 | 0.38 | 3.18 |
| Q53GM9 | Fos-related antigen 1 | FOSL1 | 0.38 | 3.36 |
| Q59E90 | Alpha-mannosidase;Lysosomal alpha-mannosidase;Lysosomal alpha-mannosidase A peptide;Lysosomal alpha-mannosidase B peptide;Lysosomal alpha-mannosidase C peptide;Lysosomal alpha-mannosidase D peptide;Lysosomal alpha-mannosidase E peptide | MAN2B1 | 0.37 | 3.63 |
| A0A140VJU5 | Endophilin-B1 | SH3GLB1 | 0.37 | 2.79 |
| P16403 | Histone H1.2 | HIST1H1C | 0.36 | 3.05 |
| P49662 | Caspase-4;Caspase-4 subunit 1;Caspase-4 subunit 2;Caspase;Caspase-5;Caspase-5 subunit p20;Caspase-5 subunit p10 | CASP4;CASP5 | 0.36 | 2.49 |
| A0A024R4X1 | Protein kinase C and casein kinase substrate in neurons protein 2 | PACSIN2 | 0.36 | 3.31 |
| Q58FF8 | Putative heat shock protein HSP 90-beta 2 | HSP90AB2P | 0.34 | 3.32 |
| B2R5U3 | EH domain-containing protein 1 | EHD1 | 0.34 | 5.77 |
| B4DL66 | Ubiquitin-conjugating enzyme E2 Z | UBE2Z | 0.34 | 2.44 |
| A0A0A7E7X3 | Endoplasmic reticulum aminopeptidase 1 | ERAP1;ARTS-1 | 0.33 | 4.56 |
| B3KYB7 | Phosphatidylinositol transfer protein beta isoform | PITPNB | 0.33 | 2.95 |
| B2RDE8 | Hepatoma-derived growth factor | HDGF | 0.33 | 3.84 |
| Q6IPH7 | RPL14 protein | RPL14 | 0.31 | 2.54 |
| Q14258 | E3 ubiquitin/ISG15 ligase TRIM25 | TRIM25 | 0.31 | 4.11 |
| B4DJI2 | Granulins;Acrogranin;Paragranulin;Granulin-1;Granulin-2;Granulin-3;Granulin-4;Granulin-5;Granulin-6;Granulin-7 | GRN | 0.31 | 4.50 |
| Q14019 | Coactosin-like protein | COTL1 | 0.30 | 5.24 |
| A0A140VK56 | Transaldolase | TALDO1 | 0.29 | 2.95 |
| P46087 | Probable 28S rRNA (cytosine(4447)-C(5))-methyltransferase | NOP2 | 0.29 | 3.59 |
| P08243 | Asparagine synthetase [glutamine-hydrolyzing] | ASNS | 0.27 | 4.81 |
| F5H6E2 | Unconventional myosin-Ic | MYO1C | 0.26 | 5.23 |
| P62906 | 60S ribosomal protein L10a;Ribosomal protein | RPL10A | 0.25 | 4.14 |
| A4QPB0 | Ras GTPase-activating-like protein IQGAP1 | IQGAP1;hCG_1991735 | 0.24 | 6.61 |
| V9HWC0 | Moesin | HEL70;MSN | 0.24 | 7.05 |

| | | | | |
|---|---|---|---|---|
| Q86U42 | Polyadenylate-binding protein 2 | PABPN1 | -0.22 | 5.36 |
| Q13813 | Spectrin alpha chain, non-erythrocytic 1 | SPTAN1 | -0.24 | 4.20 |
| A0A1C7CYX9 | Dihydropyrimidinase-related protein 2 | DPYSL2 | -0.25 | 3.98 |
| Q6IAW5 | Calumenin | CALU | -0.25 | 4.29 |
| B1AJY7 | 26S proteasome non-ATPase regulatory subunit 10 | PSMD10 | -0.27 | 3.51 |
| V9HWB9 | L-lactate dehydrogenase;L-lactate dehydrogenase A chain | HEL-S-133P;LDHA | -0.27 | 4.33 |
| V9HWG0 | Chromobox protein homolog 5 | HEL25;CBX5 | -0.28 | 3.57 |
| P11216 | Glycogen phosphorylase, brain form;Alpha-1,4 glucan phosphorylase | PYGB | -0.29 | 4.20 |
| A0A024R6H1 | Serine palmitoyltransferase 2 | SPTLC2 | -0.30 | 3.68 |
| Q68DQ4 | cAMP-dependent protein kinase type I-alpha regulatory subunit;cAMP-dependent protein kinase type I-alpha regulatory subunit, N-terminally processed | DKFZp779L0468;PRKAR1A | -0.31 | 3.79 |
| Q14315 | Filamin-C | FLNC | -0.31 | 3.98 |
| V9HW83 | Retinal dehydrogenase 1 | HEL-S-53e;HEL-9;ALDH1A1 | -0.32 | 4.08 |
| A0A024R4U3 | Tubulin--tyrosine ligase-like protein 12 | TTLL12 | -0.32 | 2.58 |
| O15231 | Zinc finger protein 185 | ZNF185;DKFZp686B22130 | -0.33 | 4.34 |
| Q5TZZ9 | Annexin;Annexin A1 | ANXA1 | -0.33 | 6.63 |
| A0A140VK39 | Protein phosphatase methylesterase 1 | PPME1 | -0.34 | 3.42 |
| Q6FHL9 | Astrocytic phosphoprotein PEA-15 | PEA15 | -0.34 | 2.77 |
| P12429 | Annexin A3;Annexin | ANXA3 | -0.35 | 4.11 |
| D6RG39 | OCIA domain-containing protein 1 | OCIAD1 | -0.36 | 2.83 |
| Q5TB52 | Bifunctional 3-phosphoadenosine 5-phosphosulfate synthase 2;Sulfate adenylyltransferase;Adenylyl-sulfate kinase | PAPSS2 | -0.38 | 5.84 |
| Q68E10 | Hexokinase;Hexokinase-2 | DKFZp686M1669;HK2 | -0.38 | 4.02 |
| Q96J85 | La-related protein 4 | LARP4 | -0.40 | 2.48 |
| A0A024QZN8 | Probable E3 ubiquitin-protein ligase HERC4 | HERC4 | -0.40 | 2.55 |
| A9UK01 | Rho GTPase-activating protein 18 | ARHGAP18 | -0.41 | 6.00 |
| H7BYY1 | Tropomyosin 1 (Alpha), isoform CRA_m | TPM1 | -0.42 | 2.00 |
| Q8IVF2 | Protein AHNAK2 | AHNAK2 | -0.42 | 5.27 |
| Q6I9R8 | Four and a half LIM domains protein 2 | FHL2;AAG11 | -0.44 | 4.03 |
| B3KY03 | Condensin complex subunit 1 | NCAPD2 | -0.45 | 2.61 |
| B4E3H8 | Multimerin-2 | MMRN2 | -0.45 | 4.14 |
| A0A024RAM4 | Microtubule-associated protein 1B;MAP1B heavy chain;MAP1 light chain LC1 | MAP1B;DKFZp686F1345 | -0.46 | 2.25 |
| B7Z653 | Band 4.1-like protein 1 | EPB41L1 | -0.46 | 3.66 |
| Q59GN2 | Putative 60S ribosomal protein L39-like 5;60S ribosomal protein L39 | RPL39P5;RPL39 | -0.46 | 4.15 |
| P46939 | Utrophin | UTRN | -0.47 | 2.35 |
| A7MD96 | Synaptopodin | SYNPO | -0.50 | 1.93 |
| Q9HD26 | Golgi-associated PDZ and coiled-coil motif-containing protein | GOPC | -0.50 | 4.15 |

| | | | | |
|---|---|---|---|---|
| Q15654 | Thyroid receptor-interacting protein 6 | TRIP6;TRIP6i4;DKFZp686J22257;TRIP6i1 | -0.50 | 2.95 |
| A8CDT9 | Unconventional myosin-Va | MYO5A | -0.52 | 3.75 |
| B2RA03 | Keratin, type I cytoskeletal 18 | KRT18 | -0.53 | 4.98 |
| E9PMS6 | LIM domain only protein 7 | LMO7 | -0.58 | 5.04 |
| Q5T9B9 | Endoglin | ENG | -0.63 | 1.87 |
| A0A0U1RQV3 | EGF-containing fibulin-like extracellular matrix protein 1 | EFEMP1 | -0.67 | 2.54 |
| A0A0S2Z4U0 | Ras and Rab interactor 1 | RIN1 | -0.70 | 4.05 |
| J3QQR8 | Intercellular adhesion molecule 2 | ICAM2 | -0.72 | 1.74 |
| Q6IBN4 | Enoyl-CoA delta isomerase 2, mitochondrial | PECI;ECI2 | -0.77 | 9.67 |
| P13073 | Cytochrome c oxidase subunit 4 isoform 1, mitochondrial | COX4I1 | -0.80 | 1.35 |
| A0A024R670 | Synaptojanin-2-binding protein | SYNJ2BP;SYNJ2BP-COX16 | -0.81 | 4.03 |
| A0A024R964 | Serine/threonine-protein kinase Nek7 | NEK7 | -0.82 | 8.19 |
| B7Z7Z3 | Nitric oxide synthase;Nitric oxide synthase, endothelial | NOS3 | -0.85 | 4.13 |
| B4E290 | Calcium-binding mitochondrial carrier protein SCaMC-1 | SLC25A24 | -1.12 | 1.47 |

Appendix Table 7: List of statistically significantly differentially regulated proteins in TNFα induced inflamed ECs in the presence of 3PO.

| Protein ID | Protein names | Gene names | log2 (3PO+TNFα vs TNFα) | -LOG(P-value) |
|---|---|---|---|---|
| B4DLP1 | IST1 homolog | IST1 | 0.53 | 1.43 |
| Q9HD26 | Golgi-associated PDZ and coiled-coil motif-containing protein | GOPC | 0.53 | 3.04 |
| E9PJ81 | UBX domain-containing protein 1 | UBXN1;LOC51035 | 0.50 | 2.03 |
| Q5TDE9 | Cancer-related nucleoside-triphosphatase | C1orf57;NTPCR | 0.44 | 2.69 |
| Q8IZ83 | Aldehyde dehydrogenase family 16 member A1 | ALDH16A1 | 0.41 | 2.93 |
| Q96P70 | Importin-9 | IPO9 | 0.40 | 4.05 |
| B2ZGL7 | Monoglyceride lipase | MGLL | 0.40 | 2.92 |
| Q5T765 | Interferon-induced protein with tetratricopeptide repeats 3 | IFIT3 | 0.37 | 2.66 |
| P43246 | DNA mismatch repair protein Msh2 | MSH2 | 0.37 | 3.42 |
| Q15654 | Thyroid receptor-interacting protein 6 | TRIP6;TRIP6i4;DKFZp686J22257;TRIP6i1 | 0.37 | 1.93 |
| A0A024R0H7 | Methylosome protein 50 | WDR77 | 0.36 | 4.18 |
| Q05BU6 | Serine/arginine-rich splicing factor 11 | SFRS11;SRSF11 | 0.36 | 2.64 |
| E7EQG2 | Eukaryotic initiation factor 4A-II;Eukaryotic initiation factor 4A-II, N-terminally processed | EIF4A2 | 0.32 | 1.90 |

| | | | | |
|---|---|---|---|---|
| B2R7C2 | Centromere/kinetochore protein zw10 homolog | ZW10 | 0.32 | 2.16 |
| Q3ZCM7 | Tubulin beta-8 chain | TUBB8 | 0.32 | 1.79 |
| P78527 | DNA-dependent protein kinase catalytic subunit | PRKDC | 0.31 | 3.68 |
| B4DEI4 | Golgi reassembly-stacking protein 2 | GORASP2 | 0.29 | 4.43 |
| Q6NUR1 | Condensin complex subunit 3 | NCAPG | 0.28 | 2.17 |
| A0A1U9X9D5 | Valine--tRNA ligase | VARS | 0.28 | 3.98 |
| A0A087X283 | Ubiquitin-conjugating enzyme E2 E1;Ubiquitin-conjugating enzyme E2 E2;Ubiquitin-conjugating enzyme E2 E3 | UBE2E2;UBE2E1; UBE2E3 | 0.28 | 2.79 |
| Q53Y97 | Thymidylate synthase | TYMS | 0.27 | 5.80 |
| Q5T6H7 | Xaa-Pro aminopeptidase 1 | XPNPEP1 | 0.27 | 2.65 |
| Q9NR30 | Nucleolar RNA helicase 2 | DDX21 | 0.27 | 3.64 |
| Q96J85 | La-related protein 4 | LARP4 | 0.26 | 2.23 |
| Q9NX58 | Cell growth-regulating nucleolar protein | LYAR | 0.26 | 2.96 |
| Q32Q12 | Nucleoside diphosphate kinase;Nucleoside diphosphate kinase B | NME1-NME2;NME2;NME 1 | 0.25 | 6.54 |
| H0YBP1 | Focal adhesion kinase 1 | PTK2;FAK;DKFZp 666O0110 | 0.25 | 2.52 |
| E9PD53 | Structural maintenance of chromosomes protein;Structural maintenance of chromosomes protein 4 | SMC4 | 0.25 | 2.90 |
| J3QLE5 | Small nuclear ribonucleoprotein-associated protein;Small nuclear ribonucleoprotein-associated protein N;Small nuclear ribonucleoprotein-associated proteins B and B | SNRPN;SNRPB | 0.24 | 2.86 |
| A0A024R3V0 | SPATS2-like protein | DNAPTP6;SPATS2 L | 0.24 | 2.80 |
| B3KQ25 | Proteasome activator complex subunit 3 | PSME3;HEL-S-283 | 0.23 | 2.96 |
| A8K9T9 | Phosphoribosylformylglycinamidine synthase | PFAS | 0.23 | 4.45 |
| A0A0S2Z4G7 | Nucleophosmin | NPM1 | 0.22 | 2.78 |
| Q9Y3U8 | 60S ribosomal protein L36 | RPL36 | 0.22 | 2.94 |
| A0A024R1N1 | Myosin-9 | MYH9 | 0.22 | 9.95 |
| E5RI99 | 60S ribosomal protein L30 | RPL30 | 0.22 | 4.77 |
| P62277 | 40S ribosomal protein S13 | RPS13 | 0.21 | 5.42 |
| A8K492 | Methionine--tRNA ligase, cytoplasmic | MARS | 0.21 | 5.03 |
| A0A024R652 | C-1-tetrahydrofolate synthase, cytoplasmic;Methylenetetrahydrofolate dehydrogenase;Methenyltetrahydrofolate cyclohydrolase;Formyltetrahydrofolate synthetase;C-1-tetrahydrofolate synthase, cytoplasmic, N-terminally processed | MTHFD1 | 0.19 | 4.52 |
| P53621 | Coatomer subunit alpha;Xenin;Proxenin | COPA | 0.18 | 5.50 |
| P26232 | Catenin alpha-2 | CTNNA2 | -0.20 | 5.52 |
| C9JZR2 | Catenin delta-1 | CTNND1;DKFZp781O2021 | -0.20 | 4.07 |
| O00469 | Procollagen-lysine,2-oxoglutarate 5-dioxygenase 2 | PLOD2 | -0.21 | 4.32 |

| | | | | |
|---|---|---|---|---|
| A0A024QZT4 | Serpin B9 | SERPINB9 | -0.22 | 2.87 |
| P52209 | 6-phosphogluconate dehydrogenase, decarboxylating | PGD | -0.23 | 5.01 |
| V9HW43 | Heat shock protein beta-1 | HEL-S-102;HSPB1 | -0.23 | 3.15 |
| P83111 | Serine beta-lactamase-like protein LACTB, mitochondrial | LACTB | -0.24 | 2.83 |
| Q9H0U4 | Ras-related protein Rab-1B | RAB1B;rab1b | -0.24 | 4.86 |
| V9HWH9 | Protein S100;Protein S100-A11;Protein S100-A11, N-terminally processed | HEL-S-43;S100A11 | -0.25 | 2.87 |
| C9JNK6 | Metaxin-2 | MTX2 | -0.25 | 2.31 |
| Q6FGE5 | Protein S100-A10 | S100A10 | -0.26 | 4.81 |
| V9HW59 | Annexin;Annexin A4 | HEL-S-274;ANXA4 | -0.26 | 3.12 |
| Q8IXB1 | DnaJ homolog subfamily C member 10 | DNAJC10 | -0.26 | 2.48 |
| A0A087WVR3 | E3 ubiquitin-protein ligase UHRF1 | UHRF1 | -0.26 | 2.35 |
| Q6FHM2 | Guanine nucleotide-binding protein G(I)/G(S)/G(T) subunit beta-2 | GNB2 | -0.26 | 4.76 |
| B2R6K4 | Guanine nucleotide-binding protein G(I)/G(S)/G(T) subunit beta-1 | GNB1 | -0.28 | 4.13 |
| Q6NTG0 | Na(+)/H(+) exchange regulatory cofactor NHE-RF2 | SLC9A3R2 | -0.28 | 3.82 |
| A0A024R6H1 | Serine palmitoyltransferase 2 | SPTLC2 | -0.28 | 2.48 |
| Q53GP1 | N-sulphoglucosamine sulphohydrolase | SGSH | -0.28 | 3.61 |
| A0A024R663 | Kinectin | KTN1 | -0.28 | 2.74 |
| B3KY56 | Extended synaptotagmin-1 | FAM62A;ESYT1 | -0.29 | 2.52 |
| Q96CP5 | Mitochondrial-processing peptidase subunit beta | PMPCB;DKFZp586I1223 | -0.29 | 2.27 |
| V9HW90 | Glutathione reductase, mitochondrial | HEL-75;GSR | -0.29 | 3.24 |
| Q7Z531 | GTP:AMP phosphotransferase AK3, mitochondrial | AK3 | -0.30 | 2.63 |
| H3BS70 | Enoyl-CoA delta isomerase 1, mitochondrial | ECI1;DCI | -0.30 | 2.27 |
| A0A024R845 | Ras-related protein Rab-14 | RAB14 | -0.31 | 3.43 |
| A4D2P1 | Ras-related C3 botulinum toxin substrate 1;Ras-related C3 botulinum toxin substrate 3;Ras-related C3 botulinum toxin substrate 2 | RAC1;hCG_20693;RAC3;RAC2 | -0.31 | 4.82 |
| A0A1W2PR68 | NAD-dependent malic enzyme, mitochondrial | ME2 | -0.31 | 1.75 |
| Q9BYN0 | Sulfiredoxin-1 | SRXN1 | -0.31 | 4.05 |
| J3KMY5 | Epididymal secretory protein E1 | NPC2 | -0.31 | 5.77 |
| Q76LA1 | Cystatin-B | CSTB | -0.31 | 1.75 |
| Q6FGX3 | Ras-related protein Rab-6A;Ras-related protein Rab-6B | RAB6A;RAB6B | -0.31 | 2.39 |
| B4E3H8 | Multimerin-2 | MMRN2 | -0.32 | 1.90 |
| Q5D1D5 | Guanylate binding protein 1 | N/A | -0.32 | 2.58 |
| A0A024R7V6 | Ras-related protein Rab-2A;Ras-related protein Rab-2B | RAB2;RAB2A;DKFZp313C1541;RAB2B | -0.33 | 3.10 |
| B4DPJ2 | Annexin;Annexin A11 | ANXA11 | -0.33 | 3.62 |
| Q15907 | Ras-related protein Rab-11B;Ras-related protein Rab-11A | RAB11B;RAB11A | -0.33 | 5.09 |

| | | | | |
|---|---|---|---|---|
| A0A024RBA9 | Ras-related protein Rab-21 | RAB21 | -0.33 | 3.68 |
| Q08257 | Quinone oxidoreductase | CRYZ | -0.33 | 3.06 |
| Q567R0 | Cytochrome b-c1 complex subunit 6, mitochondrial | UQCRH | -0.34 | 1.79 |
| Q13011 | Delta(3,5)-Delta(2,4)-dienoyl-CoA isomerase, mitochondrial | ECH1 | -0.34 | 1.64 |
| P36551 | Oxygen-dependent coproporphyrinogen-III oxidase, mitochondrial | CPOX | -0.35 | 2.06 |
| O75396 | Vesicle-trafficking protein SEC22b | SEC22B | -0.35 | 2.37 |
| A0A024RBX6 | Pirin | PIR | -0.35 | 1.98 |
| A0A0G2JP90 | Nodal modulator 1;Nodal modulator 3;Nodal modulator 2 | NOMO1;NOMO3; NOMO2 | -0.36 | 2.30 |
| A4D1N4 | MICOS complex subunit MIC19 | CHCHD3 | -0.37 | 2.35 |
| A0A0S2Z2Z6 | Annexin A6;Annexin | ANXA6 | -0.37 | 6.62 |
| Q6I9U3 | Cation-dependent mannose-6-phosphate receptor | M6PR | -0.37 | 3.82 |
| P04899 | Guanine nucleotide-binding protein G(i) subunit alpha-2 | GNAI2;WUGSC:H_LUCA16.1 | -0.38 | 2.78 |
| Q53FM7 | NADH dehydrogenase [ubiquinone] iron-sulfur protein 3, mitochondrial | NDUFS3;DKFZp586K0821 | -0.38 | 1.45 |
| A0A024R1U4 | Ras-related protein Rab-5C | RAB5C | -0.38 | 3.61 |
| B2R5P6 | Thioredoxin reductase 1, cytoplasmic | TXNRD1 | -0.39 | 4.65 |
| A0A024R972 | Laminin subunit gamma-1 | LAMC1 | -0.39 | 7.28 |
| Q9UBI6 | Guanine nucleotide-binding protein G(I)/G(S)/G(O) subunit gamma-12;Guanine nucleotide-binding protein subunit gamma | GNG12 | -0.39 | 2.22 |
| A8K5I0 | Heat shock 70 kDa protein 1B;Heat shock 70 kDa protein 1A | HEL-S-103;HSPA1B;HSPA1A | -0.40 | 4.26 |
| B7Z792 | NADH dehydrogenase [ubiquinone] iron-sulfur protein 2, mitochondrial | NDUFS2 | -0.40 | 2.18 |
| Q15843 | NEDD8 | NEDD8;NEDD8-MDP1 | -0.40 | 2.97 |
| B7Z8A2 | Prenylcysteine oxidase 1 | PCYOX1 | -0.41 | 3.96 |
| A0A0R4J2G3 | Neutral cholesterol ester hydrolase 1 | NCEH1 | -0.41 | 3.17 |
| A0A024R4X1 | Protein kinase C and casein kinase substrate in neurons protein 2 | PACSIN2 | -0.41 | 3.64 |
| B4E2S7 | Lysosome-associated membrane glycoprotein 2 | LAMP2 | -0.41 | 6.42 |
| Q5JR08 | Rho-related GTP-binding protein RhoC;Transforming protein RhoA | RHOC;hCG_2043376;RHOA | -0.41 | 5.50 |
| A8K132 | Glutaminase kidney isoform, mitochondrial | GLS | -0.42 | 1.55 |
| V9HW26 | ATP synthase subunit alpha;ATP synthase subunit alpha, mitochondrial | HEL-S-123m;ATP5A1 | -0.42 | 1.41 |
| A0A024R9D7 | 2,4-dienoyl-CoA reductase, mitochondrial | DECR1;DECR | -0.42 | 1.69 |
| Q6FHJ5 | Secretory carrier-associated membrane protein 3 | SCAMP3 | -0.43 | 3.15 |
| B4DPP0 | Tetraspanin;CD9 antigen | CD9;BTCC-1 | -0.43 | 2.50 |
| G3XAI2 | Laminin subunit beta-1 | LAMB1 | -0.44 | 4.63 |
| Q5VSQ6 | Prolyl 4-hydroxylase subunit alpha-1 | P4HA1 | -0.44 | 2.65 |

| | | | | |
|---|---|---|---|---|
| P55084 | Trifunctional enzyme subunit beta, mitochondrial;3-ketoacyl-CoA thiolase | HADHB | -0.44 | 1.52 |
| A0A024RC61 | Aminopeptidase N | ANPEP | -0.44 | 4.99 |
| A8K5W7 | Isoleucine--tRNA ligase, mitochondrial | IARS2 | -0.44 | 1.85 |
| P48507 | Glutamate--cysteine ligase regulatory subunit | GCLM | -0.44 | 1.72 |
| D3DP46 | Signal peptidase complex subunit 3 | SPCS3 | -0.45 | 2.06 |
| A0A024RB87 | Ras-related protein Rap-1b;Ras-related protein Rap-1A;Ras-related protein Rap-1b-like protein | RAP1B;RAP1A | -0.45 | 2.72 |
| A0A024RAE4 | Cell division control protein 42 homolog | CDC42;hCG_39634 | -0.46 | 3.81 |
| B3KRY3 | Lysosome-associated membrane glycoprotein 1 | LAMP1 | -0.46 | 3.73 |
| P62070 | Ras-related protein R-Ras2;Ras-related protein R-Ras | RRAS2;RRAS | -0.47 | 1.35 |
| Q5NKV8 | Intercellular adhesion molecule 1 | ICAM1 | -0.47 | 2.30 |
| Q567R6 | Single-stranded DNA-binding protein;Single-stranded DNA-binding protein, mitochondrial | SSBP1 | -0.48 | 2.14 |
| Q2TNI1 | Caveolin;Caveolin-1 | CAV1 | -0.49 | 2.81 |
| Q53SW4 | NADH dehydrogenase [ubiquinone] 1 alpha subcomplex subunit 10, mitochondrial | NDUFA10 | -0.50 | 1.46 |
| B4DKB2 | Endothelin-converting enzyme 1 | ECE1 | -0.51 | 2.35 |
| Q9UES0 | Synaptobrevin homolog YKT6 | YKT6 | -0.51 | 1.71 |
| A0A158RFU6 | Ras-related protein Rab-7a | RAB7A | -0.51 | 6.23 |
| A8K6Q8 | Transferrin receptor protein 1;Transferrin receptor protein 1, serum form | TFRC | -0.51 | 3.48 |
| A0A087WTB8 | Ubiquitin carboxyl-terminal hydrolase;Ubiquitin carboxyl-terminal hydrolase isozyme L3 | UCHL3 | -0.52 | 3.74 |
| P61026 | Ras-related protein Rab-10 | RAB10 | -0.52 | 4.98 |
| Q7Z7M4 | Superoxide dismutase;Superoxide dismutase [Mn], mitochondrial | SOD2 | -0.53 | 4.57 |
| K7EJE8 | Lon protease homolog, mitochondrial;Lon protease homolog | LONP1 | -0.54 | 1.94 |
| Q9NZM1 | Myoferlin | MYOF | -0.54 | 2.92 |
| E5RHW4 | Erlin-2 | ERLIN2 | -0.54 | 4.55 |
| Q2TSD3 | Protein kinase C;Protein kinase C alpha type | PRKCA | -0.55 | 3.17 |
| Q05DA4 | Prolyl 4-hydroxylase subunit alpha-2 | P4HA2;DKFZp686M0919 | -0.56 | 4.03 |
| Q30118 | HLA class II histocompatibility antigen, DR alpha chain;HLA class II histocompatibility antigen, DQ alpha 2 chain | HLA-DRA;HLA-DRA1;HLA-DQA1;HLA-DQA1/DRA;HLA-DQA2 | -0.56 | 2.33 |
| F5GXJ9 | CD166 antigen | ALCAM | -0.58 | 1.90 |
| E9PNW4 | CD59 glycoprotein | CD59 | -0.59 | 4.83 |
| Q53FB6 | Aldehyde dehydrogenase, mitochondrial | ALDH2 | -0.59 | 1.72 |
| B4E2V5 | Erythrocyte band 7 integral membrane protein | STOM | -0.60 | 2.79 |
| Q5ISL3 | Catenin beta-1 | CTNNB1 | -0.63 | 4.72 |
| Q6NZX3 | 5-nucleotidase | NT5E | -0.64 | 3.28 |
| P05556 | Integrin beta-1 | ITGB1 | -0.64 | 3.47 |

| | | | | |
|---|---|---|---|---|
| A8K3M3 | Tyrosine-protein phosphatase non-receptor type;Tyrosine-protein phosphatase non-receptor type 1 | PTPN1 | -0.67 | 1.93 |
| P68431 | Histone H3.1 | HIST1H3A | -0.67 | 1.53 |
| A0A0A0MS41 | Sideroflexin;Sideroflexin-3 | SFXN3 | -0.67 | 2.62 |
| A0A1W2PPX5 | Lysosome membrane protein 2 | SCARB2 | -0.68 | 6.80 |
| H0YD13 | CD44 antigen | CD44 | -0.68 | 2.72 |
| P05023 | Sodium/potassium-transporting ATPase subunit alpha-1 | ATP1A1 | -0.70 | 3.72 |
| A0A024RB01 | Integrin alpha-5;Integrin alpha-5 heavy chain;Integrin alpha-5 light chain | ITGA5 | -0.71 | 2.19 |
| Q9UNN8 | Endothelial protein C receptor | PROCR | -0.71 | 3.29 |
| Q5TEC6 | Histone H3 | HIST2H3PS2 | -0.71 | 1.35 |
| Q96AG4 | Leucine-rich repeat-containing protein 59 | LRRC59 | -0.72 | 2.38 |
| M4RCG9 | HLA class I histocompatibility antigen, A-30 alpha chain;HLA class I histocompatibility antigen, A-24 alpha chain;HLA class I histocompatibility antigen, A-69 alpha chain;HLA class I histocompatibility antigen, A-2 alpha chain;HLA class I histocompatibility antigen, A-68 alpha chain;HLA class I histocompatibility antigen, A-23 alpha chain;HLA class I histocompatibility antigen, A-11 alpha chain;HLA class I histocompatibility antigen, A-3 alpha chain;HLA class I histocompatibility antigen, A-36 alpha chain;HLA class I histocompatibility antigen, A-1 alpha chain;HLA class I histocompatibility antigen, Cw-5 alpha chain;HLA class I histocompatibility antigen, Cw-8 alpha chain | HLA-A;HLA;HLA-B;HLA-A24AK;MHC class I HLA-A;HLA-A*0226;HLA-A*02;HLA-C;HLA-Cw;HLA A | -0.75 | 4.11 |
| Q9H3N1 | Thioredoxin-related transmembrane protein 1 | TMX1 | -0.76 | 2.40 |
| Q96N83 | Podocalyxin | PODXL | -0.77 | 3.37 |
| H3BNX8 | Cytochrome c oxidase subunit 5A, mitochondrial | COX5A | -0.80 | 1.96 |
| B7Z5P4 | Ran-binding protein 3 | RANBP3 | -0.80 | 2.49 |
| Q16719 | Kynureninase | KYNU | -0.85 | 3.44 |
| P10606 | Cytochrome c oxidase subunit 5B, mitochondrial | COX5B | -0.86 | 1.55 |
| B4E2Z3 | 4F2 cell-surface antigen heavy chain | SLC3A2 | -0.89 | 2.38 |
| P54709 | Sodium/potassium-transporting ATPase subunit beta-3 | ATP1B3 | -0.92 | 3.13 |
| P47985 | Cytochrome b-c1 complex subunit Rieske, mitochondrial;Cytochrome b-c1 complex subunit 11 | UQCRFS1 | -0.93 | 1.70 |
| Q96HX3 | Dolichyl-diphosphooligosaccharide--protein glycosyltransferase subunit 1 | RPN1 | -0.96 | 4.27 |
| H3BRG4 | Cytochrome b-c1 complex subunit 2, mitochondrial | UQCRC2 | -0.97 | 2.26 |
| A0A024RBH2 | Cytoskeleton-associated protein 4 | CKAP4 | -1.04 | 3.53 |

| | | | | |
|---|---|---|---|---|
| Q6I9V5 | ADP/ATP translocase 3;ADP/ATP translocase 3, N-terminally processed;ADP/ATP translocase 1 | SLC25A6;SLC25A4 | -1.07 | 1.11 |
| Q8TCS8 | Polyribonucleotide nucleotidyltransferase 1, mitochondrial | PNPT1 | -1.08 | 3.50 |
| A0A024R4X0 | NADH-cytochrome b5 reductase;NADH-cytochrome b5 reductase 3;NADH-cytochrome b5 reductase 3 membrane-bound form;NADH-cytochrome b5 reductase 3 soluble form | CYB5R3 | -1.10 | 3.59 |
| B4DND4 | Gamma-glutamyltransferase 5;Gamma-glutamyltransferase 5 heavy chain;Gamma-glutamyltransferase 5 light chain | GGT5 | -1.15 | 1.90 |
| B2RE46 | Dolichyl-diphosphooligosaccharide--protein glycosyltransferase subunit 2 | RPN2 | -1.22 | 1.53 |
| Q9HDC9 | Adipocyte plasma membrane-associated protein | APMAP | -1.25 | 2.85 |
| P05141 | ADP/ATP translocase 2;ADP/ATP translocase 2, N-terminally processed | SLC25A5 | -1.28 | 3.06 |
| F8VVM2 | Phosphate carrier protein, mitochondrial | SLC25A3 | -1.29 | 1.62 |
| P27824 | Calnexin | CANX | -1.38 | 5.22 |
| Q9UHS8 | Sulfide:quinone oxidoreductase, mitochondrial | hCG_2001986;SQRDL | -1.48 | 1.96 |
| A0A024QZT0 | Voltage-dependent anion-selective channel protein 2 | VDAC2 | -1.51 | 4.19 |
| A0A1L1UHR1 | Voltage-dependent anion-selective channel protein 1 | VDAC1 | -1.55 | 3.51 |
| A0A0C4DGS1 | Dolichyl-diphosphooligosaccharide--protein glycosyltransferase 48 kDa subunit | DDOST | -1.66 | 3.11 |
| Q71DI3 | Histone H3.2 | HIST2H3A | -1.80 | 1.02 |
| Q16891 | MICOS complex subunit MIC60 | IMMT | -2.05 | 2.59 |
| Q8TBT6 | Cytochrome c1, heme protein, mitochondrial | CYC1 | -2.32 | 1.67 |

# 9 Supplementary Information

Table 1.S. 1: Cellular components associated with upregulated proteins found in dysfunctional ECs of AMI.

| GOID | GOTerm | Ontology Source | Group PValue | Associated Genes Found |
|---|---|---|---|---|
| GO:0022626 | cytosolic ribosome | GO_CellularComponent-EBI-QuickGO-GOA_20.11.2017_00h00 | 4.78E-13 | [RPL10, RPL14, RPL15, RPL22, RPS26, RPS26P11] |
| GO:0022626 | cytosolic ribosome | GO_CellularComponent-EBI-QuickGO-GOA_20.11.2017_00h00 | 1.41E-09 | [RPL10, RPL14, RPL15, RPL22, RPS26, RPS26P11] |
| GO:0000786 | nucleosome | GO_CellularComponent-EBI-QuickGO-GOA_20.11.2017_00h00 | 4.78E-13 | [H3F3A, H3F3C, HIST1H3A, HIST2H3A, HIST3H3] |
| GO:0015934 | large ribosomal subunit | GO_CellularComponent-EBI-QuickGO-GOA_20.11.2017_00h00 | 4.78E-13 | [NPM1, RPL10, RPL14, RPL15, RPL22] |
| GO:0015934 | large ribosomal subunit | GO_CellularComponent-EBI-QuickGO-GOA_20.11.2017_00h00 | 1.41E-09 | [NPM1, RPL10, RPL14, RPL15, RPL22] |
| GO:0000786 | nucleosome | GO_CellularComponent-EBI-QuickGO-GOA_20.11.2017_00h00 | 4.95E-09 | [H3F3A, H3F3C, HIST1H3A, HIST2H3A, HIST3H3] |
| GO:0000502 | proteasome complex | GO_CellularComponent-EBI-QuickGO-GOA_20.11.2017_00h00 | 4.78E-13 | [PSMA2, PSMB3, PSME2] |
| GO:0000788 | nuclear nucleosome | GO_CellularComponent-EBI-QuickGO-GOA_20.11.2017_00h00 | 4.95E-09 | [H3F3A, HIST1H3A, HIST3H3] |

Table 1.S. 2: Cellular components associated with down-regulated proteins found in dysfunctional ECs of AMI.

| GOID | GOTerm | Ontology Source | Group PValue | Associated Genes Found |
|---|---|---|---|---|
| GO:0044391 | ribosomal subunit | GO_CellularComponent-EBI-QuickGO-GOA_20.11.2017_00h00 | 7.84E-11 | [EIF2S1, RPL11, RPL23A, RPL27A, RPL35A, RPL36, RPL38, RPS14, RPS25, RPSA] |
| GO:0044445 | cytosolic part | GO_CellularComponent-EBI-QuickGO-GOA_20.11.2017_00h00 | 7.84E-11 | [CYB5R3, EIF2S1, RPL11, RPL23A, RPL27A, RPL35A, RPL36, RPL38, RPS14, RPS25, RPSA, UBQLN4] |

| | | | | |
|---|---|---|---|---|
| GO:0022626 | cytosolic ribosome | GO_CellularComponent-EBI-QuickGO-GOA_20.11.2017_00h00 | 7.84E-11 | [EIF2S1, RPL11, RPL23A, RPL27A, RPL35A, RPL36, RPL38, RPS14, RPS25, RPSA] |
| GO:0022627 | cytosolic small ribosomal subunit | GO_CellularComponent-EBI-QuickGO-GOA_20.11.2017_00h00 | 7.84E-11 | [EIF2S1, RPS14, RPS25, RPSA] |
| GO:0044391 | ribosomal subunit | GO_CellularComponent-EBI-QuickGO-GOA_20.11.2017_00h00 | 2.20E-10 | [EIF2S1, RPL11, RPL23A, RPL27A, RPL35A, RPL36, RPL38, RPS14, RPS25, RPSA] |
| GO:0044445 | cytosolic part | GO_CellularComponent-EBI-QuickGO-GOA_20.11.2017_00h00 | 2.20E-10 | [CYB5R3, EIF2S1, RPL11, RPL23A, RPL27A, RPL35A, RPL36, RPL38, RPS14, RPS25, RPSA, UBQLN4] |
| GO:0022626 | cytosolic ribosome | GO_CellularComponent-EBI-QuickGO-GOA_20.11.2017_00h00 | 2.20E-10 | [EIF2S1, RPL11, RPL23A, RPL27A, RPL35A, RPL36, RPL38, RPS14, RPS25, RPSA] |
| GO:0022625 | cytosolic large ribosomal subunit | GO_CellularComponent-EBI-QuickGO-GOA_20.11.2017_00h00 | 2.20E-10 | [RPL11, RPL23A, RPL27A, RPL35A, RPL36, RPL38] |
| GO:0022627 | cytosolic small ribosomal subunit | GO_CellularComponent-EBI-QuickGO-GOA_20.11.2017_00h00 | 2.20E-10 | [EIF2S1, RPS14, RPS25, RPSA] |
| GO:0071004 | U2-type prespliceosome | GO_CellularComponent-EBI-QuickGO-GOA_20.11.2017_00h00 | 1.59E-04 | [LUC7L2, SF3A1, U2AF2] |
| GO:0000502 | proteasome complex | GO_CellularComponent-EBI-QuickGO-GOA_20.11.2017_00h00 | 3.93E-04 | [UBQLN1, UBQLN4, UBXN1] |
| GO:0032154 | cleavage furrow | GO_CellularComponent-EBI-QuickGO-GOA_20.11.2017_00h00 | 4.98E-04 | [ICAM2, LIMA1, MYH10, RDX] |

Table 2.S 1: Cellular components associated with upregulated proteins found in dysfunctional ECs of CTEPH.

| GOID | GOTerm | Ontology Source | Group PValue | Associated Genes Found |
|---|---|---|---|---|
| GO:0005840 | ribosome | GO_CellularComponent-EBI-QuickGO-GOA_20.11.2017_00h00 | 1.07E-14 | [EEF2, EIF2A, RBM3, RPL10, RPL14, RPL18A, RPL19, RPL21, RPL24, RPL35A, RPL7, RPL7A, RPL8, RPS13, RPS15, RPS21, RPS27, RPS28] |
| GO:0015934 | large ribosomal subunit | GO_CellularComponent-EBI-QuickGO- | 1.07E-14 | [RBM3, RPL10, RPL14, RPL18A, RPL19, RPL21, |

| | | | | |
|---|---|---|---|---|
| | | GOA_20.11.2017_00h0 0 | | RPL24, RPL35A, RPL7, RPL7A, RPL8] |
| GO:0022626 | cytosolic ribosome | GO_CellularComponent -EBI-QuickGO- GOA_20.11.2017_00h0 0 | 1.07E-14 | [EIF2A, RPL10, RPL14, RPL18A, RPL19, RPL21, RPL24, RPL35A, RPL7, RPL7A, RPL8, RPS13, RPS15, RPS21, RPS27, RPS28] |
| GO:0022627 | cytosolic small ribosomal subunit | GO_CellularComponent -EBI-QuickGO- GOA_20.11.2017_00h0 0 | 1.07E-14 | [EIF2A, RPS13, RPS15, RPS21, RPS27, RPS28] |
| GO:0022627 | cytosolic small ribosomal subunit | GO_CellularComponent -EBI-QuickGO- GOA_20.11.2017_00h0 0 | 8.89E-14 | [EIF2A, RPS13, RPS15, RPS21, RPS27, RPS28] |
| GO:0005685 | U1 snRNP | GO_CellularComponent -EBI-QuickGO- GOA_20.11.2017_00h0 0 | 8.89E-14 | [SNRPF, SNRPG, SNRPGP15] |
| GO:0005687 | U4 snRNP | GO_CellularComponent -EBI-QuickGO- GOA_20.11.2017_00h0 0 | 8.89E-14 | [SNRPF, SNRPG, SNRPGP15] |
| GO:0005840 | ribosome | GO_CellularComponent -EBI-QuickGO- GOA_20.11.2017_00h0 0 | 5.19E-13 | [EEF2, EIF2A, RBM3, RPL10, RPL14, RPL18A, RPL19, RPL21, RPL24, RPL35A, RPL7, RPL7A, RPL8, RPS13, RPS15, RPS21, RPS27, RPS28] |
| GO:0022626 | cytosolic ribosome | GO_CellularComponent -EBI-QuickGO- GOA_20.11.2017_00h0 0 | 5.19E-13 | [EIF2A, RPL10, RPL14, RPL18A, RPL19, RPL21, RPL24, RPL35A, RPL7, RPL7A, RPL8, RPS13, RPS15, RPS21, RPS27, RPS28] |
| GO:0022627 | cytosolic small ribosomal subunit | GO_CellularComponent -EBI-QuickGO- GOA_20.11.2017_00h0 0 | 5.19E-13 | [EIF2A, RPS13, RPS15, RPS21, RPS27, RPS28] |
| GO:0022627 | cytosolic small ribosomal subunit | GO_CellularComponent -EBI-QuickGO- GOA_20.11.2017_00h0 0 | 9.83E-12 | [EIF2A, RPS13, RPS15, RPS21, RPS27, RPS28] |
| GO:0000784 | nuclear chromosome, telomeric region | GO_CellularComponent -EBI-QuickGO- GOA_20.11.2017_00h0 0 | 1.53E-09 | [CBX3, FEN1, HAT1, MCM2, MCM3, MCM5, MCM6, MCM7, PCNA] |

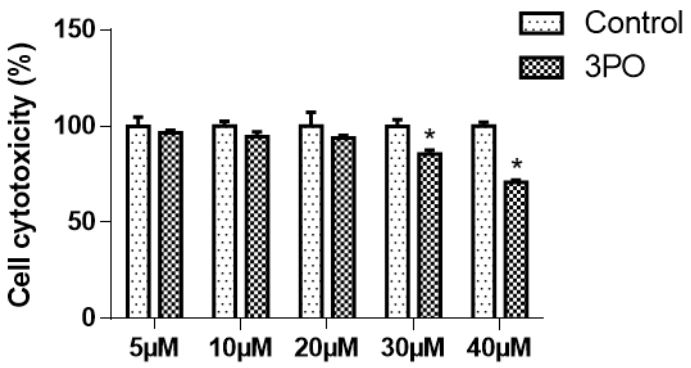


Figure S 1: Cytotoxic effect of 3PO on Ea.hy926 cells

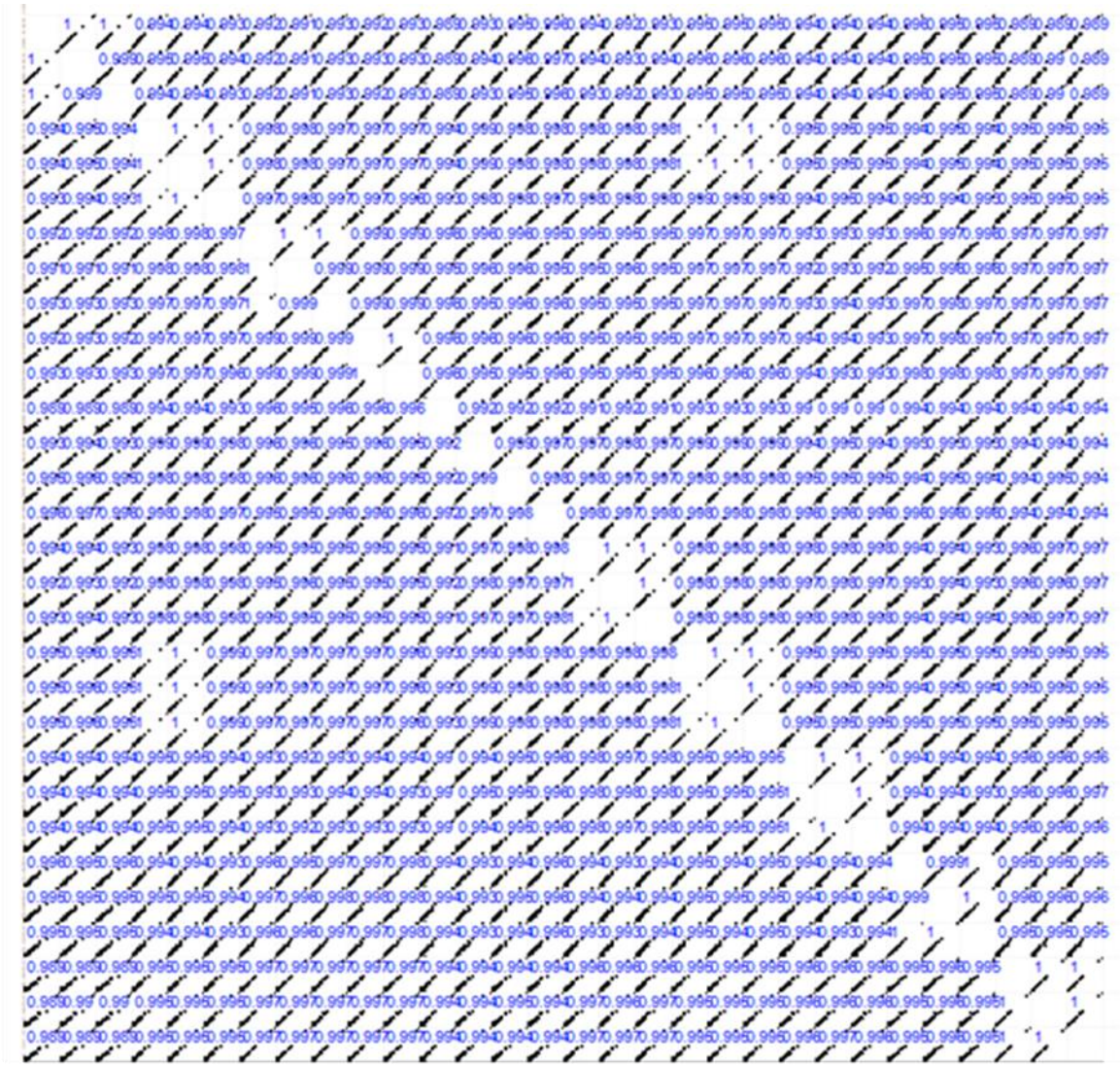

Figure S 2: The Pearson correlation among the samples.

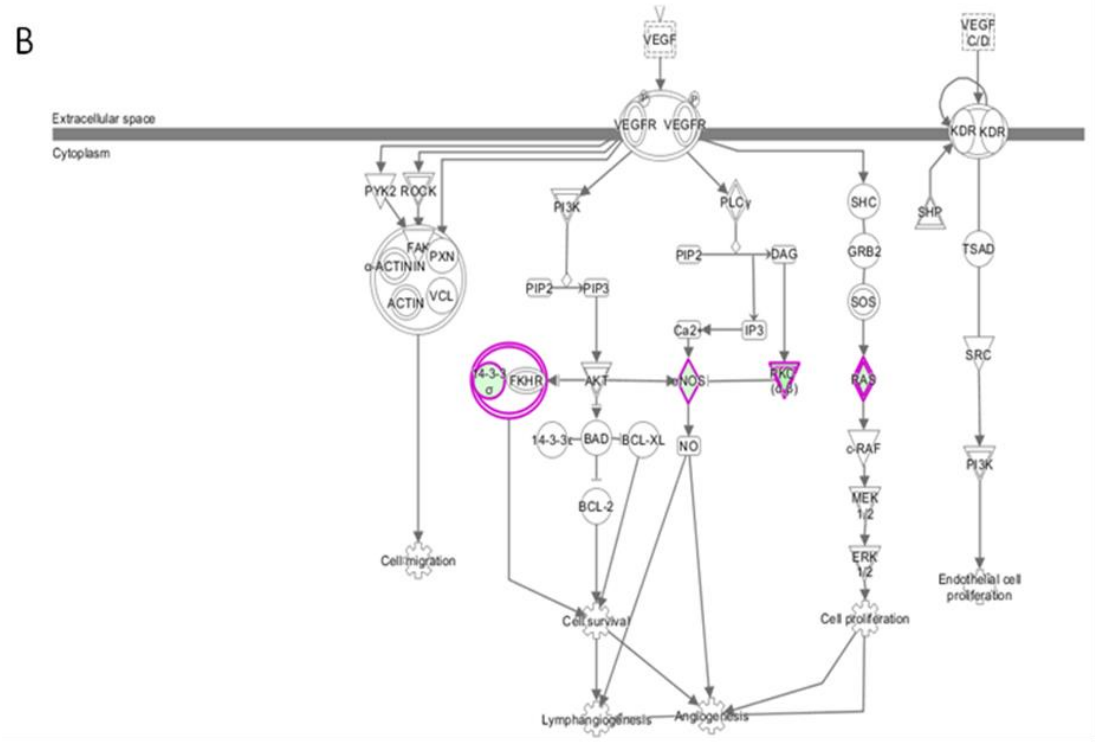


Figure S 3: Down regulation of VEGF signalling in 3PO treated cells by IPA software

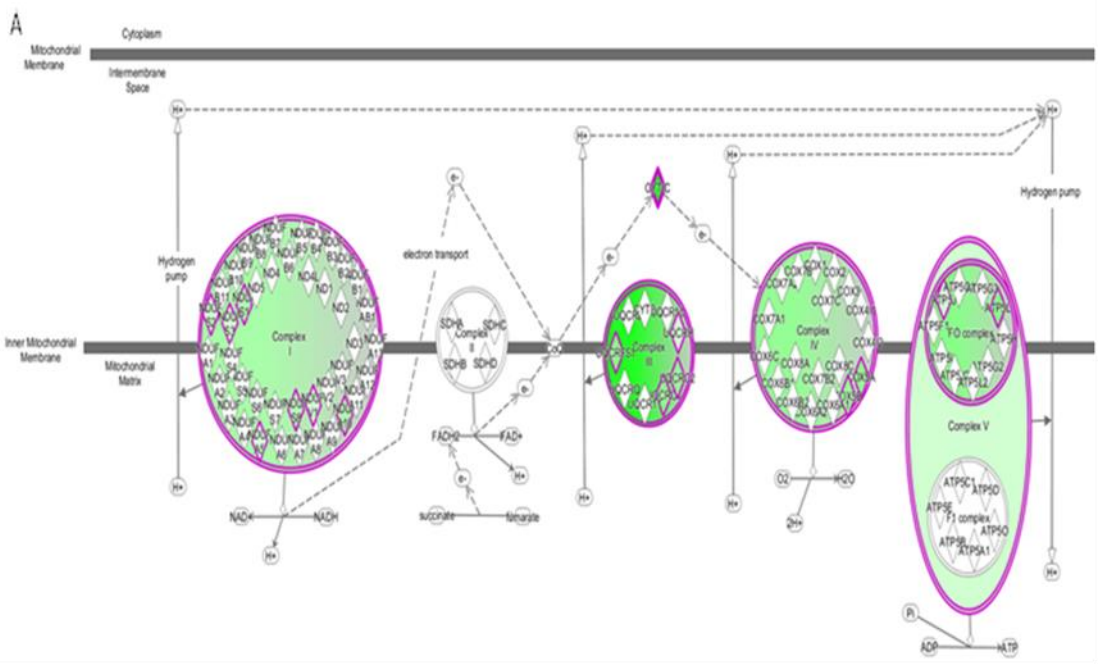


Figure S 4: Down regulation of oxidative phosphorylation in 3PO treated cells by IPA software

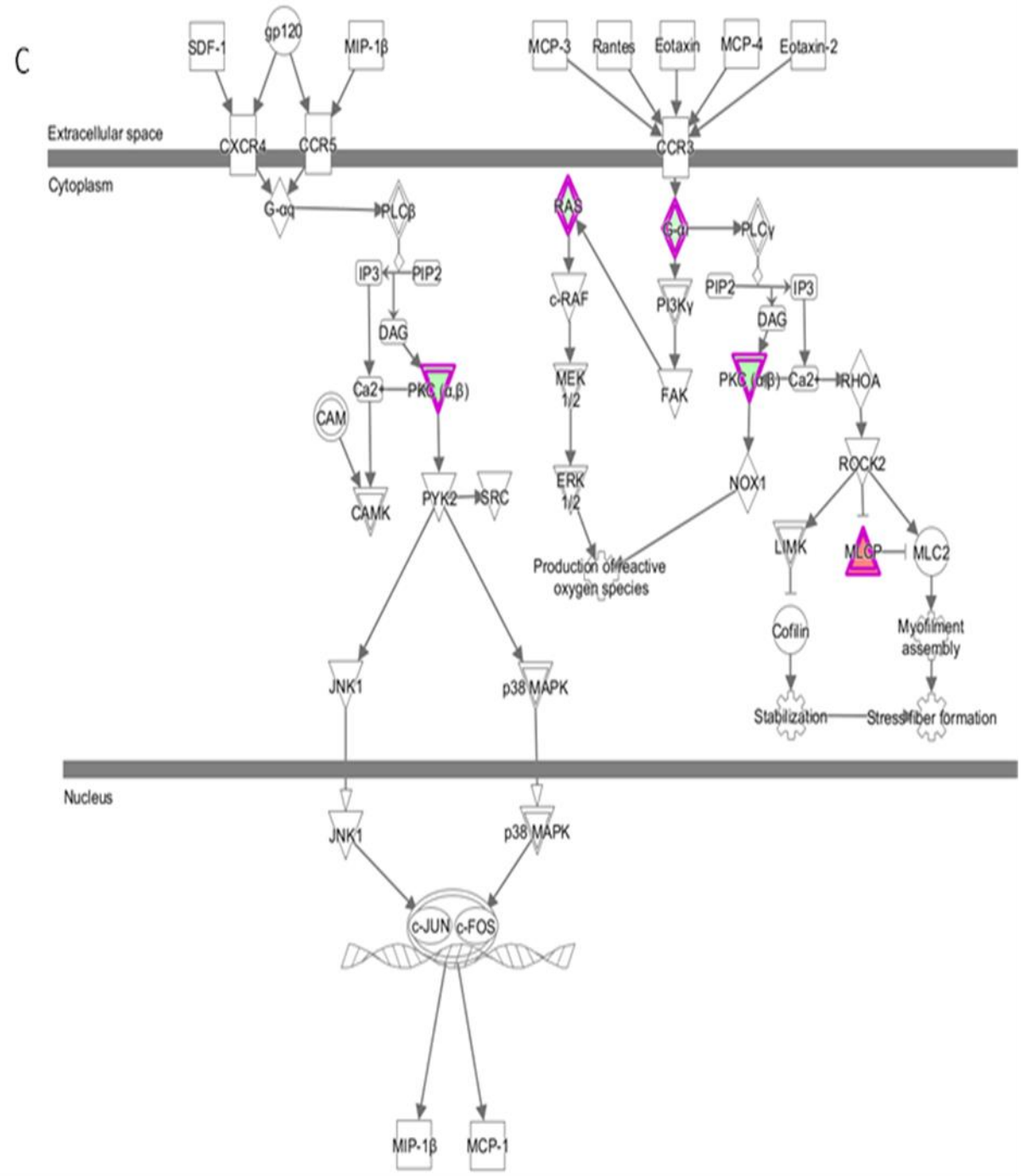


Figure S 5: Down regulation of cytokine in 3PO treated cells signaling by IPA software

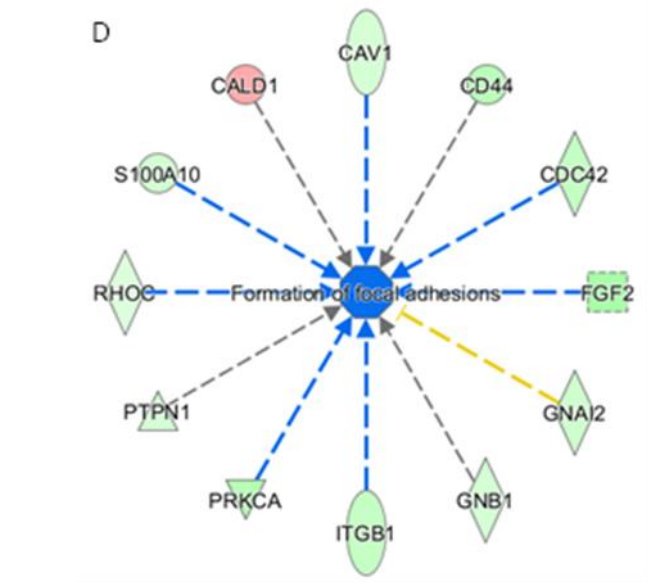


Figure S 6: Down regulation of formation of focal adhesions in 3PO treated cells signaling by IPA software

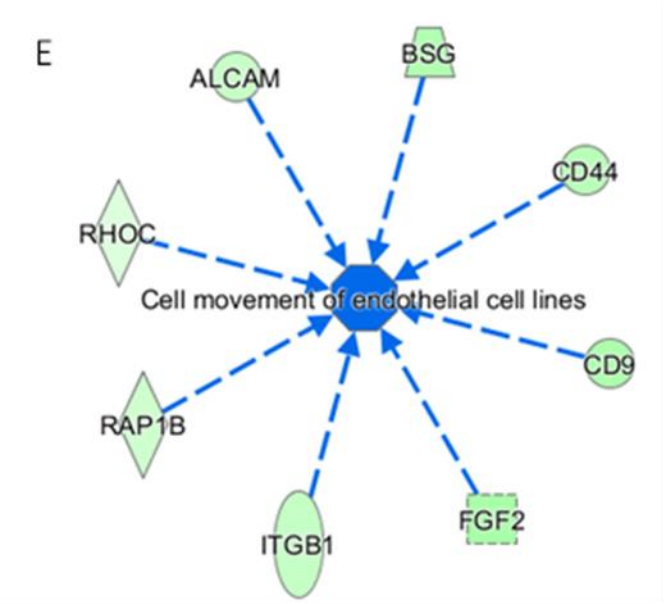


Figure S 7: Down regulation of cell movement of endothelial cell lines in 3PO treated cells signaling by IPA software